

Copyright

by

Amanda Zulema Calle Peralta

2013

**The Thesis Committee for Amanda Zulema Calle Peralta  
Certificates that this is the approved version of the following thesis:**

**Neogene sedimentation and provenance record of the  
Subandean zone and Chaco foreland basin, southern Bolivia**

**APPROVED BY  
SUPERVISING COMMITTEE:**

---

Brian K. Horton

---

Lesli J. Wood

---

Daniel F. Stockli

**Neogene sedimentation and provenance record of the  
Subandean zone and Chaco foreland basin, southern Bolivia**

**by**

**Amanda Zulema Calle Peralta, B. S. Geo.**

**Thesis**

Presented to the Faculty of the Graduate School of  
The University of Texas at Austin  
in Partial Fulfillment  
of the Requirements  
for the Degree of

**Master of Science in Geological Sciences**

**The University of Texas at Austin**  
**August 2013**

## Acknowledgements

First, I thank my supervisor Dr. Brian Horton for the challenging and fruitful discussions, and professional guidance to further pursue many interesting geologic problems. Committee members Drs. Lesli Wood and Daniel Stockli are sincerely thanked for sharing their valuable time in discussions and suggestions to improve the manuscript. Special thanks for discussions with Jonas Kley, Victor Ramos, Daniel Starck, Kitty Milliken, Antonio Teixell, and Randy Marrett.

This research was sponsored by the National Science Foundation NSF (EAR-0908518) granted to Dr. Brian Horton, the Jackson School of Geosciences, Repsol E&P Bolivia, and research grants from the Geological Society of America and Society for Sedimentary Geology.

Field and logistic assistance was graciously provided by Rodrigo Limachi, Gerardo Villacorta, Hernan Orellana, and Paul Muñoz. Discussions about Bolivian geology with Edgar Requena, Gonzalo Astorga and Rodrigo Limachi are greatly appreciated. Furthermore, I express my sincere thanks to Dr. Horton's research group for stimulating discussions and laboratory training including Nicholas Perez, Meredith Bush, Mariya Levina, Joel Saylor, Renas Mohammed, Veronica Anderson, Ryan McKenzie, and Sebastian Ramirez. My family and friends were very supportive during the whole process. I sincerely thank my parents, siblings and relatives for encouraging me to achieve my goals. Finally, I am indebted to my friends Helene Baret, David Banda, Jess Lally, Jorge Gutierrez, Edgardo Pujols, Rosmery Fernandez, Marioly Yarhui, Chelsea Underwood, and Amanda Jeffrey for their continued support during this stage.

## **Abstract**

# **Neogene sedimentation and provenance record of the Subandean zone and Chaco foreland basin, southern Bolivia**

Amanda Zulema Calle Peralta, M.S.GeoSci.

The University of Texas at Austin, 2013

Supervisor: Brian K. Horton

Evolution of the Subandean fold-thrust belt and adjacent Chaco foreland basin since their inception ~20 Myr ago has involved shortening, crustal thickening and flexural loading along the eastern margin of the central Andes in Bolivia. Few studies have assessed the linkages among surface processes and threshold responses to climate change, tectonics, and/or catchment-area modification in this thin-skinned fold-thrust belt and coupled foreland basin. Analyses of stratigraphic variations and sediment provenance within two of the proximal, westernmost sections of the Subandean zone (Bartolo and Emborozú localities) are consistent with an eastward advancing synorogenic fold-thrust system guiding deposition and facies migration within several foreland depozones. Results from Cenozoic detrital zircon U-Pb geochronology, conglomerate clast compositions, sandstone petrography and paleocurrent analyses provide information on the gradual eastward diachroneity of upward-coarsening successions and fluvial megafan deposits. New and published zircon U-Pb data for interbedded Miocene tuffs and an updated magnetostratigraphic analysis contribute to the interpretation of depositional

ages and changes in sediment accumulation rates. Regionally, the Neogene sedimentation history shows a gradually subsiding basin until 8 Ma with progressively coarser facies up to 6 Ma. High accumulation rates for proximal alluvial-fan facies and proximal fluvial megafan deposits after 6 Ma are identified and correlated with their distal counterparts in the Chaco basin. Evidence for the introduction of progressively younger rocks in uplifted sediment source areas, as documented by conglomerate counts and detrital zircon age populations, lead us to interpret protracted unroofing and sediment dispersal from the Eastern Cordillera–Interandean Zone commencing at ~23 Ma, followed by initial propagation of the deformation front into the Subandean Zone at ~20-15 Ma (as estimated from new tuff ages and accumulation rates). A temporal shift from axial to transverse fluvial drainage recorded by paleocurrent data reinforces evidence for an eastward advancing depocenter and structural partitioning of the older segments of the foreland basin, particularly from 6 Ma to present. Continued exhumation and enhancement of the drainage areas to the west (i.e., Eastern Cordillera, Interandean Zone, and actively deforming Subandean zone) reflect changes in the accumulation of coarser lithofacies in proximal areas and delivery of significant sediment volumes to modern fluvial megafans of the Chaco plain.

## Table of Contents

List of Tables .....	ix
List of Figures .....	x
<b>CHAPTER 1. INTRODUCTION AND GEOLOGIC FRAMEWORK .....</b>	<b>1</b>
Introduction.....	1
Geological setting .....	6
Andes Mountains .....	6
Central Andes.....	6
Topography .....	7
Mountain building and uplift .....	8
Shortening.....	9
Subandean foreland basin .....	9
Regional stratigraphic framework.....	13
<b>CHAPTER 2. SEDIMENTOLOGY AND STRATIGRAPHY .....</b>	<b>15</b>
Cenozoic stratigraphy .....	15
Petaca Formation .....	15
Yecua Formation.....	16
Tariquia Formation .....	16
Guandacay Formation .....	17
Emborozú Formation .....	17
Sedimentology and depositional systems .....	19
Bartolo locality.....	19
Emborozú locality.....	19
Facies associations .....	23
<b>CHAPTER 3. PROVENANCE ANALYSES .....</b>	<b>40</b>
Conglomerate clast compositions .....	40
Sandstone petrology.....	43
Paleocurrents.....	49

Detrital zircon U-Pb geochronology .....	52
<b>CHAPTER 4. U-PB GEOCHRONOLOGY AND MAGNETOSTRATIGRAPHY .....</b>	<b>63</b>
U-Pb geochronology of volcanic horizons .....	63
Magnetostratigraphy .....	64
<b>CHAPTER 5. CENOZOIC BASIN RECONSTRUCTION AND DISCUSSION.....</b>	<b>69</b>
Oligocene-Miocene boundary (~23 Ma) .....	69
~23–20 Ma .....	71
20–6 Ma .....	71
6 Ma to present.....	75
<b>CHAPTER 6. CONCLUSIONS .....</b>	<b>76</b>
Appendix 1. Recalculated modal point-count data from the Bartolo locality .....	80
Appendix 2. LA-ICP-MS analyses for detrital zircon U-Pb geochronology.....	81
Appendix 3. SHRIMP U-Pb data from detrital zircon sample VLE07-109 from Escayola et al. (2011).....	113
References.....	115
Vita.....	124

## List of Tables

Table 1. Lithofacies for the Petaca, Tariquia, Guandacay, Emborozú formations (after Miall, 1996; Uba et al., 2005 and Siks, 2011) .....	24
Table 2. Facies associations and depositional systems for the Petaca, Tariquia, Guandacay and lower Emborozú formations after Miall (1996); Uba et al. (2005); and Siks (2011).....	27
Table 3. Categories for sandstone point count analyses .....	44

## List of Figures

- Figure 1. a) Location of Central Andes in South America (yellow line). b) DEM showing tectono-morphic provinces of the Central Andes (after Uba et al., 2009), and c) location of regional map (white rectangle) of the Subandean zone and eastern Chaco plain shown in Figure 2. ....2
- Figure 2. Generalized geologic map of the (from west to east) Eastern Cordillera (mostly Ordovician exposures), Interandean zone (mostly Devonian outcrops), Subandean zone (Devonian to Paleogene exposures) and westernmost Chaco foreland basin (dominated by Quaternary deposits) in southern Bolivia from SERGEOTECMIN-YPFB (2000). Also showing major fold-thrust structures and location of Cenozoic measured sections (located at Bartolo and Emborozú) in the westernmost Subandes, tuff samples (red stars) with their U-Pb weighted age, Cenozoic samples (blue triangles) for U-Pb detrital zircon provenance and potential source samples of the Cenozoic fill (purple dots). The magnetostratigraphic study was focused at the Villamontes section. Black rectangles highlight the position of local geologic maps (Bartolo, Emborozú and Villamontes). .....4

Figure 3. Geologic maps and cross sections for: a) Bartolo (after Salinas, 1981; Giraudo and Limachi, 2001), and b) Emborozú (after Kley, 1993, and YPFB). At Bartolo, Cenozoic strata were analyzed from the Yanguilo thrust hanging-wall up to the Río Azero thrust fault. Post-Yanguilo activity of the Río Azero fault limit Cenozoic exposures. At Emborozú, deposits were measured close to an open syncline, with no observed unconformities related to coeval thrust activity.....11

Figure 4. Generalized lithostratigraphic column of Cenozoic fill in the Subandean zone and Chaco foreland basin. Lithofacies variations are observed from the basal Petaca (Oligocene-lower Miocene) to Emborozú (Plio-Pleistocene) formations. An upward coarsening trend is coupled with higher accumulation rates.....18

Figure 5. Measured stratigraphic section of the a) Bartolo and b) Emborozú stratigraphic sections displaying lithostratigraphic units (Petaca, Tariquia, Guandacay and Emborozú formations), sedimentary structures, paleocurrent directions, conglomerate clast composition stations, and sample locations for sandstone petrography, detrital zircon and newly and previously dated volcanic tuffs (U-Pb age in brackets). .....20

Figure 6. Representative lithofacies association photographs for the major Cenozoic stratigraphic units: Petaca, Tariquia, Guandacay and Emborozú. a) Pervasive calcareous paleosols (A1) widespread in the Petaca Formation. Abundant calcareous nodules displaying irregular morphologies (elongate to even vertical rhizocretions) are easily recognized for their light green and gray mottled pattern; b) facies associations-A2 and A5 of the basal Tariquia Formation at the Emborozú section. Sharp erosive basal surfaces of thick bedded sandstones (Sh) are encased in broad intervals of facies association A2 (mudstone, lithofacies Fl) and A6 (thin-bedded sandstone, lithofacies Sl) and can be traced for ten of meters; c) Finely-bedded sandstones sharply overlain by greenish gray, carbonaceous laminated siltstones, associated with facies association A7 are recorded in the lower Tariquia at the Bartolo section; d) tabular sandstones (Ss, St lithofacies) with poorly developed trough cross-stratification, and sharp erosive and sometimes irregular basal contacts (facies association A8). At Bartolo this facies association persists laterally for hundreds of meters (see vehicle in the lower right for scale) and comprises upward fining intervals underlying multistory mudstones (lithofacies Fl). e) vertically- and laterally restricted (lens shaped) finely laminated mudstones (Fl) intercalated with thinly-bedded sandstones (Fl) representing facies association A3, in the middle Tariquia section (Bartolo). Unconformably overlain are mounded interbedded lenticular sandstone and mudstone (facies associations A6) capped by thick, limited through cross-bedded sandstone (facies association A8); f) laterally extensive sandstones with

incipient erosive basal surfaces (facies association A8) interbedded with thin lenticular sandstone and mudstone of facies association A6 are observed In the middle Tariquia section of Bartolo; g) Thick-bedded sandstones (Sm), with discontinuous non-parallel erosive basal contacts are typical of the upper Guandacay Formation at Bartolo locality, they comprise facies associations A4; h) yellow, red, slightly calcareous sandstone (Pcm)- moderate developed paleosols capping upward-fining sandstones of facies associations A4 at Bartolo section; I) highly erosive basal, lenticular, upward fining, limited cross-stratified conglomerates and sandstones stacked in cycles of ~3-15 m thick represent facies association A9. Thick (~3-12 m) thin-bedded sandstones (Sl) and mudstones (Fl) are characteristic of the Guandacay Formation at the Emborozú locality. In contrast, thinner, discontinuous mudstone overlains thick-erosive conglomerates (6j) of the Emborozú Formation.

.....31

Figure 7. Conglomerate clast composition pie charts from the Guandacay Formation in the Bartolo section; n denotes the number of measured stations. .42

Figure 8. a) Q/F/L (quartz, feldspar/lithic fragment) plot (Folk, 1980) of sandstone petrographic data from Bartolo section (with 50% quartz baseline). b) Qt/F/L, and c) Qp/Lv/Ls provenance ternary diagrams (Dickinson and Suczek, 1979). Mean compositional values for the Petaca, Tariquia and Guandacay are plotted; n represents the number of samples. Arrows depict the upward increase in lithic fragments with respect to quartz grains.....47

Figure 9. Generalized Cenozoic stratigraphic column of the Subandean zone and adjacent Chaco basin including updated paleocurrent directions for the eastern (after Hullca and Heubeck, 2010) and western Subandean zone (this study). Note the paleocurrent reversal after deposition of the Petaca Formation ( $> \sim 12$  Ma). Petaca deposits record dominant paleoflows from east to west, and paleocurrent vectors above this unit show a predominant transport direction eastward. ....51

Figure 10. a) Location map of the potential source samples of the Cenozoic fill (red dots).b) Generalized stratigraphic column of Southern Bolivia (after Moretti et al., 1996), including stratigraphic position of the analyzed samples. Sample VLE07-109 from Escayola et al. (2011). ....54

Figure 11. a) Detrital zircon U-Pb spectra for Cenozoic sandstones (above red line) from the Subandean basin and modern fluvial megafans, and potential Paleozoic-Mesozoic source units (below red line) from 0-3000 Ma, and b) 400-800 Ma. Sample VLE07-109 has been analyzed previously by Escayola et al. (2011). Samples are a) Three main populations signature interpreted as recycled Amazonian craton, recycled Andean orogeny and derived from the Cenozoic magmatic arc. b) Upsection (Pliocene) increase of older Pampean ages coupled to younger (Ocloyic-Famatinian) signatures suggest a protracted unroofing of older Andean segments (Eastern Cordillera, Interandean zone). ....60

Figure 12. a) Location of the Angosto del Pilcomayo section in the eastern Subandean region, structural configuration of the nearby area (after Dunn et al., 1995), b) Stratigraphic section and U-Pb tuff ages (Uba et al., 2005), observed declination values and interpreted polarity zones with normal (black) and white (reverse) polarity intervals. c) Correlation of the polarity column with the Geomagnetic Polarity Scale (2012) (Gradstein et al., 2012). Tuff ages have been used to constrain the correlation. d) Accumulation rate diagram resulting from interpreted chrons and subchrons correlation, and compared with predicted tuff age-derived sedimentation rates. A very significant increase in the accumulation rates (from ~10 cm/kyr to ~90 cm/kyr is interpreted in the upper Miocene.....67

Figure 13. Schematic regional diagrams illustrating the proposed Cenozoic depositional systems evolution in the Subandes and Chaco foreland basin, including the Interandean-Eastern Cordillera role as a source area

.....73

# CHAPTER 1. INTRODUCTION AND GEOLOGIC FRAMEWORK

## INTRODUCTION

The Subandean zone and Chaco foreland basin are located along the eastern margin of the central Andes at 18-22°S (Figure 1). Eastward propagation of the Andean orogenic belt, coupled with crustal thickening and flexural loading resulted in Neogene development of the Subandean thin-skinned fold thrust belt and Chaco foreland basin (Figure 2; Gubbels et al., 1993; Sempere et al., 1990; Kley, 1993; Lamb et al., 1997; McQuarrie et al., 2005). The structural geometries of the evolving Andean orogenic wedge have been studied extensively (e.g., Kley, 1993; Ege et al., 2007; McQuarrie, 2002) but the configuration prior to shortening advance from the Eastern Cordillera to the Subandes has not been fully addressed. To date there has been little agreement on the timing of initial propagation of the deformation front into the Subandean zone, with various investigations suggesting ages ranging from ~20 to 5 Ma (Sempere et al., 1990; Lamb et al., 1993; Kley, 1996; Jordan et al., 1997; Echavarria et al., 2003; Ege, 2004; McQuarrie et al., 2005; Uba et al., 2006, 2009; Ege et al., 2007; Barnes et al., 2008). The activation of large thrusts and corresponding décollements (Main Interandean thrust and Main Subandean thrust) is a key element in the evolution of the central Andes (Kley, 1996; McQuarrie, 2002), but the coupled sedimentologic, stratigraphic, and geodynamic signatures in the adjacent Subandean and Chaco foreland basin remain debated (DeCelles and Horton, 2003; Echavarria et al., 2003; Uba et al., 2006, 2007, 2009).

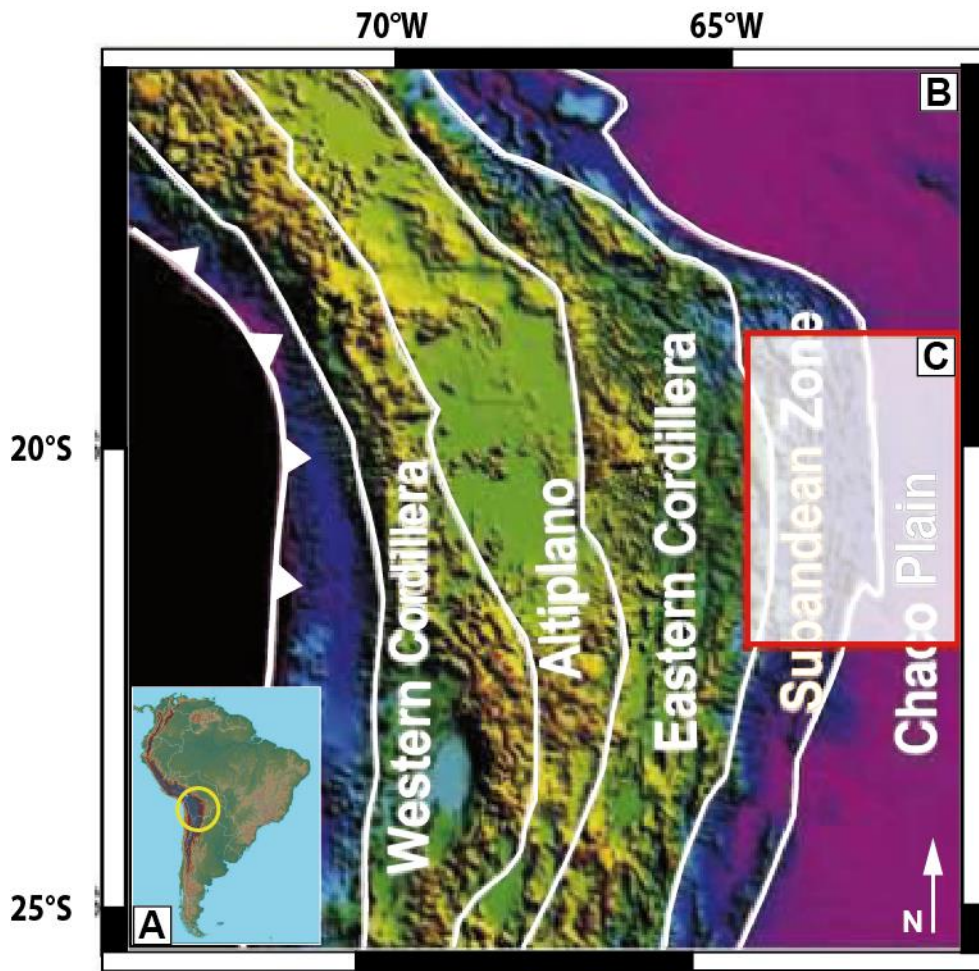


Figure 1. a) Location of Central Andes in South America (yellow line). b) DEM showing tectono-morphic provinces of the Central Andes (after Uba et al., 2009), and c) location of regional map (white rectangle) of the Subandean zone and eastern Chaco plain shown in Figure 2.

Spatial and temporal variations in the >7 km thick Cenozoic depositional record, with expected eastward shifts in facies toward the craton (Horton and DeCelles, 2001; Uba et al., 2009), have been studied from various local perspectives (Marshall et al., 1993; Erikson and Kelley, 1995; Uba et al., 2009). Depositional ages and sediment accumulation rates within the eastern Subandean region have been constrained with mammal biostratigraphy and radiometric ages of interbedded tuff layers (Marshall and

Sempere, 1991; Moretti et al., 1995; Hulka, 2005; Uba et al., 2009). However the central and western Subandean regions have a relatively poorly dated Cenozoic stratigraphy. Attempts to correlate basin-fill deposits have been focused on southernmost Bolivian localities at ~21°S and in northern Argentina (Uba et al., 2009; Echavarria et al., 2003), with little support for more-regional basin-scale correlations and depositional models.

Neogene evolution of the Subandean fold-thrust belt has resulted in shifts in sediment source regions and sedimentation pathways (Uba et al., 2005; 2006, Hulka, 2005; Hulka and Heubeck, 2010). Reconstruction of regional provenance and sediment dispersal patterns may help reconstruct the original structural and tectonomorphic configuration of the foreland basin system at various time frames (e.g., DeCelles et al., 1991). Therefore, changes in efficiency of surface processes, tectonic processes (Main Interandean and Main Subandean thrusts activation), climatic variations (Uba et al., 2007), and/or modifications in catchment areas (Mascole and Zubieta-Rosetti, 2005) in the coupled fold-thrust belt-foreland basin evolution should be recorded in the sedimentary fill.

This study attempts to provide an integrated Eocene-Holocene evolution of the Subandean zone and Chaco foreland basins. Basin subsidence response to slip of main décollements and unroofing patterns of western regions (Interandean and Eastern Cordillera) are further analyzed with a sedimentologic-stratigraphic study coupled with a provenance analysis (U-Pb detrital zircon provenance, conglomerate composition, sandstone petrography and paleocurrent directions) in two sections located in the westernmost Subandes (Bartolo and Emborozú). Depositional ages of the thick (>7 km), mostly non-marine foreland clastic deposits are bracketed with newly dated interbedded tuff horizons. An updated magnetostratigraphy study, with results herein sheds light on changes in accumulation rates observed in the eastern Subandean zone. Finally, the

combination of this study's results and previous surface and subsurface sedimentologic, stratigraphic, thermochronological and geochronological analyses by the authors will elucidate on the potential tectonic, climatic, and erosional effects on the evolution of the Subandes and Chaco foreland basin.

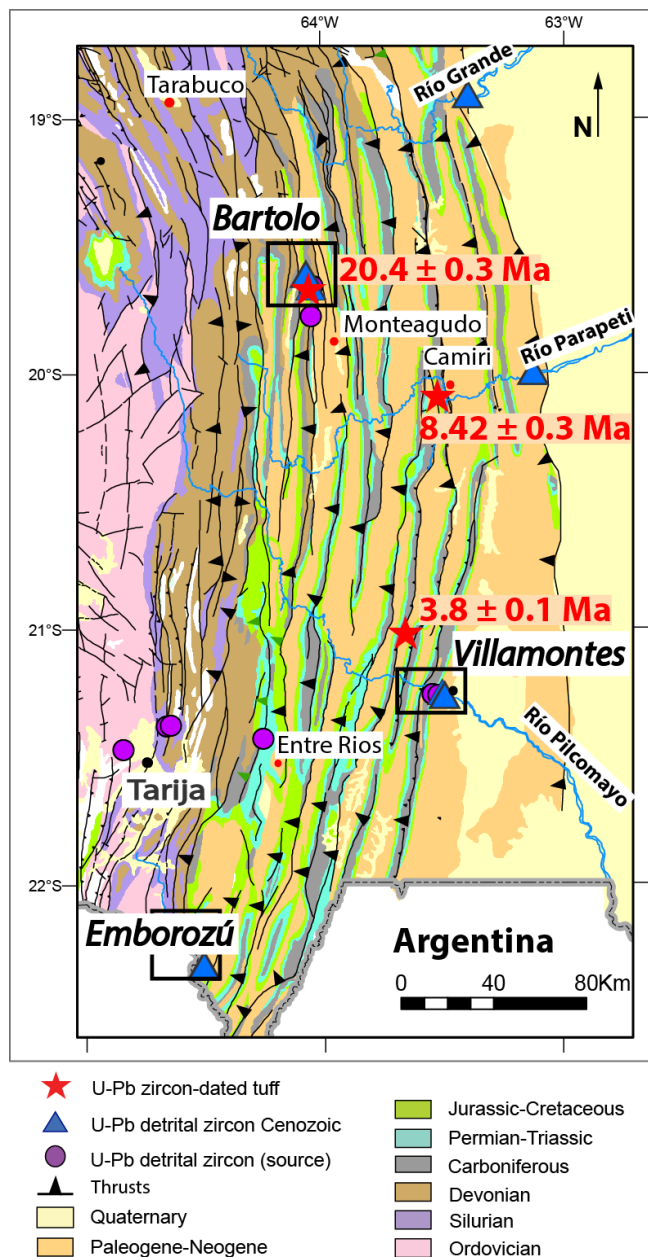


Figure 2.

Figure 2. Generalized geologic map of the (from west to east) Eastern Cordillera (mostly Ordovician exposures), Interandean zone (mostly Devonian outcrops), Subandean zone (Devonian to Paleogene exposures) and westernmost Chaco foreland basin (dominated by Quaternary deposits) in southern Bolivia from SERGEOTECMIN-YPFB (2000). Also showing major fold-thrust structures and location of Cenozoic measured sections (located at Bartolo and Emborozú) in the westernmost Subandes, tuff samples (red stars) with their U-Pb weighted age, Cenozoic samples (blue triangles) for U-Pb detrital zircon provenance and potential source samples of the Cenozoic fill (purple dots). The magnetostratigraphic study was focused at the Villamontes section. Black rectangles highlight the position of local geologic maps (Bartolo, Emborozú and Villamontes).

## GEOLOGICAL SETTING

### *Andes Mountains*

The Andes are formed by east-west shortening related to subduction of the oceanic Nazca plate beneath the continental South American plate during the Cenozoic (Isacks, 1988; Sempere et al., 1990; Gubbels, et al., 1993; Kley et al., 1997; Kley et al., 1999). Eastward propagation of the fold-thrust belt coupled with orogenic loading resulted in tectonic subsidence of eastern cratonic areas and evolution of a retroarc foreland basin (Gubbels et al., 1993; Kennan et al., 1995; Jordan et al., 1997; Horton and DeCelles, 1997). Syndeformational accumulation of mostly non-marine clastic deposits has been recognized in the evolving fold-thrust belt and foreland basin in the Central Andes (Sempere et al., 1990; Lamb et al., 1997; Jordan et al., 1997; Horton and DeCelles, 1997, 2001; Echavarria, et al., 2003; Horton, 2005; Uba et al., 2005, 2009)

### *Central Andes*

The Central Andes are formed by the following tectonomorphic units from west to east: the Peru-Chile trench, Coastal Cordillera, Longitudinal Valley, Precordillera, Western Cordillera, Altiplano, Eastern Cordillera, Interandean zone, Subandean zone and Chaco foreland basin (Figure 1, Horton et al., 2001; Beck and Zandt, 2002). The Coastal Cordillera and Precordillera are remnants of Mesozoic and Paleogene magmatic arcs, respectively. The modern forearc (Longitudinal Valley) is located between these former arc systems. Eastward, the Altiplano plateau is characterized by its anomalous crustal thickness (~65-70 km) (Zandt et al., 1996) between the Western Cordillera, the modern magmatic arc, and the Eastern Cordillera. The Interandean and Subandean thin-skinned fold thrust belts mark the leading edge of the Andes and control the configuration of the modern Chaco foreland basin (Gubbels et al., 1993; Dunn et al., 1995; Lamb et al., 1997;

and references therein). The study area is focused in the eastern segment of the fold-thrust belt: the Subandean zone and Chaco foreland basin.

### ***Topography***

In southern Bolivia, the Eastern Cordillera (3000 m average elevation) is composed by east- and west- verging thick-skinned thrust systems. The main structural feature in the east is the Sama-Yunchará anticlinorium (SYA), where mostly Ordovician rocks are exposed from 19.5°-21.5°S but Cambrian and Precambrian rocks are dominant farther south. Farther east, the Interandean zone (2000-3000 m elevation) as defined by Kley (1993, 1996), is a narrow, thin-skinned fold-thrust system developed in Silurian-Triassic strata on top of basement structures. South of 22°S, the Interandean-Eastern Cordillera boundary is obscured by widely distributed Neo-Proterozoic-Cambrian strata. The Interandean east-west extension is better developed in southern Bolivia, with a clear narrowing northward to the orocline at ~17.5°S (Kley, 1999). Lower Ordovician shales are interpreted as the main detachment level in both the Eastern Cordillera and Interandean zone.

Furthermore, the 2000-2500 m-high Subandean zone, an east vergent- thin-skinned fold thrust system, has its main décollements levels in the lower Silurian and middle Devonian shales (Baby et al., 1992; Brusset et al., 2002). The deeper structure (Silurian to Lower Devonian) is dominated by fault-bend folds, whereas tight-fault-propagation folds constitute most of the shallow structure (McQuarrie, 2002; Baby et al., 1992). Devonian to Quaternary strata are exposed in anticlines and monoclines of this zone (Figure 2). Lastly, the Chaco plain, which occupies eastern areas with elevations <300 m, is the locus of Neogene-modern wedge-top, foredeep, forebulge and backbulge

deposition in the Central Andes. It continues eastward to the Precambrian Shield in eastern Bolivia, Paraguay and westernmost Brazil (Horton and DeCelles, 1997).

Besides the structural configuration, a topographic elevation characterizes each zone individually. Kley (1999) and McQuarrie (2002) pointed out a relationship of elevation to blind basement structures (footwall and hanging-wall ramps) in both the Eastern Cordillera and Interandean zone. Slip on these large-scale features, called megathrusts, was accommodated in the Eastern Cordillera, Interandean and Subandean zone. Two main décollements, the Main Interandean thrust and Main Subandean thrust (Kley, 1996; McQuarrie, 2002), have been identified and will be discussed in this study.

### ***Mountain building and uplift***

The timing of central Andean mountain building at 18-22°S has been constrained largely by exhumation-induced cooling of upper-crustal rocks. Many studies assume that exhumation is linked with deformation, which generates relief to be eroded (Barnes et al., 2008, 2012; Ege et al., 2007). In addition, dated erosional surfaces (San Juan del Oro surface), low-temperature thermochronometry (e.g., apatite fission track) (Brusset et al., 2002; Ege et al., 2007; Barnes et al., 2008), cross-cutting structural relationships, and the stratigraphic-sedimentologic record of foreland basins (Sempere et al., 1990; Horton, 1998, 2005; Horton et al., 2001; Uba et al., 2005, 2009) have been used to constrain the evolution of the Andean orogenic wedge.

According to an integration of various methods, exhumation in the Eastern Cordillera migrated eastward from the westernmost Andes (Chilean Precordillera and Western Cordillera) in the middle Eocene to early Miocene (~45-20 Ma) (Muller et al., 2002; Ege et al., 2007; Barnes et al., 2008). Two main phases of exhumation have been identified: (1) late Eocene-Oligocene (40-30 Ma) and (2) middle Miocene to present

(roughly 15 to 0 Ma) (e.g., Barnes et al., 2006; Norabuena, et al., 1998). Exhumation propagated eastward and westward of the Eastern Cordillera resulting in east-verging and west verging large structures; following these events a period of quiescence occurred, marked by the San Juan del Oro surface (~12-8 Ma) (Gubbels et al., 1993; Kennan et al., 1995). Afterwards, exhumation shifted to the Interandean zone, from ~20 to 5 Ma (early to late Miocene) and apparently propagated into the Subandean zone after the early-middle Miocene, although this remains debated (e.g., Sempere et al., 1990; Erikson and Kelley, 1995; Kley, 1996; Brusset et al., 2002; this study).

### ***Shortening***

In terms of shortening, Oncken et al. (2006) reviewed numerous published balanced cross-sections and proposed the following values for 20-22°S. Contraction in the Eastern Cordillera and Interandean zone reached shortening values around 110 km, compared with 55-110 km of shortening in the Subandean zone. In Bolivia, Eocene to present deformation recorded the highest shortening in the Central Andes with values on the range of 250-275 km.

### ***Subandean foreland basin***

Preserved Cenozoic successions in the western Subandean zone (17°-22°S) record the eastward advance of the deformation front from the Eastern Cordillera-Interandean to the Subandean zone. Two localities in the westernmost Subandes (Bartolo and Emborozú; Figure 2) were chosen to portray and decipher the sedimentologic-stratigraphic response in the evolving retroarc foreland basin from the late Oligocene to present. Chronostratigraphic constraints (new ages for interlayered tuffs) shed light on the initiation of deformation in the Subandes, and support a proposed Neogene history of the basin evolution. In addition, an eastern section located in Angosto del Pilcomayo

(measured by Uba et al., 2005) reinforces the assessment of the depositional history, accumulation rates, age, and provenance of the Subandean Cenozoic fill.

In the northern section, at Bartolo ( $19.66^{\circ}\text{S}$ ,  $64.04^{\circ}\text{W}$ ), probable upper Oligocene-lower Miocene clastic rocks are exposed on the main road between the towns of Monteagudo and Padilla (Figure 3a). Cenozoic nonmarine strata overlying Mesozoic eolian units were analyzed within the Yanguilo thrust hanging-wall up to the Río Azero thrust fault. At Bartolo, the Yanguilo thrust defines a moderately steep ( $50^{\circ}\text{W}$ -dipping) monocline involving Devonian to Neogene rocks, that roots into a Middle Devonian detachment; no clear growth strata relationships have been recognized. Modeling of thermochronometer results shows activity on this thrust prior to 16 Ma (Barnes et al., 2008). To the west, a tight, east-vergent, out-of sequence fault-propagation anticline developed in the Rio Azero thrust sheet, which juxtaposes Middle Devonian rocks (Huamampampa Formation) on top of Miocene footwall strata (Salinas, 1981). The age of the lower section is constrained by an interbedded tuff, which although discovered previously (Erikson and Kelley, 1995), has been more accurately dated with new methods discussed in this study.

Farther south, the Emborozú section was measured near the villages of Emborozú and El Limal ( $22.33^{\circ}\text{S}$ ,  $64.50^{\circ}\text{W}$ ), along the Tarija-Bermejo highway (Figure 3b). The city of Bermejo is 65 km south of the measured section. A thick (>4 km) succession of steeply tilted ( $80^{\circ}\text{W}$ ) Cenozoic strata lies on top of Cretaceous eolian strata in the core of an open syncline whose limbs are affected by thrusts. To the west, a series of thrust sheets carrying thick Neoproterozoic to Devonian strata comprise the Interandean zone and easternmost part of the Eastern Cordillera. Motion of the Padcaya dextral-strike slip fault may have been coeval with an antecedent river (following the drainage of the Rosillas-Camacho rivers) that transported the coarsest facies at this latitude. Field

observations do not document unconformities related with coeval thrust activity, which matches reports of similar exposures in northernmost Argentina (Echavarria et al., 2003). Several interbedded tuffs record continuous sediment accumulation from the middle to late Miocene (Hulka, 2005; Uba et al., 2009).

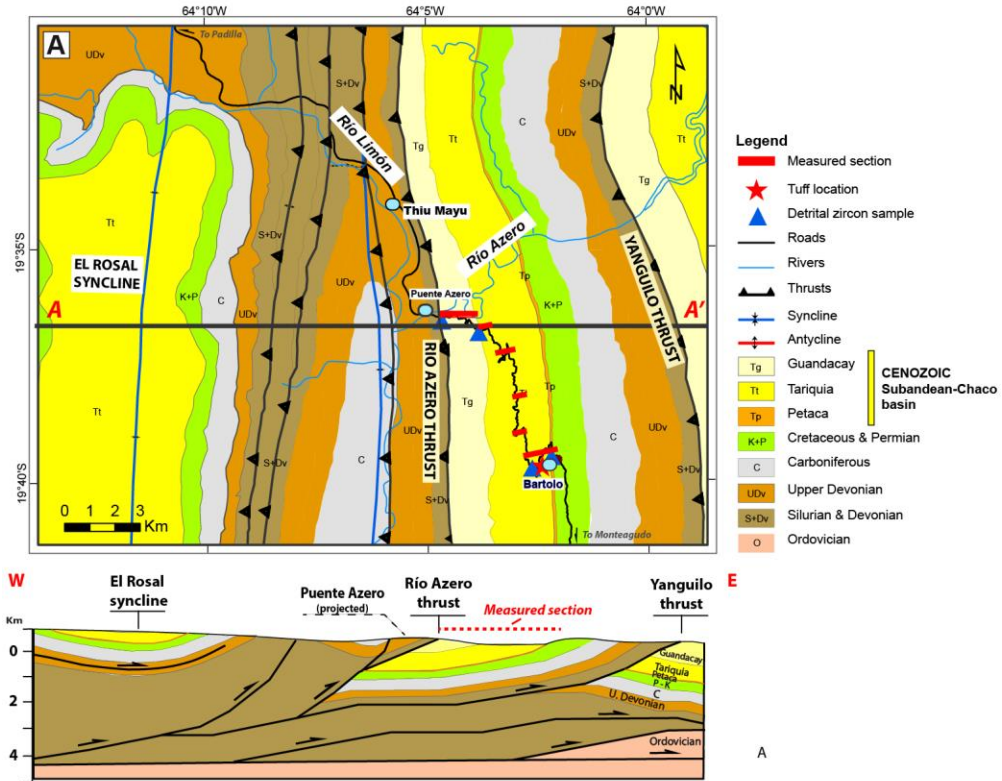


Figure 3. Geologic maps and cross sections for: a) Bartolo (after Salinas, 1981; Giraudo and Limachi, 2001), and b) Emborozú (after Kley, 1993, and YPFB). At Bartolo, Cenozoic strata were analyzed from the Yanguilo thrust hanging-wall up to the Río Azero thrust fault. Post-Yanguilo activity of the Río Azero fault limit Cenozoic exposures. At Emborozú, deposits were measured close to an open syncline, with no observed unconformities related to coeval thrust activity.

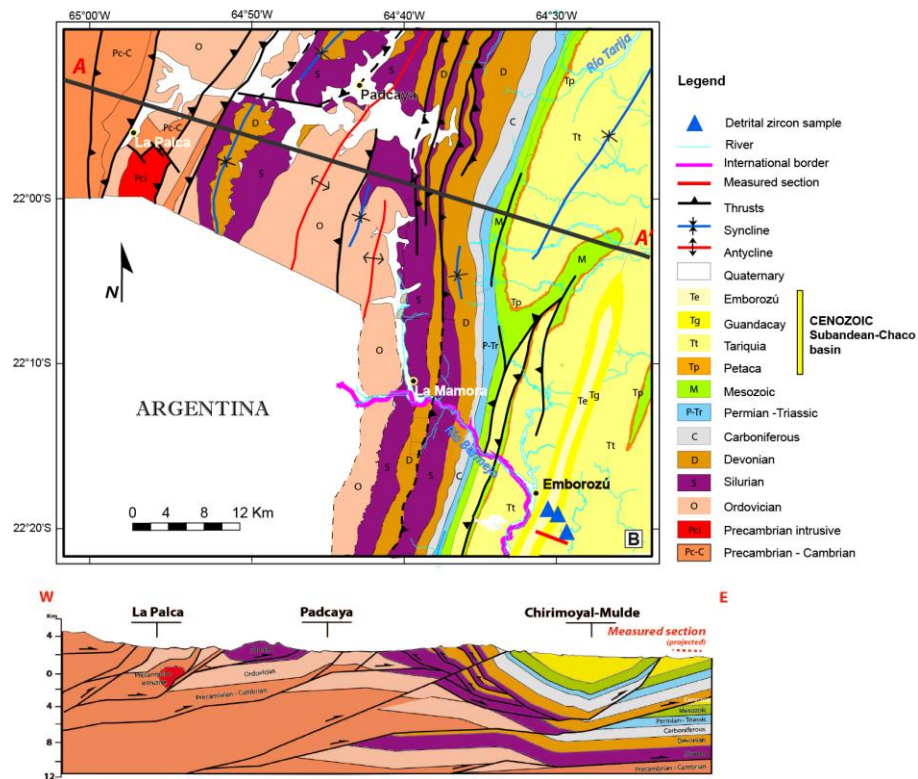


Figure 3, cont.

## **REGIONAL STRATIGRAPHIC FRAMEWORK**

Broadly, the rock record in southern Bolivia can be divided in the following tectonostratigraphic packages (Sempere, 1995; Jaillard et al., 2000; Suarez-Soruco, 2000) Neoproterozoic-lower Paleozoic igneous metasedimentary rocks (Cambrian), Paleozoic terrigenous marine sedimentary rocks (Upper Cambrian to Permian), Triassic – Cretaceous synrift and postrift deposits, and Cenozoic foreland basin deposits. Accordingly, the proposed stratigraphic division will also serve as the baseline to distinguish the various source areas from the detrital zircon U-Pb age populations obtained from the Cenozoic foreland basin fill.

Andean crystalline basement is composed of Neoproterozoic-lower Paleozoic (700-485 Ma) rocks representing the Pampean/Tilcarian (700-520 Ma) and Famatinian (500-465 Ma) orogenies. The San Cristóbal/Puncoviscana Formation (Neoproterozoic-Lower Cambrian) marks the onset of deposition in a still debatable forearc basin (Escayola et al., 2011). A thick succession of metasedimentary strata was derived from an eastern source area and records syntectonic activity with the emplacement of the Cañani/Condado, Rejará, and other granitoid intrusions (530-520 Ma; Adams et al., 2011) associated with the Tilcarian orogeny.

An unconformably overlying succession of thick (>4 km) continental to deep shelf Cambrian-Ordovician strata represents a transgressive record of the expansion of the Paleozoic basin (Egenhoff, 2007). Two main Ordovician events are recognized: volcanic-sedimentary rocks corresponding to the Famatinian arc (Early Ordovician) and subsequent Late Ordovician Ocloyic compression (~476-434 Ma; Bahlburg and Hervé, 1997; Loewy et al., 2004), both of which are better represented in NW Argentina (Suarez Soruco, 2000; Egenhoff, 2007). Continuous deposition of a roughly 4 km-thick succession with progradational cycles in an arguable foreland basin characterizes the

Silurian-Devonian record. The Carboniferous section (>2.5 km thick) recorded mixed continental-marine deposits in an intracratonic basin related to Gondwana glaciation (Starck and Del Papa, 2006). Finally, Late Carboniferous-Early Permian (320-290 Ma) denotes a discrete low-grade metamorphic event ascribed to the Hercynian orogeny (Jacobshagen et al., 2002), followed by deposition of >300 m of mixed marine-continental strata (fluvio-eolian and supratidal carbonate shelf rocks) in a higher aridity/warming climate of the Late Carboniferous and Permian (Sempere, 1995; Starck and Del Papa, 2006).

In southern Bolivia, rifting of Pangea commenced in Early-Middle Triassic time (Oller and Sempere, 1990). Fluvio-lacustrine red beds, evaporites and fluvio-eolian sandstones (~300 m thick) were deposited in restricted troughs related to initial rifting (Sempere, 1995). Accompanying alkaline and tholeiitic basalt flows, emplaced in transtensional and transpressional settings are widespread in the Eastern Cordillera and Subandean zone. In contrast, the late Triassic to mid-Cretaceous onlap of fluvial and eolian deposits (~1000 m thick) reveal a post-rift stage of sedimentation following cessation of intracontinental extension (Oller and Sempere, 1990; Lopez-Pugliessi, 1995).

Andean compression marks the Cenozoic evolution of the region, with coupled development of an adjacent retroarc foreland basin to the east (Sempere, 1990; Gubbels et al., 1993; Lamb et al., 1997; Horton and DeCelles, 1997) that recorded principally nonmarine deposition of up to 7 km of upward coarsening and thickening clastic strata. Coeval with cratonward (eastward) advance of shortening, Neogene changes in lithofacies and sedimentation rates in the foreland basin system have been interpreted to reflect deposition in several adjacent depozones (i.e., backbulge, forebulge, foredeep, wedge-top; DeCelles and Giles, 1996; Uba et al., 2005; Hulka and Heubeck, 2010).

## CHAPTER 2. SEDIMENTOLOGY AND STRATIGRAPHY

### CENOZOIC STRATIGRAPHY

In the Subandean zone and Chaco foreland basin, eolian Mesozoic facies are overlain by a >7 km-thick Cenozoic succession of mostly nonmarine siliciclastic deposits. The Oligocene to Quaternary sedimentary package recorded the deposition of five major lithostratigraphic units (Figure 4): from bottom to top, these are Petaca, Yecua, Tariquia, Guandacay and Emborozú formations (Marshall and Sempere, 1991; Gubbels et al., 1993; Jordan, et al., 1997, Kley et al., 1997, Uba et al., 2005, 2009).

The regional areal distribution of these Cenozoic units within the Chaco plain and Subandean foothills (Uba et al., 2006; YPFB data) depicts a westward pinchout of the oldest unit (Petaca Formation) toward the Andean hinterland. In contrast, younger units show maximum thicknesses in the westernmost Chaco plain, attributable to accumulation within the foredeep depozone. The thick foredeep deposits show a pattern of eastward thinning, possibly linked to a forebulge depozone coinciding with an eastward basement high distribution (Alto del Izozog), and westward thinning toward the western Subandean zone, which may be the product of selective erosion of proximal synorogenic strata (e.g. Simpson, 2006).

In the following text, the key characteristics of the different units are briefly outlined:

#### ***Petaca Formation***

The up to 250 m-thick Petaca Formation has a Deseadan to Chasican age according to mammal biostratigraphy (Sempere et al., 1990; Marshall and Sempere, 1991; Marshall et al., 1993). It is composed predominantly of sandstone and conglomerate deposited in braided fluvial systems (Uba et al., 2005). Most of the deposits

appear to be diagenetically altered to paleosols, with many clasts formed by pedogenic calcareous nodules and concretions of the underlying Mesozoic eolian sandstones. Deposition of the Petaca Formation has been attributed to accumulation in the most distal, back-bulge region of an incipient foreland basin. Therefore, this unit marks the late Oligocene to middle Miocene eastern edge of an evolving foreland basin linked to shortening and crustal loading in the Eastern Cordillera (Horton and DeCelles, 1997; DeCelles and Horton, 2003; Uba et al., 2005).

### ***Yecua Formation***

According to previous studies, the Yecua Formation represents several short-lived marine incursions during the middle to late Miocene (12.4-8 Ma; Marshall et al., 1993; Hulka et al., 2006; Hernandez et al., 2005; Uba et al., 2007). This unit is up to 500 m-thick and comprises an intercalation of mudstone, marl, sandstone and limestone stacked in 1-8 m thick, rhythmic packages. The deposits contain foraminifera, bivalves, ostracods, and gastropods as well as ichnofossils. This unit is restricted to the eastern margin of the Subandean zone and adjacent Chaco foreland basin.

### ***Tariquia Formation***

In the western Subandean zone, the thick (~4500 m) Miocene Tariquia Formation directly overlies the Petaca Formation, without a record of an intervening Yecua unit. A ~22- 6 Ma depositional age for the Tariquia Formation is constrained by interbedded tuffs (Uba et al., 2005, 2009; this study). Tariquia facies consist predominantly of sandstone and mudstone deposited in a mixed fluvial system containing a variety of anastomosing, braided and meandering channels, probably associated with the distal portions of fluvial-dominated megafans (Uba et al., 2005). The temporal and spatial

distribution of the Tariquia Formation suggests that it represents Miocene accumulation in the foredeep depozone.

### ***Guandacay Formation***

Capping the Tariquia Formation is the 1500 m-thick upward-coarsening, conglomeratic Guandacay Formation of late Miocene-early Pliocene age (~6-2 Ma) (Moretti et al., 1996; Uba et al., 2005). This unit is the product of braided fluvial systems that deposited coarse sediments in the medial portions of a fluvial-dominated megafan (Uba et al., 2005, 2006). Growth strata within this unit have been recognized in seismic reflection lines of the easternmost Subandean zone, revealing synorogenic deposition in a wedge-top depozone of the proximal foreland basin (Moretti et al., 1996; Horton and DeCelles, 1997; Uba et al., 2009).

### ***Emborozú Formation***

Unconformable deposition of the Pliocene-Quaternary Emborozú Formation upon the Guandacay Formation is observed in exposures of the southwestern Subandean zone and at the Rio Grande river mouth, as well as interpreted in subsurface data from the Chaco foreland basin (Ayaviri, 1971; Dunn et al., 1995; Moretti et al., 1996; Echavarria et al., 2003; Uba et al., 2005; Barnes and Heins, 2009). This unit tapers eastward from ~1500 m in the modern foredeep depozone to a few tens of meters close to the modern forebulge. Sediment gravity and braided fluvial processes deposited pebble-cobble conglomerate and interbedded sandstone and thin mudstone in proximal portions of the fluvial-dominated megafan and alluvial fan settings (Uba et al., 2005; this study).

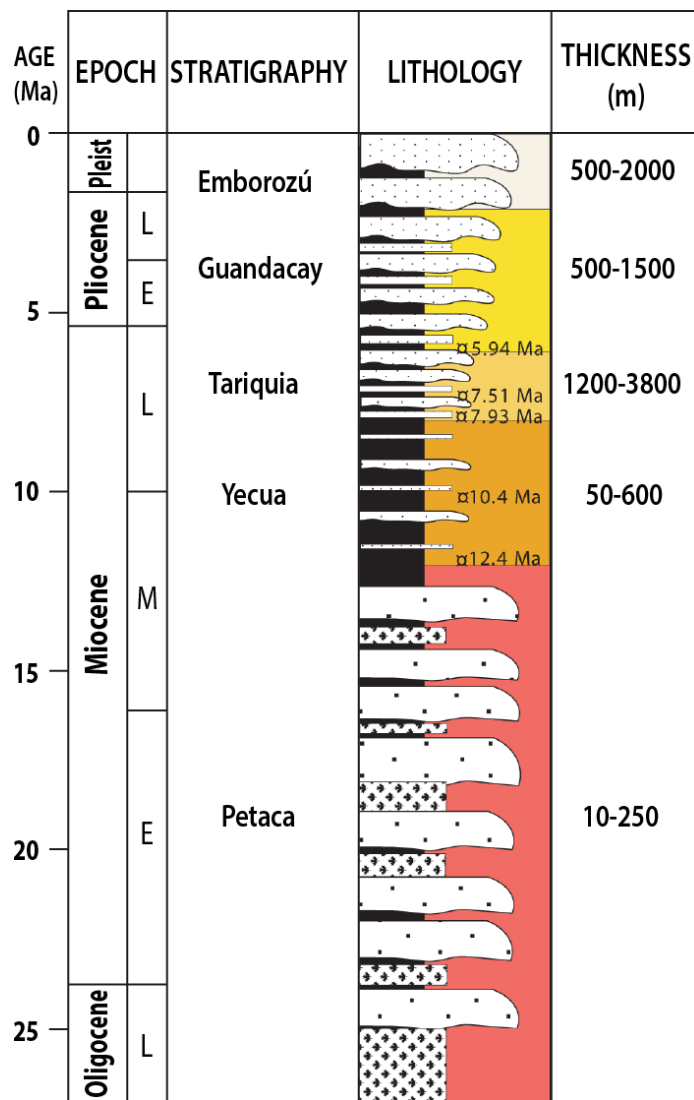


Figure 4. Generalized lithostratigraphic column of Cenozoic fill in the Subandean zone and Chaco foreland basin. Lithofacies variations are observed from the basal Petaca (Oligocene-lower Miocene) to Emborozú (Plio-Pleistocene) formations. An upward coarsening trend is coupled with higher accumulation rates.

## **SEDIMENTOLOGY AND DEPOSITIONAL SYSTEMS**

Cenozoic basin fill was described, measured, and sampled in two locations within the western Subandean zone: the northern (Bartolo) and southern (Emborozú) localities. Detailed facies descriptions and interpretations are presented below.

### ***Bartolo locality***

The Cenozoic succession at Bartolo (Figure 5a) exceeds 2.6 km in thickness and comprises a semi-continuous succession from the Upper Oligocene-Miocene Petaca Formation to the Miocene Guandacay Formation. Data collected from this section include a total of 19 paleocurrent measurement stations (from clast imbrications, flute marks, ripples and channel axis), 16 stations of conglomerate counts and 19 sandstone petrology samples. A tuff sample for U-Pb geochronology was collected along with four detrital zircon sandstone samples for U-Pb provenance analyses.

### ***Emborozú locality***

At the Emborozú locality, the exposed Cenozoic stratigraphic section exceeds 2.9 km in thickness (Figure 5b) and spans the middle Miocene Tariquia to upper Pliocene-lower Pleistocene Emborozú formations. To constrain sediment provenance, paleocurrent measurements were collected at 18 stations from mainly clast imbrication and trough cross-strata, and three samples were collected for detrital zircon U-Pb age analyses.

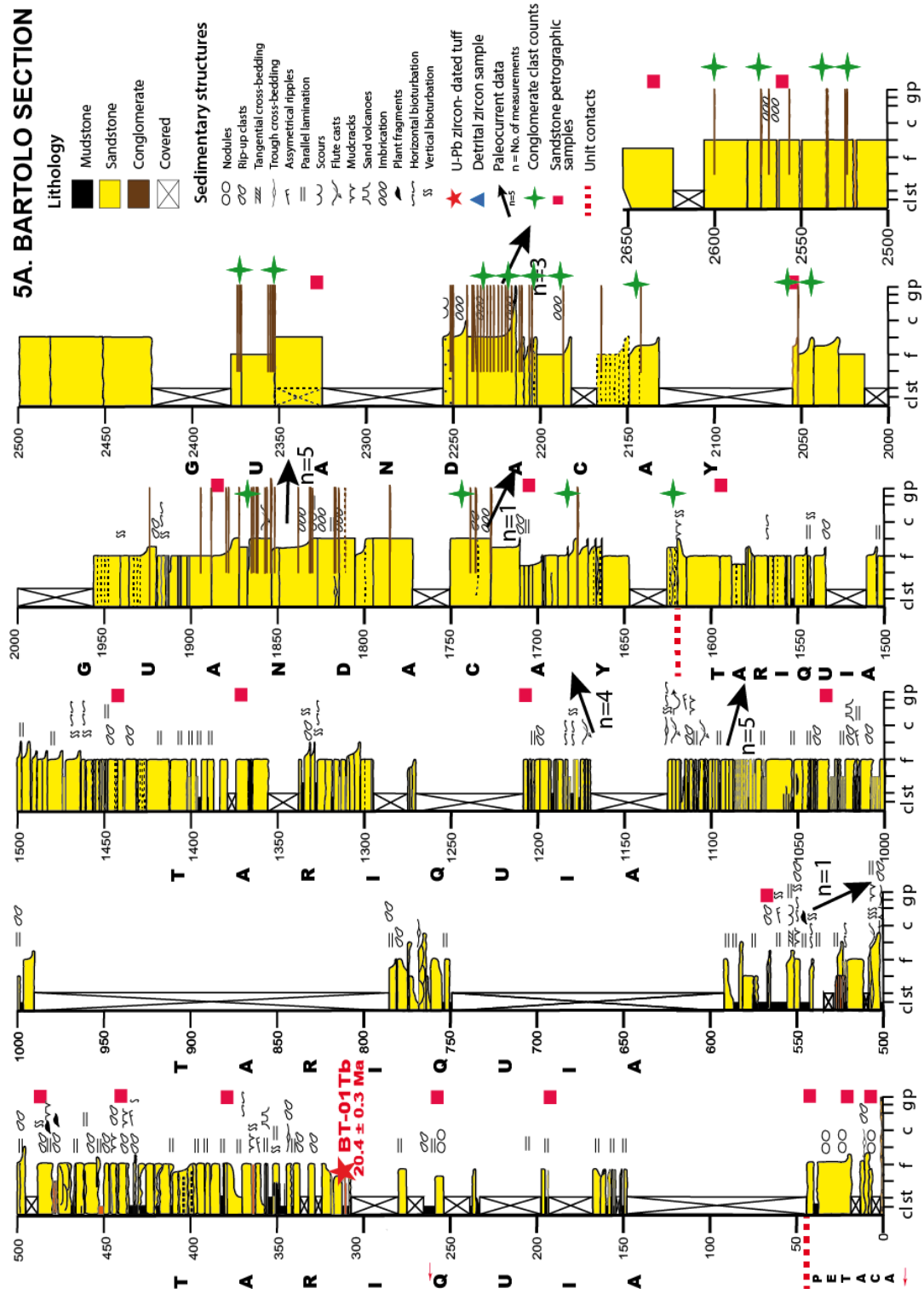


Figure 5.

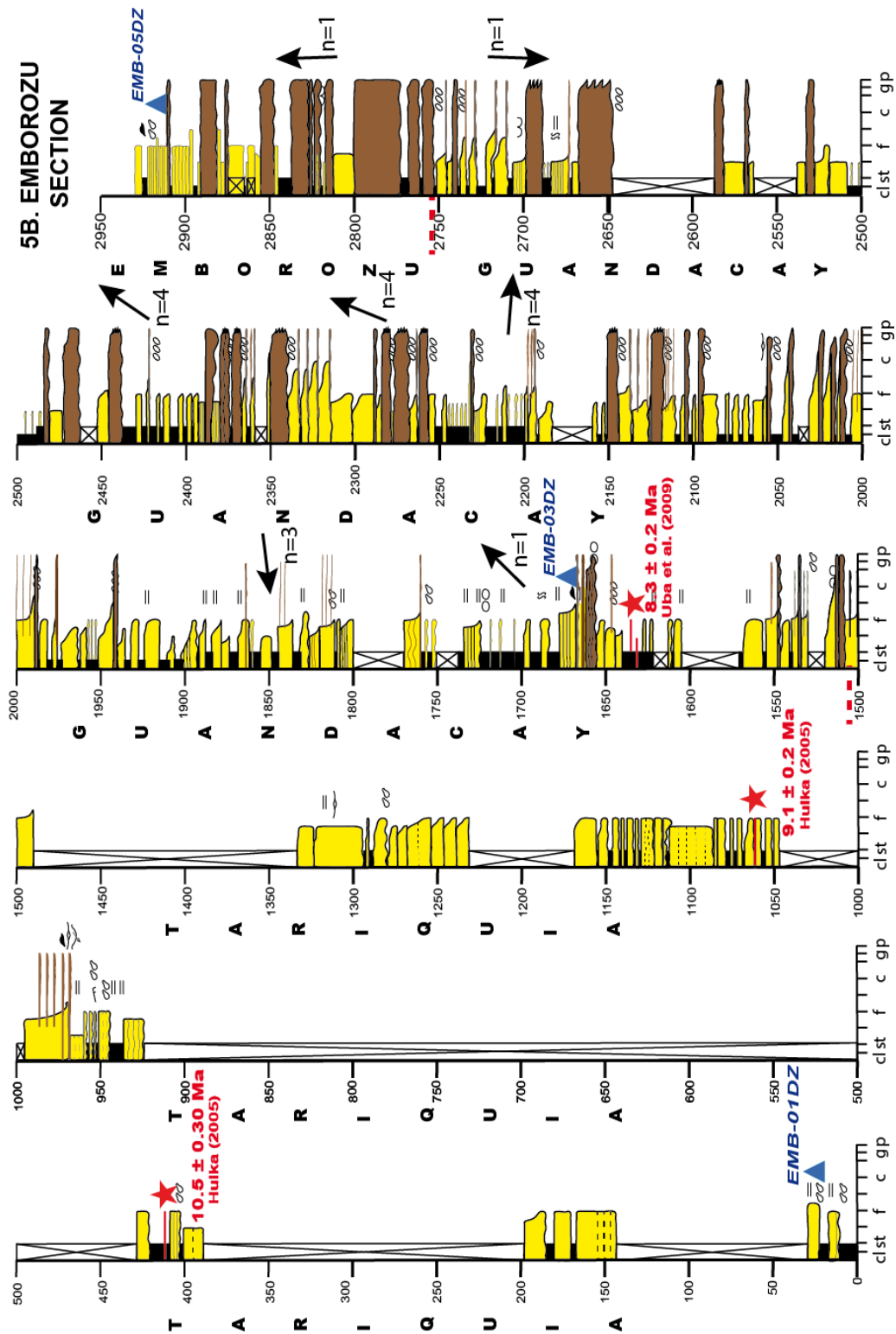


Figure 5.

Figure 5. Measured stratigraphic section of the a) Bartolo and b) Emborozú stratigraphic sections displaying lithostratigraphic units (Petaca, Tariquia, Guandacay and Emborozú formations), sedimentary structures, paleocurrent directions, conglomerate clast composition stations, and sample locations for sandstone petrography, detrital zircon and newly and previously dated volcanic tuffs (U-Pb age in brackets).

## FACIES ASSOCIATIONS

At both localities, the sections were measured using a 1.5 m Jacob staff. At Bartolo, bed sets were measured at an approximate 1:100 scale within the Petaca-Tariquia interval and a 1:500 scale within the massive Guandacay Formation. At Emborozú, the entire section was measured at an approximate 1:1000 scale. Field observations of the Cenozoic succession define four lithostratigraphic units (Petaca, Tariquia, Guandacay and Emborozú); due to its restricted position in the distal foredeep, facies of the Yecua lithostratigraphic unit are not recognized in the western Subandean zone. A total of ten facies associations (Table 2) have been interpreted according to field sedimentological descriptions in both sections, and are interpreted to have been deposited by anastomosing, mixed meandering-braided, and exclusive braided fluvial systems, all active in a megafan setting comparable to the setting which characterizes the modern foreland basin (Horton and DeCelles, 2001; Uba et al., 2005). Sets of lithofacies categories were defined after Miall (1996), Uba et al. (2005) and Sinks (2011) on the basis of sedimentary structures, lithology, and degree of pedogenesis. Overall, the individual lithofacies (described in Table 1) have been used as framework elements to define the broader facies associations (Table 2).

Table 1. Lithofacies for the Petaca, Tariquia, Guandacay, and Emborozú formations  
 (after Miall, 1996; Uba et al., 2005 and Siks, 2011)

Code	Description	Thickness	Interpretation
<b>Ps</b>	Silcrete, strongly developed with chert nodules, massive, no original sedimentary structures, chalcedony cement	0.5 to 2 m	Mature paleosol
<b>Pc</b>	Calcrete, well-developed with calcareous nodules, massive, poor sorted and spar-filled tubules	1-2 m	Mature paleosol
<b>Pcm</b>	Calcrete, moderately-developed with calcareous patches, massive, structureless, fair-poor sorted, very fine to medium grained with floating granules of chert and quartz. Irregular bedding contacts	0.2-2 m	Moderately-developed paleosoil
<b>C</b>	Dark gray, brown carbonaceous mudstones, lignite fragments, chips	0.1-0.3 m	Vegetated swamp deposits
<b>Fl</b>	Finely laminated dark red, dark brown claystones, siltstones. Sharp planar basal contacts. Scattered chips of organic material, occasional ripples	0.003-3 m	Floodbasin deposits, overbank deposits, abandoned channel
<b>Fm</b>	Red, massive mudstones (siltstones-claystones)	1 m	Overbank deposits
<b>Fb</b>	Bioturbated, red claystones	0.5- 1 m	Overbank deposits
<b>Fbt</b>	Bioturbated, very thin-thinly bedded, very fine-grained sandstone, siltstone, with calcareous nodules, and occasional reduction spots	0.5-1 m	Levee, moderate paleosol
<b>Shl</b>	Horizontally, thinly-bedded sandstone. Very fine-fine grained, fair-sorted, subangular-subrounded. Sharp contacts and occasionally syndeformational structures, scattered chips of organic material	5-10 cm	Plane-bed flow
<b>Sh</b>	Horizontally-bedded sandstone. Fair sorted, fine grained, subangular sandstone. Sharp erosional basal contacts containing intraformational red clay rip-up clasts	0.6-7 m	Migration of 2D dunes, in channels
<b>Sl</b>	Planar, medium-bedded sandstone. Fine grained, fair-poor sorted, subangular, very fine sand matrix, weakly calcareous, occasional ripples	0.1-0.3 m	Overbank deposits (crevasse splays)
<b>Sp</b>	Low-angle, tabular cross-bedded sandstone. Coarse to medium-grained, well-sorted, rounded, base-only normal grading. Erosive basal contact	0.2-1 m	Transverse and linguoid bedforms (migration of 2D dunes in channels)
<b>Smd</b>	Trough-cross bedded, channel-like, medium-bedded sandstone. Fine-grained, well-sorted, subrounded-rounded. Vertical and horizontal burrows, desiccation marks	0.08-0.15 m	Sinuous-crested and linguoid dunes (Migration of 3D dunes in flashy events)

Table 1 (continued)

<b>St</b>	Very limited trough cross-bedded sandstone. Lenticular-shaped, fair-well sorted, very fine-fine grained, subangular sandstone. Highly erosive basal contacts with frequently red clay rip-up clasts. Scattered desiccation marks on the top and bioturbation	0.10-2.5 m	Dune migration, lower flow regime, abandoned channel
<b>Ss</b>	Lenticular, medium-bedded sandstone. Fine-grained, poor-fair sorted, red clay matrix; broad, shallow scours	0.01- 0.5 m	Scour fill
<b>Sm</b>	Structureless sandstone. Wavy, non-parallel bedded, fine-medium-grained, fair-poor sorted, subangular-subrounded, scattered-subrounded chert, rose and white, quartz floating granules, and altered feldspars, occasionally mica chips (muscovite); slightly calcareous	0.2-5 m	Longitudinal bar
<b>Gh</b>	Low-angle, tabular cross-bedded, channel-like, pebble-cobble conglomerate. Subrounded clasts, medium grained sandstone - matrix supported, (maximum clast size 30 cm), weak imbrication of clasts and scattered red clay rip-up clasts, normal grading; barely calcareous cement. Erosive basal contact	0.05-3 m	Longitudinal bedforms, lag deposits
<b>Gt</b>	Trough cross-bedded, granule-cobble conglomerate. Normal grading, clast-supported, with clast imbrication	0.5-3 m	Channel fill

## A1. Paleosols

In the Bartolo section, the lowermost deposits are dominated by paleosols of the Petaca Formation. The 2 m-thick basal silcrete deposits are overlain by up to 35 m of calcareous paleosols and isolated calcretes. The basal silcrete displays a pseudo-pebble conglomerate appearance, with highly indurated dark gray, dark brown, subangular-angular chert nodules surrounded by a fine-grained sandstone matrix. In places, some larger nodules have a clear central core of well-sorted, medium-grained eolian sandstone of the subjacent Cretaceous section. Chalcedony and iron oxide minerals are the main cements in this level. The overlying interval of calcareous paleosols and calcretes contain abundant calcareous nodules displaying irregular morphologies ranging from moderately elongate (even vertical rhizocretions: 2-3 cm wide, 20-50 cm long, Figure 6a) to semi-

spherical forms within a matrix composed of medium-grained, reddish brown granule sandstone. The nodules are easily distinguished from the matrix because of their light green and gray mottled pattern (Figure 6a). Throughout the Petaca Formation, the more developed paleosols are located near upper bedding contacts. In selected localized areas, the basal Petaca section lacks such pervasive paleosol deposits and maintains some original depositional structures such as irregular erosive contacts, tabular cross-stratification, or mudstone rip-up clasts.

### **Interpretation**

Evidence of siliceous and calcareous nodules reveals the action of post-depositional physical and chemical processes within a distal braided fluvial system. Illuviation and precipitation of SiO<sub>2</sub> and CaCO<sub>3</sub> leading to diagenetic chert and calcareous nodule formation, along with destruction of all original sedimentary texture and fabric point to pedogenic activity (Stow, 2012). In situ alteration of silica-rich materials, such as those from the underlying Cretaceous eolian succession, would promote silica precipitation close to the water table in a relatively high pH setting. This process likely explains the development of the siliceous paleosols and silcretes of the basal Petaca Formation (e.g. Thiry and Maréchal, 2001; Nash et al., 2004; Blanco et al., 2008). In contrast, the overlying main body of the Petaca Formation exhibits a characteristically paler color and more poorly sorted and coarser-grained texture, along with the moderate to abundant presence of calcareous nodules within a section dominated by braided-fluvial channel sandstones. These deposits affected by pedogenesis are considered the result of calcite precipitation from groundwater leaching, and therefore interpreted as a calcrete subsoil or fossil horizon B. Additionally; these paleosols are commonly diagnostic of high rates of evaporation typical of a semi-arid to arid climate (Tucker, 2003; Stow, 2005).

**Table 2. Facies associations and depositional systems for the Petaca, Tariquia, Guandacay and lower Emborozú formations after Miall (1996); Ubá et al., (2005); and Siks (2011)**

Code	Facies associations	Lithofacies	Description	Interval thickness	Stratigraphic occurrence	Interpretation
A1	Paleosol	Ps, Pcm, Sm	Massive, fine to medium grained-sandstones, poor-fair sorted, calcareous nodules, floating structures. Upward, associated with SI facies association	≤ 10 m	Petaca	Pedogenesis
A2	Mudstone	Fm, Fbt, Fl, Fb, C	Structureless, laminated, thin-bedded very fine-grained sandy siltstone, mudstones; pedogenically altered. Alternated with S2 and S3 facies associations	0.8 - 12 m	Petaca, Tariquia, Guandacay (Bartolo), Tariquia, Guandacay and Emborozú (Emborozú)	Overbank and suspended fluvial facies (braided) with pedogenic structures
A3	Finely interbedded mudstones and sandstones	Fl, Shl	Finely-laminated, very-thin, thin interbedded muds and fine sandstones. Rhythmic alternation of 8-15 cm, respectively.	≤ 2 m	Tariquia (Bartolo)	Abandoned (meandering) channel plug
A4	Structureless, thick-bedded sandstone	Sm, Pcm, Geo, Gh	Structureless, wavy-discontinuous non-parallel sandstone, fine-medium-grained, fair-poor sorted, subangular-subrounded, scattered subrounded chert, rose and white quartz, floating subangular-angular granules, slightly calcareous. It includes a 5-10 cm veneer/lenses of conglomerate lags	1.5 m	Petaca, Guandacay (Bartolo)	Braided fluvial channel
A5	Thick-bedded sandstone	Sh, Sp, Fbt	Horizontally-bedded sandstone, fair sorted, fine grained, subangular sandstone. Sharp erosive basal, and top contacts; normally graded upward to Fl, and interbedded SS facies associations	0.6 - 10 m	Tariquia (Bartolo and Emborozú)	Anastomosing fluvial channel
A6	Interbedded lenticular sandstone and mudstone	Sm, Sl, Fl, Fbt	Tabular bedded, fine-grained, fair to poor sorted sandstone. Commonly associated with Fl, S2 and GI facies associations	0.5 - 12 m	Tariquia (Bartolo and Emborozú), Guandacay and Emborozú (Emborozú)	Crevasse splays, levees
A7	Tabular, thin-bedded sandstone and carbonaceous mudstones	Shl, C	Thick-laminated, very fine-fine grained, fair-sorted sandstone. Sharp contacts and occasionally syndeformational structures, scattered chips of organic material	≤ 2 m	Tariquia (Bartolo)	Intechannel lacustrine deposits (braided)
A8	Thick, limited trough cross-bedded sandstone	Sm, Smtd, Sp, Sh	Tabular-bedded sandstones medium to fine grained, very limited cross stratified, with erosive basal contacts. Commonly associated with facies association Fl, SS and S4	≤ 7 m	Tariquia (Bartolo and Emborozú), Guandacay (Bartolo)	Braided fluvial channel
A9	Upward fining, cross-stratified conglomerates and sandstones	Gh, Q, St, Sh, Shl, Pcm, Fln, Fl, C	Lenticular conglomerate, Subangular-subrounded, polymictic clasts, weak-moderately imbricated, clast-supported. Common erosive basal contacts. It grades upward to facies association SS, S3 and Fl.	≤ 10 m	Guandacay and Emborozú (Emborozú)	Gravel-sand braided channel

## A2. Mudstones

Fine-grained mudstone lithofacies are dominant in exposures of the Tariquia Formation at both outcrop sections measured for this study, as well as in exposures of the Guandacay Formation at the Emborozú section. These deposits are less common in the Guandacay and Petaca units in the north (Bartolo locality), and in the Emborozú unit at the southern (Emborozú) locality. This facies association encompasses finely laminated, massive, bioturbated mudstones, as well as mudstones with pedogenic structures consisting of small (~ 1-2 cm) calcareous nodules and reduction spots. These deposits are typically located within the upper part of upward fining successions. Carbonaceous mudstones are also part of this association, although they have not been widely described in the record. Individual bed thickness in these facies associations range from 5 cm to 2 m, and stacked (amalgamated) mudstone packages can reach up to 12 m in thickness. The lateral continuity of this facies association is also governed by the overlying lithofacies but field observations reveal packages that persist for at least 200 m laterally (Figure 6d).

### Interpretation

This facies association is interpreted as fine-grained overbank sediments deposited in floodplain environments within broader fluvial systems. The bioturbated and moderately pedogenically affected mudstone facies is the likely result of deposition in interfluves in which subaerial exposure after flood events transitions to a zone prone to bioturbation and coeval pedogenic activity (e.g. McCarthy et al., 1997). By contrast, the laminated, thin-bedded mudstone facies represent slow, sporadic deposition on a distal floodplain. The thick massive mudstone facies are interpreted as avulsion products reflecting deposition of suspended flows in overbank areas during flood stage (Galloway and Hobday, 1996). The distal position and low rates of sediment accumulation were

beneficial for colonization by vegetation, as evidenced in the presence of carbonaceous mudstones and chips of preserved organic material.

### **A3. Finely interbedded sandstones and mudstones**

Finely laminated mudstones (Fl) up to 2 m thick, alternating with very thin, very fine sandstones (Shl, ~2 -6 cm thick) on a quasi-regular pattern represent this facies association (Figure 6b). The mudstones are highly restricted with lateral continuity limited to 5-7 m with the deposit exhibiting a clear lensoid shape (Figure 6e). In general, the succession is upward fining, with dominance of mudstones at the top.

#### **Interpretation**

This facies association represent mud deposition as an isolated plug in an abandoned (meandering) channel. The mostly finely laminated mudstone facies represents slow suspension deposition within the abandoned channel. The thin-bedded sandstones are interpreted as distal portions of crevasse splays sourced from a coeval, laterally adjacent, active channel. Migration of the channel belt is further documented by the presences of overlying mounded levee deposits (Figure 6e; e.g., Brierley et al., 1997).

### **A4. Structureless, thick-bedded sandstones**

At Bartolo, deposits of the upper Petaca and upper Guandacay units are characterized by facies association A4. Thick (1-5 m) bedded intervals of fine to medium grained sandstones (Sm), with discontinuous non-parallel erosive basal contacts, comprise this assemblage. The sandstone beds are usually massive and contain scattered floating clasts of subangular-angular chert, rose and white quartz granules and even some angular-subangular limestone cobbles in the Guandacay Formation (Figure 6g). In the Guandacay interval, a thin (5-30 cm thick) lag of pebble-cobble conglomerate facies(Gh, Gco) defines the basal contact, whereas the upper levels reveal pedogenic modification including thin (0.2-2 m thick) light yellow, red, green poorly sorted, slightly calcareous

sandstone facies (Pcm) capping upward fining and thinning successions (Figure 6h). A few mudstone rip-up clasts also are present in the basal conglomerate lenses. In general, the degree of lateral continuity (>100 m) and vertical stacking increases in upper levels of the section.

### **Interpretation**

The thick structureless sandstones are attributed to channel deposition. These sandstones represent low-sinuosity, predominantly sand-load, longitudinal braided channels (Sm). The lateral continuity along with the conglomerate lags show deposition within channel systems of variable competence. Vertically stacked multilateral channel fills dominate the floodplain facies, with the former documenting pedogenesis (Pcm). The overall vertical stacking pattern, paucity of overbank facies, and aggradational flood plain architecture reveal relatively limited channel migration (Uba et al., 2005). Additionally, the bases of the conglomerate channels document two types of scouring processes. On one hand, rapid transport conditions promote lengthening of gravel lags faster than they can aggrade, giving rise to widespread flat, low inclined, thin-bedded (5-10 cm; Gco) conglomerate lags (Miall, 1996). On the other hand, traction load during seasonal flooding or changing hydraulic conditions may induce erosion of underlying (thalweg) and flanking (cutbank) fill, promoting deposition of conglomerate lags (Gh) and intraformational mudstone rip-up clasts.

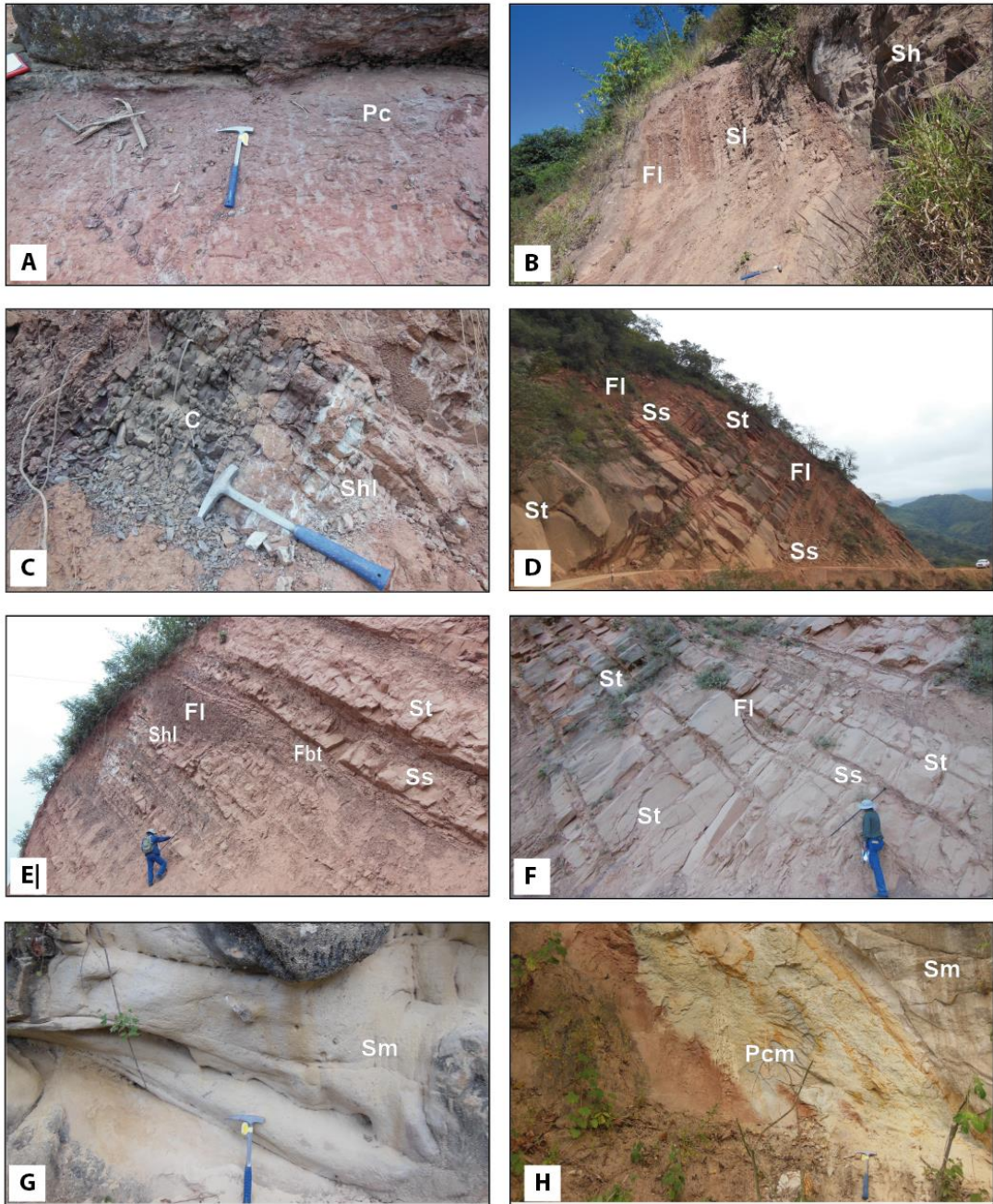


Figure 6.



Figure 6.

Figure 6. Representative lithofacies association photographs for the major Cenozoic stratigraphic units: Petaca, Tariquia, Guandacay and Emborozú. a) Pervasive calcareous paleosols (A1) widespread in the Petaca Formation. Abundant calcareous nodules displaying irregular morphologies (elongate to even vertical rhizocretions) are easily recognized for their light green and gray mottled pattern; b) facies associations-A2 and A5 of the basal Tariquia Formation at the Emborozú section. Sharp erosive basal surfaces of thick bedded sandstones (Sh) are encased in broad intervals of facies association A2 (mudstone, lithofacies Fl) and A6 (thin-bedded sandstone, lithofacies Sl) and can be traced for ten of meters; c) Finely-bedded sandstones sharply overlain by greenish gray, carbonaceous laminated siltstones, associated with facies association A7 are recorded in the lower Tariquia at the Bartolo section; d) tabular sandstones (Ss, St lithofacies) with poorly developed trough cross-stratification, and sharp erosive and sometimes irregular basal contacts (facies association A8). At Bartolo this facies association persists laterally for hundreds of meters (see vehicle in the lower right for scale) and comprises upward fining intervals underlying multistory mudstones (lithofacies Fl). e) vertically- and laterally restricted (lens shaped) finely laminated mudstones (Fl) intercalated with thinly-bedded sandstones (Fl) representing facies association A3, in the middle Tariquia section (Bartolo). Unconformably overlain are mounded interbedded lenticular sandstone and mudstone (facies associations A6) capped by thick, limited through cross-bedded sandstone (facies association A8); f) laterally extensive sandstones with incipient erosive basal surfaces (facies association A8) interbedded with thin lenticular sandstone and mudstone of facies association A6 are observed In the middle Tariquia section of Bartolo; g) Thick-bedded sandstones (Sm), with discontinuous non-parallel erosive basal contacts are typical of the upper Guandacay Formation at Bartolo locality, they comprise facies associations A4; h) yellow, red, slightly calcareous sandstone (Pcm)-moderate developed paleosols capping upward-fining sandstones of facies associations A4 at Bartolo section; I) highly erosive basal, lenticular, upward fining, limited cross-stratified conglomerates and sandstones stacked in cycles of ~3-15 m thick represent facies association A9. Thick (~3-12 m) thin-bedded sandstones (Sl) and mudstones (Fl) are characteristic of the Guandacay Formation at the Emborozú locality. In contrast, thinner, discontinuous mudstone overlains thick-erosive conglomerates (6j) of the Emborozú Formation.

### **A5. Thick-bedded sandstone**

Light brown, reddish brown, thick-bedded sandstones (1-22 m) encompass this facies association. Fine-grained, fair-well sorted, with marks of sharp erosive basal surfaces characterize the lower Tariquia Formation in both sections. Reworking of older deposits is represented by red claystone rip-up clasts (1-12 cm) on top of thin (0.2-0.5 m) dark red, laminated claystones. Horizontally stratified sandstones (Sh) are widely distributed with minor tabular cross-bedded sandstones (Sp). The thick sandstones are typically conformably overlain by thin bedded, fair to poorly sorted sandstones with pedogenic structures (Fbt). Individual beds show a predominantly uniform texture, with a subordinate amount showing a limited upward fining pattern. Both upward thinning and upward thickening stacking patterns are present. This facies persists for tens of meters laterally, and is especially well represented at the Emborozú locality. Meanwhile, there is not a clear pattern in the degree of vertical connectedness. This facies association is commonly encased in broader intervals of facies association A2 (mudstone) and A6 (thin-bedded sandstone) (see Figure 6b).

#### **Interpretation**

The limited lateral continuity, limited degree of vertical connectedness, scarcity of lateral accretion deposits, and overall ribbon sandstone geometries—coupled with their close association to overbank deposits—are interpreted as suspended-load channels (Eberth and Miall, 1991). These channels are tentatively interpreted as vertically aggrading, anastomosed channels. Consequently, the thick sandstones are attributed to multistorey channels (up to 22 m-thick), and in some cases to bank accretion (Galloway and Hobday, 1996). Abrupt lateral transitions associated with avulsive activities are characteristic of most sandstone bodies, and supported by an abundance of mudstone rip-

up clasts and sharp erosional bases. Subaerial exposure is reflected in the development of moderate paleosol horizons (Miall, 1996).

#### **A6. Interbedded lenticular sandstone and mudstone**

This facies association consists of light brown, reddish brown lenticular (Ss), tabular (Sl)-bedded, fine-medium grained, fair to poorly sorted sandstone (up to 12 m-thick) alternating with interbedded mudstones (0.05-2 m-thick) corresponding to facies association A2. Most beds are composed of slightly calcareous sandstones showing erosive basal surfaces, with some sandstone bodies showing sharp nonerosive basal contacts. Crude horizontal stratification is the main characteristic of these sandstone bodies, and subplanar cross lamination. Individual beds are not greater than 0.5 m in thickness and persist laterally for more than 50 m (Figures 6c, 6d, 6e). The lenticular sandstones pinch out over a comparable lateral distance (~50-70 m) and pass laterally into adjacent mudstones.

In general, the lenticular sandstone bodies display a low relief (1 m maximum) and are regularly interbedded with finer overbank facies (F1) that encompass laminated (Fl) and pedogenic (Fbtl) mudstones. This assemblage usually occupies the uppermost levels of fining and thinning upward intervals (facies association A8 and A9).

#### **Interpretation**

This facies association is interpreted as the deposits of a sand-dominated floodplain with overbank deposition (crevasse splays) linked to adjacent sandy channel systems. Repeated injection of sand into the floodplain environment is attributed to overbank deposition of suspended load during high flood events in proximity to major avulsed channel systems. The channel avulsion process is reflected in the complex stratigraphic stacking generally involving upward fining and thinning patterns. This stacking pattern may be interpreted as initial deposition of new, small, ephemeral

channels close to the trunk channel followed by periodic deposition of suspended load in the overbank area. Consecutive flooding stages would reflect deposition of several crevasses splay and finer facies, representative of progradation of the crevasse lobe into the floodplain (Galloway and Hobday, 1996; McCarthy et al., 1997). The lateral continuity, and in some case the pronounced cycle thickness (Sl+Fl+Fbt; >10 m), can be attributed to deposition in a low relief, rapidly aggrading floodplain. Intermittent subaerial exposure in the floodplain is demonstrated by bioturbated sandstones and weakly developed paleosols.

#### **A7. Tabular, thin-bedded sandstone and carbonaceous mudstones**

The mixed thin sandstones and organic-rich mudstones of this facies association are restricted to the intermediate levels of the Tariquia Formation at the Bartolo locality, approximately 40 m above the newly dated tuff. The facies is composed of white and pale red, tabular, 5-10 cm-bedded, thin-laminated, fine-grained, moderately sorted sandstones that are sharply overlain by greenish gray, finely laminated siltstones. Proportionally, the base is dominated by fine grained sandstones capped by carbonaceous mudstones, within a broad upward fining interval. The lithologies persist laterally for ~15 m, and are underlain and overlain by mudstones of facies association A2. The upper bedding contacts are occasionally marked by syndepositional flame structures (Figure 6c).

#### **Interpretation**

Facies characteristics are consistent with interfluvial lacustrine deposition within this S4 facies associations. Rapid deceleration of flows into ephemeral standing bodies of water may be indicated by finely laminated sandstones (Shl). A rapid rate of aggradation is marked, in turn by internal soft-sediment deformation structures (Shl; Miall, 1996). A potential decrease in accumulation rates may be recorded by deposition

of carbonaceous muds in abandoned or less-active interfluvial channels or local lacustrine zones.

#### **A8. Thick, limited trough cross-bedded sandstone**

At Bartolo, thick cross-stratified sandstones of this facies association compose the bulk of the upper Tariquia Formation (above the tuff bed) and lower Guandacay Formation. Similarly, at Emborozú, these facies are typically distributed within the upper Tariquia Formation (above the  $9.1 \pm 0.2$  Ma tuff) and very scattered in the Guandacay and Emborozú formations, constituting the upward fining sets of facies association G1. This association is characterized by thick (2-13 m) medium-fine grained sandstones that are generally tabular with sharp erosive and sometimes irregular basal contacts (Figures 6d, 6e, 6f). Although it is very difficult to recognize internal sedimentary structures, the majority represent poorly developed trough cross-stratification with subordinate low-angle cross-stratification and horizontal stratification. Abundant red claystone rip-up clasts are common along basal contacts, and discrete desiccation cracks, ripples, and moderate bioturbation along upper contacts. With several exceptions in upper stratigraphic levels, this assemblage generally grades upward to interbedded lenticular sandstones and mudstones (A6 and A2 facies associations, respectively) (see Figure 6d, 6f).

At Bartolo, individual beds generally persist laterally for several hundred meters (~200-500 m). Most individual packages present a fining and thinning upward pattern ranging from 1.5 to 8 m thick. The finer facies become less abundant upsection, insomuch as the cycles are sandstone-dominated with limited or very thin (3-10 cm) mudstones. The intermediate levels of the Bartolo section present multistory sandstone bodies with main bodies reaching up to 50 m in thickness and persisting laterally as far as 400 m (Figure 6d). The deposits comprising three or more symmetric, concentric upward

fining intervals with erosive basal contacts (with 2-3 m of relief) encased in underlying multistory mudstones. The upper levels of the Bartolo section have similar or more laterally extensive sandstone bodies with less erosive basal surfaces (with <1 m of relief) (Figure 6f).

### **Interpretation**

This facies association is attributed to deposition within braided fluvial channels. The stratigraphic expression of individual lithofacies and cycle are consistent with multiple laterally adjacent channels deposited by low-sinuosity, dominantly sand-bedload channels (Galloway and Hobday, 1996; Gibling, 2006). The presence of intraformational rip-up clasts indicates erosion of previous overbank deposits. Interpretation of waning flow conditions is supported by deposition of longitudinal and linguoid braided bars (Sm, Smd, St) followed by ripple laminated facies (Fl). Evidence of abandoned channels, possibly associated with avulsion in the lower Bartolo section, is corroborated by the presence of dessication cracks, bioturbation, and poorly developed paleosols (Miall, 1996).

In general, the coupled upsection decrease in relief and thickness of overbank deposits (facies associations A6 and A2) may be associated with a change from avulsive behavior to very limited channel migration, likely coupled with an increase in sand load. Furthermore, the prominent vertical accretion suggests deposition in unconfined plains, potentially in highly aggradational setting such as a medial fluvial megafan adjacent to an active mountain front (e.g. Horton and DeCelles, 2001; Uba et al., 2005, 2009).

### **A9. Upward fining, limited cross-stratified conglomerates and sandstones**

This facies association is represented in the Guandacay and Emborozú formations at the Emborozú locality. It contains a plethora of lithofacies within well-developed

upward thinning and fining packages. At the base, this assemblage has a 1-16 m-thick, highly erosive basal, lenticular, granule-cobble, conglomerate (Figures 6i, 6j). Subrounded clasts of variable lithology include intraformational rip-up mudstone clasts concentrated at the bases of individual beds. The conglomerate beds are normally graded, slightly to well-imbricated, and locally exhibit trough cross-stratification. Maximum clast size is 30 cm. The beds range from around 0.6 to 3 m in thickness, with basal erosive relief up to ~1 m, and persist laterally for a few tens of meters, pinching out into adjacent mudstones or sandstones. Vertically, these beds grade into thick (1-12 m) light brown, moderately sorted, horizontally stratified, locally trough cross-stratified, and tabular sandstones of facies association A8 and A6. At the top, thin (20-50 cm-thick) laminated and bioturbated mudstones of facies association (A2) are present (Figure 6i, 6j). Volumetrically, the conglomerate facies composes 50-70% of the assemblage, and the overlying sandstone and mudstone facies the remaining 50-30%. Upsection, thicker conglomerate levels are observed in deposits of the Emborozú locality.

### **Interpretation**

Facies association A9 is interpreted as deposits of a gravelly-sandy braided channel system. The moderate degree of organization, clast roundness, along with the erosive basal contacts and clast imbrication point to traction-load deposition of high-energy, low-sinuosity, gravelly channels with the characteristic development of longitudinal bars (Miall, 1977). Subsequent waning flood flow promoted upward fining patterns produced by deposition of capping dune sand deposits (Sh, Shl; Miall, 1977) followed by suspension sedimentation in overbanks areas (Galloway and Hobday, 1996). Abandonment or subaerial exposure of these finer facies in overbank areas made these zones favorable to the development of moderate paleosols and vegetation expansion (McCarthy et al., 1997).

## CHAPTER 3. PROVENANCE ANALYSES

### *Conglomerate clast compositions*

#### **Methods**

Conglomerate clast composition data were collected in the field at 16 stations throughout the upper Bartolo section (Figure 5a). Due to the limited areal exposure of conglomerate facies, most clast counts were visually estimated within outcrop areas  $<0.7\text{ m}^2$ . The process was carried out in moderately organized pebble-cobble conglomerates. Individual clasts and clast populations were differentiated according to typical lithologies present in regionally extensive stratigraphic units exposed in the Subandean zone, Interandean zone, and Eastern Cordillera (McQuarrie, 2002). (1) Lower Paleozoic clasts were identified as follows: white fine-grained quartzites associated with Ordovician units (likely Anzaldo and/or San Benito formations); (2) greenish and yellowish brown fine-grained sandstones and black chert potentially derived from Silurian units (likely the Cancañiri and Kirusillas formations); (3) medium gray, white, purple sandstone, fine-grained sandstones with parallel-aligned mica flakes derived from Devonian units (potentially Icla and/or Huamampampa formations). In contrast, upper Paleozoic clasts include the following lithologies: (4) pale red, coarse-grained sandstones derived from Carboniferous units (plausible from Tupambi, Chorro, Escarpment); (5) Permian carbonates (light-medium gray mudstones with stromatolitic structures, mostly present as floating clasts); and (6) black chert derived from the Vitiacua Formation.

#### **Results and interpretation**

Conglomerate clast counts within the upper Bartolo section document exhumation of the western Interandean zone. For the Guandacay Formation (Figure 7), there is a predominance of Devonian sandstone clasts at lower levels, followed by a clear input of Silurian quartzarenites together with Devonian and Carboniferous sandstone clasts by

intermediate levels. This significant upsection increase in Silurian clasts at the expense of Devonian and Carboniferous clasts represents a normal unroofing pattern of nearby source terranes, as commonly observed in thrust-related basins (e.g. DeCelles et al., 1998, Colombo, 1994). The broad distribution of Silurian rocks in the Interandean Zone, in contrast to adjacent tectonomorphic zones, help identify it as the main source of these older clasts. Because cooling ages for the Interandean zone reveal thrust activity after ~40 Ma (IA1 sample, Barnes et al., 2008) we tentatively attribute the unroofing sequence to slip on the Main Interandean thrust (Kley, 1996; McQuarry, 2002; Oncken et al., 2006).

Farther upsection, in the upper Guandacay Formation, the greatest population of clasts is composed of Permian carbonates, followed by moderate amounts of Silurian, Devonian and Carboniferous clasts. The Permian carbonate clasts include numerous pebbles to large cobbles ( $\leq 20$  cm) suggestive of a relatively proximal source area. According to the regional distribution of Permian strata (Oviedo, 1974), the source area appears to be limited to the western Subandean zone. The upsection appearance of Permian clasts at the expense of Silurian clasts suggests a shift in clast dispersal, which may be ascribed to drainage reorganization (likely headward enhancement or elaboration of the drainage network) leading to capture of new sources areas. Alternatively, a new deformation episode with associated thrust activity and erosion of younger successions within new thrust sheets could also explain the change of clast populations. Perhaps the most plausible scenario is a composite interpretation in which the distribution of clasts is associated both with contemporaneous thrusting near the Interandean-Subandean boundary as well as reorganization or expansion of the catchment area resulting in incorporation of younger rocks from less-exhumed thrust sheets and potential recycling of older synorogenic fill of the more-proximal foreland basin (e.g. Colombo, 1994).

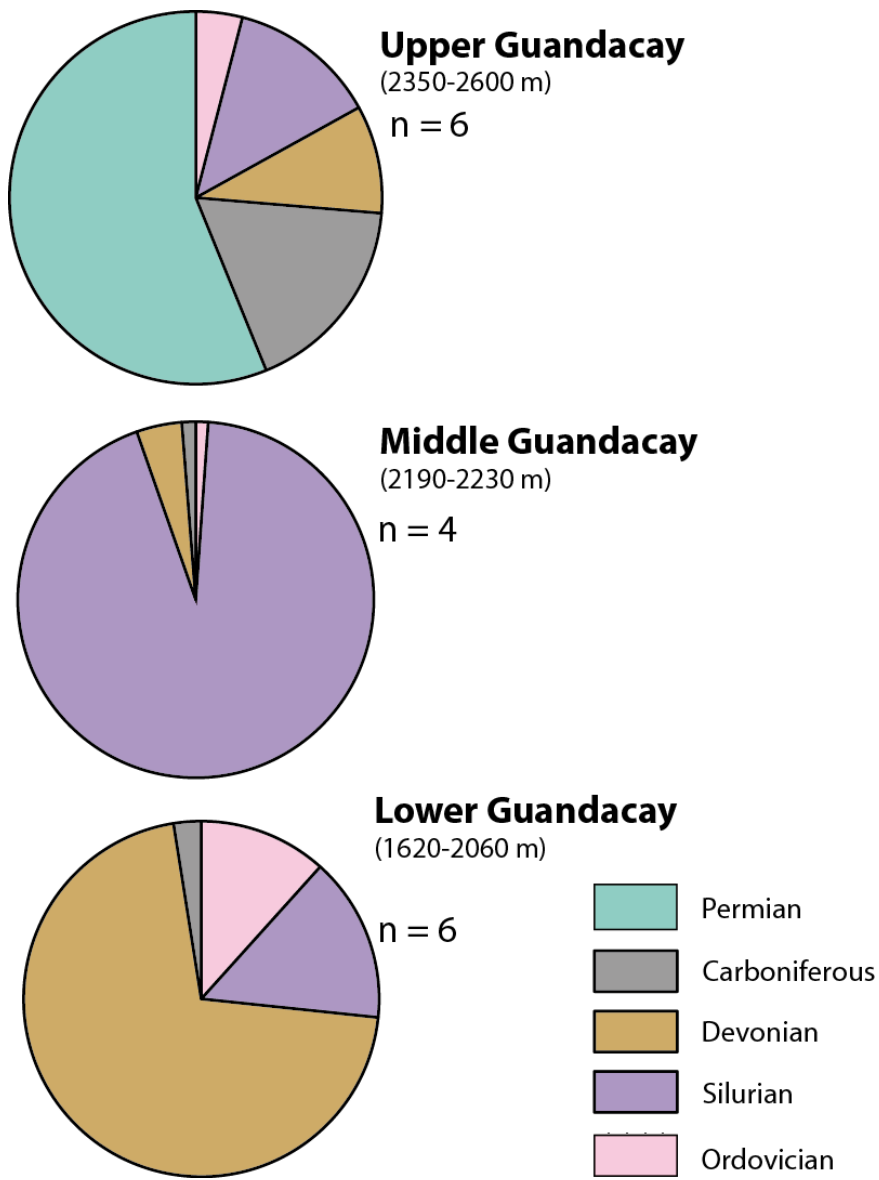


Figure 7. Conglomerate clast composition pie charts from the Guandacay Formation in the Bartolo section; n denotes the number of measured stations.

## **Sandstone petrology**

### **Methods**

In order to determine the compositional variations of sandstones and assess the provenance of the Cenozoic Subandean basin, detailed petrographic studies were conducted on 19 medium-grained sandstones. The collected samples are distributed uniformly within the four lithostratigraphic units exposed in the Bartolo section (Figure 5a). Thin sections were constructed following standard procedures to facilitate conventional transmitted polarized-light microscopic analysis. To discriminate primary and secondary porosity, the samples were injected with blue-dye epoxy. They were also stained for potassium feldspar and plagioclase feldspar to assist grain identification. Point counts of 350 framework grains per thin section were carried out following the Gazzi-Dickinson method (Dickinson and Suczek, 1979; Ingersoll et al., 1984; Dickinson, 1985). Mineral grains and rock fragments were classified according to Table 3.

### **Results**

Standard ternary diagrams are employed to display the results of the sandstone point counts. Figure 8 shows the three distinct ternary diagrams used for each formation set of samples. An explanation of the parameters employed in each diagram is provided below, and the recalculated parameters are included in Table 3:

Whereas the (A) QtFL diagram of Folk (1980) considers total quartz, feldspar, and lithic fragments (Figure 8a), the other two diagrams (Figure 8b, 8c) constructed according to Dickinson and Suczek (1979) discriminate: (B) Q / F / L: quartz, feldspar, and lithic fragments; (C) Qp / Lv / Ls: polycrystalline quartz, and volcanic (Lv) and sedimentary (Ls) lithic fragments. The last two diagrams have been designed to best assist in the general discrimination of the contrasting provenance of various plate tectonic settings (Dickinson, 1985).

Table 3. Categories for sandstone point count analyses

Symbol	Grain categories	Recalculated parameters
Qm	Monocrystalline quartz	<b>Q-F-L</b>
Qp	Polycrystalline quartz	$Q = Qm + Qp + Qpt + C$
Qpt	Polycrystalline quartz with tectonic fabric	$F = P + K$
K	Potassium feldspar	$L = Lv + Ls + Lmu$
P	Plagioclase feldspar	$Ls = Lss + Lzls + Lmu$
Lv	Volcanic lithic fragments	$Lmu = Lmp + Lms$
Lss	Sandstone lithic fragment	<b>Qm-F-Lt</b>
Lzls	Siltstone lithic fragment	$Qm = Qm$
Lmu	Mudrock lithic fragment	$F = P + K$
C	Chert sedimentary lithic fragment	$Lt = Lv + Ls + Lmu + Qp + Qpt + C$
Lmp	Phyllite metamorphic lithic fragment	<b>Lv-Lm-Ls</b>
Lms	Schist metamorphic lithic fragment	$Lv = Lv$
A	Accessory minerals (heavy minerals and micas)	$Lm = Lmp + Lms$
		$Ls = Lss + Lzls + Lmu$

The point-count data generated in this study show that the samples are quartz-rich (>80%), with monocrystalline quartz as the most common framework grain. The percentage of feldspar decreases upsection, coincident with an increase in lithic fragments. Metamorphic lithic fragments (phyllites and schists in minor quantities) are almost exclusively encountered in the intermediate levels of the section, in contrast with the sedimentary (siltstone and fine-grained sandstone) and volcanic (mostly felsitic and lathwork) counterparts documented in the upper levels of the section. Chert, organic matter (bitumen), and accessory minerals such as micas, amphiboles, tourmaline, hematite, pyroxenes, etc. are very scattered throughout the section. Overall, primary porosity has been reduced in most of the samples, as no further diagenetic processes have conspired to generate significant secondary porosity (e.g. grain dissolution).

The Petaca Formation consists of a poor to moderately sorted, subangular-subrounded quartz-grain dominated sandstone with calcite cement and some relicts of clay matrix introduced by infiltration. According to the compositional classification of Folk (1980), they classify as subarkoses (Figure 8a). The average quartz content of 81% is composed exclusively of monocrystalline quartz, followed by 17% feldspar and 2% lithic fragments. Potassium feldspar dominates with respect to plagioclase feldspar. In general, orthoclase grains are highly altered, most commonly to clays but also to iron oxides; a similar high degree of alteration is observed in a small percentage of plagioclase grains. The compositionally Petaca Formation sandstones are interpreted as submature to immature.

Sandstones of the overlying Tariquia Formation are composed mainly of subangular-subrounded monocrystalline quartz grains (with the exception of a few distinctive well-rounded grains), lithic fragments immersed in a considerable amount of clay pseudomatrix that diminishes upsection. The majority (80%) of the samples correspond to sublitharenites (Figure 8a). In addition to monocrystalline quartz (with a high percentage of undulose extinction), there is an appearance and progressive increase in chert grains. The most important populations of lithic fragments are associated with dominantly (~80%) metasedimentary lithic fragments in the basal Tariquia, followed upsection by volcanic rock fragments and finally predominantly sedimentary lithic fragments (siltstones and fine-grained sandstones) in the upper Tariquia. In contrast to the underlying Petaca unit, feldspar grains are restricted to potassium feldspar (orthoclase), the overall proportion decreases toward the top (from ~9% to 2%), and they show progressively less alteration from bottom to top. A low percentage of bitumen is observed in many samples. On the basis of framework grain compositions for the Tariquia

Formation, a relative increase in maturity is observed (submature) with respect to the Petaca samples.

In general, the Guandacay Formation is distinguished by medium-grained sandstones of sublitharenitic composition with subrounded grains, slight calcareous cement, and thinly-covered cutans. The feldspar proportion remains relatively uniform compared to the underlying Tariqua unit. Likewise, a change in the lithic fragments is evidenced by the input of metasedimentary lithic fragments (dominantly phyllites). In the upper levels of the Guandacay Formation, there is contribution of chert and volcanic (felsitic) rock fragments consistent with conglomerate clast counts. Also, the main accessory mineral is the iron oxide, hematite. Overall, the Guandacay sandstone samples show a submature to immature composition.

### **Interpretation**

Cenozoic sandstones of lowermost basin fill at the Bartolo section show predominantly quartz-rich compositions with an important percentage of both potassium and plagioclase feldspars. According to compositional classifications and ternary diagrams best suited for plate-tectonic discrimination (Figure 8b), they may correspond to erosion of a transitional continental block from a craton interior. If we consider the degree of maturity and sedimentological evidence for depositional processes, these sandstones may have been derived from a relatively close source area and/or a source area rich in feldspars. The most probable sources areas for these deposits can be assigned to either the Amazonian craton or pre-Cenozoic deposits rich in feldspars. Paleocurrent and detrital zircon provenance signatures (discussed below) shed more light about these proposed source areas.

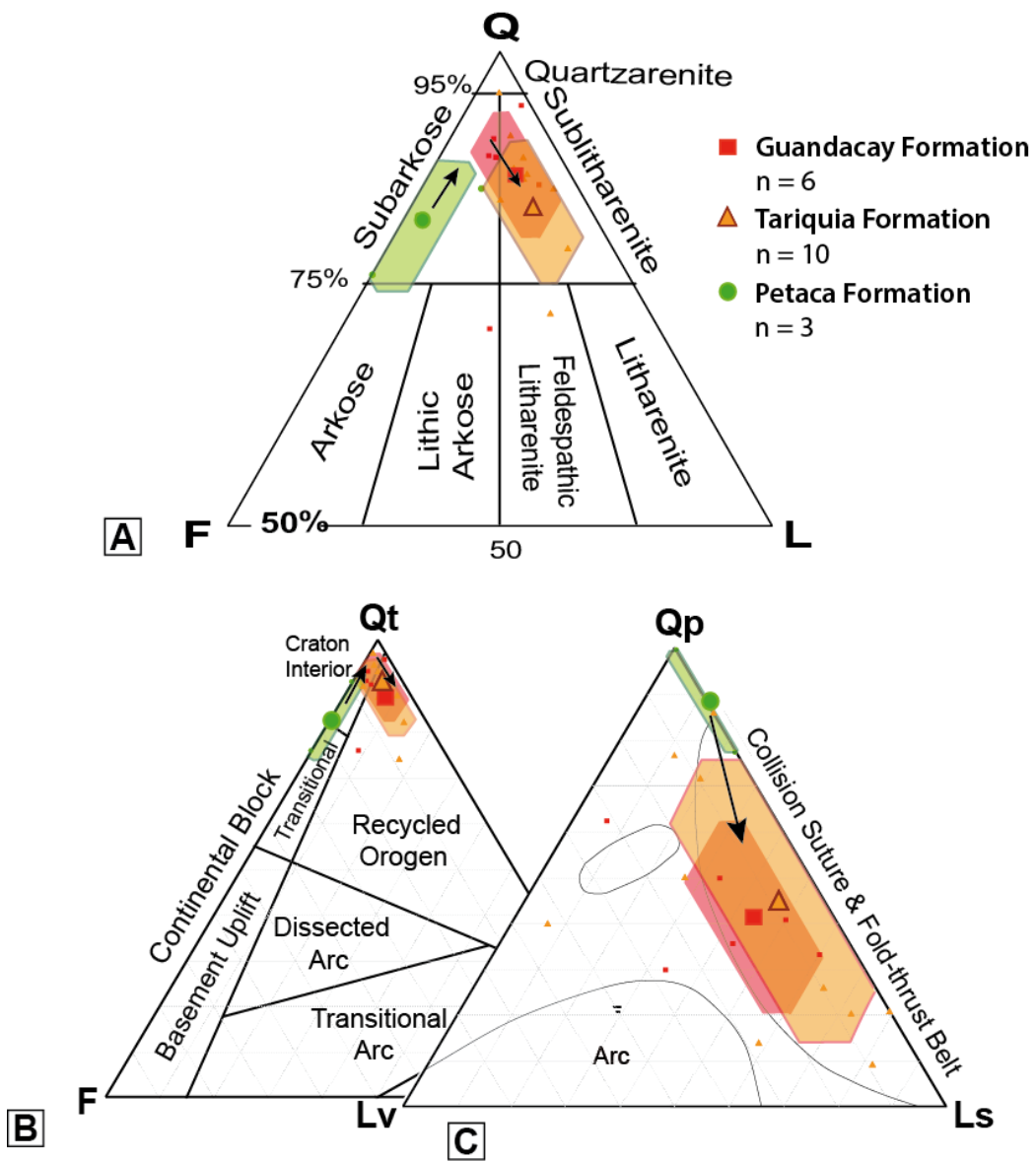


Figure 8. a) Q/F/L (quartz, feldspar/lithic fragment) plot (Folk, 1980) of sandstone petrographic data from Bartolo section (with 50% quartz baseline). b) Qt/F/L, and c) Qp/Lv/Ls provenance ternary diagrams (Dickinson and Suczek, 1979). Mean compositional values for the Petaca, Tariquia and Guandacay are plotted; n represents the number of samples. Arrows depict the upward increase in lithic fragments with respect to quartz grains.

Upsection, the clear input of lithic fragments in the Tariquia Formation, at the expense of feldspar grains, can be coupled to a shift in the principal sediment source region (Figure 8b, 8c), an interpretation supported by previous sedimentological studies (Uba et al., 2005, Hulka, 2005). During Tariquia deposition, a recycled orogen represented by the Andean fold-thrust belt to the west would have become the dominant source area. Erosion of pre-Cenozoic units is documented in the field by conglomerate clast compositions and confirmed in the sandstone petrographic analysis. For example, the identification of well-rounded, spherical monocrystalline rose quartz grains derived from Mesozoic eolian units, helped support the increase of lithic fragments attributed to this provenance shift. It is important to note that even though volcanic lithic fragments are present in the lower Tariquia Formation, the degree of grain roundness and distant position of the Cenozoic magmatic arc (>300 km to the west) during the time of deposition (>15 Ma) suggest they are more likely derived from older sublitharenites of Paleozoic age (e.g. Schonian and Egenhoff, 2007).

Finally, the sublitharenites of the Guandacay Formation reflect a persistent recycled orogen provenance. The textural maturity of these sandstones (submature to immature) coupled with increased preservation of sedimentary lithic fragments (principally siltstone and fine-grained sandstones) may indicate a change in the proximity and/or source units in the fold-thrust belt. Similar to the conglomerate clast compositional record, the input of chert grains suggests the introduction of Permian and other Paleozoic units in the drainage networks that largely tapped into the growing topography of the Interandean zone.

## **Paleocurrents**

### **Methods**

Paleocurrent data were collected from individual genetic lithofacies units (e.g. DeCelles and Cavazza, 1999). Although the quality of exposure and nature of primary current structures prevented continuous data collection in both sections, measurements were carried out for a series of horizons (19 stations in Bartolo section, 18 stations in Emborozú section), mostly located in the Tariquia and Guandacay formations. Flute marks, asymmetric ripples, channel axes, and trough-cross strata were the main sedimentary structures measured in the Tariquia Formation. In the coarser facies of the Guandacay and Emborozú formations, measurements of clast imbrication (consisting of 6 or more imbricated clasts) define the mean paleocurrent direction in small outcrop areas (less than 2 m<sup>2</sup>).

### **Results and interpretation**

This study augments the paleoflow directions previously presented for Cenozoic strata exposed in the eastern Subandean zone and Chaco foreland basin (Uba et al., 2005, 2006; Hulka, 2005; Hulka and Heubeck, 2010), allowing extrapolation of sediment dispersal patterns throughout the Subandean region. Arrows representing the mean paleoflow direction of a group of stations (numbered vectors in Figures 5a and 5b) are portrayed in the stratigraphic columns. These data form the basis of an updated synthesis (Figure 9) incorporating the measurements of this study with respect to each lithostratigraphic unit or formation.

The updated database reveals a pronounced mid-Cenozoic reversal in paleocurrent directions. Whereas the lower Cenozoic section (Petaca Formation) shows a predominant transport direction from east to west, the paleocurrent vectors above this unit show a general eastward flow (Figure 9). Further interpretations are made on the

basis of scattered paleocurrent directions (azimuthal variation along  $180^{\circ}$ ) observed in the younger units. Hulka (2005) proposes the channel type and flexural response of the foredeep as the main variables to control this dispersal pattern. An analysis based solely on paleoflow indicators from the Emborozú section reveals a clear axial (north-south) paleoflow pattern during deposition of the Guandacay Formation. Conversely, the uppermost stratigraphic levels show a return to dominantly east-directed paleoflow, suggesting a rejuvenation of a drainage system characterized by transverse (east-west) flow. This pattern of alternating transverse and axial flow is not well expressed at Bartolo, where paleocurrent indicators above the basal unit (Petaca Formation) show consistently east-directed paleoflow.

The azimuthal range in paleocurrent directions potentially reflects the advancement of a fluvial megafan system as observed in the proximal western sector of the foreland basin adjacent to the north-south-striking deformation front of the Andes (Horton and DeCelles, 2001; Horton, 2005). Moreover, results presented here support an early Miocene onset of major erosion of developing western sediment sources (Interandean, Eastern Cordillera), coincident with the paleoflow reversal. This interpretation is further supported by sandstone petrologic results, conglomerate clast compositions, and detrital zircon U-Pb provenance analyses (described below).

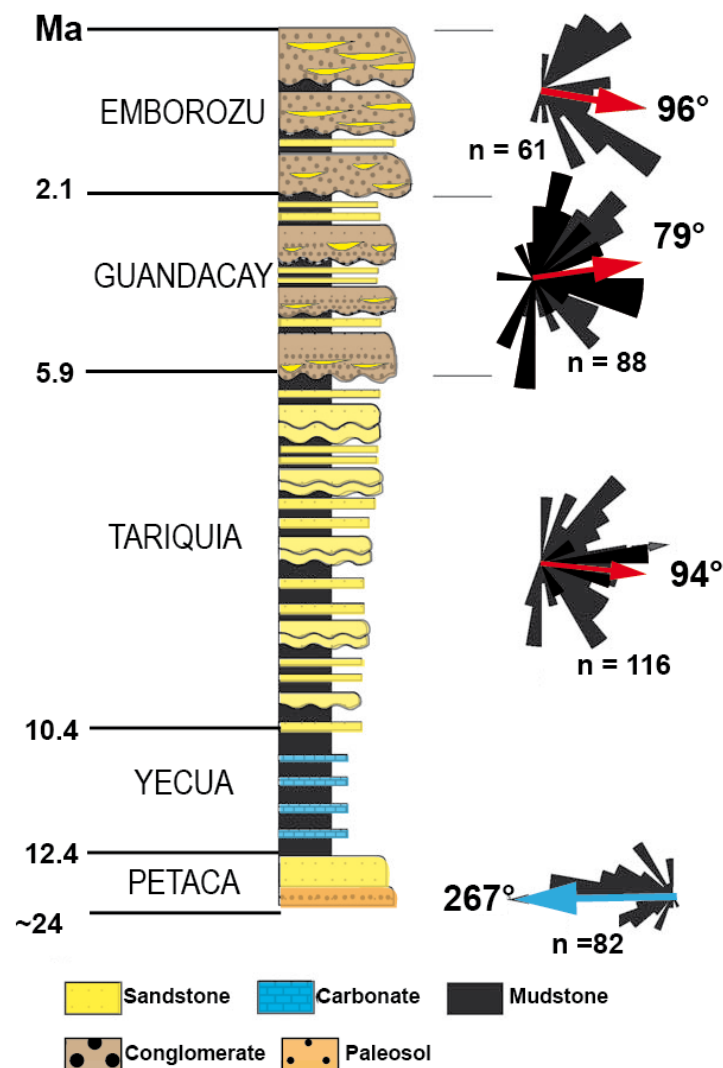


Figure 9. Generalized Cenozoic stratigraphic column of the Subandean zone and adjacent Chaco basin including updated paleocurrent directions for the eastern (after Hullca and Heubeck, 2010) and western Subandean zone (this study). Note the paleocurrent reversal after deposition of the Petaca Formation ( $>\sim 12$  Ma). Petaca deposits record dominant paleoflows from east to west, and paleocurrent vectors above this unit show a predominant transport direction eastward.

## ***Detrital zircon U-Pb geochronology***

### **Methods**

A total of 15 medium-grained Phanerozoic sandstones were analyzed using U-Pb geochronology to assess the provenance of detrital zircon grains. A subgroup of nine Cenozoic samples, derived from the Bartolo, Emborozú and Villamontes sections (Figure 2, 5a and 5b) were targeted to define U-Pb age signatures within the Subandean-Chaco foreland basin. An additional six samples of pre-Cenozoic sandstone were also analyzed to enable accurate discrimination of potential source areas within the central Andes. Figure 10 shows the location and stratigraphic position of the samples analyzed for source discrimination.

The procedure for separation of zircon minerals from each sample included: crushing, grinding, Wilfley table water separation, heavy liquid (bromo) separation, followed by magnetic separation (Frantz). The non-magnetic fraction was then subjected to MEI heavy liquid separation, with the resulting heavier fraction (mostly zircon grains) carefully poured onto a reticulated tape mount without discrimination of grains due to color, size, shape, roundness, or other physical parameter. Zircon grains were analyzed at the (U-Th)/He Geo- and Thermochronometry Lab at the University of Texas at Austin using laser ablation high resolution inductively coupled plasma mass spectrometry (LA-HR-ICP-MS). This involved loading of sample mounts into a large-volume Helex sample cell system and analyzing them with a magnetic sector, single collector Element2 HR-ICP-MS attached to an Excimer laser ablation system (<http://www.jsg.utexas.edu/he-lab/u-thhe-and-upb-hr-icp-ms-lab/>).

The analytical procedure involved random selection of ~120 zircon grains, with placement of the laser ablation spot (diameter = 30  $\mu\text{m}$ ) on clean surfaces of individual grains, attempting to best avoid cracks, inclusions, and grain edges. With one exception

(SLL-03), 120 initial detrital grains were initially analyzed for all samples. Two age standards were analyzed to correct for inter-elemental fractionation: (1) GJ-1, with a known age of  $600.4 \pm 0.1$  Ma, and (2) the Plesovice standard (PL-1) with a known age of  $337.2 \pm 0.4$  Ma. All grains analyzed are subjected to an ablation pit, which produces a depth profile for the outermost layer of the grain (10  $\mu\text{m}$ ), rendering the technique sensitive to potential age or compositional zonation within individual grains.

Next, the data were reduced using Iolite software, an industry standard for U-Pb geochronology. Few grains showed clear overgrowths or age variation from rim to core; therefore, in most cases, both rim ages and core ages were taken into account in the data analysis. Analytical data are reported in Appendix 2. Results shown in this table are reported at the  $1\sigma$  level and include data with uncertainties less than 10% ( $1\sigma$ ) in  $^{206}\text{Pb}/^{238}\text{U}$ , <30% discordance, and <5% reverse discordance. Recognizing the strong signature of the Grenville/Sunsas orogeny in Bolivia, an age cut-off age of 950 Ma was applied to determine the best age, with  $^{206}\text{Pb}/^{238}\text{U}$  ages reported for younger grains <950 Ma and  $^{206}\text{Pb}/^{207}\text{Pb}$  ages reported for older grains >950 Ma.

U-Pb results are grouped according to formation units, including five stratigraphic units (9 samples) from Cenozoic basin fill as well as six pre-Cenozoic units (6 samples) representing potential sediment sources. In addition, we include results from a sample of the Neoproterozoic-Cambrian Puncoviscana Formation analyzed by Escayola et al. (2011). All age data are plotted in relative probability distribution curves shown in Figure 11a.

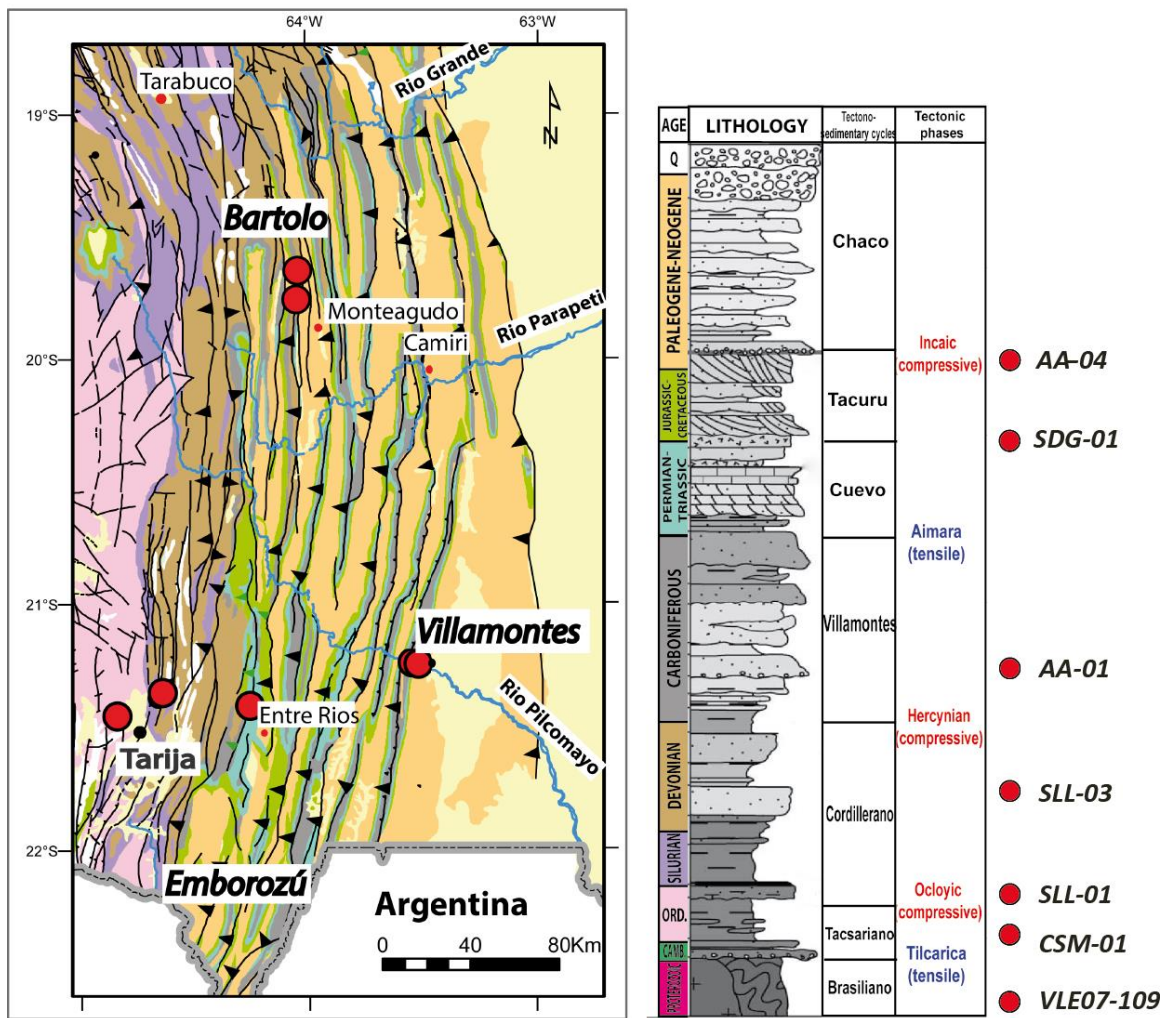


Figure 10. a) Location map of the potential source samples of the Cenozoic fill (red dots). b) Generalized stratigraphic column of Southern Bolivia (after Moretti et al., 1996), including stratigraphic position of the analyzed samples. Sample VLE07-109 from Escayola et al. (2011).

### Interpretation

The detrital zircon U-Pb results from Oligocene-Holocene samples reveal three main populations interpreted as signatures (detrital zircon “petrofacies”) of (a) recycled Amazonian craton (>1000 Ma), (b) recycled Andean orogen (<700 Ma), and (c)

Cenozoic magmatic arc (<70 Ma). These populations can be further subdivided according to known tectonomagmatic events of the Central Andes.

The Amazonian age population is mostly represented by grains ultimately derived from:

- (1) the Sunsas-Aguapei province (Grenville Gondwana counterpart) (1300-950 Ma; Litherland and Bloomfield, 1981; Ramos, 2010; Texeira et al., 2010), extensively imprinted in the Guaporé craton, and the Arequipa-Antofalla terrane. A strong detrital zircon signature of this age is documented in the Neoproterozoic –Cambrian Puncoviscana (San Cristobal) Formation (Adams et al., 2011; Toselli et al., 2012).
- (2) the Rondonian-San Ignacio province (1.56-1.30 Ga; Bettencourt et al., 2010). This province is one of the most important areally extensive source regions in eastern Bolivia (Matos et al., 2010).
- (3) the Rio Negro-Jurena province (1.8-1.5 Ga), broadly distributed across SSE Brazil, but not represented in the Arequipa-Antofalla terrane (Loewy et al., 2004); and,
- (4) the Ventuari-Tapajos province (2 - 1.8 Ga), a signature present in both the Guaporé craton and the Arequipa-Antofalla terrane.

Age populations characterizing the recycled Andean signature include the following:

- (1) Pampean/Tilcarian signature (700-520 Ma), widely recognized in the Eastern Cordillera, Altiplano/Puna, Subandean zones of northern Argentina, Chile, Perú and northern regions (Chew et al., 2008; Escayola et al., 2011; Reimann et al., 2010; Ramos, 2008; Leier et al., 2010; Hauser

et al., 2011; Bahlburg et al., 2011; McLeod et al., 2013) and in some SW inliers of the Amazon craton (Litherland et al., 1989),

- (2) Famatinian signature (500-465 Ma) documented in NW Argentina during the deposition of volcaniclastic sediments on the area between the Pampean block and the southern edge of the Arequipa-Antofalla terrane (Ramos, 2008); and finally by
- (3) Ocloyic signature (~476-434 Ma), evidenced by uplift/metamorphism of granitic intrusions of northern Chile and deformation of the Proto-Cordillera of the region between Chile and northern Argentina (Bahlburg et al., 1994; Bahlburg and Hervé, 1997, Loewy et al., 2004). This assemblage is considered the main source area during the Ordovician (Egenhoff and Lucassen, 2003) and until the Devonian (Sempere, 1995).
- (4) Cenozoic detrital zircon ages (65-0 Ma), are ascribed to first-cycle volcanic zircon derived from the evolving Andean magmatic arc (Wotzlaw et al., 2011).

In considering the U-Pb age distributions of potential sources areas (Figure 11a), several key trends can be observed. Directly capping granitic basement, at the base of the sedimentary cover succession, a diluted Sunsas/Grenville signal (1200-950 Ma) is expressed in the Neoproterozoic-Cambrian Puncoviscana Formation and followed upsection by a strong Pampean (700-600 Ma) fingerprint. Upsection, the Lower Ordovician, Upper Ordovician and Devonian samples display a very limited population of recycled Amazonian petrofacies, constraining a recycled Andean petrofacies (700-350 Ma). This composite population (Figure 11b) show a systematic shift in detrital zircon ages further upsection, with the loss of older Pampean ages, identified as petrofacies P1 (680-655 Ma), P2 (655-635 Ma), and P3 (630-600 Ma) in the lower Ordovician), and the

strengthening of younger ages as petrofacies P4 (595-580 Ma) and P5 (550-540 Ma), trends that are coupled with an input of exotic Famatinian (490-470 Ma) and less pronounced Ocloyic (465-445 Ma) signals. Next, the U-Pb geochronologic record of Carboniferous to Cretaceous samples is marked by a recovering Amazonian population (more prominent in the Cretaceous sample), which is largely restricted to the Sunsas/Grenville signal. Pampean petrofacies are represented only for two persistent petrofacies (P3, P4), and a less-persistent P5 petrofacies during the Triassic. As observed in the Devonian samples, a very incipient Famatinian signal is also documented for the late Paleozoic-Mesozoic samples (Figure 11b).

The Oligocene-lower Miocene Petaca Formation has conspicuous younger Pampean ages (P3= 630-600 Ma, P4 = 595-580 Ma, and P5 = 550-445 Ma; Figure 11b), as well as a nearly continuous record of younger recycled Amazonian grains from 1800-1000 Ma (Figure 11a), with the strongest peak at 1050 Ma of Sunsas/Grenville affinity. The persistent recycled Amazonian signal, along with the paleocurrent trends at the time of deposition suggest an important source located in eastern regions (likely the Guaporé craton exposed in the SW portion of the broader Amazonian craton). The consistent identification of Neoproterozoic ages representative of a Pampean signal, until the upper Ordovician, may indicate a recycled origin. Tentatively, Triassic strata may be suggested as a potential source unit, since the Petaca Formation preserves the same Pampean detrital zircon petrofacies (P3-P4-P5) but lacks the Famatinian signature. However, the restricted areal distribution of the Triassic deposits, currently limited to a north-south belt in the Subandean zone (Oviedo, 1974), questions its potential as a major unique source for the Petaca Formation, which is distributed across the Subandean-Chaco region. Alternatively, a recycled source area of Paleozoic-Mesozoic age prominently expressed to the east, near the Amazon craton (with progressive eastward pinchout toward the Alto

del Izozog) could represent a more plausible source area. Nonetheless, the question of whether pre- Cenozoic deposits (Cretaceous) constituted the dominant source has not been fully elucidated yet, and should be better constrained by further paleogeographic reconstructions.

The overlying Upper Miocene Tariquia Formation displays a relatively diluted Amazonian craton petrofacies limited to Sunsas/Grenville peak at 1050 Ma (Figure 11a), a more robust Pampean representation attributed to petrofacies P2, P3, P4 and P5 (655-540 Ma), and a pronounced Famatinian signal (490-470 Ma; Figure 11b). The Sunsas/Grenville signal suggests a combination of different Paleozoic and Mesozoic sources. The widespread distribution in the Tariquia of well-rounded, nearly spherical monocrystalline quartz grains, typical of the Mesozoic eolian units (Ichoa Formation), implicates the Cretaceous section as one of the potential sources. However, this hypothesis is not completely supported due to different U-Pb Pampean distributions. The input of older and younger U-Pb zircon populations with respect to Petaca, P4 and Famatinian, respectively, mark a broadening, or capture, of different sources. For instance, unusual older Pampean ages (P4) are restricted to Ordovician deposits, whereas Famatinian prominent signal is characteristic of Devonian and Triassic rocks. Therefore, the observed populations are interpreted as a mixing of at least three sources, most likely associated with Ordovician-Cretaceous rocks exposed in western sources. Therefore, the Tariquia Formation is a fundamental unit that marks the initial uplift/unroofing of the Andes.

Input of older Pampean petrofacies (P1, 680.655 Ma) characterizes the lower Pliocene Guandacay Formation. Recycled Amazonian craton petrofacies continue to be relatively underrepresented in the record (Figure 11a). The strong lower Pampean petrofacies can be ascribed solely to lower Ordovician sources, and the similarity and

continuous distribution with results from the underlying upper Miocene deposits, suggest a similar orogenic source area with continued exhumation of lower Ordovician deposits. Given the geological distribution of older Ordovician strata in the Eastern Cordillera, it is interpreted that the lower Pliocene fill of the Subandean basin was the product of major sediment delivery from the lower stratigraphic levels of the Eastern Cordillera.

The significant loss of Pampean peaks in the Pleistocene Emborozú Formation is compensated by the increased importance of Cenozoic arc petrofacies (<67Ma; Figure 11a). Due to the areal restriction of this coarse-grained Emborozú deposits, it mostly reflects (Figure 11b) nearby sources (likely <60 km) such as: younger Puncoviscana deposits (P4: 595-580 Ma), granitic intrusions (e.g. Rejará) represented by petrofacies P5 (550-540 Ma), and Devonian deposits (Famatinian signature; ~475 Ma). Despite the restricted location of this unit and hence detrital zircon distribution, it elucidates modifications to the catchment areas during the Quaternary, with the capture and recording of representative Cenozoic arc petrofacies, located more than 100 km to the west.

Finally, the Holocene fluvial megafans deposits depict a complete distribution of detrital zircon petrofacies. Pampean (P4, P5), Famatinian, Ocloyic, Cenozoic arc, and less distributed recycled Amazonian craton petrofacies (Figures 11a and 11b) are all recognized in the population. This distribution appears to confirm the simultaneous contribution of sediments derived from the Eastern Cordillera, Interandean and Subandean and reflects the ongoing exhumation/unroofing of these zones. However, some degree of recycling of Cenozoic basin fill is considered likely. Ultimately, these data help decipher the temporal shifts in source areas and support the basin evolution model.

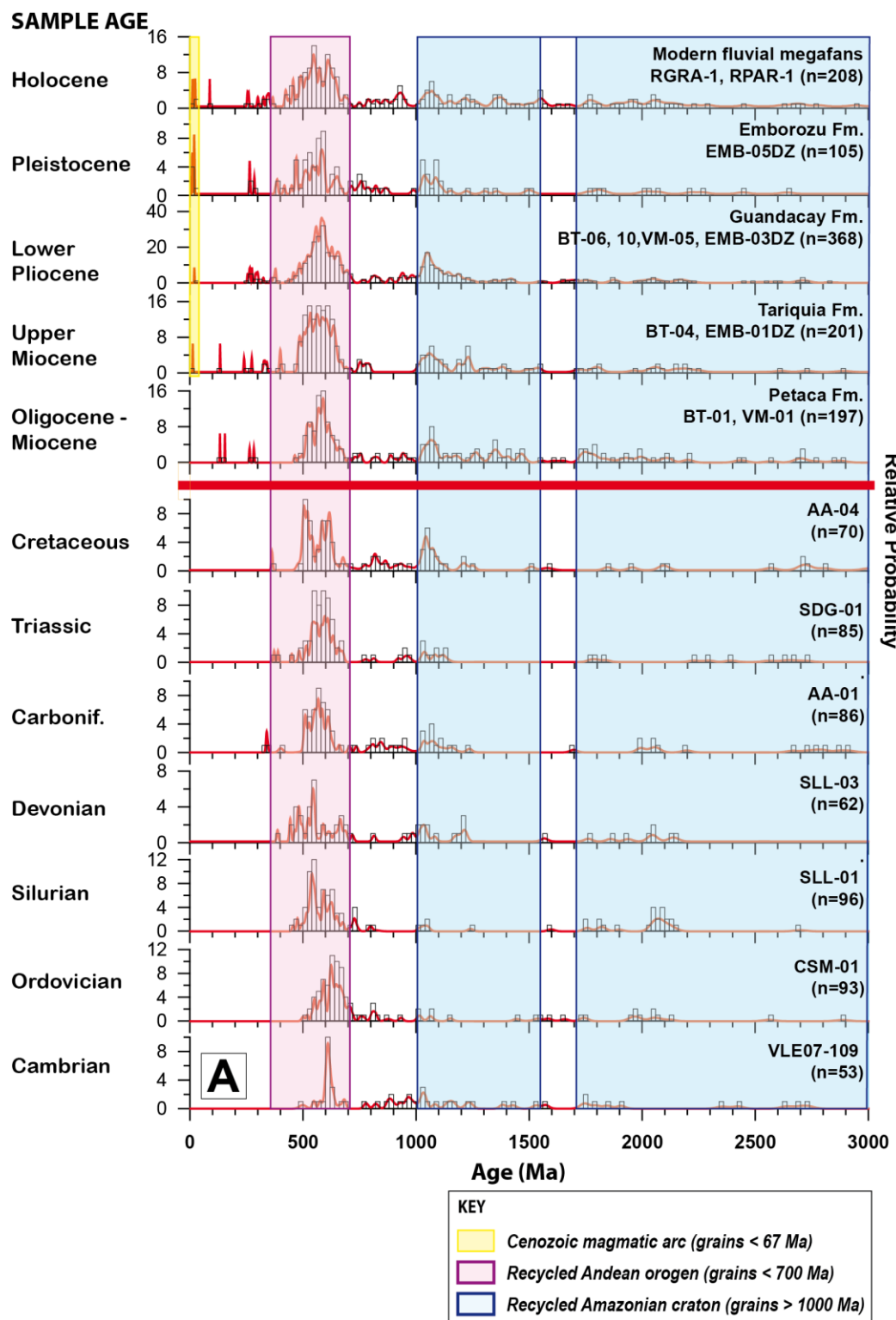


Figure 11.

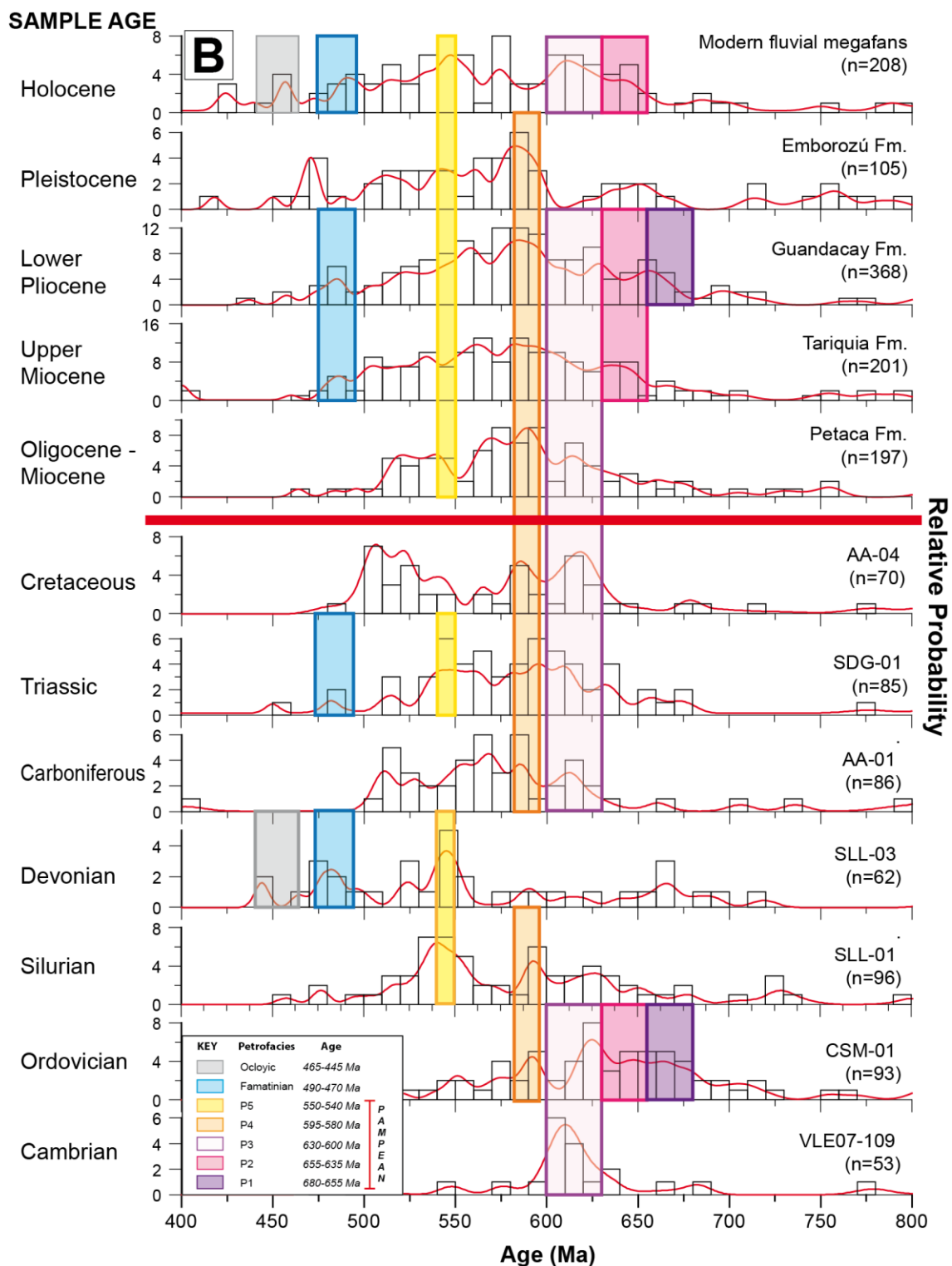


Figure 11.

Figure 11. a) Detrital zircon U-Pb spectra for Cenozoic sandstones (above red line) from the Subandean basin and modern fluvial megafans, and potential Paleozoic-Mesozoic source units (below red line) from 0-3000 Ma, and b) 400-800 Ma. Sample VLE07-109 has been analyzed previously by Escayola et al. (2011). Samples are a) Three main populations signature interpreted as recycled Amazonian craton, recycled Andean orogeny and derived from the Cenozoic magmatic arc. b) Upsection (Pliocene) increase of older Pampean ages coupled to younger (Ocloyic-Famatinian) signatures suggest a protracted unroofing of older Andean segments (Eastern Cordillera, Interandean zone).

## CHAPTER 4. U-PB GEOCHRONOLOGY AND MAGNETOSTRATIGRAPHY

### *U-Pb geochronology of volcanic horizons*

U-Pb geochronological results from two ash-fall tuffs and one reworked tuff from the Tariquia and Guandacay formations shed light on the poorly dated depositional history of the central Andean foreland basin. Although one tuff from the Bartolo section was dated previously (Erikson and Kelley, 1995), it was collected for more accurate dating in order to constrain the depositional age of the westernmost Subandean basin fill. Analyses were performed at the (U-Th)/He Geo- and Thermochronometry Lab at the University of Texas at Austin using laser ablation high-resolution inductively coupled plasma mass spectrometry (LA-HR-ICP-MS). The procedure for mineral separation and mounting for the two primary tuffs was the same as that for detrital zircons. For the reworked tuff sample, the analysis was focused on euhedral, inclusion-free grains that were individually picked and mounted.

The stratigraphically lowest sample, collected from the lower Bartolo section, shows limited reworking (Figure 5a). The reworked Camiri tuff was sampled ~5 km SSE of Camiri along the Camiri-Salinas highway. The Quebrada Seca ash-fall tuff was taken from Quebrada Seca creek in the footwall of the Mandiyuti thrust, roughly 32 km northwest of Villamontes. The oldest analyzed sample, exposed in Bartolo (BT-01Tb), has a weighted mean age of  $20.8 \pm 0.4$  Ma ( $n = 37$  U-Pb zircon grains). The reworked tuff near Camiri (CM-01) has a weighted mean age of  $8.42 \pm 0.3$  Ma ( $n = 21$  U-Pb zircon grains). The Quebrada Seca ash fall tuff (QSC-01) has a weighted mean age of  $3.8 \pm 0.1$  Ma ( $n = 38$  U-Pb zircon grains).

According to the U-Pb results from the lower Miocene Bartolo tuff near the eastern boundary of the Interandean zone, we estimate the propagation of the deformation

front from the Interandean zone to Subandean zone at ~20-15 Ma, on the basis of estimated accumulation rates. The other two tuff ages further constrain the late Miocene to Pliocene ages for deposition and facies migration in the Subandean region, supporting a proposed reconstruction of basin evolution.

### ***Magnetostratigraphy***

#### **Methods**

An updated magnetostratigraphic analysis was carried out on paleomagnetic samples from the Villamontes section of the easternmost Subandean zone. The original paleomagnetic cores were collected by Dr. Brian Horton and Nicholas Perez from the Angosto del Pilcomayo section, which was first measured by Uba et al. (2005). A total of 207 paleomagnetic sites were collected, with each site consisting of a minimum of three core samples (labeled as A, B, C). To more accurately constrain accumulation rates for the middle-upper Miocene section, we supplemented the original demagnetization measurements and magnetic polarity analyses of Perez (2009). At the Paleomagnetics Laboratory at the University of Texas at Austin, we analyzed one additional set of samples (C samples) and incorporated these new results with the original dataset (A and B samples) of Perez (2009). A total of three sample sets (A, B, and C samples) comprise the updated database; each core sample was subjected to a series of thermal demagnetization steps at progressively higher temperatures (e.g., 0, 100, 200, 300, 400, 450, 475, 500, 525, 550, 575, and 600°C), with measurements carried out following techniques outlined by Perez (2009), following the methodology of Butler (1992).

The complete thermal demagnetization dataset was reduced using PaleoMag software v.3.1b2. Representative primary magnetization vectors were chosen using at least three consecutive temperature steps in tilt-corrected Zijderveld diagrams and corresponding

stereographic projections. We then compared the individual vector results from the three sample for each paleomagnetic site and assigned variable letter codes on the basis of a predominantly normal ( $0^\circ \pm 45^\circ$ ) or reverse ( $180^\circ \pm 45^\circ$ ) polarity direction. Three informal codes were chosen: code A for cases where all three samples yield the same polarity; code B when two samples display the same polarity; and code C when the data lacked internal consistency and appeared random. Code C data were excluded from further consideration. Code A and B data were used to construct a magnetic polarity stratigraphy for the Villamontes section (Figure 12). We then considered various potential correlations of the Villamontes magnetic polarity data with individual chrons and subchrons of the Geomagnetic Polarity TimeScale (GPTS) of Gradstein et al. (2012). Figure 12 shows our preferred correlation, along with a least-squares stratigraphic plot that provides the basis for calculation of sediment accumulation rates through time. Temporal variations in accumulation rate are displayed in Figure 12d.

### **Results and interpretation**

The magnetic polarity stratigraphy of the Villamontes section reveals a drastic increase in sediment accumulation rates during the late Miocene. Whereas the middle Miocene Yecua Formation is characterized by an accumulation rate of 20 m/Myr (2 cm/kyr), late Miocene rates achieve values of 110 m/Myr. During deposition of the upper Miocene Tariquia Formation, the accumulation increased by nearly an order of magnitude to 880 m/Myr, before decreasing to 250 m/Myr. Comparable rates of accumulation are calculated on the basis of age data for intercalated volcanic ashes in the section (Figure 12d).

The late Miocene increase in sedimentation rates for the Villamontes section could be associated with climatic variability (monsoon activity), increased sediment delivery, and/or accelerated tectonic subsidence as proposed by (Echavarria et al., 2003;

Ege et al., 2007; Uba et al., 2007; Mulch et al., 2010). However, the implications of these results at a regional scale remain unclear, as shifts in sediment accumulation could be variably attributed to these different processes or a plausible interrelation of various processes. The results from thermochronologic analyses for the Subandean zone have not been definitive, largely owing to the apparent lack of sufficient overburden to fully reset apatites for apatite fission-track thermochronology (e.g., Ege et al., 2007; Barnes et al., 2008). Further detailed analyses using lower temperature thermochronometers, such as apatite (U-Th)/He techniques, should shed light on the unroofing history of the Subandean zone and better discriminate among competing tectonic vs. climatic interpretations.

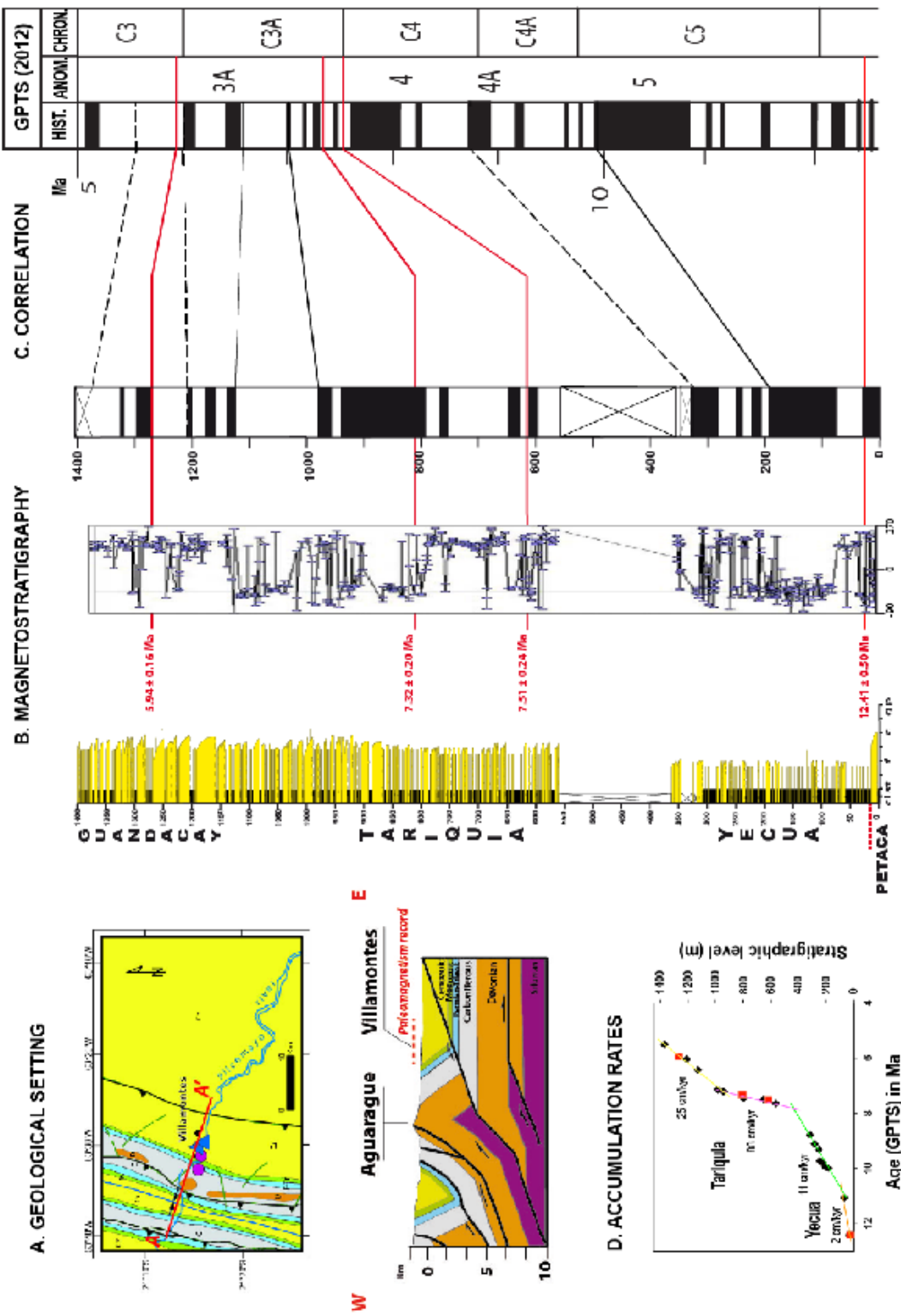


Figure 12.

Figure 12. a) Location of the Angosto del Pilcomayo section in the eastern Subandean region, structural configuration of the nearby area (after Dunn et al., 1995). b) Stratigraphic section and U-Pb tuff ages (Uba et al., 2005), observed declination values and interpreted polarity zones with normal (black) and white (reverse) polarity intervals. c) Correlation of the polarity column with the Geomagnetic Polarity Scale (2012) (Gradstein et al., 2012). Tuff ages have been used to constrain the correlation. d) Accumulation rate diagram resulting from interpreted chrons and subchrons correlation, and compared with predicted tuff age-derived sedimentation rates. A very significant increase in the accumulation rates (from ~10 cm/kyr to ~90 cm/kyr is interpreted in the upper Miocene.

## CHAPTER 5. CENOZOIC BASIN RECONSTRUCTION AND DISCUSSION

The Cenozoic depositional record of the Subandean zone and Chaco foreland basin reflects the cratonward advance of Andean retroarc shortening from the Oligocene to present. A new interpretation presented here is based on a synthesis of lithofacies assemblages, new and previous isotopic ages for interbedded tuffs, paleocurrents, conglomerate clast compositions, sandstone mineralogy, and detrital zircon U-Pb age populations for two clastic nonmarine successions in the western Subandean zone. These data are integrated with new age control from a pilot magnetostratigraphic study to propose a schematic evolution of the foreland basin system of southern Bolivia (Figure 13).

### *Oligocene-Miocene boundary (~23 Ma)*

Low-sinuosity braided fluvial systems represented by fine-grained sandstones (subarkoses) with subordinate conglomerates and thin mudstones were deposited at this time, coeval with development of pervasive paleosols (calcretes and silcretes) (Uba et al., 2005). These clastic sediments were likely deposited in a distal, back-bulge depozone in which subsidence was associated with flexural loading in hinterland regions to the west. These deposits are considered the distal equivalent of a more proximal foreland basin preserved in the Eastern Cordillera (Horton and DeCelles, 1997; DeCelles and Horton, 2003; Uba et al., 2005). This timeframe is marked by low rates of aggradation coupled with a relatively arid climate. Interpretation of a westward pinchout of these distal deposits is evidenced by a condensed (<50 m-thick) succession preserved in the northern section of the Bartolo locality. Paleocurrent measurements show sediment transport from east to west (Uba et al., 2005; Hulka and Heubeck, 2010), indicative of an eastern source

area in the distal foreland (Figures 9 and 13a). Moreover, U-Pb detrital zircon ages are limited to the 445-1050 Ma span, with the most important signals represented by the younger Pampean (630-445 Ma) and Sunsas/Grenville (1050 Ma) ages representative of basement ages in the westernmost segments of the Amazonian craton.

A comparison of detrital age distributions suggests that the provenance signatures are not exclusively recycled from the underlying Cretaceous section. Dissimilar Pampean populations characterize the Cretaceous and the upper Oligocene-lower Miocene units, though they have comparable Sunsas/Grenville signatures. The persistence of a recycled Sunsas/Grenville population coupled with west-directed paleocurrents and subarkose sandstone compositions support an eastern cratonic source area. However, the differences within the Pampean signatures suggest a slight departure from this simple interpretation in which cover strata from non-basement source areas, also potentially in the east, may have contributed sediments to this distal part of the foreland basin. A better understanding of the pre-Cenozoic basin configuration should shed light on the sediment dispersal patterns and further constrain different source areas in the east.

Despite the apparent dominance of eastern, non-orogenic sources, there is evidence for coeval deformation farther to the west, including possible motion on the Main Interandean thrust that may reflect eastward advance of the Andean fold-thrust wedge and associated initial exhumation along this zone (Ege et al., 2007; Barnes et al., 2008). A further record of more-proximal wedge-top and foredeep deposits (e.g., Camargo, Incapampa) helps define an older segment of the foreland basin system in the Eastern Cordillera (Horton and DeCelles, 2001; Horton, 2005).

### **~23–20 Ma**

This time frame is marked by suspended-load deposition of fine-grained sand and mud in avulsive, ribbon-shaped fluvial channels. From the early Miocene onward, the paleoflows record a mean transport direction from west to east (Hulka and Heubeck, 2010). This period is also marked by the appearance of submature lithic sandstones. The common framework lithic fragments are of metasedimentary origin, with minor proportions of volcanic lithic grains. The presence of subrounded metasedimentary lithic fragments may indicate recycling of preexisting lithic fragments. Thus, the source area may potentially represent lithic-rich sandstones from Carboniferous and Silurian units (Schonian and Egenhoff, 2007). The stratigraphic architecture of ribbon sandstone bodies encased in overbank facies suggests deposition in low-gradient fluvial settings, with a probable increase in aggradation rates.

Eastward advance of the Main Interandean thrust may have triggered similar activation and propagation of additional east-directed thrust sheets along with continued crustal shortening and exhumation in the Interandean Zone. Collectively, the combination of an influx of lithic fragments, reversal in paleocurrents, and associated depositional setting indicates (1) a change to a western provenance area associated with the Interandean Zone, (2) initiation of a major depocenter on the eastern flank of the Interandean Zone, and (3) deposition in a distal foredeep setting.

### **20–6 Ma**

Diachronous deposition of braided-fluvial systems, potentially including channels of fluvial megafans in the proximal foreland basin (Uba et al., 2005), is documented consistently in two sections of the western Subandean zone. New and previously dated interbedded tuffs and a nearly ten-fold increase in sediment accumulation rates in the late Miocene help constrain the evolution of the orogenic wedge. A general eastward flow is

recorded in available deposits. The introduction of clasts derived from middle and upper Paleozoic rocks suggests proximal sources corresponding to older segments of the Interandean zone. Additionally, detrital zircon U-Pb age signatures are characterized by the progressively enhanced input of older Pampean ages (from 550 Ma to 655 Ma) relative to younger Famatinian (490-470 Ma) signatures.

The integrated results suggest progressive diachronous deposition of lithic-rich sandstones in braided and mixed braided-meandering fluvial channels in the western zones, coeval with meandering-anastomosing fluvial counterparts in the distal foredeep (Villamontes, Charagua, Abapo, etc.) (Uba et al., 2005). Evidence for the introduction of progressively younger rocks in the sediment source areas, as documented by conglomerate counts and detrital zircon age populations, lead us to interpret (1) protracted unroofing and sediment dispersal from the Eastern Cordillera–Interandean Zone commencing at ~20-15 Ma (as estimated from new tuff ages and accumulation rates) followed by (2) initial propagation of the deformation front into the Subandean Zone during the late Miocene, implying activation of the Main Subandean thrust. A temporal shift from axial to transverse fluvial drainage recorded by paleocurrent data reinforces the interpretation of an eastward advancing depocenter and progressive structural partitioning of the older segments of the Subandean foreland basin, particularly after 8 Ma.

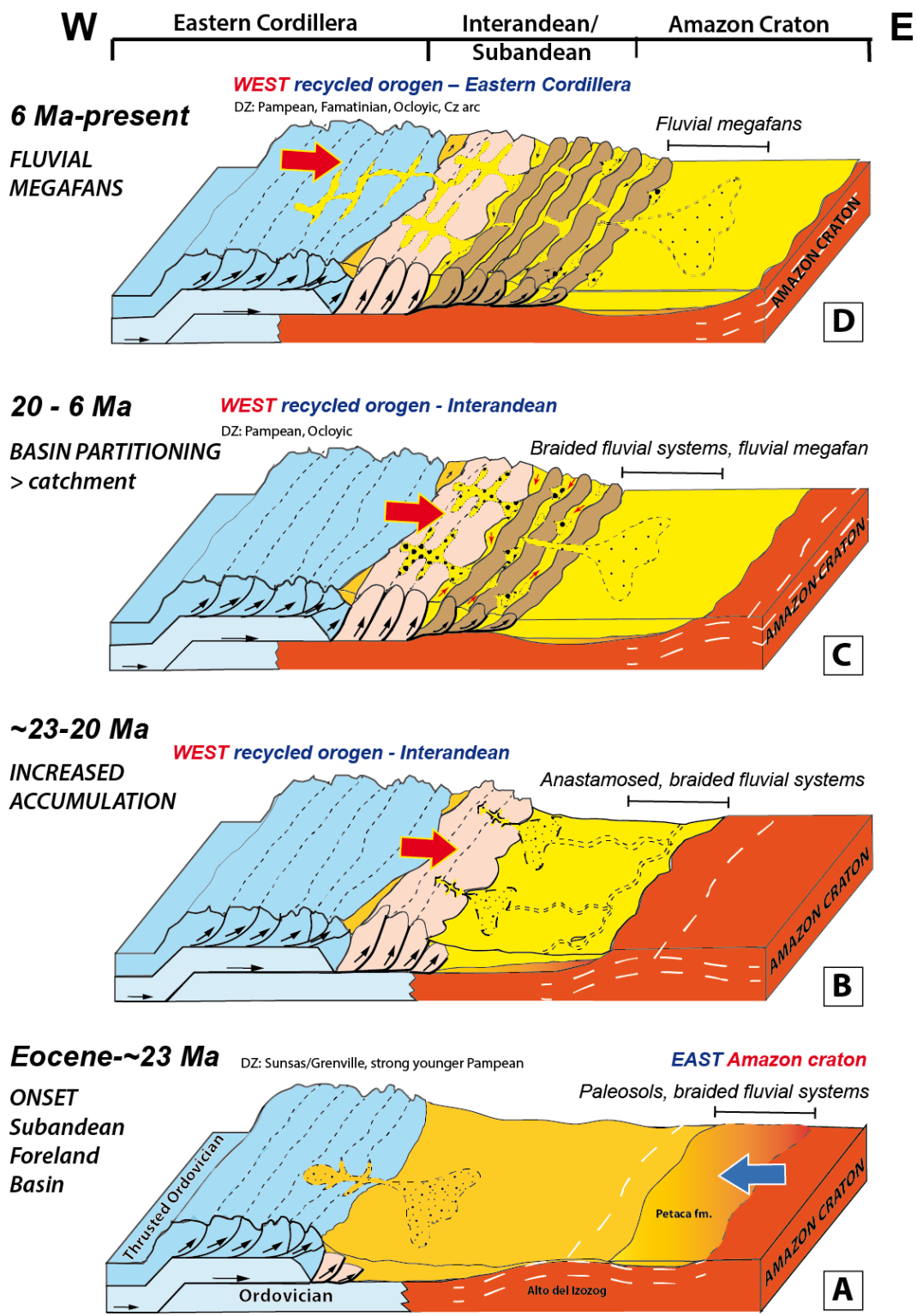


Figure 13.

Figure 13. Schematic regional diagrams illustrating the proposed Cenozoic depositional systems evolution in the Subandes and Chaco foreland basin, including the Interandean-Eastern Cordillera role as a source area

## ***6 Ma to present***

Gravelly–sandy braided channel systems dominate the depositional record from the latest Miocene to present. More-proximal sources are interpreted relative to older deposits, and attributed to alluvial fan and proximal fluvial megafan deposition (Horton and DeCelles, 2001; Uba et al., 2005; Hulka, 2005). Radial paleoflow patterns principally directed toward the east are characteristic of deposits of this age, as well as the current geomorphic distribution in the Chaco plain. Synorogenic deposition in wedge-top segments of the most-proximal basin are recognized along the eastern (frontal) margin of the fold-thrust wedge (Moretti et al., 1996; Uba et al., 2009). A diverse collection of detrital zircon U-Pb age spectra are represented by Pampean (655-540 Ma), Famatinian (550-540 Ma), Ocloyic (465-445 Ma), Cenozoic magmatic arc (<67 Ma) signature, as well as a Sunsas/Grenville (1300-1000 Ma). Differences between the detrital zircon populations of Pleistocene versus Holocene deposits are attributed to localized deposition of gravelly-braided channels in the western Subandes (Emborozú locality).

Continued exhumation and enhancement of the drainage area to the west (i.e., drainage expansion to include the Eastern Cordillera, Interandean Zone, and actively deforming Subandean zone) are interpreted to reflect changes to accumulation of coarser lithofacies in proximal areas (e.g., Emborozú locality), and delivery of significant sediment volumes to the Chaco plain. Modern fluvial megafans (Pilcomayo, Parapeti and Grande) in fact are the repository of Holocene sediments which have an estimated volume of  $\sim 6.4 \times 10^4 \text{ km}^3$  (Barnes et al., 2009).

## CHAPTER 6. CONCLUSIONS

Analyses of Cenozoic stratigraphic variations and sediment provenance within two proximal successions of the western Subandean zone (Bartolo and Emborozú localities) at 19-21°S in southern Bolivia provide insights into synorogenic sedimentation in a foreland basin generated by eastward advance of the central Andean fold-thrust system responsible for crustal thickening, loading, and flexural subsidence. New and previously published zircon U-Pb geochronological data for interbedded Miocene tuffs and updated magnetostratigraphic results constrain an assessment of the linkages between surface processes, tectonics, catchment-area modification, and potential climate change in this thin-skinned fold-thrust belt and coupled foreland basin.

1.- The Cenozoic sedimentary record preserved in the Bartolo and Emborozú sections provide information on the eastward progradation of upward-coarsening successions and fluvial megafan deposits. Sedimentological analyses of lithofacies and facies associations support the interpretation of initial mid-Cenozoic deposition of a braided-fluvial system with substantial pedogenic processes. Upsection shifts to more distal Miocene facies associated with anastomosed fluvial systems, followed by mixed braided-meandering fluvial systems, sandy-gravelly braided systems, and ultimately proximal alluvial-fan deposits reveal the progressive eastward migration of depositional systems and their increasing proximity to positive topography and sediment source areas.

2.- U-Pb ages for interbedded tuffs within the Tariquia and Guandacay formations provide key temporal constraints for eastward advance of shortening from the Interandean to Subandean zone. These results help constrain the migration of foreland basin depozones and the timing of Subandean fold-thrust deformation. A zircon U-Pb age of  $20.8 \pm 0.4$  Ma for a key tuff horizon in the Tariquia Formation (Bartolo locality) marks

early Miocene accumulation in the Subandean fold-thrust belt. A second tuff from the Tariquia Formation near the city of Camiri in the eastern Subandean zone yields a U-Pb age of  $8.42 \pm 0.1$  Ma. These tuff ages support a proposed spatiotemporal evolution of depositional systems and migration of sedimentary facies from 20 to 8 Ma. A younger tuff preserved in the middle Guandacay Formation near the Pilcomayo river (Quebrada Seca) in the eastern Subandean zone yields a U-Pb age of  $3.8 \pm 0.1$  Ma. This indicates a Pliocene depositional age and demonstrates the continuous history of late Cenozoic deposition for the youngest and coarsest facies in the foreland basin of southern Bolivia.

3.- Sediment provenance information derived from sandstone petrography, conglomerate clast compositions, and paleocurrent data indicate a dramatic shift in source areas from Oligocene to Holocene time. During the late Oligocene-early Miocene, quartzose sandstones with a significant percentage of feldspars were derived from a continental source region consisting of the Amazonian craton and/or pre-Cenozoic strata rich in feldspar. Upsection changes toward lithic-rich sandstones with variable proportions of recycled volcanic lithic, metasedimentary lithic, and predominantly sedimentary lithic fragments at the top reveal a shift in the principal sediment source region to an Andean recycled orogen provenance. Conglomerate clast compositions, in turn, differentiate the introduction of early-mid Paleozoic clasts reflecting a normal unroofing pattern of the Interandean zone and potential displacement on the Main Interandean thrust. The upsection introduction of a late Paleozoic clast population is associated with additional thrusting near the Interandean-Subandean boundary, with reorganization and possible (headward) expansion of the catchment area. Finally, an updated database on sediment dispersal patterns reveals a pronounced mid-Cenozoic reversal in paleocurrents. An of  $\sim 180^\circ$  azimuthal variation in paleocurrents for the middle Miocene–Pliocene interval of the Emborozú section is interpreted as a signal of axial

(north-south) paleoflow followed by reestablishment of a drainage system characterized by transverse (east-west) flow.

4.- New detrital zircon U-Pb ages from Cenozoic sandstones demonstrate cratonic then Andean sediment sources with enhancement of montane catchment areas. A recycled Pampean (540-655 Ma) age signature persists throughout the Cenozoic succession, somewhat obscuring unambiguous identification of discrete source units. For the upper Oligocene-Miocene Petaca Formation, U-Pb ages reveal a significant recycled Amazonian (1800-1000 Ma) signature indicative of a basement craton provenance. However, the remaining younger Pampean populations (P4 and P5; 540-595 Ma) suggest an additional or alternative source in the foreland near the Paleozoic-Mesozoic exposures of Alto del Izozog. Upsection, the progressive Miocene introduction of older Pampean ages (P1, P2; 680-635 Ma) and a Famatinian signature (490-470 Ma) indicates incorporation of orogenic material derived from the Interandean zone and Eastern Cordillera. For modern sediments, Andean exhumation and drainage patterns are reflected in diverse detrital zircon spectra: Pampean (655-540 Ma), Famatinian (550-540 Ma), Ocloyic (465-445 Ma), Cenozoic magmatic arc (<67 Ma) signature, and Sunsas/Grenville (1300-1000 Ma) and signatures.

5.- Syntheses of lithofacies assemblages, isotopic ages of interbedded tuffs, paleocurrents, conglomerate clast compositions, sandstone mineralogy, and detrital zircon U-Pb age populations for two sections in the westernmost Subandean zone, combined with updated magnetostratigraphic results, support a reconstruction of the Oligocene to Holocene evolution of the Subandean zone and Chaco foreland basin. The reconstruction proposes: (1) late Oligocene-early Miocene accumulation of cratonic sediment in a back-bulge depozone generated by flexural loading in the older, Eastern Cordillera sector of the Andean fold-thrust belt; (2) early Miocene initiation of distal

foredeep depozone in the western Subandes associated with flexural subsidence of the developing Interandean fold-thrust system and consequent establishment of new sediment sources; (3) widespread middle-late Miocene deposition and increased aggradation in a flexurally subsiding foredeep depozone, with continued sediment delivery from the Interandean zone and eastward propagation of shortening into the Subandean zone (initial displacement on the Main Subandean thrust); and (4) Pliocene to Holocene structural partitioning of the proximal foreland basin along with westward (headward) expansion of the montane drainage areas (encompassing the western Subandean zone, Interandean zone, and Eastern Cordillera), resulting in deposition of large fluvial megafans in the Chaco plain.

## Appendix 1. Recalculated modal point-count data from the Bartolo locality

Unit	Sample	Level (mabs)	QFL (%)			QmFLt (%)			QmPK (%)			LmLvLs (%)		
			Q	F	L	Qm	F	Lt	Qm	P	K	Lm	Lv	Ls
Petaca	<b>BT-01PF</b>	9.0	90.9	9.1	0.0	85.1	9.1	5.8	90.3	2.1	7.6	77.8	0.0	22.2
	<b>BT-02PF</b>	21.8	75.9	24.1	0.0	75.9	24.1	0.0	75.9	13.6	10.5	0.0	0.0	0.0
	<b>BT-03PF</b>	44.8	83.6	16.4	0.0	82.2	16.4	1.4	83.3	5.1	11.6	100.0		
	Average		83.4	16.6	0.0	81.0	16.6	2.4	83.2	6.9	9.9	88.9	0.0	11.1
	Std. Deviation		36.5	8.9	0.0	35.3	8.9	2.4	36.4	5.2	4.5	42.9	0.0	10.5
Tariquia	<b>BT-05PF</b>	194.7	73.8	9.3	16.9	72.0	9.3	18.7	88.5	1.6	9.8	13.8	27.6	58.6
	<b>BT-06PF</b>	263.0	87.6	5.2	7.1	87.1	5.2	7.6	94.3	0.5	5.2	9.1	9.1	81.8
	<b>BT-08PF</b>	380.0	87.9	2.6	9.4	84.9	2.6	12.5	97.0	0.0	3.0	25.8	9.7	64.5
	<b>BT-02</b>	437.0	81.9	4.4	13.7	78.6	4.4	16.9	94.7	0.5	4.9	20.0	7.5	72.5
	<b>BT-04</b>	567.0	90.7	4.8	4.5	86.2	4.8	9.0	94.7	0.8	4.5	50.0	23.1	26.9
	<b>BT-12PF</b>	491.4	93.0	3.7	3.3	90.6	3.7	5.7	96.1	0.0	3.9	40.0	53.3	6.7
	<b>BT-17PF</b>	1037.3	88.3	4.3	7.4	86.3	4.3	9.4	95.3	1.3	3.4	20.8	0.0	79.2
	<b>BT-19PF</b>	1198.7	89.7	8.0	2.3	84.0	8.0	8.0	91.3	0.8	7.9	71.4	9.5	19.0
	<b>BT-21PF</b>	1444.4	94.3	3.8	1.9	88.2	3.8	8.0	95.9	0.0	4.1	76.5	11.8	11.8
	<b>BT-22PF</b>	1595.0	97.2	2.5	0.4	95.1	2.5	2.5	97.5	0.0	2.5	85.7	0.0	14.3
	Average		88.4	4.9	6.7	85.3	4.9	9.8	94.5	0.6	4.9	41.3	15.2	43.5
	Std. Deviation		6.3	2.1	5.1	6.0	2.1	4.7	2.6	0.6	2.2	26.6	15.2	28.9
Guandacay	<b>BT-24PF</b>	1710.5	95.7	1.1	3.2	93.9	1.1	5.0	98.9	0.0	1.1	35.7	21.4	42.9
	<b>BT-25PF</b>	1875.0	90.9	6.7	2.4	88.6	6.7	4.7	93.0	0.0	7.0	50.0	16.7	33.3
	<b>BT-26PF</b>	2060.1	75.7	15.8	8.5	70.3	15.8	13.9	81.7	0.4	17.9	40.9	9.1	50.0
	<b>BT-27PF</b>	2315.0	90.2	6.2	3.6	88.4	6.2	5.5	93.5	0.0	6.5	33.3	6.7	60.0
	<b>BT-28PF</b>	2564.9	88.8	3.6	7.6	85.6	3.6	10.8	96.0	0.0	4.0	30.0	36.7	33.3
	<b>BT-29PF</b>	2636.9	93.0	5.3	1.6	90.4	5.3	4.3	94.4	0.8	4.7	62.5	31.3	6.3
	Average		89.1	6.4	4.5	86.2	6.4	7.4	92.9	0.2	6.9	42.1	20.3	37.6
	Std. Deviation		6.4	4.6	2.6	7.5	4.6	3.7	5.4	0.3	5.3	11.1	10.9	16.8

\* mabs = meters above base section

## Appendix 2. LA-ICP-MS analyses for detrital zircon U-Pb geochronology

Analysis	Isotope ratios					Apparent ages (Ma)								
	207Pb*	± 1σ	206Pb*	± 1σ	error	206Pb*	± 1σ	207Pb*	± 1σ	206Pb*	± 1σ	Best age	± 1σ	Conc
	235U*	(%)	238U	(%)	corr.	238U*	(Ma)	235U	(Ma)	207Pb*	(Ma)	(Ma)	(Ma)	(%)
<b>CSM-01, Lower Ordovician Iscayachi Formation (N=93). 21.47°S, 64.83°W</b>														
CSM_01_14	0.6550	0.0	0.0808	0.0	0.60	501.0	7.1	511.0	5.1	578.0	19.4	501.0	7.1	86.7
CSM_01_80	0.6790	0.0	0.0841	0.0	0.29	520.8	3.3	526.0	3.3	546.0	10.7	520.8	3.3	95.4
CSM_01_57	0.7500	0.0	0.0872	0.0	0.15	539.1	3.8	567.9	3.2	637.0	11.2	539.1	3.8	84.6
CSM_01_73	0.7440	0.0	0.0888	0.0	0.44	548.4	4.3	565.0	6.6	603.0	21.9	548.4	4.3	90.9
CSM_01_7	0.7560	0.0	0.0890	0.0	0.80	550.0	5.1	572.4	4.1	629.0	7.1	550.0	5.1	87.4
CSM_01_75	0.7210	0.0	0.0894	0.0	0.66	552.1	4.4	551.3	4.5	543.0	10.7	552.1	4.4	101.7
CSM_01_9	0.7630	0.0	0.0899	0.0	0.26	555.2	3.8	575.4	3.4	642.0	11.2	555.2	3.8	86.5
CSM_01_45	0.7470	0.0	0.0913	0.0	0.48	563.2	4.0	566.3	3.8	596.0	11.2	563.2	4.0	94.5
CSM_01_16	0.7580	0.0	0.0927	0.0	0.60	571.3	3.7	572.3	3.1	574.0	8.7	571.3	3.7	99.5
CSM_01_34	0.7780	0.0	0.0927	0.0	0.73	571.6	4.1	584.0	4.3	609.0	8.2	571.6	4.1	93.9
CSM_01_88	0.8270	0.0	0.0938	0.0	0.66	578.0	5.1	611.6	4.3	718.0	9.7	578.0	5.1	80.5
CSM_01_65	0.7780	0.0	0.0938	0.0	0.45	578.2	3.1	583.8	3.1	587.0	9.2	578.2	3.1	98.5
CSM_01_67	0.7900	0.0	0.0953	0.0	0.56	586.6	3.5	590.9	3.5	611.0	8.7	586.6	3.5	96.0
CSM_01_17	0.7930	0.0	0.0959	0.0	0.07	590.0	6.6	592.0	5.6	595.0	17.9	590.0	6.6	99.2
CSM_01_69	0.7907	0.0	0.0961	0.0	0.49	591.5	2.9	591.4	2.0	597.0	5.6	591.5	2.9	99.1
CSM_01_8	0.7860	0.0	0.0962	0.0	0.58	592.3	3.9	589.6	3.8	599.0	9.7	592.3	3.9	98.9
CSM_01_49	0.8320	0.0	0.0961	0.0	0.66	592.8	4.3	614.3	3.5	679.0	8.2	592.8	4.3	87.3
CSM_01_24	0.8120	0.0	0.0967	0.0	0.19	594.7	4.6	603.0	5.1	638.0	13.3	594.7	4.6	93.2
CSM_01_40	0.8520	0.0	0.0967	0.0	0.42	595.0	6.1	624.0	8.7	781.0	26.5	595.0	6.1	76.2
CSM_01_1	0.8140	0.0	0.0977	0.0	0.37	601.0	6.1	602.0	9.7	629.0	22.4	601.0	6.1	95.5
CSM_01_104	0.8130	0.0	0.0978	0.0	0.74	601.0	13.3	603.0	7.7	585.0	20.9	601.0	13.3	102.7
CSM_01_41	0.8380	0.0	0.1008	0.0	0.44	618.8	4.3	619.2	3.8	633.0	10.2	618.8	4.3	97.8
CSM_01_38	0.8340	0.0	0.1009	0.0	0.35	619.0	6.1	618.0	7.1	622.0	17.9	619.0	6.1	99.5
CSM_01_79	0.8470	0.0	0.1008	0.0	0.60	619.0	5.6	622.5	4.4	648.0	10.2	619.0	5.6	95.5
CSM_01_103	0.8670	0.0	0.1010	0.0	0.21	620.0	5.6	634.0	6.1	681.0	19.4	620.0	5.6	91.0
CSM_01_81	0.8510	0.0	0.1012	0.0	0.32	621.0	5.1	625.0	6.1	664.0	26.0	621.0	5.1	93.5
CSM_01_102	0.8720	0.0	0.1013	0.0	0.75	622.0	8.2	637.0	6.1	685.0	9.7	622.0	8.2	90.8
CSM_01_13	0.8840	0.0	0.1015	0.0	0.37	624.6	5.0	643.9	3.7	717.0	10.7	624.6	5.0	87.1
CSM_01_82	0.9000	0.0	0.1016	0.0	0.24	626.0	6.1	651.1	4.8	710.0	21.9	626.0	6.1	88.2
CSM_01_3	0.8620	0.0	0.1021	0.0	0.58	626.4	4.9	631.6	3.6	663.0	8.7	626.4	4.9	94.5
CSM_01_101	0.8540	0.0	0.1022	0.0	0.70	627.0	6.1	626.5	3.7	633.0	8.2	627.0	6.1	99.1
CSM_01_70	0.8680	0.0	0.1022	0.0	0.37	627.1	4.2	633.9	4.1	666.0	11.2	627.1	4.2	94.2
CSM_01_68	0.8590	0.0	0.1024	0.0	0.81	628.1	4.8	630.1	3.4	633.0	7.1	628.1	4.8	99.2
CSM_01_30	0.8820	0.0	0.1032	0.0	0.61	633.1	3.9	642.1	3.1	674.0	6.1	633.1	3.9	93.9
CSM_01_37	0.8810	0.0	0.1033	0.0	0.25	633.5	4.5	642.4	4.7	677.0	10.7	633.5	4.5	93.6
CSM_01_60	0.8810	0.0	0.1034	0.0	0.61	634.0	5.6	641.0	4.7	681.0	11.2	634.0	5.6	93.1
CSM_01_76	0.8810	0.0	0.1049	0.0	0.68	642.7	4.6	641.9	3.8	649.0	7.1	642.7	4.6	99.0
CSM_01_43	0.8815	0.0	0.1050	0.0	0.53	643.5	3.1	642.2	2.2	630.0	6.1	643.5	3.1	102.1
CSM_01_12	0.8930	0.0	0.1051	0.0	0.57	644.0	4.4	647.4	3.1	646.0	6.6	644.0	4.4	99.7
CSM_01_78	0.8800	0.0	0.1053	0.0	0.69	645.4	4.8	641.6	3.3	636.0	7.7	645.4	4.8	101.5

CSM_01_66	0.8870	0.0	0.1051	0.0	0.57	646.0	7.1	644.2	4.3	675.0	13.3	646.0	7.1	95.7
CSM_01_26	0.8900	0.0	0.1061	0.0	0.49	650.2	3.9	646.1	3.5	640.0	9.7	650.2	3.9	101.6
CSM_01_15	0.9110	0.0	0.1065	0.0	0.29	652.0	6.6	656.0	5.6	669.0	16.3	652.0	6.6	97.5
CSM_01_52	0.8950	0.0	0.1066	0.0	0.54	652.9	3.4	648.5	3.0	642.0	8.2	652.9	3.4	101.7
CSM_01_11	1.0170	0.0	0.1072	0.0	0.14	656.2	4.9	713.0	6.1	871.0	23.0	656.2	4.9	75.3
CSM_01_62	0.9069	0.0	0.1077	0.0	0.46	659.5	3.0	655.2	2.5	641.0	7.1	659.5	3.0	102.9
CSM_01_77	0.9140	0.0	0.1082	0.0	0.46	662.0	5.1	658.8	4.0	654.0	9.7	662.0	5.1	101.2
CSM_01_44	0.9270	0.0	0.1086	0.0	0.48	664.5	3.2	665.4	3.5	674.0	9.2	664.5	3.2	98.6
CSM_01_97	0.9480	0.0	0.1087	0.0	0.30	665.2	4.6	676.8	3.7	721.0	12.2	665.2	4.6	92.3
CSM_01_21	1.0100	0.0	0.1089	0.0	0.38	666.1	3.4	711.7	4.7	854.0	13.3	666.1	3.4	78.0
CSM_01_42	0.9170	0.0	0.1091	0.0	0.46	668.0	5.6	660.2	4.5	644.0	11.7	668.0	5.6	103.7
CSM_01_35	0.9630	0.0	0.1103	0.0	0.09	674.0	9.7	684.0	10.2	705.0	17.3	674.0	9.7	95.6
CSM_01_54	0.9360	0.0	0.1102	0.0	0.78	674.0	5.6	670.1	4.9	653.0	7.1	674.0	5.6	103.2
CSM_01_93	0.9370	0.0	0.1105	0.0	0.19	676.4	3.6	670.9	2.9	660.0	6.1	676.4	3.6	102.5
CSM_01_87	0.9670	0.0	0.1111	0.0	0.37	679.0	5.6	686.3	5.0	719.0	15.3	679.0	5.6	94.4
CSM_01_23	1.0080	0.0	0.1116	0.0	0.74	682.0	6.1	707.0	5.1	778.0	8.7	682.0	6.1	87.7
CSM_01_20	0.9800	0.0	0.1115	0.0	0.66	683.0	7.7	694.0	5.6	723.0	17.3	683.0	7.7	94.5
CSM_01_2	0.9660	0.0	0.1138	0.0	0.74	695.0	7.7	686.0	4.6	681.0	9.7	695.0	7.7	102.1
CSM_01_4	0.9830	0.0	0.1140	0.0	-0.10	696.0	7.7	694.0	7.7	697.0	16.3	696.0	7.7	99.9
CSM_01_58	0.9900	0.0	0.1155	0.0	0.53	704.4	4.1	698.3	2.9	686.0	6.1	704.4	4.1	102.7
CSM_01_72	1.0900	0.0	0.1165	0.0	-0.01	710.5	4.0	748.1	3.2	831.0	7.1	710.5	4.0	85.5
CSM_01_18	1.0650	0.0	0.1166	0.0	0.56	710.7	3.7	736.0	2.9	792.0	5.6	710.7	3.7	89.7
CSM_01_25	1.0190	0.0	0.1183	0.0	0.50	721.0	6.6	716.0	5.1	699.0	13.8	721.0	6.6	103.1
CSM_01_19	1.0950	0.0	0.1241	0.0	0.42	754.0	5.6	750.6	3.0	761.0	9.7	754.0	5.6	99.1
CSM_01_56	1.1230	0.0	0.1269	0.0	0.88	770.0	8.7	764.0	6.1	768.0	7.1	770.0	8.7	100.3
CSM_01_100	1.2260	0.0	0.1330	0.0	0.81	805.0	6.1	813.0	4.4	819.0	6.6	805.0	6.1	98.3
CSM_01_83	1.2110	0.0	0.1335	0.0	0.09	807.5	3.5	805.3	2.7	798.0	6.6	807.5	3.5	101.2
CSM_01_89	1.2140	0.0	0.1354	0.0	0.39	819.0	5.6	806.7	4.6	791.0	9.7	819.0	5.6	103.5
CSM_01_74	1.2410	0.0	0.1362	0.0	0.60	823.0	6.1	819.2	3.2	793.0	8.2	823.0	6.1	103.8
CSM_01_61	1.3720	0.0	0.1444	0.0	0.76	877.0	14.3	882.0	14.3	942.0	23.0	877.0	14.3	93.1
CSM_01_95	1.6180	0.0	0.1559	0.0	0.49	934.0	8.7	980.0	7.1	1087.0	13.8	934.0	8.7	85.9
CSM_01_48	1.6840	0.0	0.1698	0.0	0.67	1011.0	6.6	1002.0	5.1	1011.0	6.1	1011.0	6.1	100.0
CSM_01_36	1.8030	0.0	0.1787	0.0	0.49	1059.0	9.7	1046.0	5.6	1020.0	8.2	1020.0	8.2	103.8
CSM_01_59	1.8720	0.0	0.1816	0.0	0.85	1075.0	12.8	1071.0	6.6	1063.0	8.2	1063.0	8.2	101.1
CSM_01_92	1.7770	0.0	0.1716	0.0	0.34	1021.0	12.2	1040.0	8.7	1068.0	16.8	1068.0	16.8	95.6
CSM_01_94	2.1880	0.0	0.2012	0.0	0.44	1181.0	7.7	1178.0	6.1	1153.0	10.7	1153.0	10.7	102.4
CSM_01_6	3.0300	0.0	0.2446	0.0	0.78	1410.0	8.7	1414.6	4.9	1445.3	4.7	1445.3	4.7	97.6
CSM_01_64	3.3380	0.0	0.2528	0.0	0.71	1452.0	16.3	1488.0	9.7	1538.0	10.2	1538.0	10.2	94.4
CSM_01_84	2.8600	0.1	0.2105	0.0	0.24	1231.0	10.2	1367.0	25.5	1550.0	51.0	1550.0	51.0	79.4
CSM_01_47	3.7280	0.0	0.2745	0.0	0.62	1563.0	9.2	1578.1	4.1	1585.0	6.6	1585.0	6.6	98.6
CSM_01_29	3.9090	0.0	0.2813	0.0	0.78	1597.0	13.3	1614.0	8.7	1658.0	7.7	1658.0	7.7	96.3
CSM_01_71	4.0110	0.0	0.2713	0.0	0.68	1547.0	11.7	1638.0	5.6	1737.0	7.1	1737.0	7.1	89.1
CSM_01_33	4.7490	0.0	0.3216	0.0	0.63	1797.0	12.2	1775.0	6.1	1749.0	6.1	1749.0	6.1	102.7
CSM_01_63	5.8000	0.1	0.3509	0.0	0.66	1939.0	11.7	1946.0	7.7	1945.0	6.1	1945.0	6.1	99.7
CSM_01_39	6.0800	0.1	0.3629	0.0	0.83	1995.0	17.3	1987.0	7.7	1967.0	6.6	1967.0	6.6	101.4
CSM_01_53	5.1020	0.0	0.3044	0.0	0.69	1713.0	10.7	1836.0	5.1	1970.0	5.1	1970.0	5.1	87.0
CSM_01_50	6.1120	0.0	0.3614	0.0	0.37	1988.0	9.2	1991.0	5.6	1992.0	6.1	1992.0	6.1	99.8
CSM_01_99	5.3200	0.1	0.3083	0.0	0.84	1730.0	18.4	1871.0	11.2	2042.0	7.7	2042.0	7.7	84.7
CSM_01_27	5.9870	0.0	0.3400	0.0	0.75	1886.0	14.8	1973.0	6.6	2056.0	6.1	2056.0	6.1	91.7
CSM_01_91	5.9760	0.0	0.3404	0.0	0.70	1887.0	19.9	1971.0	7.1	2079.0	7.7	2079.0	7.7	90.8
CSM_01_90	6.8400	0.1	0.3789	0.0	0.80	2069.0	20.4	2092.0	9.2	2124.0	7.1	2124.0	7.1	97.4
CSM_01_51	11.2500	0.2	0.4805	0.0	0.51	2528.0	14.8	2541.0	13.8	2562.0	20.9	2562.0	20.9	98.7
CSM_01_5	17.0800	0.2	0.5880	0.0	0.53	2979.0	23.0	2941.0	9.2	2886.0	10.2	2886.0	10.2	103.2

**SLL-01, Upper Ordovician, Cancañiri Formation (N=96). 21.38°S, 64.66°W**

SLL01_90	0.5930	0.0	0.0735	0.0	0.46	457.0	5.1	473.0	7.1	549.0	22.4	457.0	5.1	83.2
SLL01_16	0.5978	0.0	0.0764	0.0	0.53	474.3	2.4	475.5	2.8	513.0	9.2	474.3	2.4	92.5
SLL01_72	0.6041	0.0	0.0770	0.0	0.49	478.3	3.0	479.6	2.4	486.0	8.7	478.3	3.0	98.4
SLL01_92	0.6610	0.0	0.0797	0.0	0.69	494.0	5.1	514.7	4.8	630.0	14.3	494.0	5.1	78.4
SLL01_111	0.6430	0.0	0.0812	0.0	0.52	503.0	3.7	503.4	3.8	524.0	8.7	503.0	3.7	96.0
SLL01_102	0.6826	0.0	0.0829	0.0	0.55	513.1	3.6	528.1	3.0	582.0	8.2	513.1	3.6	88.2
SLL01_82	0.6730	0.0	0.0835	0.0	0.23	517.0	4.5	521.8	5.1	545.0	17.3	517.0	4.5	94.9
SLL01_43	0.7360	0.0	0.0836	0.0	0.10	517.2	3.9	559.4	4.9	710.0	16.8	517.2	3.9	72.8
SLL01_104	0.6852	0.0	0.0850	0.0	0.38	525.7	2.9	530.4	3.0	541.0	10.2	525.7	2.9	97.2
SLL01_101	0.7010	0.0	0.0855	0.0	0.76	528.8	4.0	540.2	3.4	586.0	6.1	528.8	4.0	90.2
SLL01_8	0.6750	0.0	0.0856	0.0	0.37	529.5	3.0	523.7	3.3	514.0	10.7	529.5	3.0	103.0
SLL01_106	0.6870	0.0	0.0861	0.0	0.30	533.2	3.5	530.3	4.5	548.0	11.7	533.2	3.5	97.3
SLL01_27	0.7063	0.0	0.0866	0.0	0.49	535.1	3.0	542.3	2.8	553.0	5.6	535.1	3.0	96.8
SLL01_91	0.6980	0.0	0.0869	0.0	0.45	537.1	3.6	537.3	4.9	543.0	9.2	537.1	3.6	98.9
SLL01_44	0.7250	0.0	0.0871	0.0	0.41	538.0	5.6	553.5	5.0	596.0	16.3	538.0	5.6	90.3
SLL01_39	0.7033	0.0	0.0871	0.0	0.25	538.4	2.3	540.6	2.1	540.0	6.6	538.4	2.3	99.7
SLL01_34	0.7090	0.0	0.0872	0.0	0.47	539.1	4.3	543.5	4.0	586.0	10.7	539.1	4.3	92.0
SLL01_86	0.7058	0.0	0.0873	0.0	0.39	539.5	2.7	542.1	2.3	544.0	7.7	539.5	2.7	99.2
SLL01_58	0.7032	0.0	0.0877	0.0	0.35	541.6	2.3	540.4	2.7	526.0	9.2	541.6	2.3	103.0
SLL01_49	0.7180	0.0	0.0879	0.0	0.51	542.8	3.2	549.3	2.4	568.0	7.1	542.8	3.2	95.6
SLL01_61	0.7370	0.0	0.0879	0.0	0.58	543.0	8.2	560.5	4.9	653.0	14.3	543.0	8.2	83.2
SLL01_47	0.7144	0.0	0.0885	0.0	0.64	546.3	3.3	547.7	2.6	548.0	6.1	546.3	3.3	99.7
SLL01_77	0.7230	0.0	0.0887	0.0	0.33	547.9	3.9	552.0	3.8	616.0	11.2	547.9	3.9	88.9
SLL01_18	0.7195	0.0	0.0889	0.0	0.36	549.0	3.2	550.1	2.9	543.0	10.2	549.0	3.2	101.1
SLL01_67	0.7440	0.0	0.0890	0.0	0.21	549.8	4.5	564.0	5.6	611.0	19.4	549.8	4.5	90.0
SLL01_84	0.7210	0.0	0.0891	0.0	0.25	550.1	3.4	550.7	3.3	561.0	11.2	550.1	3.4	98.1
SLL01_103	0.7540	0.0	0.0898	0.0	-0.15	554.3	3.3	571.5	3.6	609.0	14.8	554.3	3.3	91.0
SLL01_12	0.7270	0.0	0.0899	0.0	0.57	554.9	4.3	555.4	3.9	548.0	9.7	554.9	4.3	101.3
SLL01_74	0.7420	0.0	0.0904	0.0	0.54	557.7	4.3	563.1	3.4	586.0	7.1	557.7	4.3	95.2
SLL01_22	0.7351	0.0	0.0907	0.0	0.45	559.7	2.3	559.3	2.4	548.0	6.1	559.7	2.3	102.1
SLL01_13	0.7400	0.0	0.0915	0.0	0.71	565.3	4.3	562.1	3.1	546.0	7.7	565.3	4.3	103.5
SLL01_107	0.7520	0.0	0.0924	0.0	0.41	569.5	3.8	568.9	3.7	585.0	9.7	569.5	3.8	97.4
SLL01_88	0.7610	0.0	0.0930	0.0	0.50	573.4	4.5	574.2	3.9	564.0	11.2	573.4	4.5	101.7
SLL01_53	0.8060	0.0	0.0938	0.0	0.68	578.0	7.1	599.0	5.1	704.0	10.7	578.0	7.1	82.1
SLL01_81	0.8000	0.0	0.0956	0.0	0.54	588.4	4.0	597.1	3.6	629.0	9.2	588.4	4.0	93.5
SLL01_108	0.7810	0.0	0.0960	0.0	0.43	591.0	7.7	588.0	6.6	604.0	17.3	591.0	7.7	97.8
SLL01_55	0.8070	0.0	0.0961	0.0	0.26	591.4	3.6	601.2	4.4	643.0	11.7	591.4	3.6	92.0
SLL01_24	0.7890	0.0	0.0963	0.0	0.35	592.6	2.7	591.6	3.7	594.0	10.2	592.6	2.7	99.8
SLL01_23	0.7990	0.0	0.0963	0.0	0.29	592.7	4.4	595.9	3.4	606.0	11.7	592.7	4.4	97.8
SLL01_71	0.7895	0.0	0.0964	0.0	0.46	593.4	2.9	590.6	2.6	598.0	8.2	593.4	2.9	99.2
SLL01_38	0.8220	0.0	0.0966	0.0	0.55	595.0	5.1	608.9	3.5	649.0	10.2	595.0	5.1	91.7
SLL01_15	0.8180	0.0	0.0982	0.0	0.34	603.5	3.6	606.6	3.5	600.0	11.2	603.5	3.6	100.6
SLL01_96	0.8500	0.0	0.0982	0.0	0.63	603.7	4.7	624.5	3.8	709.0	8.2	603.7	4.7	85.1
SLL01_78	0.8590	0.0	0.0990	0.0	0.54	608.0	11.2	629.0	12.2	695.0	19.4	608.0	11.2	87.5
SLL01_76	0.8260	0.0	0.0993	0.0	0.42	610.3	5.1	610.7	4.5	641.0	13.3	610.3	5.1	95.2
SLL01_41	0.8300	0.0	0.1002	0.0	0.59	615.0	6.1	613.3	4.1	616.0	11.2	615.0	6.1	99.8
SLL01_87	0.8520	0.0	0.1005	0.0	0.37	617.1	4.6	625.5	3.7	672.0	13.3	617.1	4.6	91.8
SLL01_97	0.8550	0.0	0.1011	0.0	0.25	620.7	3.9	626.8	4.6	642.0	13.3	620.7	3.9	96.7
SLL01_59	0.8830	0.0	0.1013	0.0	0.26	622.0	6.1	641.0	7.7	683.0	25.0	622.0	6.1	91.1
SLL01_75	0.8540	0.0	0.1022	0.0	0.62	626.9	4.8	626.6	2.9	636.0	9.2	626.9	4.8	98.6
SLL01_48	0.8510	0.0	0.1026	0.0	0.54	629.4	4.5	625.7	3.9	634.0	10.2	629.4	4.5	99.3

SLL01_113	0.8760	0.0	0.1027	0.0	0.70	630.3	4.8	639.4	3.5	677.0	8.2	630.3	4.8	93.1
SLL01_62	0.8630	0.0	0.1030	0.0	0.50	632.0	6.1	631.4	4.4	616.0	11.2	632.0	6.1	102.6
SLL01_46	0.9100	0.0	0.1032	0.0	0.54	633.0	6.1	656.0	5.1	755.0	13.8	633.0	6.1	83.8
SLL01_45	0.8970	0.0	0.1056	0.0	0.36	647.4	3.4	650.0	3.2	660.0	6.6	647.4	3.4	98.1
SLL01_28	0.8912	0.0	0.1060	0.0	0.46	649.2	2.9	646.9	2.1	635.0	6.6	649.2	2.9	102.2
SLL01_65	0.8940	0.0	0.1063	0.0	0.54	651.1	4.1	649.8	3.1	648.0	7.7	651.1	4.1	100.5
SLL01_31	0.9110	0.0	0.1079	0.0	0.46	660.4	4.5	657.3	3.7	644.0	9.7	660.4	4.5	102.5
SLL01_10	0.9380	0.0	0.1104	0.0	0.69	674.9	4.4	672.6	3.8	686.0	7.1	674.9	4.4	98.4
SLL01_30	0.9370	0.0	0.1111	0.0	0.40	679.0	3.9	670.9	3.4	656.0	7.7	679.0	3.9	103.5
SLL01_60	0.9770	0.0	0.1157	0.0	0.13	705.0	9.7	694.0	9.7	706.0	24.5	705.0	9.7	99.9
SLL01_9	1.1000	0.0	0.1193	0.0	0.58	726.0	10.2	754.0	6.6	837.0	18.4	726.0	10.2	86.7
SLL01_35	1.0390	0.0	0.1194	0.0	0.79	727.0	6.6	722.7	4.4	706.0	7.1	727.0	6.6	103.0
SLL01_109	1.0640	0.0	0.1194	0.0	0.84	727.0	6.6	735.0	5.6	755.0	8.7	727.0	6.6	96.3
SLL01_29	1.1130	0.0	0.1215	0.0	0.63	739.0	9.2	759.0	6.6	809.0	15.3	739.0	9.2	91.3
SLL01_37	1.1940	0.0	0.1320	0.0	0.52	799.4	3.7	797.4	3.1	776.0	6.6	799.4	3.7	103.0
SLL01_57	1.2730	0.0	0.1346	0.0	0.42	812.0	21.4	837.0	14.3	910.0	33.2	812.0	21.4	89.2
SLL01_79	1.7810	0.0	0.1752	0.0	0.51	1041.0	6.1	1039.2	4.7	1016.0	9.7	1016.0	9.7	102.5
SLL01_112	1.7850	0.0	0.1768	0.0	0.60	1049.0	9.7	1040.0	6.1	1034.0	7.7	1034.0	7.7	101.5
SLL01_94	1.6720	0.0	0.1627	0.0	0.57	971.0	13.8	1002.0	8.2	1045.0	15.3	1045.0	15.3	92.9
SLL01_36	1.8500	0.0	0.1794	0.0	0.59	1064.0	5.6	1063.8	3.8	1053.5	4.7	1053.5	4.7	101.0
SLL01_54	2.3530	0.0	0.2095	0.0	0.85	1225.0	11.2	1228.0	6.6	1241.0	6.1	1241.0	6.1	98.7
SLL01_20	3.4320	0.0	0.2516	0.0	0.79	1446.0	12.8	1511.0	10.7	1598.0	11.2	1598.0	11.2	90.5
SLL01_66	4.7170	0.0	0.3196	0.0	0.72	1787.0	11.7	1771.0	5.6	1754.0	5.6	1754.0	5.6	101.9
SLL01_21	4.6030	0.0	0.3133	0.0	0.46	1757.0	10.7	1749.0	6.1	1760.0	7.1	1760.0	7.1	99.8
SLL01_32	4.9020	0.0	0.3205	0.0	0.85	1791.0	14.8	1801.0	7.7	1814.7	5.0	1814.7	5.0	98.7
SLL01_70	4.9540	0.0	0.3247	0.0	0.63	1812.0	10.2	1812.4	4.8	1818.0	6.1	1818.0	6.1	99.7
SLL01_100	5.1070	0.0	0.3290	0.0	0.74	1833.0	11.7	1836.0	6.1	1833.5	4.4	1833.5	4.4	100.0
SLL01_56	5.6480	0.0	0.3492	0.0	0.59	1930.0	14.8	1923.0	6.6	1899.0	6.6	1899.0	6.6	101.6
SLL01_7	5.1040	0.0	0.2946	0.0	0.77	1664.0	9.7	1835.0	7.7	2038.0	7.7	2038.0	7.7	81.6
SLL01_42	5.0220	0.0	0.2896	0.0	0.78	1645.0	14.8	1822.0	8.2	2046.0	7.7	2046.0	7.7	80.4
SLL01_1	5.0800	0.0	0.2916	0.0	0.54	1648.0	15.3	1832.0	6.1	2055.0	8.7	2055.0	8.7	80.2
SLL01_85	6.8300	0.0	0.3883	0.0	0.54	2119.0	11.7	2089.0	5.6	2056.0	6.6	2056.0	6.6	103.1
SLL01_50	6.5600	0.1	0.3740	0.0	0.90	2046.0	20.4	2051.0	8.7	2057.0	6.6	2057.0	6.6	99.5
SLL01_52	6.3490	0.0	0.3612	0.0	0.64	1992.0	18.9	2024.0	6.6	2063.0	9.2	2063.0	9.2	96.6
SLL01_89	6.4870	0.0	0.3665	0.0	0.55	2012.0	8.7	2043.6	4.2	2080.0	4.8	2080.0	4.8	96.7
SLL01_93	6.0580	0.0	0.3387	0.0	0.82	1879.0	15.3	1985.0	6.6	2082.0	5.6	2082.0	5.6	90.2
SLL01_51	6.6750	0.0	0.3783	0.0	0.61	2068.0	10.7	2070.0	5.6	2082.0	6.1	2082.0	6.1	99.3
SLL01_98	6.7800	0.0	0.3805	0.0	0.80	2078.0	12.8	2083.0	5.6	2082.0	4.1	2082.0	4.1	99.8
SLL01_69	6.8080	0.1	0.3782	0.0	0.82	2067.0	15.8	2086.0	6.6	2088.0	5.1	2088.0	5.1	99.0
SLL01_25	6.8740	0.0	0.3835	0.0	0.68	2092.0	9.2	2094.8	4.1	2101.4	4.0	2101.4	4.0	99.6
SLL01_33	7.2200	0.1	0.3967	0.0	0.62	2153.0	15.3	2140.0	7.1	2119.0	6.6	2119.0	6.6	101.6
SLL01_110	7.1020	0.0	0.3908	0.0	0.44	2128.0	8.2	2123.9	3.3	2122.0	5.1	2122.0	5.1	100.3
SLL01_6	7.1700	0.1	0.3931	0.0	0.70	2137.0	12.8	2134.0	6.6	2124.0	5.1	2124.0	5.1	100.6
SLL01_14	7.1880	0.0	0.3896	0.0	0.57	2121.0	7.7	2134.7	3.1	2150.1	3.4	2150.1	3.4	98.6
SLL01_105	13.3300	0.2	0.5260	0.0	0.75	2723.0	29.6	2701.0	10.7	2700.0	13.3	2700.0	13.3	100.9

#### SLL-03, Lower Devonian Santa Rosa Formation (N=62). 21.38°S, 64.64°W

SSL03_12	0.5530	0.0	0.0713	0.0	0.29	444.2	2.1	446.7	2.4	485.0	7.7	444.2	2.1	91.6
SSL03_51	0.5540	0.0	0.0714	0.0	0.31	444.7	3.0	447.4	3.0	487.0	11.7	444.7	3.0	91.3
SSL03_33	0.6050	0.0	0.0748	0.0	0.61	464.9	4.7	480.4	3.9	547.0	13.3	464.9	4.7	85.0
SSL03_14	0.6088	0.0	0.0765	0.0	0.46	475.0	2.3	482.7	1.9	502.0	7.1	475.0	2.3	94.6
SSL03_29	0.6310	0.0	0.0772	0.0	0.20	479.6	3.3	495.9	5.0	561.0	19.9	479.6	3.3	85.5
SSL03_24	0.6110	0.0	0.0774	0.0	0.84	480.0	5.6	486.0	6.1	517.0	8.7	480.0	5.6	92.8

SSL03_35	0.6150	0.0	0.0784	0.0	0.63	486.6	2.7	486.3	3.4	505.0	10.7	486.6	2.7	96.4
SSL03_31	0.6226	0.0	0.0798	0.0	0.46	495.1	2.2	491.8	2.0	494.0	5.6	495.1	2.2	100.2
SSL03_1	0.6785	0.0	0.0853	0.0	0.23	527.6	2.8	526.2	2.7	524.0	7.7	527.6	2.8	100.7
SSL03_36	0.6996	0.0	0.0874	0.0	0.37	540.0	4.2	538.3	2.8	555.0	9.7	540.0	4.2	97.3
SSL03_17	0.7050	0.0	0.0875	0.0	0.55	540.8	2.8	541.6	3.2	542.0	9.2	540.8	2.8	99.8
SSL03_39	0.7040	0.0	0.0881	0.0	0.52	544.0	5.6	541.0	5.6	549.0	14.3	544.0	5.6	99.1
SSL03_46	0.7085	0.0	0.0886	0.0	0.32	547.3	3.0	544.3	2.6	535.0	10.2	547.3	3.0	102.3
SSL03_43	0.7120	0.0	0.0892	0.0	0.46	550.0	6.1	546.0	5.1	527.0	16.8	550.0	6.1	104.4
SSL03_42	0.7180	0.0	0.0890	0.0	0.68	550.7	4.4	548.8	3.5	534.0	7.7	550.7	4.4	103.1
SSL03_9	0.7590	0.0	0.0926	0.0	0.76	571.0	16.8	572.0	14.8	600.0	24.5	571.0	16.8	95.2
SSL03_27	0.8190	0.0	0.0956	0.0	0.58	588.3	3.9	607.1	3.5	666.0	12.2	588.3	3.9	88.3
SSL03_11	0.8230	0.0	0.0964	0.0	0.69	593.4	4.5	610.4	3.2	675.0	6.6	593.4	4.5	87.9
SSL03_55	0.8825	0.0	0.1066	0.0	0.46	653.1	3.5	642.1	2.7	622.0	7.1	653.1	3.5	105.0
SSL03_30	0.9140	0.0	0.1083	0.0	0.51	664.0	5.1	658.4	4.3	634.0	10.7	664.0	5.1	104.7
SSL03_3	0.9270	0.0	0.1087	0.0	-0.02	665.0	5.1	665.8	3.6	682.0	9.7	665.0	5.1	97.5
SSL03_26	0.9380	0.0	0.1117	0.0	0.57	682.4	3.4	671.5	2.8	667.0	6.6	682.4	3.4	102.3
SSL03_20	0.9690	0.0	0.1135	0.0	0.36	692.9	4.0	688.6	4.0	690.0	9.7	692.9	4.0	100.4
SSL03_52	1.0430	0.0	0.1181	0.0	0.80	719.0	7.1	725.0	5.6	764.0	7.7	719.0	7.1	94.1
SSL03_2	1.5290	0.0	0.1580	0.0	0.72	945.0	10.7	941.0	7.1	925.0	11.7	945.0	10.7	102.2
SSL03_10	1.7170	0.0	0.1697	0.0	0.71	1010.0	11.2	1014.0	6.1	1019.0	8.2	1019.0	8.2	99.1
SSL03_54	1.7490	0.0	0.1720	0.0	0.52	1023.0	8.7	1028.0	7.1	1034.0	8.2	1034.0	8.2	98.9
SSL03_21	1.7150	0.0	0.1688	0.0	0.58	1005.4	5.0	1014.9	3.1	1036.0	6.1	1036.0	6.1	97.0
SSL03_47	1.8310	0.0	0.1811	0.0	0.16	1073.0	10.2	1057.0	9.7	1048.0	18.4	1048.0	18.4	102.4
SSL03_53	2.1560	0.0	0.1987	0.0	0.62	1168.4	4.3	1166.6	4.0	1173.0	5.1	1173.0	5.1	99.6
SSL03_38	2.0200	0.0	0.1850	0.0	0.73	1094.0	10.7	1128.0	5.6	1190.0	7.7	1190.0	7.7	91.9
SSL03_19	2.4220	0.0	0.2176	0.0	0.58	1269.0	7.1	1248.6	4.1	1216.0	6.6	1216.0	6.6	104.4
SSL03_40	2.2790	0.0	0.2062	0.0	0.34	1208.0	9.7	1205.0	7.7	1217.0	11.2	1217.0	11.2	99.3
SSL03_37	4.7960	0.0	0.3219	0.0	0.61	1802.0	8.2	1783.9	4.3	1762.0	6.6	1762.0	6.6	102.3
SSL03_7	5.2600	0.1	0.3337	0.0	0.67	1855.0	18.4	1861.0	9.2	1861.0	8.2	1861.0	8.2	99.7
SSL03_22	5.3180	0.0	0.3244	0.0	0.68	1811.0	11.7	1873.0	6.6	1938.0	6.6	1938.0	6.6	93.4
SLL01_7	5.1040	0.0	0.2946	0.0	0.77	1664.0	9.7	1835.0	7.7	2038.0	7.7	2038.0	7.7	81.6
SLL01_42	5.0220	0.0	0.2896	0.0	0.78	1645.0	14.8	1822.0	8.2	2046.0	7.7	2046.0	7.7	80.4
SLL01_1	5.0800	0.0	0.2916	0.0	0.54	1648.0	15.3	1832.0	6.1	2055.0	8.7	2055.0	8.7	80.2
SSL03_25	7.2590	0.0	0.3984	0.0	0.40	2161.0	6.1	2143.4	3.5	2130.9	4.1	2130.9	4.1	101.4
SSL03_49	6.9830	0.0	0.3789	0.0	0.59	2071.0	11.7	2110.0	5.6	2147.0	5.6	2147.0	5.6	96.5
SSL03_15	23.5700	0.2	0.5990	0.0	0.81	3038.0	23.5	3250.0	7.7	3377.0	6.6	3377.0	6.6	90.0
SSL03_16	28.8300	0.3	0.7150	0.0	0.83	3477.0	25.5	3447.0	8.7	3429.0	6.1	3429.0	6.1	101.4

#### AA-01, Carboniferous Tupambi Formation (N=97). 21.26°S, 63.54°W

AA01-1	0.4049	5.1	0.0541	0.9	0.18	339.7	3.0	345.2	14.8	382.3	112.0	339.7	3.0	NA
AA01-38	0.4137	10.3	0.0547	2.4	0.23	343.4	8.1	351.6	30.6	405.8	224.4	343.4	8.1	NA
AA01-57	0.4920	6.4	0.0645	5.4	0.83	402.8	20.9	406.3	21.5	426.0	79.0	402.8	20.9	94.5
AA01-50	0.5692	7.3	0.0755	2.4	0.33	468.9	10.8	457.5	26.8	400.6	154.3	468.9	10.8	117.1
AA01-61	0.6209	11.1	0.0802	1.3	0.12	497.5	6.4	490.4	43.2	457.4	244.9	497.5	6.4	108.8
AA01-103	0.6129	6.5	0.0810	2.0	0.30	502.0	9.5	485.4	25.0	407.9	138.3	502.0	9.5	123.0
AA01-62	0.6582	3.7	0.0816	1.1	0.29	505.9	5.2	513.5	14.8	547.4	76.9	505.9	5.2	92.4
AA01-28	0.6468	6.2	0.0824	1.7	0.27	510.1	8.2	506.5	24.8	490.1	132.2	510.1	8.2	104.1
AA01-67	0.6606	2.2	0.0825	1.4	0.61	511.1	6.7	515.0	8.9	532.1	38.2	511.1	6.7	96.0
AA01-7	0.6723	2.0	0.0826	0.8	0.41	511.7	4.0	522.1	8.1	567.9	39.4	511.7	4.0	90.1
AA01-9	0.6729	3.9	0.0834	1.6	0.42	516.2	8.1	522.5	15.9	549.9	77.1	516.2	8.1	93.9
AA01-18	0.5315	28.5	0.0838	9.0	0.31	518.6	44.6	432.8	100.8	-1.7	663.0	518.6	44.6	NA
AA01-87	0.6858	7.3	0.0848	3.8	0.53	524.9	19.4	530.3	30.1	553.3	134.9	524.9	19.4	94.9
AA01-48	0.6708	3.2	0.0851	1.2	0.36	526.5	5.8	521.2	13.2	498.3	66.5	526.5	5.8	105.7

AA01-22	0.6945	2.4	0.0853	1.5	0.61	527.8	7.6	535.5	10.2	568.3	42.0	527.8	7.6	92.9
AA01-29	0.6432	10.6	0.0854	2.4	0.23	528.5	12.2	504.3	42.3	396.1	232.8	528.5	12.2	133.4
AA01-80	0.6866	10.3	0.0860	1.9	0.18	532.0	9.5	530.7	42.5	525.4	222.3	532.0	9.5	101.3
AA01-14	0.6982	1.9	0.0874	1.6	0.86	539.9	8.4	537.7	7.9	528.3	21.0	539.9	8.4	102.2
AA01-86	0.7139	2.1	0.0882	1.0	0.50	545.1	5.3	547.1	8.7	555.2	39.0	545.1	5.3	98.2
AA01-37	0.7315	3.9	0.0883	1.8	0.46	545.2	9.3	557.4	16.6	607.5	74.2	545.2	9.3	89.8
AA01-52	0.7238	1.6	0.0894	0.9	0.59	551.9	4.8	552.9	6.6	557.0	27.4	551.9	4.8	99.1
AA01-68	0.6978	3.4	0.0894	1.8	0.52	551.9	9.3	537.5	14.0	476.6	63.4	551.9	9.3	115.8
AA01-17	0.7371	4.4	0.0896	1.8	0.41	553.3	9.5	560.7	18.8	590.9	86.5	553.3	9.5	93.6
AA01-54	0.7275	2.1	0.0900	0.8	0.36	555.4	4.0	555.1	8.9	554.0	42.4	555.4	4.0	100.2
AA01-6	0.7291	1.0	0.0900	0.8	0.73	555.5	4.1	556.1	4.5	558.4	15.8	555.5	4.1	99.5
AA01-4	0.7175	11.5	0.0903	2.9	0.25	557.2	15.3	549.2	49.0	516.1	246.0	557.2	15.3	108.0
AA01-73	0.7475	4.8	0.0912	4.2	0.87	562.9	22.4	566.7	20.8	582.3	51.4	562.9	22.4	96.7
AA01-27	0.7330	6.4	0.0913	1.3	0.21	563.0	7.2	558.3	27.6	539.2	137.7	563.0	7.2	104.4
AA01-65	0.7445	1.5	0.0916	1.0	0.65	564.9	5.2	565.0	6.4	565.3	24.5	564.9	5.2	99.9
AA01-90	0.7706	10.5	0.0919	3.2	0.30	566.6	17.1	580.1	46.3	633.2	215.7	566.6	17.1	89.5
AA01-45	0.7710	9.0	0.0922	3.0	0.34	568.3	16.4	580.3	39.8	627.7	182.9	568.3	16.4	90.5
AA01-78	0.7178	13.7	0.0922	2.9	0.21	568.7	15.5	549.4	58.0	470.2	296.9	568.7	15.5	120.9
AA01-69	0.7574	6.1	0.0924	0.8	0.13	569.8	4.5	572.5	26.8	583.2	131.6	569.8	4.5	97.7
AA01-104	0.7947	4.9	0.0925	2.0	0.41	570.0	10.8	593.9	21.9	685.9	94.9	570.0	10.8	83.1
AA01-63	0.7147	7.4	0.0925	1.9	0.25	570.4	10.3	547.5	31.5	453.5	160.0	570.4	10.3	125.8
AA01-76	0.7557	1.4	0.0926	0.8	0.60	571.0	4.5	571.6	6.0	573.8	23.8	571.0	4.5	99.5
AA01-88	0.7693	1.9	0.0933	0.9	0.46	575.1	4.7	579.4	8.2	595.9	35.7	575.1	4.7	96.5
AA01-91	0.7508	6.6	0.0947	2.7	0.41	583.5	14.8	568.7	28.6	510.1	132.0	583.5	14.8	114.4
AA01-11	0.7987	4.1	0.0949	2.8	0.69	584.2	15.7	596.1	18.4	641.7	63.4	584.2	15.7	91.0
AA01-81	0.7701	8.3	0.0950	1.3	0.15	585.0	7.2	579.8	36.8	559.5	179.4	585.0	7.2	104.6
AA01-53	0.7867	2.0	0.0950	1.1	0.57	585.0	6.3	589.3	8.8	605.8	35.1	585.0	6.3	96.6
AA01-55	0.7776	1.5	0.0950	1.2	0.80	585.1	6.9	584.1	6.8	580.4	20.1	585.1	6.9	100.8
AA01-85	0.8075	3.6	0.0955	1.0	0.28	588.1	5.6	601.0	16.3	650.0	74.0	588.1	5.6	90.5
AA01-84	0.8612	4.9	0.0957	4.7	0.96	589.1	26.3	630.8	22.9	783.1	29.1	589.1	26.3	75.2
AA01-77	0.7752	7.3	0.0968	1.9	0.25	595.4	10.5	582.8	32.5	533.8	155.4	595.4	10.5	111.5
AA01-46	0.8279	1.3	0.0969	1.1	0.87	596.4	6.5	612.5	6.0	672.2	13.7	596.4	6.5	88.7
AA01-12	0.8086	5.5	0.0983	2.0	0.36	604.4	11.4	601.7	24.9	591.4	110.9	604.4	11.4	102.2
AA01-25	0.8133	6.6	0.0985	2.5	0.38	605.6	14.7	604.3	30.2	599.2	132.6	605.6	14.7	101.1
AA01-16	0.8393	4.6	0.0996	2.1	0.45	611.9	12.2	618.8	21.4	643.8	88.7	611.9	12.2	95.1
AA01-3	0.8339	1.0	0.0997	0.7	0.69	612.9	4.2	615.8	4.8	626.2	16.4	612.9	4.2	97.9
AA01-42	0.8368	1.5	0.1002	0.8	0.55	615.4	4.8	617.4	6.9	624.6	26.8	615.4	4.8	98.5
AA01-10	0.8354	5.9	0.1005	2.2	0.36	617.4	12.7	616.6	27.3	613.5	119.0	617.4	12.7	100.6
AA01-66	0.8462	5.0	0.1012	4.4	0.88	621.4	26.0	622.6	23.2	626.6	50.5	621.4	26.0	99.2
AA01-13	0.8582	4.3	0.1025	2.5	0.59	628.8	15.0	629.1	20.0	630.5	74.4	628.8	15.0	99.7
AA01-60	0.8582	9.5	0.1034	5.9	0.63	634.5	35.8	629.1	44.4	609.8	159.8	634.5	35.8	104.0
AA01-24	0.9247	6.4	0.1080	1.8	0.27	661.2	11.0	664.8	31.3	677.1	131.8	661.2	11.0	97.7
AA01-89	0.9896	4.1	0.1158	1.3	0.31	706.1	8.4	698.5	20.6	674.0	82.8	706.1	8.4	104.8
AA01-51	1.1402	2.4	0.1209	2.1	0.87	736.0	14.4	772.6	12.8	879.8	24.0	736.0	14.4	83.7
AA01-44	1.1778	3.9	0.1312	3.4	0.88	794.6	25.3	790.3	21.2	778.0	38.7	794.6	25.3	102.1
AA01-101	1.2859	2.5	0.1342	1.5	0.61	811.7	11.8	839.5	14.5	913.8	41.6	811.7	11.8	88.8
AA01-70	1.2277	6.8	0.1351	6.6	0.97	816.9	50.9	813.3	38.2	803.4	33.8	816.9	50.9	101.7
AA01-75	1.2814	8.6	0.1385	2.3	0.26	836.0	17.7	837.5	49.2	841.6	173.5	836.0	17.7	99.3
AA01-15	1.3322	3.5	0.1422	2.3	0.65	857.3	18.2	859.8	20.4	866.5	55.7	857.3	18.2	98.9
AA01-83	1.5557	4.3	0.1598	3.7	0.85	955.8	32.9	952.7	26.9	945.7	46.7	945.7	46.7	101.1
AA01-36	1.5589	2.5	0.1598	1.7	0.70	955.6	15.4	954.0	15.4	950.4	36.5	950.4	36.5	100.5
AA01-30	1.3731	2.7	0.1402	1.9	0.68	845.9	14.7	877.5	16.1	958.1	41.1	958.1	41.1	88.3
AA01-98	1.4757	3.4	0.1500	3.0	0.87	901.0	24.9	920.5	20.5	967.3	33.6	967.3	33.6	93.1

AA01-31	1.4493	2.7	0.1470	2.7	0.99	884.4	22.0	909.6	16.2	971.2	8.6	971.2	8.6	91.1
AA01-79	1.5502	4.8	0.1550	3.8	0.79	929.0	33.1	950.6	29.8	1001.0	59.9	1001.0	59.9	92.8
AA01-82	1.7829	3.7	0.1765	1.8	0.47	1047.8	17.0	1039.3	24.2	1021.3	66.4	1021.3	66.4	102.6
AA01-8	1.7627	1.4	0.1734	1.2	0.85	1030.8	11.3	1031.8	9.1	1034.0	15.0	1034.0	15.0	99.7
AA01-71	1.8243	9.8	0.1793	9.8	1.00	1063.4	95.8	1054.2	64.4	1035.3	18.0	1035.3	18.0	102.7
AA01-99	1.7227	7.3	0.1678	4.6	0.63	1000.0	42.8	1017.0	47.0	1053.9	114.2	1053.9	114.2	94.9
AA01-43	1.8267	1.8	0.1770	1.4	0.78	1050.5	13.7	1055.1	12.0	1064.8	23.2	1064.8	23.2	98.7
AA01-21	1.7435	3.0	0.1689	2.4	0.81	1006.0	22.7	1024.8	19.4	1065.0	35.5	1065.0	35.5	94.5
AA01-34	1.9225	4.4	0.1853	2.2	0.50	1095.8	22.2	1088.9	29.2	1075.3	75.8	1075.3	75.8	101.9
AA01-40	1.8677	3.8	0.1796	3.0	0.78	1065.0	29.2	1069.7	25.2	1079.2	47.9	1079.2	47.9	98.7
AA01-49	1.8512	1.5	0.1778	1.0	0.66	1055.0	9.3	1063.9	9.6	1082.1	22.0	1082.1	22.0	97.5
AA01-5	1.7443	5.6	0.1655	2.1	0.38	987.3	19.2	1025.0	35.8	1106.5	102.8	1106.5	102.8	89.2
AA01-41	1.9740	2.1	0.1862	1.1	0.51	1100.7	11.1	1106.7	14.5	1118.5	36.8	1118.5	36.8	98.4
AA01-39	1.8313	4.2	0.1693	2.5	0.60	1008.1	23.3	1056.8	27.5	1158.6	66.8	1158.6	66.8	87.0
AA01-2	1.8487	4.7	0.1708	4.6	0.96	1016.3	42.8	1063.0	31.3	1160.1	26.7	1160.1	26.7	87.6
AA01-32	2.1704	3.3	0.1928	3.2	0.96	1136.3	33.0	1171.6	22.8	1237.5	16.9	1237.5	16.9	91.8
AA01-58	4.3050	3.2	0.2999	3.1	0.96	1690.8	46.0	1694.3	26.5	1698.7	15.8	1698.7	15.8	99.5
AA01-26	6.0316	2.3	0.3576	2.3	0.99	1970.7	38.3	1980.4	19.9	1990.6	6.0	1990.6	6.0	99.0
AA01-23	6.1843	1.3	0.3653	1.3	0.98	2007.2	22.3	2002.2	11.6	1997.1	4.9	1997.1	4.9	100.5
AA01-64	6.4391	1.6	0.3710	1.6	0.99	2034.0	27.5	2037.6	14.0	2041.3	4.0	2041.3	4.0	99.6
AA01-33	6.2062	1.4	0.3542	1.4	0.98	1954.4	23.3	2005.3	12.3	2058.1	5.1	2058.1	5.1	95.0
AA01-47	6.2694	3.2	0.3553	3.1	0.99	1959.8	52.9	2014.2	27.8	2070.4	8.9	2070.4	8.9	94.7
AA01-95	7.5509	1.0	0.3978	1.0	0.95	2158.8	18.0	2179.0	9.2	2198.1	5.6	2198.1	5.6	98.2
AA01-100	9.1699	4.0	0.3666	4.0	1.00	2013.3	69.3	2355.1	36.8	2665.9	5.5	2665.9	5.5	75.5
AA01-94	13.5902	1.2	0.5225	1.1	0.97	2709.9	24.6	2721.6	10.9	2730.3	4.9	2730.3	4.9	99.3
AA01-74	12.9801	1.7	0.4845	1.7	0.99	2546.9	35.9	2678.2	16.3	2778.9	4.6	2778.9	4.6	91.7
AA01-102	11.2847	7.9	0.4150	7.9	1.00	2237.8	148.7	2546.9	73.8	2803.2	11.7	2803.2	11.7	79.8
AA01-97	12.2113	3.5	0.4306	3.3	0.95	2308.6	64.0	2620.8	32.5	2871.7	17.1	2871.7	17.1	80.4
AA01-59	11.6862	8.2	0.4003	8.1	0.99	2170.2	150.2	2579.6	76.9	2919.0	16.2	2919.0	16.2	74.3
AA01-20	21.2875	1.8	0.6095	1.6	0.92	3068.2	40.2	3151.8	17.4	3205.5	11.2	3205.5	11.2	95.7

#### SDG-01, Triassic Ipaguazu/San Diego Formation (N=85). 21.44°S, 64.25°W

SDG_01_2	0.4425	0.0	0.0595	0.0	0.59	372.6	1.9	371.9	1.7	364.0	6.6	372.6	1.9	102.4
SDG_01_77	0.4713	0.0	0.0622	0.0	0.33	389.2	2.6	391.9	2.3	424.0	10.7	389.2	2.6	91.8
SDG_01_78	0.5620	0.0	0.0724	0.0	0.06	450.8	3.6	453.2	3.9	455.0	15.8	450.8	3.6	99.1
SDG_01_67	0.6115	0.0	0.0777	0.0	0.46	482.3	2.7	484.3	2.7	499.0	6.6	482.3	2.7	96.7
SDG_01_49	0.6140	0.0	0.0781	0.0	0.57	485.0	10.7	485.0	13.3	499.0	34.2	485.0	10.7	97.2
SDG_01_17	0.6581	0.0	0.0824	0.0	0.53	510.4	2.6	514.3	2.3	532.0	8.2	510.4	2.6	95.9
SDG_01_7	0.6960	0.0	0.0833	0.0	0.57	515.8	4.5	535.7	4.2	613.0	12.2	515.8	4.5	84.1
SDG_01_11	0.6940	0.0	0.0838	0.0	0.57	518.7	3.8	536.3	3.4	594.0	7.1	518.7	3.8	87.3
SDG_01_90	0.6950	0.0	0.0862	0.0	0.33	532.8	4.6	535.1	4.8	568.0	13.8	532.8	4.6	93.8
SDG_01_96	0.6980	0.0	0.0867	0.0	0.64	536.1	2.6	537.3	3.5	536.0	7.7	536.1	2.6	100.0
SDG_01_47	0.7021	0.0	0.0873	0.0	0.19	539.6	2.9	539.9	2.3	559.0	7.7	539.6	2.9	96.5
SDG_01_29	0.7100	0.0	0.0874	0.0	0.58	540.2	3.9	544.2	3.7	550.0	9.2	540.2	3.9	98.2
SDG_01_56	0.7250	0.0	0.0875	0.0	-0.25	541.0	6.6	553.0	9.2	604.0	21.4	541.0	6.6	89.6
SDG_01_44	0.7058	0.0	0.0876	0.0	0.27	541.3	1.9	542.1	1.9	533.0	5.6	541.3	1.9	101.6
SDG_01_84	0.7370	0.0	0.0886	0.0	0.31	547.1	4.4	560.0	3.6	612.0	10.2	547.1	4.4	89.4
SDG_01_15	0.7240	0.0	0.0888	0.0	0.46	548.4	3.3	552.8	3.3	581.0	10.7	548.4	3.3	94.4
SDG_01_55	0.7250	0.0	0.0889	0.0	0.13	549.1	3.7	554.1	4.2	579.0	11.7	549.1	3.7	94.8
SDG_01_16	0.7390	0.0	0.0893	0.0	0.32	551.5	3.1	561.7	3.5	604.0	12.2	551.5	3.1	91.3
SDG_01_63	0.7220	0.0	0.0901	0.0	0.23	556.0	5.1	552.3	4.6	537.0	17.3	556.0	5.1	103.5
SDG_01_8	0.7330	0.0	0.0902	0.0	0.44	556.5	5.1	557.0	5.1	564.0	14.3	556.5	5.1	98.7
SDG_01_21	0.7540	0.0	0.0906	0.0	0.17	559.0	6.1	563.0	9.2	619.0	31.1	559.0	6.1	90.3

SDG_01_64	0.7360	0.0	0.0912	0.0	0.59	562.6	3.9	561.1	3.9	571.0	8.2	562.6	3.9	98.5
SDG_01_68	0.7530	0.0	0.0913	0.0	0.06	563.0	9.2	568.0	9.7	613.0	37.2	563.0	9.2	91.8
SDG_01_31	0.7540	0.0	0.0915	0.0	0.19	564.2	4.3	571.4	3.9	577.0	17.9	564.2	4.3	97.8
SDG_01_34	0.7449	0.0	0.0915	0.0	0.60	564.6	3.1	565.7	2.9	564.0	8.2	564.6	3.1	100.1
SDG_01_51	0.8280	0.0	0.0922	0.0	0.15	568.4	4.5	612.0	6.6	800.0	23.0	568.4	4.5	71.1
SDG_01_73	0.7890	0.0	0.0934	0.0	0.41	577.0	4.7	590.2	3.6	656.0	10.2	577.0	4.7	88.0
SDG_01_14	0.7890	0.0	0.0938	0.0	0.39	578.0	6.1	589.0	7.1	664.0	16.8	578.0	6.1	87.0
SDG_01_93	0.7810	0.0	0.0938	0.0	0.49	578.0	4.2	585.4	3.5	622.0	11.2	578.0	4.2	92.9
SDG_01_27	0.7640	0.0	0.0944	0.0	0.50	581.7	3.1	575.9	3.4	564.0	9.7	581.7	3.1	103.1
SDG_01_92	0.7900	0.0	0.0946	0.0	0.19	582.0	6.6	590.0	5.6	607.0	17.9	582.0	6.6	95.9
SDG_01_102	0.7824	0.0	0.0951	0.0	0.47	586.4	2.5	586.6	2.5	585.0	6.1	586.4	2.5	100.2
SDG_01_22	0.7860	0.0	0.0954	0.0	0.53	587.1	3.9	588.3	3.5	587.0	10.2	587.1	3.9	100.0
SDG_01_37	0.7800	0.0	0.0965	0.0	0.62	593.0	7.7	585.0	5.6	582.0	9.7	593.0	7.7	101.9
SDG_01_98	0.8000	0.0	0.0966	0.0	0.45	594.4	3.4	596.3	3.2	593.0	7.1	594.4	3.4	100.2
SDG_01_20	0.8340	0.0	0.0966	0.0	0.09	594.6	4.2	615.0	5.6	705.0	13.3	594.6	4.2	84.3
SDG_01_62	0.7919	0.0	0.0969	0.0	0.42	595.9	2.9	592.0	2.3	583.0	5.6	595.9	2.9	102.2
SDG_01_3	0.7970	0.0	0.0969	0.0	0.33	596.1	3.6	594.7	3.5	594.0	10.2	596.1	3.6	100.4
SDG_01_40	0.8010	0.0	0.0973	0.0	0.53	599.0	5.1	598.0	4.5	596.0	13.8	599.0	5.1	100.5
SDG_01_38	0.8140	0.0	0.0980	0.0	0.43	602.0	5.6	603.9	4.6	623.0	9.2	602.0	5.6	96.6
SDG_01_54	0.8190	0.0	0.0987	0.0	0.67	606.0	8.7	611.0	6.1	606.0	15.3	606.0	8.7	100.0
SDG_01_36	0.8190	0.0	0.0991	0.0	0.21	609.2	3.9	608.0	4.0	602.0	12.8	609.2	3.9	101.2
SDG_01_9	0.8240	0.0	0.0992	0.0	0.42	609.9	3.5	610.9	2.9	605.0	7.7	609.9	3.5	100.8
SDG_01_4	0.8190	0.0	0.0993	0.0	0.41	610.0	5.1	606.0	6.1	582.0	14.3	610.0	5.1	104.8
SDG_01_5	0.8220	0.0	0.0994	0.0	0.37	610.5	2.8	608.8	3.0	599.0	7.7	610.5	2.8	101.9
SDG_01_45	0.8440	0.0	0.0994	0.0	0.39	610.7	4.8	621.0	3.6	667.0	13.3	610.7	4.8	91.6
SDG_01_86	0.8330	0.0	0.1000	0.0	0.23	614.0	5.6	615.0	6.1	622.0	22.4	614.0	5.6	98.7
SDG_01_26	0.8260	0.0	0.1002	0.0	0.33	615.6	4.0	613.0	4.2	594.0	12.2	615.6	4.0	103.6
SDG_01_48	0.8543	0.0	0.1020	0.0	0.21	625.9	3.0	626.9	2.1	618.0	12.2	625.9	3.0	101.3
SDG_01_71	0.8660	0.0	0.1026	0.0	0.54	629.0	6.1	632.7	4.6	648.0	11.2	629.0	6.1	97.1
SDG_01_1	0.8670	0.0	0.1030	0.0	0.38	631.9	3.4	633.3	3.7	629.0	9.2	631.9	3.4	100.5
SDG_01_53	0.8960	0.0	0.1034	0.0	0.41	634.0	4.2	649.1	3.8	696.0	11.7	634.0	4.2	91.1
SDG_01_60	0.8900	0.0	0.1036	0.0	0.62	635.2	5.1	645.8	4.7	702.0	8.7	635.2	5.1	90.5
SDG_01_43	0.8840	0.0	0.1042	0.0	0.50	639.0	4.6	642.5	4.5	659.0	10.7	639.0	4.6	97.0
SDG_01_101	0.9060	0.0	0.1073	0.0	0.54	656.7	3.9	654.4	3.8	658.0	12.2	656.7	3.9	99.8
SDG_01_46	0.9060	0.0	0.1073	0.0	0.18	657.2	3.3	654.5	3.5	645.0	6.6	657.2	3.3	101.9
SDG_01_41	0.9240	0.0	0.1082	0.0	0.60	662.0	10.2	666.0	7.1	673.0	19.9	662.0	10.2	98.4
SDG_01_99	0.9400	0.0	0.1097	0.0	0.59	671.0	6.1	673.6	4.9	668.0	9.7	671.0	6.1	100.4
SDG_01_81	0.9440	0.0	0.1109	0.0	0.13	678.0	5.1	674.0	7.1	673.0	19.4	678.0	5.1	100.7
SDG_01_50	1.1810	0.0	0.1282	0.0	0.41	777.0	12.2	791.0	7.7	786.0	16.3	777.0	12.2	98.9
SDG_01_70	1.2760	0.0	0.1345	0.0	0.72	813.0	9.2	836.0	6.6	892.0	10.7	813.0	9.2	91.1
SDG_01_82	1.7240	0.0	0.1536	0.0	0.77	921.0	9.2	1017.0	6.1	1239.0	7.7	921.0	9.2	74.3
SDG_01_97	1.6500	0.0	0.1581	0.0	0.58	946.0	8.2	989.0	5.6	1114.0	9.2	946.0	8.2	84.9
SDG_01_94	1.6350	0.0	0.1671	0.0	0.62	996.0	7.7	986.0	5.1	960.0	7.7	960.0	7.7	103.8
SDG_01_57	1.6070	0.0	0.1627	0.0	0.84	971.0	11.7	971.0	10.7	973.0	11.7	973.0	11.7	99.8
SDG_01_100	1.7790	0.0	0.1753	0.0	0.45	1041.0	6.6	1038.3	4.5	1022.0	8.7	1022.0	8.7	101.9
SDG_01_6	1.7860	0.0	0.1763	0.0	0.71	1047.0	7.1	1039.7	4.6	1036.0	7.1	1036.0	7.1	101.1
SDG_01_103	1.8480	0.0	0.1830	0.0	0.32	1083.0	7.1	1063.0	5.1	1036.0	10.7	1036.0	10.7	104.5
SDG_01_85	1.8380	0.0	0.1815	0.0	0.56	1075.0	6.1	1061.0	5.6	1045.0	7.1	1045.0	7.1	102.9
SDG_01_42	1.8080	0.0	0.1744	0.0	0.37	1036.0	7.7	1049.0	6.6	1076.0	12.8	1076.0	12.8	96.3
SDG_01_75	1.7970	0.0	0.1727	0.0	0.65	1026.0	8.2	1043.0	5.1	1083.0	8.7	1083.0	8.7	94.7
SDG_01_74	1.6670	0.0	0.1591	0.0	0.56	951.0	14.8	994.0	7.7	1096.0	15.3	1096.0	15.3	86.8
SDG_01_24	1.9390	0.0	0.1828	0.0	0.55	1082.0	10.2	1093.0	7.1	1117.0	10.7	1117.0	10.7	96.9
SDG_01_72	1.9100	0.0	0.1791	0.0	0.20	1062.0	10.2	1083.0	8.7	1126.0	18.4	1126.0	18.4	94.3

SDG_01_79	1.7720	0.0	0.1588	0.0	0.66	955.0	12.2	1029.0	13.3	1129.0	17.9	1129.0	17.9	84.6
SDG_01_88	4.2710	0.0	0.2869	0.0	0.47	1626.0	11.2	1687.0	6.6	1771.0	9.7	1771.0	9.7	91.8
SDG_01_95	4.9690	0.0	0.3260	0.0	0.74	1818.0	13.3	1813.0	5.6	1798.0	5.6	1798.0	5.6	101.1
SDG_01_91	5.1610	0.0	0.3319	0.0	0.85	1847.0	14.8	1844.0	7.1	1839.0	5.6	1839.0	5.6	100.4
SDG_01_10	7.7200	0.1	0.3969	0.0	0.78	2154.0	15.8	2198.0	6.1	2230.5	4.9	2230.5	4.9	96.6
SDG_01_13	8.5800	0.1	0.4282	0.0	0.73	2297.0	16.8	2294.0	6.1	2293.0	7.7	2293.0	7.7	100.2
SDG_01_66	8.5000	0.1	0.3969	0.0	0.68	2154.0	12.2	2285.0	6.1	2392.0	5.6	2392.0	5.6	90.1
SDG_01_12	11.6800	0.1	0.4908	0.0	0.78	2573.0	20.4	2578.0	8.2	2561.0	5.6	2561.0	5.6	100.5
SDG_01_52	12.2700	0.1	0.5042	0.0	0.83	2631.0	15.3	2624.0	6.1	2628.1	4.0	2628.1	4.0	100.1
SDG_01_69	11.2700	0.1	0.4490	0.0	0.72	2394.0	16.8	2547.0	6.1	2669.0	5.6	2669.0	5.6	89.7
SDG_01_25	13.0900	0.2	0.4990	0.0	0.87	2607.0	25.0	2684.0	11.2	2723.0	8.7	2723.0	8.7	95.7

**AA-04, Cretaceous Ichoa Formation (N=98). 21.27°S, 63.52°W**

AA04-86	0.4180	3.7	0.0573	1.4	0.39	359.3	5.0	354.6	11.2	324.2	78.2	359.3	5.0	NA
AA04-90	0.4318	2.4	0.0583	2.0	0.82	365.1	7.1	364.5	7.5	360.4	31.2	365.1	7.1	NA
AA04-64	0.5721	4.4	0.0772	1.8	0.41	479.5	8.4	459.4	16.3	360.1	90.5	479.5	8.4	133.2
AA04-91	0.6281	16.5	0.0776	4.2	0.25	481.8	19.4	494.9	64.8	556.1	350.8	481.8	19.4	86.6
AA04-11	0.6482	4.0	0.0810	3.2	0.79	501.9	15.4	507.4	16.1	532.2	54.2	501.9	15.4	94.3
AA04-71	0.6108	7.0	0.0811	3.3	0.48	502.4	16.2	484.1	26.9	398.1	137.7	502.4	16.2	126.2
AA04-97	0.6518	4.6	0.0815	3.4	0.74	504.9	16.6	509.6	18.4	530.8	67.3	504.9	16.6	95.1
AA04-49	0.6486	3.1	0.0816	2.6	0.85	505.6	12.9	507.6	12.5	516.4	36.4	505.6	12.9	97.9
AA04-36	0.6565	3.3	0.0816	2.2	0.67	505.9	10.6	512.5	13.1	542.0	53.2	505.9	10.6	93.3
AA04-29	0.6832	11.5	0.0817	4.4	0.38	506.4	21.3	528.7	47.3	626.4	229.2	506.4	21.3	80.8
AA04-14	0.6490	5.7	0.0820	2.7	0.47	507.9	13.2	507.8	22.9	507.5	111.0	507.9	13.2	100.1
AA04-40	0.6627	6.4	0.0821	3.0	0.47	508.9	14.8	516.2	25.9	549.0	123.1	508.9	14.8	92.7
AA04-9	0.6930	7.6	0.0830	7.0	0.92	514.2	34.4	534.6	31.6	622.4	65.7	514.2	34.4	82.6
AA04-69	0.6732	3.6	0.0835	3.2	0.89	517.0	15.8	522.7	14.6	547.5	35.8	517.0	15.8	94.4
AA04-101	0.7194	6.0	0.0837	2.4	0.40	517.9	11.8	550.3	25.4	686.6	117.4	517.9	11.8	75.4
AA04-99	0.6757	5.2	0.0846	3.7	0.71	523.6	18.5	524.2	21.1	526.7	79.2	523.6	18.5	99.4
AA04-20	0.6786	1.7	0.0847	1.4	0.82	523.9	7.1	525.9	7.1	534.8	21.9	523.9	7.1	98.0
AA04-24	0.7174	6.7	0.0847	1.5	0.22	524.0	7.5	549.1	28.4	654.9	140.0	524.0	7.5	80.0
AA04-25	0.6831	2.0	0.0847	1.6	0.80	524.2	8.1	528.7	8.2	547.7	26.0	524.2	8.1	95.7
AA04-66	0.5675	17.8	0.0849	5.3	0.30	525.6	26.7	456.4	65.5	121.3	402.9	525.6	26.7	433.3
AA04-98	0.7516	15.3	0.0854	7.1	0.46	528.6	36.1	569.1	66.7	734.8	287.8	528.6	36.1	71.9
AA04-96	0.6951	3.1	0.0867	2.2	0.72	536.2	11.6	535.9	13.0	534.6	47.4	536.2	11.6	100.3
AA04-60	0.7185	1.9	0.0871	1.7	0.87	538.3	8.6	549.8	8.1	597.8	19.9	538.3	8.6	90.0
AA04-87	0.6920	24.7	0.0877	8.0	0.32	542.1	41.4	534.0	103.0	499.7	521.8	542.1	41.4	108.5
AA04-44	0.7202	2.0	0.0883	1.0	0.49	545.3	5.3	550.8	8.7	573.5	38.8	545.3	5.3	95.1
AA04-37	0.7096	5.4	0.0885	1.4	0.26	546.8	7.3	544.5	22.8	534.9	114.7	546.8	7.3	102.2
AA04-26	0.6565	13.5	0.0905	4.7	0.35	558.5	25.0	512.5	54.4	311.9	289.2	558.5	25.0	179.0
AA04-7	0.7166	13.6	0.0910	6.0	0.44	561.3	32.4	548.6	57.7	496.3	269.7	561.3	32.4	113.1
AA04-80	0.7483	1.9	0.0915	1.4	0.76	564.5	7.6	567.3	8.1	578.2	26.5	564.5	7.6	97.6
AA04-79	0.7500	2.2	0.0917	2.1	0.91	565.7	11.1	568.2	9.8	578.4	19.8	565.7	11.1	97.8
AA04-4	0.7339	5.7	0.0923	2.3	0.40	569.3	12.5	558.8	24.5	516.4	114.6	569.3	12.5	110.3
AA04-41	0.7456	2.8	0.0927	1.9	0.66	571.4	10.1	565.6	12.1	542.7	45.9	571.4	10.1	105.3
AA04-46	0.8320	4.1	0.0941	3.5	0.85	580.0	19.2	614.7	18.9	745.0	46.1	580.0	19.2	77.9
AA04-19	0.7781	3.7	0.0945	2.5	0.69	581.8	14.2	584.4	16.3	594.4	57.4	581.8	14.2	97.9
AA04-6	0.7878	2.1	0.0949	1.6	0.79	584.5	9.2	589.9	9.3	610.9	27.2	584.5	9.2	95.7
AA04-92	0.8010	3.5	0.0952	3.2	0.91	586.1	17.7	597.4	15.6	640.4	30.1	586.1	17.7	91.5
AA04-95	0.7966	2.8	0.0955	2.5	0.92	588.3	14.3	594.9	12.4	620.4	23.1	588.3	14.3	94.8
AA04-105	0.9042	6.2	0.0956	5.8	0.93	588.4	32.5	654.0	29.9	887.2	45.9	588.4	32.5	66.3
AA04-22	0.7951	3.0	0.0956	2.2	0.72	588.7	12.4	594.1	13.7	614.4	45.5	588.7	12.4	95.8
AA04-39	0.8641	4.3	0.0969	3.5	0.83	596.4	20.2	632.3	20.0	763.1	49.7	596.4	20.2	78.2

AA04-53	0.8055	3.2	0.0971	3.1	0.95	597.5	17.4	599.9	14.5	609.0	21.0	597.5	17.4	98.1
AA04-75	0.7708	4.3	0.0972	2.2	0.51	598.2	12.5	580.2	18.8	510.4	80.6	598.2	12.5	117.2
AA04-47	0.8485	3.0	0.0987	2.4	0.79	606.8	13.7	623.8	14.0	686.0	39.7	606.8	13.7	88.5
AA04-102	0.8581	6.3	0.0993	3.0	0.47	610.6	17.5	629.1	29.7	696.3	119.2	610.6	17.5	87.7
AA04-82	0.8184	3.7	0.0995	2.2	0.61	611.4	13.1	607.2	16.9	591.5	63.8	611.4	13.1	103.4
AA04-104	0.8460	4.2	0.0999	3.3	0.79	613.6	19.4	622.4	19.5	654.5	55.2	613.6	19.4	93.8
AA04-51	0.8692	3.6	0.1005	3.2	0.88	617.1	18.8	635.2	17.1	700.1	36.4	617.1	18.8	88.1
AA04-89	0.8644	2.4	0.1007	1.4	0.58	618.7	8.2	632.5	11.3	682.3	41.7	618.7	8.2	90.7
AA04-5	0.8362	3.7	0.1009	2.1	0.57	619.9	12.3	617.0	17.0	606.5	65.2	619.9	12.3	102.2
AA04-76	0.8595	3.9	0.1016	1.3	0.35	623.6	8.0	629.9	18.2	652.5	78.3	623.6	8.0	95.6
AA04-81	0.8470	5.6	0.1017	3.1	0.55	624.6	18.3	623.0	26.0	617.4	100.7	624.6	18.3	101.2
AA04-30	0.8580	2.9	0.1018	1.7	0.61	624.9	10.4	629.0	13.5	643.9	49.4	624.9	10.4	97.0
AA04-23	0.8686	2.8	0.1032	1.9	0.67	633.4	11.5	634.8	13.4	639.9	45.0	633.4	11.5	99.0
AA04-55	0.8981	3.7	0.1059	3.4	0.91	648.8	20.7	650.7	17.8	657.4	33.7	648.8	20.7	98.7
AA04-31	0.9724	3.4	0.1109	2.1	0.61	678.3	13.4	689.7	17.2	727.2	58.0	678.3	13.4	93.3
AA04-13	0.9763	5.9	0.1123	4.7	0.80	686.4	30.8	691.7	29.6	709.1	75.0	686.4	30.8	96.8
AA04-12	1.0476	7.6	0.1181	7.2	0.94	719.4	49.2	727.7	39.7	753.4	52.9	719.4	49.2	95.5
AA04-35	1.2334	3.5	0.1282	3.3	0.94	777.3	24.0	815.9	19.5	922.6	23.7	777.3	24.0	84.3
AA04-43	1.2492	5.9	0.1346	5.2	0.89	814.0	40.0	823.1	33.0	847.7	54.4	814.0	40.0	96.0
AA04-8	1.2696	3.1	0.1351	3.0	0.98	816.6	23.2	832.2	17.6	874.1	12.5	816.6	23.2	93.4
AA04-32	1.2558	2.4	0.1357	1.4	0.60	820.1	11.0	826.0	13.5	841.9	39.9	820.1	11.0	97.4
AA04-77	1.3366	5.7	0.1424	5.2	0.90	858.4	41.5	861.7	33.4	870.5	52.2	858.4	41.5	98.6
AA04-88	1.3887	2.3	0.1440	2.1	0.91	867.2	17.0	884.2	13.6	926.9	19.6	867.2	17.0	93.6
AA04-38	1.4760	5.0	0.1517	3.4	0.68	910.7	28.7	920.6	30.1	944.4	74.9	944.4	74.9	96.4
AA04-54	1.5751	4.1	0.1604	3.8	0.91	958.8	33.6	960.4	25.7	964.3	34.6	964.3	34.6	99.4
AA04-63	1.7167	3.4	0.1700	1.9	0.55	1011.9	17.4	1014.8	21.8	1021.0	57.5	1021.0	57.5	99.1
AA04-28	1.5793	2.6	0.1562	2.5	0.99	935.5	22.0	962.1	15.9	1023.2	8.6	1023.2	8.6	91.4
AA04-59	1.7960	5.1	0.1768	4.8	0.94	1049.4	46.5	1044.0	33.3	1032.6	35.4	1032.6	35.4	101.6
AA04-68	1.7424	3.1	0.1710	2.1	0.70	1017.5	20.1	1024.4	19.8	1039.1	44.3	1039.1	44.3	97.9
AA04-103	1.7565	3.8	0.1722	3.5	0.92	1024.4	33.6	1029.6	24.8	1040.5	29.5	1040.5	29.5	98.5
AA04-78	1.7996	2.5	0.1762	1.7	0.67	1046.2	16.1	1045.3	16.1	1043.3	36.8	1043.3	36.8	100.3
AA04-67	1.7307	1.9	0.1695	1.4	0.71	1009.2	12.7	1020.0	12.3	1043.3	27.3	1043.3	27.3	96.7
AA04-84	1.7075	1.7	0.1671	1.1	0.69	996.1	10.6	1011.4	10.7	1044.7	24.6	1044.7	24.6	95.3
AA04-83	1.7041	2.3	0.1666	2.1	0.91	993.5	19.2	1010.1	14.6	1046.2	18.8	1046.2	18.8	95.0
AA04-3	1.8497	2.3	0.1807	2.1	0.93	1070.6	20.6	1063.3	14.8	1048.5	17.1	1048.5	17.1	102.1
AA04-33	1.7780	4.5	0.1724	4.0	0.90	1025.4	38.3	1037.5	29.3	1063.0	39.8	1063.0	39.8	96.5
AA04-21	1.7482	2.6	0.1686	2.5	0.96	1004.5	23.0	1026.5	16.6	1073.8	14.4	1073.8	14.4	93.5
AA04-16	1.7133	2.2	0.1652	2.1	0.94	985.5	19.1	1013.5	14.3	1074.6	15.5	1074.6	15.5	91.7
AA04-70	1.8330	2.1	0.1761	1.8	0.89	1045.6	17.7	1057.4	13.6	1081.8	19.1	1081.8	19.1	96.7
AA04-42	1.8968	1.7	0.1812	1.1	0.64	1073.6	10.5	1080.0	11.1	1092.9	25.7	1092.9	25.7	98.2
AA04-50	1.7704	3.9	0.1681	3.8	0.99	1001.8	35.3	1034.7	25.0	1104.8	12.8	1104.8	12.8	90.7
AA04-72	1.4718	4.5	0.1387	3.7	0.82	837.4	28.8	918.9	27.1	1120.0	51.5	1120.0	51.5	74.8
AA04-17	1.8363	2.5	0.1723	2.5	0.98	1024.8	23.3	1058.5	16.5	1128.7	8.9	1128.7	8.9	90.8
AA04-15	2.2186	2.2	0.1998	1.5	0.69	1174.4	16.2	1186.9	15.4	1209.8	31.6	1209.8	31.6	97.1
AA04-62	2.1803	2.8	0.1958	2.4	0.86	1152.9	25.3	1174.8	19.4	1215.3	27.8	1215.3	27.8	94.9
AA04-65	2.3912	1.8	0.2107	1.6	0.89	1232.3	18.4	1240.0	13.1	1253.2	16.0	1253.2	16.0	98.3
AA04-2	3.2811	3.3	0.2527	3.2	0.95	1452.3	41.1	1476.6	25.8	1511.6	18.6	1511.6	18.6	96.1
AA04-93	3.5796	4.1	0.2656	3.1	0.75	1518.4	41.9	1545.0	32.6	1581.6	50.5	1581.6	50.5	96.0
AA04-18	4.9861	2.7	0.3197	2.6	0.97	1788.3	41.4	1817.0	23.2	1849.9	12.9	1849.9	12.9	96.7
AA04-61	5.5673	5.2	0.3360	5.2	0.99	1867.4	83.6	1911.0	44.8	1958.8	12.2	1958.8	12.2	95.3
AA04-52	6.4381	3.0	0.3612	3.0	0.99	1988.0	50.5	2037.5	26.1	2087.9	5.5	2087.9	5.5	95.2
AA04-27	6.6185	2.4	0.3670	2.4	1.00	2015.5	41.8	2061.8	21.4	2108.4	2.9	2108.4	2.9	95.6
AA04-94	10.8886	2.9	0.4610	2.8	0.97	2443.9	57.3	2513.7	26.9	2570.5	10.8	2570.5	10.8	95.1

AA04-34	12.9028	6.7	0.5023	6.6	1.00	2623.6	143.2	2672.6	62.9	2709.9	8.7	2709.9	8.7	96.8
AA04-73	12.4304	1.3	0.4814	1.3	0.99	2533.3	27.7	2637.5	12.5	2718.4	2.3	2718.4	2.3	93.2
AA04-100	10.3333	4.2	0.3954	4.2	1.00	2147.9	76.7	2465.1	39.0	2738.1	5.7	2738.1	5.7	78.4
AA04-45	12.8179	4.0	0.4696	3.9	0.98	2481.7	81.2	2666.4	37.9	2809.6	13.1	2809.6	13.1	88.3
AA04-85	15.5063	2.6	0.5032	2.6	1.00	2627.7	56.6	2846.9	25.1	3005.9	3.3	3005.9	3.3	87.4

## CENOZOIC FILL

### BT-01, Oligocene-Miocene Petaca Formation (N=98). 19.66°S, 64.04°W

BT_01_110	0.6410	0.0	0.0800	0.0	0.30	496.1	2.9	503.4	3.2	549.0	10.2	496.1	2.9	90.4
BT_01_29	0.6622	0.0	0.0822	0.0	0.67	509.2	1.8	515.8	1.7	540.1	4.5	509.2	1.8	94.3
BT_01_1	0.6958	0.0	0.0832	0.0	0.50	515.1	2.2	536.1	2.2	599.0	8.7	515.1	2.2	86.0
BT_01_43	0.6930	0.0	0.0838	0.0	0.61	518.0	5.1	535.0	5.6	579.0	16.8	518.0	5.1	89.5
BT_01_104	0.6855	0.0	0.0845	0.0	0.66	523.8	3.9	529.8	2.9	563.0	8.2	523.8	3.9	93.0
BT_01_63	0.6930	0.0	0.0849	0.0	0.56	525.1	2.9	534.1	4.2	578.0	13.3	525.1	2.9	90.8
BT_01_60	0.6782	0.0	0.0850	0.0	0.41	525.7	2.3	525.4	2.9	532.0	9.7	525.7	2.3	98.8
BT_01_70	0.6857	0.0	0.0857	0.0	0.65	529.9	2.9	530.1	1.9	520.0	6.1	529.9	2.9	101.9
BT_01_2	0.6889	0.0	0.0858	0.0	0.54	530.4	2.5	531.8	3.0	534.0	7.1	530.4	2.5	99.3
BT_01_79	0.6898	0.0	0.0859	0.0	0.42	531.2	3.0	534.0	2.9	523.0	11.2	531.2	3.0	101.6
BT_01_77	0.7600	0.0	0.0868	0.0	0.07	536.6	3.0	573.4	4.0	724.0	13.3	536.6	3.0	74.1
BT_01_84	0.6988	0.0	0.0877	0.0	0.38	541.9	2.7	537.9	2.4	540.0	9.2	541.9	2.7	100.4
BT_01_16	0.7180	0.0	0.0878	0.0	0.44	542.6	2.0	549.4	1.8	580.0	6.1	542.6	2.0	93.6
BT_01_76	0.7850	0.0	0.0879	0.0	0.10	543.0	4.3	588.0	3.2	752.0	20.9	543.0	4.3	72.2
BT_01_3	0.7370	0.0	0.0887	0.0	0.46	547.9	2.6	561.1	3.3	599.0	9.7	547.9	2.6	91.5
BT_01_13	0.7470	0.0	0.0903	0.0	0.29	557.3	3.2	565.9	3.2	607.0	10.2	557.3	3.2	91.8
BT_01_109	0.7420	0.0	0.0912	0.0	0.44	562.8	2.6	564.9	3.1	584.0	7.7	562.8	2.6	96.4
BT_01_57	0.7458	0.0	0.0914	0.0	0.57	563.9	2.1	565.7	1.9	588.8	4.5	563.9	2.1	95.8
BT_01_33	0.7750	0.0	0.0915	0.0	0.76	564.5	4.7	582.3	4.4	645.0	8.7	564.5	4.7	87.5
BT_01_7	0.7610	0.0	0.0921	0.0	0.51	567.9	3.5	574.5	3.6	616.0	9.2	567.9	3.5	92.2
BT_01_41	0.8610	0.0	0.0932	0.0	0.16	574.0	5.6	630.3	3.6	814.0	18.9	574.0	5.6	70.5
BT_01_98	0.7860	0.0	0.0934	0.0	0.26	575.6	2.7	588.6	3.4	642.0	8.2	575.6	2.7	89.7
BT_01_114	0.7750	0.0	0.0938	0.0	0.46	577.7	3.5	582.4	3.3	609.0	12.2	577.7	3.5	94.9
BT_01_25	0.8230	0.0	0.0942	0.0	0.81	580.0	7.7	610.0	8.7	742.0	15.8	580.0	7.7	78.2
BT_01_78	0.7860	0.0	0.0951	0.0	0.19	585.9	2.2	590.2	3.0	605.0	9.2	585.9	2.2	96.8
BT_01_30	0.7795	0.0	0.0955	0.0	0.30	587.7	2.2	585.0	2.1	580.0	6.6	587.7	2.2	101.3
BT_01_64	0.8001	0.0	0.0957	0.0	0.80	589.0	3.3	596.7	2.4	622.0	5.1	589.0	3.3	94.7
BT_01_8	0.8390	0.0	0.0959	0.0	0.38	590.3	2.6	619.4	3.7	728.0	10.2	590.3	2.6	81.1
BT_01_59	0.7890	0.0	0.0959	0.0	0.57	590.4	3.0	588.2	3.3	579.0	9.7	590.4	3.0	102.0
BT_01_51	0.8158	0.0	0.0964	0.0	0.27	593.0	2.1	606.3	2.7	647.0	9.7	593.0	2.1	91.7
BT_01_45	0.8450	0.0	0.0967	0.0	0.74	594.7	4.9	621.0	5.6	688.0	9.2	594.7	4.9	86.4
BT_01_103	0.8390	0.0	0.0973	0.0	0.38	598.4	2.7	617.0	5.6	684.0	16.8	598.4	2.7	87.5
BT_01_24	0.8334	0.0	0.0984	0.0	0.55	604.7	2.9	615.8	1.9	652.0	6.6	604.7	2.9	92.7
BT_01_99	0.8370	0.0	0.1003	0.0	0.54	616.1	3.6	617.3	3.3	608.0	9.7	616.1	3.6	101.3
BT_01_67	0.8500	0.0	0.1004	0.0	0.19	616.9	3.8	623.9	3.7	645.0	12.8	616.9	3.8	95.6
BT_01_61	0.8790	0.0	0.1010	0.0	0.35	619.9	2.7	640.0	3.0	726.0	8.2	619.9	2.7	85.4
BT_01_91	0.8610	0.0	0.1024	0.0	0.81	628.6	4.7	630.3	3.9	641.0	7.7	628.6	4.7	98.1
BT_01_102	0.8690	0.0	0.1026	0.0	0.75	629.7	4.3	634.4	4.2	644.0	5.6	629.7	4.3	97.8
BT_01_94	0.9760	0.0	0.1053	0.0	0.62	645.0	7.7	691.0	6.1	851.0	17.9	645.0	7.7	75.8
BT_01_108	0.9382	0.0	0.1101	0.0	0.51	673.2	2.1	671.7	2.3	663.3	4.7	673.2	2.1	101.5
BT_01_39	1.1010	0.0	0.1157	0.0	0.61	705.9	3.0	754.5	3.6	886.0	8.2	705.9	3.0	79.7
BT_01_92	1.0580	0.0	0.1196	0.0	0.31	728.2	3.8	732.4	4.1	750.0	11.7	728.2	3.8	97.1
BT_01_23	1.1730	0.0	0.1244	0.0	0.76	755.5	4.9	788.5	4.4	873.0	6.1	755.5	4.9	86.5
BT_01_73	1.3070	0.0	0.1361	0.0	0.46	822.0	5.1	849.0	7.1	914.0	12.2	822.0	5.1	89.9
BT_01_69	1.5580	0.0	0.1565	0.0	0.58	937.2	3.9	952.9	4.0	983.0	6.6	937.2	3.9	95.3

BT_01_50	1.5880	0.0	0.1577	0.0	0.34	944.1	3.9	965.0	3.3	1013.0	7.7	944.1	3.9	93.2
BT_01_88	1.7810	0.0	0.1744	0.0	0.38	1037.5	4.4	1038.2	3.2	1050.0	6.6	1050.0	6.6	98.8
BT_01_90	1.8150	0.0	0.1771	0.0	0.70	1051.0	6.6	1052.1	4.6	1054.0	6.1	1054.0	6.1	99.7
BT_01_85	1.8050	0.0	0.1746	0.0	0.37	1037.2	3.5	1047.5	2.7	1062.0	5.1	1062.0	5.1	97.7
BT_01_93	1.9250	0.0	0.1836	0.0	0.64	1088.0	7.1	1088.9	4.7	1072.0	6.6	1072.0	6.6	101.5
BT_01_100	1.8320	0.0	0.1770	0.0	0.72	1051.0	6.6	1056.5	4.5	1086.0	7.1	1086.0	7.1	96.8
BT_01_54	1.7020	0.0	0.1624	0.0	0.77	970.0	5.6	1010.0	4.6	1087.1	4.1	1087.1	4.1	89.2
BT_01_105	1.8280	0.0	0.1737	0.0	0.60	1032.0	5.1	1056.1	3.0	1106.0	5.6	1106.0	5.6	93.3
BT_01_75	2.0860	0.0	0.1926	0.0	0.73	1135.4	4.0	1144.6	2.5	1163.4	3.1	1163.4	3.1	97.6
BT_01_83	2.1590	0.0	0.1981	0.0	0.73	1165.1	5.1	1168.4	3.3	1174.2	4.8	1174.2	4.8	99.2
BT_01_68	2.1630	0.0	0.1951	0.0	0.69	1147.0	17.3	1169.0	9.2	1187.0	19.9	1187.0	19.9	96.6
BT_01_21	1.9760	0.0	0.1809	0.0	0.65	1074.0	6.6	1107.0	5.1	1188.0	9.2	1188.0	9.2	90.4
BT_01_52	1.9570	0.0	0.1730	0.0	0.40	1028.4	3.9	1099.0	9.7	1225.0	25.0	1225.0	25.0	84.0
BT_01_56	2.1310	0.0	0.1859	0.0	0.42	1102.0	10.7	1160.0	5.6	1259.0	18.4	1259.0	18.4	87.5
BT_01_5	2.2810	0.0	0.1996	0.0	0.52	1173.1	5.1	1207.8	3.4	1261.0	5.6	1261.0	5.6	93.0
BT_01_12	2.0850	0.0	0.1830	0.0	0.76	1083.0	8.7	1144.6	4.7	1269.0	5.6	1269.0	5.6	85.3
BT_01_17	1.9590	0.0	0.1696	0.0	0.21	1009.9	4.7	1100.0	9.7	1275.0	26.0	1275.0	26.0	79.2
BT_01_81	2.6040	0.0	0.2256	0.0	0.39	1311.0	6.1	1301.5	3.3	1283.0	5.1	1283.0	5.1	102.2
BT_01_32	2.7130	0.0	0.2286	0.0	0.70	1327.1	4.1	1331.9	2.7	1328.6	3.1	1328.6	3.1	99.9
BT_01_107	2.8090	0.0	0.2370	0.0	0.47	1371.0	5.6	1357.8	2.6	1344.5	4.4	1344.5	4.4	102.0
BT_01_111	2.7940	0.0	0.2350	0.0	0.49	1360.5	4.3	1353.8	2.4	1355.4	3.4	1355.4	3.4	100.4
BT_01_71	2.6980	0.0	0.2246	0.0	0.54	1306.0	6.1	1327.3	3.7	1360.0	5.1	1360.0	5.1	96.0
BT_01_48	2.7820	0.0	0.2303	0.0	0.69	1335.0	9.2	1353.0	5.6	1381.0	7.7	1381.0	7.7	96.7
BT_01_113	2.7950	0.0	0.2224	0.0	0.39	1294.4	4.8	1353.9	3.7	1460.0	5.1	1460.0	5.1	88.7
BT_01_66	3.1780	0.0	0.2504	0.0	0.59	1441.0	5.1	1451.5	3.0	1468.0	4.4	1468.0	4.4	98.2
BT_01_14	3.1670	0.0	0.2500	0.0	0.67	1438.0	6.1	1448.5	4.1	1479.8	4.8	1479.8	4.8	97.2
BT_01_86	3.7930	0.0	0.2861	0.0	0.61	1622.0	7.7	1590.9	3.5	1556.1	4.4	1556.1	4.4	104.2
BT_01_22	3.2700	0.0	0.2225	0.0	0.26	1295.0	5.6	1472.0	6.6	1732.0	6.6	1732.0	6.6	74.8
BT_01_28	4.3700	0.1	0.2971	0.0	0.83	1680.0	15.3	1701.0	12.8	1733.0	10.7	1733.0	10.7	96.9
BT_01_4	4.4290	0.0	0.3011	0.0	0.70	1696.0	8.2	1717.2	3.7	1736.5	4.5	1736.5	4.5	97.7
BT_01_46	4.3980	0.0	0.2975	0.0	0.51	1679.0	6.6	1711.5	3.5	1745.0	5.6	1745.0	5.6	96.2
BT_01_42	4.0750	0.0	0.2764	0.0	0.71	1573.0	10.7	1648.0	6.6	1756.0	7.1	1756.0	7.1	89.6
BT_01_89	4.5930	0.0	0.3083	0.0	0.63	1732.0	5.6	1747.7	2.7	1763.8	3.1	1763.8	3.1	98.2
BT_01_20	4.8370	0.0	0.3228	0.0	0.57	1803.0	7.1	1791.1	3.5	1774.6	3.7	1774.6	3.7	101.6
BT_01_36	4.4990	0.0	0.2951	0.0	0.46	1669.0	6.6	1731.1	5.0	1789.0	6.1	1789.0	6.1	93.3
BT_01_9	3.6000	0.1	0.2350	0.0	0.32	1360.0	6.1	1543.0	22.4	1794.0	46.9	1794.0	46.9	75.8
BT_01_27	4.5570	0.0	0.2949	0.0	0.77	1665.0	10.7	1741.1	3.3	1833.0	6.6	1833.0	6.6	90.8
BT_01_116	4.4400	0.0	0.2865	0.0	0.32	1624.0	7.7	1720.9	4.9	1839.0	8.7	1839.0	8.7	88.3
BT_01_74	5.2360	0.0	0.3193	0.0	0.88	1785.0	12.2	1857.6	4.9	1931.6	5.1	1931.6	5.1	92.4
BT_01_38	5.7020	0.0	0.3425	0.0	0.72	1898.0	6.1	1931.3	3.1	1954.9	2.9	1954.9	2.9	97.1
BT_01_95	4.6170	0.0	0.2743	0.0	0.85	1562.0	11.7	1752.0	7.1	1992.0	5.6	1992.0	5.6	78.4
BT_01_40	6.1490	0.0	0.3589	0.0	0.51	1977.0	7.7	1997.0	4.7	2003.0	4.2	2003.0	4.2	98.7
BT_01_18	6.2970	0.0	0.3632	0.0	0.56	1997.0	7.1	2017.8	4.1	2045.6	4.3	2045.6	4.3	97.6
BT_01_34	7.0120	0.0	0.3875	0.0	0.34	2111.0	7.1	2113.4	3.0	2110.4	4.6	2110.4	4.6	100.0
BT_01_87	7.7000	0.0	0.4042	0.0	0.15	2188.0	9.2	2195.8	4.4	2200.9	3.9	2200.9	3.9	99.4
BT_01_96	5.5100	0.1	0.2885	0.0	0.50	1634.0	6.6	1899.0	10.2	2204.0	16.8	2204.0	16.8	74.1
BT_01_31	9.3880	0.0	0.4252	0.0	0.65	2284.0	8.2	2378.5	4.2	2446.9	3.9	2446.9	3.9	93.3
BT_01_82	11.7400	0.1	0.4869	0.0	0.48	2556.0	16.8	2585.0	6.6	2572.0	9.2	2572.0	9.2	99.4
BT_01_106	12.9600	0.1	0.5081	0.0	0.71	2647.0	13.8	2675.0	5.1	2688.1	4.9	2688.1	4.9	98.5
BT_01_97	11.4800	0.1	0.4480	0.0	0.08	2388.0	10.2	2564.3	4.7	2708.0	10.7	2708.0	10.7	88.2
BT_01_55	13.1000	0.1	0.4908	0.0	0.76	2573.0	12.2	2687.0	5.6	2775.0	4.2	2775.0	4.2	92.7
BT_01_15	14.2900	0.1	0.5088	0.0	0.77	2651.0	8.7	2770.3	3.8	2858.9	3.1	2858.9	3.1	92.7
BT_01_115	21.5000	0.1	0.6217	0.0	0.86	3116.0	10.7	3160.9	4.0	3195.1	2.1	3195.1	2.1	97.5

**BT-04, Miocene Tariquia Formation (N=96). 19.67°S, 64.05°W**

BT_04_35	0.1571	0.0	0.0211	0.0	0.47	134.8	0.8	147.9	2.4	339.0	23.5	134.8	0.8	NA
BT_04_65	0.2746	0.0	0.0380	0.0	0.56	240.5	2.2	245.3	2.5	289.0	15.3	240.5	2.2	83.2
BT_04_98	0.4942	0.0	0.0644	0.0	0.73	402.1	1.6	407.7	1.7	430.0	7.1	402.1	1.6	93.5
BT_04_62	0.6420	0.0	0.0770	0.0	0.74	478.0	4.1	503.2	3.5	623.0	9.7	478.0	4.1	76.7
BT_04_86	0.6520	0.0	0.0810	0.0	0.39	502.1	2.3	509.3	4.1	531.0	12.8	502.1	2.3	94.6
BT_04_84	0.6531	0.0	0.0812	0.0	0.51	503.1	2.4	510.1	2.9	538.0	9.7	503.1	2.4	93.5
BT_04_52	0.6525	0.0	0.0813	0.0	0.63	503.7	3.4	509.8	2.7	562.0	10.7	503.7	3.4	89.6
BT_04_64	0.6823	0.0	0.0839	0.0	0.27	519.0	1.9	528.1	1.6	562.0	6.1	519.0	1.9	92.3
BT_04_61	0.7480	0.0	0.0842	0.0	0.40	521.1	3.3	567.0	7.1	743.0	24.5	521.1	3.3	70.1
BT_04_95	0.6777	0.0	0.0842	0.0	0.49	521.3	1.8	525.3	1.5	543.0	5.1	521.3	1.8	96.0
BT_04_100	0.6823	0.0	0.0848	0.0	0.69	524.6	3.4	527.9	2.8	535.0	7.1	524.6	3.4	98.1
BT_04_102	0.7440	0.0	0.0864	0.0	0.12	534.1	2.9	563.0	5.1	686.0	17.9	534.1	2.9	77.9
BT_04_14	0.7135	0.0	0.0864	0.0	0.27	534.2	1.9	546.5	2.9	591.0	11.2	534.2	1.9	90.4
BT_04_76	0.7800	0.0	0.0864	0.0	0.45	534.3	3.6	583.0	7.7	757.0	21.4	534.3	3.6	70.6
BT_04_44	0.7103	0.0	0.0871	0.0	0.18	538.0	2.4	546.0	2.8	582.0	9.7	538.0	2.4	92.4
BT_04_17	0.7100	0.0	0.0872	0.0	0.19	539.1	2.1	545.1	3.1	576.0	9.7	539.1	2.1	93.6
BT_04_67	0.7378	0.0	0.0875	0.0	0.45	540.5	2.4	561.0	1.9	642.6	4.5	540.5	2.4	84.1
BT_04_58	0.7670	0.0	0.0885	0.0	0.28	546.4	2.1	577.2	4.5	676.0	14.8	546.4	2.1	80.8
BT_04_18	0.7124	0.0	0.0885	0.0	0.37	546.6	1.8	546.1	1.6	540.0	6.1	546.6	1.8	101.2
BT_04_82	0.7840	0.0	0.0888	0.0	-0.16	548.3	2.6	587.1	4.6	708.0	16.8	548.3	2.6	77.4
BT_04_53	0.7460	0.0	0.0889	0.0	0.59	548.8	3.8	565.7	3.2	636.0	10.2	548.8	3.8	86.3
BT_04_93	0.7510	0.0	0.0892	0.0	0.39	550.6	2.8	568.3	3.8	643.0	12.8	550.6	2.8	85.6
BT_04_85	0.7660	0.0	0.0895	0.0	0.57	552.7	3.0	576.9	4.5	663.0	15.3	552.7	3.0	83.4
BT_04_87	0.7489	0.0	0.0901	0.0	0.25	556.5	2.1	568.0	2.3	616.0	6.6	556.5	2.1	90.3
BT_04_111	0.7340	0.0	0.0907	0.0	0.30	559.4	2.9	558.5	3.6	539.0	10.2	559.4	2.9	103.8
BT_04_13	0.7597	0.0	0.0910	0.0	0.56	561.4	2.4	573.6	2.7	624.0	7.1	561.4	2.4	90.0
BT_04_99	0.7990	0.0	0.0910	0.0	0.38	561.4	3.7	596.2	4.5	740.0	22.4	561.4	3.7	75.9
BT_04_25	0.7485	0.0	0.0910	0.0	0.45	561.8	1.7	567.7	1.5	599.3	4.8	561.8	1.7	93.7
BT_04_3	0.7511	0.0	0.0917	0.0	0.29	565.7	1.6	568.8	1.8	585.0	5.6	565.7	1.6	96.7
BT_04_101	0.7480	0.0	0.0921	0.0	0.78	568.1	3.6	566.8	3.5	566.0	6.6	568.1	3.6	100.4
BT_04_31	0.7720	0.0	0.0921	0.0	-0.06	568.2	3.6	580.2	3.7	621.0	14.3	568.2	3.6	91.5
BT_04_6	0.7459	0.0	0.0925	0.0	0.34	570.0	1.7	565.8	1.4	557.2	3.8	570.0	1.7	102.3
BT_04_46	0.7721	0.0	0.0928	0.0	0.62	572.3	1.7	580.9	1.6	618.2	3.7	572.3	1.7	92.6
BT_04_12	0.7677	0.0	0.0941	0.0	0.17	579.4	2.0	578.9	2.0	588.0	8.2	579.4	2.0	98.5
BT_04_48	0.7976	0.0	0.0940	0.0	0.66	579.4	3.8	595.2	2.8	656.0	8.7	579.4	3.8	88.3
BT_04_2	0.7882	0.0	0.0941	0.0	0.21	579.8	2.7	589.8	2.9	621.0	8.7	579.8	2.7	93.4
BT_04_74	0.7940	0.0	0.0942	0.0	0.51	580.4	2.5	593.3	3.0	645.0	9.7	580.4	2.5	90.0
BT_04_89	0.8530	0.0	0.0944	0.0	0.52	581.3	2.9	621.0	6.6	773.0	18.9	581.3	2.9	75.2
BT_04_70	0.8170	0.0	0.0955	0.0	0.29	588.0	2.3	606.0	5.1	688.0	18.4	588.0	2.3	85.5
BT_04_27	0.7890	0.0	0.0956	0.0	0.15	588.6	3.6	589.8	4.3	598.0	14.8	588.6	3.6	98.4
BT_04_71	0.8238	0.0	0.0956	0.0	0.17	590.0	2.4	609.9	2.6	663.0	8.7	590.0	2.4	89.0
BT_04_8	0.7964	0.0	0.0971	0.0	0.55	597.4	2.2	594.7	1.9	600.2	4.9	597.4	2.2	99.5
BT_04_37	0.8480	0.0	0.0981	0.0	0.83	603.3	3.8	624.1	3.8	690.0	7.7	603.3	3.8	87.4
BT_04_15	0.8110	0.0	0.0984	0.0	0.80	605.0	4.0	604.2	4.5	611.0	8.2	605.0	4.0	99.0
BT_04_29	0.9020	0.0	0.0984	0.0	0.27	606.2	4.9	652.0	7.7	831.0	18.9	606.2	4.9	72.9
BT_04_80	0.8500	0.0	0.0995	0.0	0.58	611.5	3.8	624.6	2.9	658.0	8.7	611.5	3.8	92.9
BT_04_30	0.8264	0.0	0.0997	0.0	0.40	612.8	2.0	611.5	1.5	615.1	4.8	612.8	2.0	99.6
BT_04_21	0.8500	0.0	0.0999	0.0	0.67	613.6	3.8	625.2	3.7	671.0	10.2	613.6	3.8	91.4
BT_04_36	0.8400	0.0	0.1004	0.0	0.35	616.9	2.2	619.5	2.0	639.0	6.6	616.9	2.2	96.5
BT_04_4	0.9090	0.0	0.1005	0.0	-0.11	617.1	3.5	651.0	7.7	742.0	26.0	617.1	3.5	83.2
BT_04_41	0.8550	0.0	0.1015	0.0	0.40	623.2	3.5	626.9	3.5	644.0	8.2	623.2	3.5	96.8

BT_04_108	0.9270	0.0	0.1015	0.0	0.49	623.3	3.3	665.2	4.1	800.0	10.2	623.3	3.3	77.9
BT_04_16	0.8731	0.0	0.1029	0.0	0.51	631.1	2.1	637.1	1.9	657.0	5.6	631.1	2.1	96.1
BT_04_32	0.9470	0.0	0.1033	0.0	0.32	633.7	2.3	672.8	2.8	819.0	9.7	633.7	2.3	77.4
BT_04_39	0.9453	0.0	0.1039	0.0	0.31	637.4	3.3	675.5	2.1	786.0	8.2	637.4	3.3	81.1
BT_04_106	0.9110	0.0	0.1049	0.0	0.33	642.9	2.2	657.5	3.2	691.0	8.2	642.9	2.2	93.0
BT_04_47	0.9970	0.0	0.1133	0.0	0.21	691.9	3.2	702.9	3.3	726.0	8.2	691.9	3.2	95.3
BT_04_96	1.1460	0.0	0.1230	0.0	0.60	747.6	3.8	775.0	3.4	856.0	6.6	747.6	3.8	87.3
BT_04_79	1.1790	0.0	0.1245	0.0	0.89	756.0	5.6	790.0	5.6	900.0	6.6	756.0	5.6	84.0
BT_04_43	1.1900	0.0	0.1279	0.0	0.15	776.0	4.2	795.1	5.0	831.0	13.8	776.0	4.2	93.4
BT_04_26	1.6790	0.0	0.1663	0.0	0.50	991.0	6.1	1000.0	3.6	1030.0	7.7	1030.0	7.7	96.2
BT_04_50	1.6830	0.0	0.1658	0.0	0.34	988.6	4.1	1003.2	3.3	1031.0	7.1	1031.0	7.1	95.9
BT_04_7	1.6810	0.0	0.1659	0.0	0.61	989.4	4.1	1001.9	3.2	1031.3	4.9	1031.3	4.9	95.9
BT_04_24	1.7500	0.0	0.1717	0.0	0.35	1021.3	4.0	1026.7	3.6	1048.0	5.6	1048.0	5.6	97.5
BT_04_110	1.8320	0.0	0.1768	0.0	0.56	1049.0	6.1	1056.6	3.7	1054.0	6.1	1054.0	6.1	99.5
BT_04_1	1.7580	0.0	0.1701	0.0	0.59	1012.5	4.3	1029.9	3.4	1075.0	5.6	1075.0	5.6	94.2
BT_04_60	1.6860	0.0	0.1617	0.0	0.27	966.3	4.4	1002.4	4.8	1078.0	9.7	1078.0	9.7	89.6
BT_04_55	1.7230	0.0	0.1664	0.0	0.66	992.8	3.6	1018.9	4.7	1083.0	8.2	1083.0	8.2	91.7
BT_04_88	1.8630	0.0	0.1780	0.0	0.29	1056.0	5.6	1067.0	4.9	1097.0	8.2	1097.0	8.2	96.3
BT_04_20	1.9090	0.0	0.1805	0.0	0.18	1069.7	2.5	1083.9	2.2	1125.1	5.0	1125.1	5.0	95.1
BT_04_11	2.0320	0.0	0.1911	0.0	0.48	1127.3	3.4	1126.7	3.4	1135.0	5.1	1135.0	5.1	99.3
BT_04_73	1.7720	0.0	0.1617	0.0	0.22	966.4	3.3	1034.7	4.1	1181.0	10.7	1181.0	10.7	81.8
BT_04_5	2.0600	0.0	0.1871	0.0	0.72	1105.0	5.6	1135.2	2.8	1188.0	5.1	1188.0	5.1	93.0
BT_04_104	2.0330	0.0	0.1804	0.0	0.52	1069.0	5.6	1126.3	3.1	1227.0	5.6	1227.0	5.6	87.1
BT_04_40	2.4450	0.0	0.2178	0.0	0.47	1269.9	4.9	1255.7	3.6	1232.2	4.7	1232.2	4.7	103.1
BT_04_34	1.9170	0.0	0.1711	0.0	0.51	1018.1	4.1	1087.4	4.0	1235.0	9.2	1235.0	9.2	82.4
BT_04_10	2.3030	0.0	0.2044	0.0	0.62	1198.9	3.7	1212.9	1.8	1235.6	3.8	1235.6	3.8	97.0
BT_04_77	2.4620	0.0	0.2142	0.0	0.34	1251.3	4.8	1260.6	4.0	1289.3	5.1	1289.3	5.1	97.1
BT_04_51	2.5450	0.0	0.2182	0.0	0.24	1272.5	4.6	1284.6	2.9	1309.0	5.6	1309.0	5.6	97.2
BT_04_66	2.4880	0.0	0.2114	0.0	0.55	1236.0	4.6	1268.5	2.8	1325.3	4.4	1325.3	4.4	93.3
BT_04_72	2.0340	0.0	0.1684	0.0	0.71	1003.0	7.7	1127.0	7.7	1385.0	11.2	1385.0	11.2	72.4
BT_04_91	2.3700	0.1	0.1939	0.0	0.72	1142.0	14.8	1228.0	15.8	1408.0	30.1	1408.0	30.1	81.1
BT_04_75	3.2360	0.0	0.2461	0.0	0.46	1418.0	5.6	1465.5	3.5	1544.8	3.9	1544.8	3.9	91.8
BT_04_105	3.9320	0.0	0.2720	0.0	0.46	1551.0	8.2	1620.8	4.4	1711.0	6.1	1711.0	6.1	90.6
BT_04_56	4.5280	0.0	0.2980	0.0	0.82	1681.0	11.2	1738.0	5.6	1804.0	5.1	1804.0	5.1	93.2
BT_04_97	5.9540	0.0	0.3431	0.0	0.63	1901.0	7.7	1968.5	4.9	2049.0	5.6	2049.0	5.6	92.8
BT_04_42	5.8960	0.0	0.3329	0.0	0.77	1852.0	13.8	1960.0	6.6	2063.0	6.6	2063.0	6.6	89.8
BT_04_49	6.3100	0.1	0.3631	0.0	0.68	1997.0	13.8	2019.0	7.7	2064.0	8.7	2064.0	8.7	96.8
BT_04_92	4.8990	0.0	0.2747	0.0	0.56	1565.0	6.6	1801.0	5.6	2085.0	9.2	2085.0	9.2	75.1
BT_04_45	5.9600	0.0	0.3245	0.0	0.77	1811.0	11.7	1969.2	4.6	2146.0	7.7	2146.0	7.7	84.4
BT_04_22	7.0210	0.0	0.3739	0.0	0.66	2047.0	7.7	2115.1	2.9	2190.7	3.0	2190.7	3.0	93.4
BT_04_69	7.1700	0.0	0.3712	0.0	0.41	2034.0	8.2	2132.0	5.6	2220.0	6.1	2220.0	6.1	91.6
BT_04_28	7.3000	0.1	0.3768	0.0	0.84	2060.0	16.3	2150.0	9.2	2255.0	8.2	2255.0	8.2	91.4
BT_04_68	10.2400	0.1	0.4198	0.0	0.82	2258.0	17.3	2453.0	9.7	2615.1	4.9	2615.1	4.9	86.3
BT_04_81	9.8390	0.0	0.3800	0.0	0.66	2076.0	8.2	2419.3	3.8	2725.0	3.6	2725.0	3.6	76.2
BT_04_90	13.6700	0.1	0.4755	0.0	0.70	2507.0	10.2	2727.4	4.2	2891.1	3.4	2891.1	3.4	86.7

#### BT-06, Miocene Guandacay Formation (N=87). 19.62°S, 64.07°W

BT_06_13	0.3729	0.0	0.0517	0.0	0.33	325.1	2.4	322.2	2.7	321.0	13.8	325.1	2.4	101.3
BT_06_12	0.4560	0.0	0.0609	0.0	0.56	380.9	3.4	381.1	3.8	387.0	14.3	380.9	3.4	98.4
BT_06_86	0.5811	0.0	0.0740	0.0	0.32	460.1	2.3	465.0	2.2	485.0	9.2	460.1	2.3	94.9
BT_06_95	0.6499	0.0	0.0807	0.0	0.58	500.1	3.3	508.7	3.2	525.0	8.2	500.1	3.3	95.3
BT_06_10	0.6970	0.0	0.0819	0.0	0.41	507.0	6.1	538.0	8.2	621.0	20.9	507.0	6.1	81.6
BT_06_17	0.6420	0.0	0.0822	0.0	0.60	509.0	5.6	505.4	4.5	505.0	12.8	509.0	5.6	100.8

BT_06_52	0.7110	0.0	0.0845	0.0	0.20	522.6	3.0	545.7	3.7	641.0	9.7	522.6	3.0	81.5
BT_06_34	0.7260	0.0	0.0868	0.0	0.49	536.7	5.1	553.6	4.2	624.0	14.8	536.7	5.1	86.0
BT_06_101	0.7150	0.0	0.0882	0.0	0.53	544.7	3.7	547.5	4.3	546.0	10.7	544.7	3.7	99.8
BT_06_16	0.7950	0.0	0.0890	0.0	0.09	549.3	4.4	593.0	5.6	776.0	24.5	549.3	4.4	70.8
BT_06_67	0.7340	0.0	0.0898	0.0	0.63	554.0	6.1	558.0	5.1	576.0	11.7	554.0	6.1	96.2
BT_06_91	0.7280	0.0	0.0898	0.0	0.48	554.1	3.7	555.0	3.5	571.0	8.2	554.1	3.7	97.0
BT_06_90	0.7310	0.0	0.0906	0.0	0.30	558.8	3.1	557.1	3.0	552.0	9.7	558.8	3.1	101.2
BT_06_72	0.7940	0.0	0.0913	0.0	0.56	563.0	6.1	594.0	6.1	745.0	15.8	563.0	6.1	75.6
BT_06_78	0.7567	0.0	0.0914	0.0	0.29	563.9	2.6	571.9	2.2	601.0	8.7	563.9	2.6	93.8
BT_06_92	0.8020	0.0	0.0918	0.0	0.54	566.0	6.6	596.0	7.1	675.0	17.9	566.0	6.6	83.9
BT_06_9	0.7571	0.0	0.0920	0.0	0.17	567.5	2.8	572.1	2.7	582.0	9.2	567.5	2.8	97.5
BT_06_94	0.7410	0.0	0.0928	0.0	0.42	571.7	4.4	562.0	5.1	524.0	15.8	571.7	4.4	109.1
BT_06_49	0.7720	0.0	0.0938	0.0	0.32	577.7	4.3	580.7	3.8	596.0	11.7	577.7	4.3	96.9
BT_06_79	0.7665	0.0	0.0939	0.0	0.39	578.6	3.5	578.2	2.7	564.0	9.2	578.6	3.5	102.6
BT_06_89	0.7880	0.0	0.0943	0.0	0.46	580.8	4.5	589.4	5.0	649.0	16.8	580.8	4.5	89.5
BT_06_20	0.7970	0.0	0.0945	0.0	0.13	581.9	4.5	594.6	4.8	659.0	15.8	581.9	4.5	88.3
BT_06_8	0.8080	0.0	0.0947	0.0	0.39	584.2	4.1	601.0	5.6	662.0	14.8	584.2	4.1	88.2
BT_06_18	0.7827	0.0	0.0950	0.0	0.55	585.0	3.3	587.6	2.6	608.0	6.1	585.0	3.3	96.2
BT_06_84	0.7950	0.0	0.0961	0.0	0.59	591.0	5.1	595.1	4.4	584.0	10.2	591.0	5.1	101.2
BT_06_1	0.8500	0.0	0.0964	0.0	0.35	593.0	5.6	627.0	6.1	762.0	13.8	593.0	5.6	77.8
BT_06_50	0.8110	0.0	0.0967	0.0	0.20	594.9	3.8	602.0	5.6	640.0	19.4	594.9	3.8	93.0
BT_06_6	0.7997	0.0	0.0969	0.0	0.35	596.0	3.3	596.4	2.6	584.0	8.7	596.0	3.3	102.1
BT_06_44	0.8160	0.0	0.0974	0.0	0.40	599.0	5.1	605.0	5.1	613.0	15.8	599.0	5.1	97.7
BT_06_103	0.7950	0.0	0.0980	0.0	0.40	602.5	4.4	593.8	3.4	570.0	11.7	602.5	4.4	105.7
BT_06_102	0.8300	0.0	0.0987	0.0	0.16	606.5	4.3	613.0	5.1	641.0	16.3	606.5	4.3	94.6
BT_06_87	0.8420	0.0	0.0987	0.0	0.03	606.5	3.9	619.5	3.9	675.0	16.3	606.5	3.9	89.9
BT_06_63	0.8010	0.0	0.0987	0.0	0.36	606.7	4.9	598.0	2.9	566.0	9.7	606.7	4.9	107.2
BT_06_15	0.8170	0.0	0.0997	0.0	0.14	612.0	5.1	608.0	5.6	587.0	15.8	612.0	5.1	104.3
BT_06_58	0.8450	0.0	0.1018	0.0	0.52	625.0	5.6	622.2	3.5	614.0	9.7	625.0	5.6	101.8
BT_06_32	0.8630	0.0	0.1022	0.0	0.34	628.4	3.9	631.4	4.1	640.0	14.3	628.4	3.9	98.2
BT_06_31	0.8410	0.0	0.1032	0.0	0.41	633.0	4.0	619.7	3.0	598.0	9.2	633.0	4.0	105.9
BT_06_76	0.9170	0.0	0.1055	0.0	0.44	646.0	6.1	660.0	6.6	710.0	15.3	646.0	6.1	91.0
BT_06_68	0.8970	0.0	0.1056	0.0	0.53	647.0	7.1	649.5	4.2	659.0	10.2	647.0	7.1	98.2
BT_06_98	0.9630	0.0	0.1057	0.0	-0.04	648.0	6.1	685.0	7.7	779.0	28.6	648.0	6.1	83.2
BT_06_39	0.8810	0.0	0.1059	0.0	0.25	651.4	4.6	641.7	4.8	611.0	12.2	651.4	4.6	106.6
BT_06_41	0.9250	0.0	0.1081	0.0	0.36	661.6	3.4	665.4	3.6	669.0	9.2	661.6	3.4	98.9
BT_06_7	0.9100	0.0	0.1088	0.0	0.67	665.0	5.6	656.7	4.2	618.0	7.1	665.0	5.6	107.6
BT_06_24	0.9250	0.0	0.1087	0.0	0.47	665.1	4.9	664.4	4.3	688.0	10.2	665.1	4.9	96.7
BT_06_36	0.9171	0.0	0.1091	0.0	0.33	667.2	3.6	660.7	2.2	619.0	8.2	667.2	3.6	107.8
BT_06_22	0.9440	0.0	0.1099	0.0	0.53	672.3	4.5	674.8	3.3	641.0	7.7	672.3	4.5	104.9
BT_06_11	0.9250	0.0	0.1108	0.0	0.50	677.0	8.2	666.0	7.1	623.0	17.3	677.0	8.2	108.7
BT_06_26	1.0930	0.0	0.1119	0.0	0.08	683.0	5.6	747.0	10.7	929.0	42.3	683.0	5.6	73.5
BT_06_80	0.9560	0.0	0.1123	0.0	0.23	685.9	3.8	681.9	4.3	662.0	11.7	685.9	3.8	103.6
BT_06_104	0.9890	0.0	0.1151	0.0	0.67	702.1	4.8	697.7	4.0	681.0	7.1	702.1	4.8	103.1
BT_06_100	1.2190	0.0	0.1362	0.0	0.44	823.0	6.1	808.8	5.1	775.0	10.2	823.0	6.1	106.2
BT_06_75	1.3320	0.0	0.1375	0.0	0.61	830.2	4.2	859.3	3.6	938.0	5.6	830.2	4.2	88.5
BT_06_14	1.4160	0.0	0.1506	0.0	0.33	904.0	6.1	897.2	4.6	859.0	12.8	904.0	6.1	105.2
BT_06_96	1.8590	0.0	0.1832	0.0	0.34	1084.0	6.6	1065.0	7.1	1015.0	10.2	1015.0	10.2	106.8
BT_06_27	1.7380	0.0	0.1727	0.0	0.50	1027.0	7.1	1022.3	3.9	1015.0	9.2	1015.0	9.2	101.2
BT_06_23	1.8440	0.0	0.1828	0.0	0.44	1082.0	6.1	1062.1	4.2	1026.0	8.2	1026.0	8.2	105.5
BT_06_69	1.8430	0.0	0.1826	0.0	0.57	1081.0	9.2	1060.0	5.1	1027.0	11.2	1027.0	11.2	105.3
BT_06_38	1.7870	0.0	0.1766	0.0	0.53	1048.0	5.0	1041.0	3.0	1032.0	5.6	1032.0	5.6	101.6
BT_06_33	1.8870	0.0	0.1842	0.0	0.34	1090.0	5.1	1076.1	3.9	1049.0	7.7	1049.0	7.7	103.9

BT_06_57	1.8160	0.0	0.1771	0.0	0.52	1051.0	7.7	1051.7	4.5	1052.0	8.7	1052.0	8.7	99.9
BT_06_4	1.7470	0.0	0.1704	0.0	0.23	1014.0	6.6	1027.0	7.7	1062.0	12.8	1062.0	12.8	95.5
BT_06_35	1.8820	0.0	0.1813	0.0	0.56	1074.0	4.4	1074.6	3.4	1066.0	6.1	1066.0	6.1	100.8
BT_06_77	2.0640	0.0	0.1995	0.0	0.77	1172.0	9.2	1136.0	5.1	1088.0	6.6	1088.0	6.6	107.7
BT_06_5	1.7590	0.0	0.1682	0.0	0.79	1002.0	13.3	1030.0	6.6	1088.0	10.2	1088.0	10.2	92.1
BT_06_25	1.9890	0.0	0.1888	0.0	0.50	1115.0	6.6	1113.6	4.3	1098.0	8.2	1098.0	8.2	101.5
BT_06_40	1.9820	0.0	0.1884	0.0	0.50	1112.0	7.1	1108.4	4.9	1103.0	9.2	1103.0	9.2	100.8
BT_06_83	2.0080	0.0	0.1916	0.0	0.54	1130.0	7.1	1117.0	5.6	1111.0	8.2	1111.0	8.2	101.7
BT_06_60	2.1250	0.0	0.1955	0.0	0.41	1151.0	8.2	1158.0	7.7	1174.0	14.8	1174.0	14.8	98.0
BT_06_48	2.3060	0.0	0.2096	0.0	0.56	1226.0	6.6	1215.7	3.8	1189.0	6.1	1189.0	6.1	103.1
BT_06_43	1.9600	0.0	0.1755	0.0	0.54	1042.0	9.2	1101.2	4.3	1204.0	11.7	1204.0	11.7	86.5
BT_06_88	2.2530	0.0	0.2022	0.0	0.14	1187.0	9.2	1197.0	6.1	1215.0	7.1	1215.0	7.1	97.7
BT_06_65	2.5540	0.0	0.2265	0.0	0.67	1316.0	5.6	1287.3	3.5	1239.5	4.5	1239.5	4.5	106.2
BT_06_29	2.4580	0.0	0.2207	0.0	0.68	1284.0	21.4	1261.0	13.3	1240.0	20.9	1240.0	20.9	103.5
BT_06_73	2.2670	0.0	0.1947	0.0	0.76	1147.0	8.2	1201.0	6.1	1297.0	6.6	1297.0	6.6	88.4
BT_06_51	2.8580	0.0	0.2418	0.0	0.35	1396.0	8.7	1373.0	6.1	1339.0	8.7	1339.0	8.7	104.3
BT_06_82	2.4420	0.0	0.2056	0.0	0.03	1205.0	8.2	1256.3	4.2	1345.0	18.9	1345.0	18.9	89.6
BT_06_28	3.3680	0.0	0.2697	0.0	0.62	1539.0	10.2	1497.0	5.1	1436.0	8.7	1436.0	8.7	107.2
BT_06_66	3.7130	0.0	0.2767	0.0	0.59	1574.0	10.7	1575.0	6.6	1564.0	7.7	1564.0	7.7	100.6
BT_06_30	5.0130	0.0	0.3373	0.0	0.70	1873.0	10.2	1821.1	4.5	1761.9	4.5	1761.9	4.5	106.3
BT_06_93	5.5840	0.0	0.3518	0.0	0.67	1942.0	14.8	1913.0	5.6	1878.0	6.1	1878.0	6.1	103.4
BT_06_2	5.5650	0.0	0.3509	0.0	0.74	1938.0	16.3	1910.0	5.6	1883.0	9.2	1883.0	9.2	102.9
BT_06_70	6.3300	0.1	0.3760	0.0	0.71	2053.0	32.7	2018.0	16.8	1974.0	11.7	1974.0	11.7	104.0
BT_06_47	6.6590	0.0	0.3809	0.0	0.70	2080.0	10.2	2067.5	4.3	2051.0	5.6	2051.0	5.6	101.4
BT_06_61	7.1600	0.1	0.3910	0.0	0.75	2127.0	23.0	2131.0	7.7	2147.0	6.1	2147.0	6.1	99.1
BT_06_37	10.5500	0.1	0.4647	0.0	0.00	2459.0	15.3	2481.0	8.2	2500.0	9.7	2500.0	9.7	98.4
BT_06_74	11.7600	0.1	0.4540	0.0	0.77	2412.0	14.8	2589.0	6.6	2724.1	4.4	2724.1	4.4	88.5
BT_06_3	15.7500	0.1	0.5616	0.0	0.78	2872.0	18.4	2861.0	6.6	2836.4	4.3	2836.4	4.3	101.3

#### BT-10, Miocene Guandacay Formation (N=91). 19.61°S, 64.08°W

BT_10_18	0.3440	0.0	0.0477	0.0	0.49	300.6	1.6	300.1	1.7	322.0	8.2	300.6	1.6	93.4
BT_10_58	0.6580	0.0	0.0817	0.0	0.52	506.0	5.1	514.1	3.7	549.0	12.2	506.0	5.1	92.2
BT_10_28	0.6980	0.0	0.0845	0.0	0.61	522.7	4.6	537.0	4.8	587.0	11.7	522.7	4.6	89.0
BT_10_50	0.7110	0.0	0.0862	0.0	0.30	533.0	5.6	544.8	4.4	615.0	14.3	533.0	5.6	86.7
BT_10_59	0.6890	0.0	0.0866	0.0	0.24	535.0	7.1	530.0	7.7	594.0	20.9	535.0	7.1	90.1
BT_10_77	0.7160	0.0	0.0878	0.0	0.12	542.1	2.8	547.6	3.7	594.0	12.2	542.1	2.8	91.3
BT_10_101	0.7970	0.0	0.0891	0.0	0.21	550.0	5.1	594.9	4.6	783.0	20.9	550.0	5.1	70.2
BT_10_102	0.7160	0.0	0.0898	0.0	0.36	554.1	4.3	547.5	4.3	547.0	16.8	554.1	4.3	101.3
BT_10_23	0.8140	0.0	0.0900	0.0	0.28	555.0	7.1	606.0	9.2	791.0	28.1	555.0	7.1	70.2
BT_10_79	0.7330	0.0	0.0902	0.0	0.39	558.0	4.6	557.8	4.3	563.0	12.8	558.0	4.6	99.1
BT_10_72	0.7570	0.0	0.0911	0.0	0.12	562.0	4.5	572.5	4.7	601.0	17.3	562.0	4.5	93.5
BT_10_70	0.7360	0.0	0.0911	0.0	0.54	562.2	3.8	560.4	3.9	539.0	9.2	562.2	3.8	104.3
BT_10_40	0.7310	0.0	0.0913	0.0	0.38	562.9	4.8	556.7	4.1	522.0	13.3	562.9	4.8	107.8
BT_10_69	0.7480	0.0	0.0914	0.0	0.68	563.0	6.1	567.1	4.6	556.0	11.7	563.0	6.1	101.3
BT_10_90	0.7530	0.0	0.0922	0.0	0.63	568.6	3.7	569.5	3.6	579.0	7.1	568.6	3.7	98.2
BT_10_91	0.8100	0.0	0.0921	0.0	0.33	571.0	10.7	602.0	9.7	720.0	28.1	571.0	10.7	79.3
BT_10_1	0.7520	0.0	0.0928	0.0	0.56	572.1	4.3	568.9	3.7	565.0	9.2	572.1	4.3	101.3
BT_10_52	0.7530	0.0	0.0929	0.0	0.43	573.0	5.6	572.0	6.6	582.0	16.8	573.0	5.6	98.5
BT_10_81	0.7400	0.0	0.0933	0.0	0.57	574.9	3.7	562.2	3.0	538.0	7.1	574.9	3.7	106.9
BT_10_39	0.7990	0.0	0.0935	0.0	0.19	576.0	7.1	596.0	6.6	676.0	27.6	576.0	7.1	85.2
BT_10_29	0.7570	0.0	0.0938	0.0	0.39	577.9	4.6	571.6	3.6	551.0	9.7	577.9	4.6	104.9
BT_10_6	0.7480	0.0	0.0941	0.0	0.50	579.8	3.1	567.6	3.3	532.0	8.7	579.8	3.1	109.0
BT_10_24	0.7670	0.0	0.0941	0.0	0.20	581.0	6.1	577.0	5.6	579.0	16.3	581.0	6.1	100.3

BT_10_98	0.7620	0.0	0.0944	0.0	0.54	581.1	4.3	575.5	3.3	558.0	8.7	581.1	4.3	104.1
BT_10_22	0.7610	0.0	0.0946	0.0	0.19	583.6	3.7	574.4	3.4	562.0	11.7	583.6	3.7	103.8
BT_10_107	0.7770	0.0	0.0949	0.0	0.59	584.2	3.9	583.1	3.8	582.0	11.2	584.2	3.9	100.4
BT_10_35	0.7770	0.0	0.0952	0.0	0.54	586.4	4.4	583.0	5.6	583.0	13.8	586.4	4.4	100.6
BT_10_16	0.7790	0.0	0.0955	0.0	0.56	588.0	4.1	586.4	4.4	595.0	11.2	588.0	4.1	98.8
BT_10_61	0.7810	0.0	0.0959	0.0	0.35	591.4	3.9	585.8	3.4	551.0	11.2	591.4	3.9	107.3
BT_10_51	0.7830	0.0	0.0959	0.0	0.48	592.0	5.1	588.0	3.8	609.0	10.7	592.0	5.1	97.2
BT_10_15	0.7810	0.0	0.0964	0.0	0.43	593.0	4.3	585.5	3.7	565.0	10.2	593.0	4.3	105.0
BT_10_87	0.8360	0.0	0.0964	0.0	0.59	593.0	9.2	619.0	8.2	728.0	21.4	593.0	9.2	81.5
BT_10_64	0.7850	0.0	0.0966	0.0	0.29	594.3	4.5	588.0	5.1	593.0	15.8	594.3	4.5	100.2
BT_10_17	0.7980	0.0	0.0970	0.0	0.47	596.6	4.8	595.0	4.9	605.0	14.3	596.6	4.8	98.6
BT_10_34	0.8050	0.0	0.0970	0.0	0.48	597.0	3.5	599.9	2.9	603.0	7.7	597.0	3.5	99.0
BT_10_78	0.7920	0.0	0.0971	0.0	0.49	597.5	4.5	591.8	3.6	567.0	8.7	597.5	4.5	105.4
BT_10_86	0.7860	0.0	0.0973	0.0	0.59	599.0	5.1	588.2	3.8	564.0	10.2	599.0	5.1	106.2
BT_10_31	0.8140	0.0	0.0975	0.0	0.47	600.8	4.7	603.0	6.1	644.0	12.2	600.8	4.7	93.3
BT_10_76	0.7950	0.0	0.0982	0.0	0.36	603.7	4.5	593.5	3.9	557.0	13.3	603.7	4.5	108.4
BT_10_84	0.8100	0.0	0.0986	0.0	0.60	606.0	4.3	603.4	4.3	584.0	9.2	606.0	4.3	103.8
BT_10_95	0.8130	0.0	0.0985	0.0	0.60	606.3	4.0	604.0	3.1	588.0	6.1	606.3	4.0	103.1
BT_10_20	0.8130	0.0	0.0992	0.0	0.73	609.0	5.6	604.4	3.9	572.0	8.2	609.0	5.6	106.5
BT_10_106	0.8250	0.0	0.0999	0.0	0.35	613.8	3.1	610.3	4.1	607.0	11.2	613.8	3.1	101.1
BT_10_14	0.8180	0.0	0.1003	0.0	0.60	616.0	8.7	608.0	5.6	589.0	16.8	616.0	8.7	104.6
BT_10_75	0.8370	0.0	0.1005	0.0	0.43	617.0	7.1	616.0	7.1	611.0	19.4	617.0	7.1	101.0
BT_10_43	0.8100	0.0	0.1005	0.0	0.67	617.1	4.1	602.1	3.0	561.0	7.1	617.1	4.1	110.0
BT_10_11	0.8560	0.0	0.1020	0.0	0.14	626.0	7.7	625.0	11.7	600.0	33.2	626.0	7.7	104.3
BT_10_44	0.8437	0.0	0.1022	0.0	0.56	627.0	2.6	621.6	2.2	612.0	5.1	627.0	2.6	102.5
BT_10_103	0.8680	0.0	0.1021	0.0	0.26	627.0	5.6	634.0	5.6	676.0	16.8	627.0	5.6	92.8
BT_10_71	0.8540	0.0	0.1021	0.0	0.18	628.0	5.6	626.0	4.5	631.0	16.8	628.0	5.6	99.5
BT_10_74	0.8250	0.0	0.1027	0.0	0.58	630.0	5.1	611.9	3.9	574.0	9.2	630.0	5.1	109.8
BT_10_26	0.8710	0.0	0.1040	0.0	0.58	638.0	5.6	635.7	4.4	632.0	9.7	638.0	5.6	100.9
BT_10_82	0.9270	0.0	0.1049	0.0	0.37	643.0	6.6	665.0	6.1	767.0	15.8	643.0	6.6	83.8
BT_10_41	0.8970	0.0	0.1054	0.0	0.62	646.0	6.1	650.6	4.6	678.0	9.7	646.0	6.1	95.3
BT_10_21	0.8670	0.0	0.1057	0.0	0.52	647.7	4.7	633.5	3.5	597.0	9.2	647.7	4.7	108.5
BT_10_62	0.8920	0.0	0.1063	0.0	0.67	653.0	6.6	647.3	4.3	631.0	10.2	653.0	6.6	103.5
BT_10_83	0.8960	0.0	0.1067	0.0	0.33	654.0	5.6	649.0	6.6	623.0	18.4	654.0	5.6	105.0
BT_10_49	0.8780	0.0	0.1074	0.0	0.61	657.5	3.9	639.9	3.1	604.0	8.2	657.5	3.9	108.9
BT_10_32	0.9450	0.0	0.1091	0.0	0.62	667.0	6.6	676.0	4.3	670.0	11.2	667.0	6.6	99.6
BT_10_56	0.9240	0.0	0.1094	0.0	0.31	669.0	6.1	664.0	5.6	634.0	12.8	669.0	6.1	105.5
BT_10_66	0.9330	0.0	0.1117	0.0	0.64	682.0	7.1	669.0	6.1	640.0	13.8	682.0	7.1	106.6
BT_10_42	0.9590	0.0	0.1122	0.0	0.61	685.0	6.1	682.0	6.6	646.0	11.7	685.0	6.1	106.0
BT_10_5	0.9370	0.0	0.1126	0.0	0.49	687.9	4.0	671.1	3.0	632.0	6.6	687.9	4.0	108.8
BT_10_46	0.9800	0.0	0.1140	0.0	0.71	696.0	6.1	692.9	5.1	685.0	8.2	696.0	6.1	101.6
BT_10_99	0.9940	0.0	0.1140	0.0	0.76	696.0	7.1	700.0	5.6	716.0	9.7	696.0	7.1	97.2
BT_10_68	1.0030	0.0	0.1152	0.0	0.33	703.0	6.6	704.0	6.1	750.0	15.8	703.0	6.6	93.7
BT_10_4	1.0160	0.0	0.1178	0.0	0.61	718.0	6.6	712.6	4.0	697.0	8.7	718.0	6.6	103.0
BT_10_54	1.2620	0.0	0.1328	0.0	0.67	804.0	8.2	828.0	5.6	876.0	10.7	804.0	8.2	91.8
BT_10_36	1.2540	0.0	0.1385	0.0	0.50	836.3	4.6	824.9	3.1	802.0	6.1	836.3	4.6	104.3
BT_10_97	1.6830	0.0	0.1719	0.0	0.55	1022.0	7.1	1001.6	4.9	961.0	8.2	961.0	8.2	106.3
BT_10_2	1.6760	0.0	0.1659	0.0	0.64	987.0	19.4	1000.0	11.2	1000.0	30.6	1000.0	30.6	98.7
BT_10_100	1.7400	0.0	0.1751	0.0	0.64	1039.0	17.9	1028.0	12.8	1001.0	18.4	1001.0	18.4	103.8
BT_10_25	1.6970	0.0	0.1691	0.0	0.29	1009.0	10.7	1004.0	10.7	1004.0	23.5	1004.0	23.5	100.5
BT_10_60	1.7410	0.0	0.1727	0.0	0.38	1029.0	8.7	1028.0	10.2	1023.0	16.3	1023.0	16.3	100.6
BT_10_27	1.9750	0.0	0.1926	0.0	0.64	1138.0	9.2	1106.0	5.1	1039.0	8.7	1039.0	8.7	109.5
BT_10_10	1.9410	0.0	0.1919	0.0	0.56	1131.0	9.7	1096.0	5.1	1049.0	11.7	1049.0	11.7	107.8

BT_10_30	1.8530	0.0	0.1837	0.0	0.61	1087.0	8.7	1065.2	5.0	1053.0	9.2	1053.0	9.2	103.2
BT_10_85	1.9780	0.0	0.1944	0.0	0.79	1145.0	15.8	1107.0	8.7	1055.0	10.7	1055.0	10.7	108.5
BT_10_105	1.9240	0.0	0.1868	0.0	0.64	1104.0	10.2	1090.0	6.1	1055.0	9.2	1055.0	9.2	104.6
BT_10_45	1.8760	0.0	0.1822	0.0	0.42	1079.0	10.2	1072.0	6.1	1064.0	10.7	1064.0	10.7	101.4
BT_10_63	1.8210	0.0	0.1775	0.0	0.68	1053.0	9.7	1052.0	5.6	1068.0	10.2	1068.0	10.2	98.6
BT_10_47	1.8320	0.0	0.1800	0.0	0.45	1067.0	10.7	1059.0	9.7	1089.0	15.3	1089.0	15.3	98.0
BT_10_80	1.9100	0.0	0.1802	0.0	0.30	1072.0	13.8	1083.0	9.2	1123.0	19.9	1123.0	19.9	95.5
BT_10_9	2.4160	0.0	0.2182	0.0	0.73	1272.0	11.7	1248.0	7.1	1224.0	10.7	1224.0	10.7	103.9
BT_10_19	4.1360	0.0	0.2969	0.0	0.70	1678.0	9.2	1662.1	4.9	1646.0	5.6	1646.0	5.6	101.9
BT_10_7	6.4000	0.1	0.3715	0.0	0.76	2035.0	15.3	2035.0	7.1	2029.0	7.7	2029.0	7.7	100.3
BT_10_8	8.0400	0.1	0.4280	0.0	0.72	2296.0	16.8	2234.0	6.1	2184.0	4.1	2184.0	4.1	105.1
BT_10_3	8.1100	0.1	0.4182	0.0	0.87	2251.0	13.8	2241.0	6.6	2231.3	3.2	2231.3	3.2	100.9
BT_10_38	13.4900	0.1	0.5247	0.0	0.74	2718.0	16.8	2715.0	6.6	2709.1	4.6	2709.1	4.6	100.3
BT_10_93	11.8600	0.1	0.4615	0.0	0.83	2444.0	19.4	2593.0	7.7	2720.0	6.1	2720.0	6.1	89.9
BT_10_57	19.5300	0.4	0.6010	0.0	0.91	3027.0	33.2	3049.0	23.0	3058.0	19.9	3058.0	19.9	99.0

**EMB-01DZ, Miocene Tariquia Formation (N=107). 22.33°S, 64.50°W**

EMB01DZ_25	0.0134	0.0	0.0020	0.0	0.18	13.1	0.2	13.5	0.3	258.0	31.1	13.1	0.2	NA
EMB01DZ_7	0.3232	0.0	0.0435	0.0	0.32	274.2	2.0	285.3	3.2	340.0	14.3	274.2	2.0	80.6
EMB01DZ_31	0.3842	0.0	0.0522	0.0	0.50	327.8	1.5	330.1	1.7	354.0	5.6	327.8	1.5	92.6
EMB01DZ_64	0.3880	0.0	0.0531	0.0	-0.06	333.3	2.8	334.1	4.1	368.0	24.5	333.3	2.8	90.6
EMB01DZ_44	0.4035	0.0	0.0545	0.0	0.51	341.8	0.9	344.1	1.8	370.0	8.7	341.8	0.9	92.4
EMB01DZ_14	0.4826	0.0	0.0639	0.0	0.24	399.0	1.4	399.8	1.6	404.0	7.7	399.0	1.4	98.8
EMB01DZ_17	0.4891	0.0	0.0642	0.0	0.59	401.1	2.8	404.0	3.0	431.0	7.7	401.1	2.8	93.1
EMB01DZ_46	0.6102	0.0	0.0771	0.0	0.53	479.5	2.2	483.5	2.3	500.0	6.1	479.5	2.2	95.9
EMB01DZ_8	0.6374	0.0	0.0777	0.0	0.42	482.3	2.2	500.6	2.6	575.0	9.2	482.3	2.2	83.9
EMB01DZ_27	0.6126	0.0	0.0783	0.0	0.02	486.2	1.9	485.1	1.9	484.0	5.1	486.2	1.9	100.5
EMB01DZ_5	0.6223	0.0	0.0784	0.0	0.30	486.7	1.6	491.8	2.1	500.0	5.6	486.7	1.6	97.3
EMB01DZ_54	0.6245	0.0	0.0785	0.0	0.20	487.3	2.0	492.4	2.9	511.0	8.7	487.3	2.0	95.4
EMB01DZ_29	0.6223	0.0	0.0787	0.0	0.36	488.5	2.2	491.8	2.8	503.0	10.2	488.5	2.2	97.1
EMB01DZ_38	0.6179	0.0	0.0795	0.0	0.21	493.0	2.3	489.0	2.7	489.0	9.7	493.0	2.3	100.8
EMB01DZ_62	0.6258	0.0	0.0800	0.0	0.11	496.1	1.8	493.3	2.3	498.0	7.7	496.1	1.8	99.6
EMB01DZ_12	0.6534	0.0	0.0810	0.0	0.58	502.1	2.6	510.4	2.9	536.0	7.1	502.1	2.6	93.7
EMB01DZ_4	0.6656	0.0	0.0811	0.0	0.65	502.8	3.4	517.9	2.9	594.0	11.2	502.8	3.4	84.6
EMB01DZ_48	0.6610	0.0	0.0817	0.0	0.15	506.1	2.4	514.9	4.0	573.0	16.8	506.1	2.4	88.3
EMB01DZ_45	0.6559	0.0	0.0825	0.0	0.36	511.1	2.5	512.0	2.2	534.0	7.1	511.1	2.5	95.7
EMB01DZ_3	0.6780	0.0	0.0827	0.0	0.33	511.9	2.4	525.1	3.7	570.0	15.3	511.9	2.4	89.8
EMB01DZ_33	0.6610	0.0	0.0831	0.0	0.53	514.3	3.2	514.9	3.0	540.0	10.2	514.3	3.2	95.2
EMB01DZ_20	0.6630	0.0	0.0835	0.0	0.20	516.8	4.0	516.1	4.6	553.0	14.3	516.8	4.0	93.5
EMB01DZ_13	0.6722	0.0	0.0836	0.0	0.82	517.5	2.8	522.5	1.7	544.0	5.6	517.5	2.8	95.1
EMB01DZ_47	0.6730	0.0	0.0838	0.0	0.06	518.0	8.2	523.0	12.2	582.0	30.6	518.0	8.2	89.0
EMB01DZ_19	0.6883	0.0	0.0852	0.0	0.74	527.0	2.3	532.2	2.3	554.8	4.4	527.0	2.3	95.0
EMB01DZ_7	0.6810	0.0	0.0852	0.0	0.54	527.2	3.7	528.4	3.8	537.0	8.2	527.2	3.7	98.2
EMB01DZ_50	0.6870	0.0	0.0857	0.0	0.01	529.8	3.8	536.0	5.1	553.0	18.4	529.8	3.8	95.8
EMB01DZ_2	0.6953	0.0	0.0860	0.0	0.12	532.0	1.8	535.8	2.4	541.0	6.6	532.0	1.8	98.3
EMB01DZ_21	0.6946	0.0	0.0861	0.0	0.50	532.5	2.8	535.3	2.5	560.0	7.7	532.5	2.8	95.1
EMB01DZ_31	0.6958	0.0	0.0865	0.0	0.51	534.9	3.0	536.1	2.4	540.0	6.6	534.9	3.0	99.1
EMB01DZ_15	0.6940	0.0	0.0866	0.0	0.55	535.5	4.0	534.9	4.6	497.0	11.7	535.5	4.0	107.7
EMB01DZ_6	0.6983	0.0	0.0868	0.0	0.39	536.4	1.9	537.6	2.4	531.0	7.1	536.4	1.9	101.0
EMB01DZ_16	0.7170	0.0	0.0896	0.0	0.05	553.2	4.0	548.6	4.1	528.0	14.8	553.2	4.0	104.8
EMB01DZ_24	0.7336	0.0	0.0901	0.0	0.28	556.2	2.1	559.6	2.0	565.0	7.1	556.2	2.1	98.4
EMB01DZ_9	0.7620	0.0	0.0907	0.0	0.73	559.9	4.1	574.9	3.3	624.0	6.1	559.9	4.1	89.7
EMB01DZ_32	0.7499	0.0	0.0912	0.0	0.50	562.3	3.2	568.0	2.3	596.0	7.1	562.3	3.2	94.3

EMB01DZ_46	0.7746	0.0	0.0919	0.0	0.50	567.8	3.5	582.2	2.8	655.0	6.1	567.8	3.5	86.7
EMB01DZ_24	0.7761	0.0	0.0926	0.0	0.21	571.1	3.2	583.0	2.9	641.0	9.2	571.1	3.2	89.1
EMB01DZ_15	0.7630	0.0	0.0927	0.0	0.50	571.4	4.4	575.6	3.9	588.0	9.2	571.4	4.4	97.2
EMB01DZ_30	0.7757	0.0	0.0945	0.0	0.29	582.2	2.2	582.9	2.0	595.0	6.6	582.2	2.2	97.8
EMB01DZ_48	0.7890	0.0	0.0947	0.0	0.06	583.5	4.0	590.6	4.4	633.0	15.8	583.5	4.0	92.2
EMB01DZ_60	0.7720	0.0	0.0952	0.0	0.20	586.0	3.1	580.8	3.1	583.0	10.7	586.0	3.1	100.5
EMB01DZ_2	0.7910	0.0	0.0956	0.0	0.64	589.4	3.5	591.1	3.7	589.0	8.2	589.4	3.5	100.1
EMB01DZ_33	0.8030	0.0	0.0962	0.0	0.34	592.0	5.1	598.0	5.6	629.0	17.9	592.0	5.1	94.1
EMB01DZ_34	0.7930	0.0	0.0964	0.0	0.44	593.0	2.8	592.6	3.1	596.0	7.7	593.0	2.8	99.5
EMB01DZ_25	0.8100	0.0	0.0965	0.0	0.04	594.0	3.3	602.8	4.0	639.0	12.8	594.0	3.3	93.0
EMB01DZ_32	0.8200	0.0	0.0974	0.0	0.82	599.0	6.1	607.0	5.1	621.0	7.7	599.0	6.1	96.5
EMB01DZ_8	0.8087	0.0	0.0978	0.0	0.32	601.6	2.5	602.1	2.3	602.0	7.1	601.6	2.5	99.9
EMB01DZ_51	0.8570	0.0	0.0979	0.0	0.69	602.3	3.7	628.0	5.6	707.0	12.8	602.3	3.7	85.2
EMB01DZ_57	0.8207	0.0	0.0981	0.0	0.32	603.5	2.3	608.2	2.7	631.0	6.6	603.5	2.3	95.6
EMB01DZ_47	0.8240	0.0	0.0982	0.0	0.27	603.7	2.9	610.9	3.4	637.0	7.1	603.7	2.9	94.8
EMB01DZ_56	0.8580	0.0	0.0984	0.0	0.19	604.9	3.1	628.9	3.1	726.0	9.7	604.9	3.1	83.3
EMB01DZ_42	0.8320	0.0	0.0998	0.0	0.18	613.2	4.0	614.5	3.8	613.0	11.2	613.2	4.0	100.0
EMB01DZ_36	0.9030	0.0	0.1008	0.0	0.19	618.9	3.7	653.0	5.6	760.0	18.4	618.9	3.7	81.4
EMB01DZ_11	0.9170	0.0	0.1019	0.0	0.77	626.0	12.8	661.0	7.1	767.0	10.2	626.0	12.8	81.6
EMB01DZ_49	0.8581	0.0	0.1022	0.0	0.52	627.1	2.9	628.9	2.4	645.0	7.7	627.1	2.9	97.2
EMB01DZ_35	0.8610	0.0	0.1029	0.0	0.39	631.5	2.4	630.1	3.1	642.0	9.2	631.5	2.4	98.4
EMB01DZ_22	0.8760	0.0	0.1031	0.0	0.30	632.7	4.0	638.4	3.2	637.0	10.7	632.7	4.0	99.3
EMB01DZ_6	0.8757	0.0	0.1038	0.0	0.47	636.9	2.1	638.5	1.8	636.5	4.6	636.9	2.1	100.1
EMB01DZ_26	0.8760	0.0	0.1040	0.0	0.65	637.8	4.2	639.5	3.5	666.0	7.1	637.8	4.2	95.8
EMB01DZ_29	0.8730	0.0	0.1042	0.0	0.63	639.0	3.1	637.0	2.7	629.0	5.6	639.0	3.1	101.6
EMB01DZ_39	0.8768	0.0	0.1047	0.0	0.57	641.6	2.1	639.1	2.0	644.0	5.1	641.6	2.1	99.6
EMB01DZ_18	0.8900	0.0	0.1052	0.0	0.23	644.9	3.3	645.8	3.4	652.0	8.7	644.9	3.3	98.9
EMB01DZ_40	0.9020	0.0	0.1057	0.0	0.48	648.4	3.1	652.5	3.0	678.0	6.6	648.4	3.1	95.6
EMB01DZ_43	0.9180	0.0	0.1060	0.0	0.75	649.6	3.7	660.8	4.1	703.0	6.6	649.6	3.7	92.4
EMB01DZ_10	0.8820	0.0	0.1061	0.0	0.58	650.2	4.1	641.7	3.6	617.0	7.7	650.2	4.1	105.4
EMB01DZ_37	0.9000	0.0	0.1063	0.0	0.13	651.0	4.9	654.0	6.6	679.0	17.9	651.0	4.9	95.9
EMB01DZ_30	0.9300	0.0	0.1083	0.0	0.33	662.7	3.4	667.3	3.3	685.0	9.2	662.7	3.4	96.7
EMB01DZ_13	0.9130	0.0	0.1092	0.0	0.75	668.0	4.9	659.4	4.4	640.0	6.6	668.0	4.9	104.4
EMB01DZ_19	0.9320	0.0	0.1103	0.0	0.39	674.4	4.6	669.0	4.1	657.0	13.3	674.4	4.6	102.6
EMB01DZ_1	1.0150	0.0	0.1164	0.0	0.59	709.6	3.3	711.2	2.6	710.0	5.1	709.6	3.3	99.9
EMB01DZ_35	1.1040	0.0	0.1247	0.0	0.47	757.7	4.8	755.0	3.8	751.0	10.2	757.7	4.8	100.9
EMB01DZ_5	1.1900	0.0	0.1283	0.0	0.22	778.0	8.7	794.0	9.2	889.0	20.9	778.0	8.7	87.5
EMB01DZ_50	1.2470	0.0	0.1304	0.0	0.19	790.4	3.1	822.7	3.0	909.0	7.1	790.4	3.1	87.0
EMB01DZ_55	1.2020	0.0	0.1314	0.0	0.51	796.0	4.3	803.5	3.7	819.0	7.7	796.0	4.3	97.2
EMB01DZ_36	1.6400	0.0	0.1644	0.0	0.73	981.1	4.7	985.5	3.2	1010.0	4.0	1010.0	4.0	97.1
EMB01DZ_16	1.6630	0.0	0.1657	0.0	0.68	988.0	11.2	994.0	12.8	1017.0	17.3	1017.0	17.3	97.1
EMB01DZ_1	1.7930	0.0	0.1763	0.0	0.35	1046.6	4.3	1042.3	3.5	1022.0	6.1	1022.0	6.1	102.4
EMB01DZ_37	1.6730	0.0	0.1647	0.0	0.69	983.0	5.1	997.9	3.8	1047.0	7.1	1047.0	7.1	93.9
EMB01DZ_23	1.7640	0.0	0.1723	0.0	0.70	1024.6	3.9	1032.1	2.9	1052.2	4.6	1052.2	4.6	97.4
EMB01DZ_9	1.6960	0.0	0.1635	0.0	0.90	976.0	6.6	1006.0	6.1	1061.0	5.6	1061.0	5.6	92.0
EMB01DZ_58	1.8050	0.0	0.1753	0.0	0.69	1040.9	4.3	1047.0	3.3	1062.2	4.6	1062.2	4.6	98.0
EMB01DZ_17	1.8970	0.0	0.1852	0.0	0.39	1095.2	4.1	1079.9	3.0	1065.0	5.6	1065.0	5.6	102.8
EMB01DZ_22	1.8030	0.0	0.1741	0.0	0.82	1034.0	14.8	1044.0	12.2	1070.0	13.3	1070.0	13.3	96.6
EMB01DZ_12	1.9140	0.0	0.1833	0.0	0.35	1085.0	6.1	1089.0	5.1	1086.0	11.2	1086.0	11.2	99.9
EMB01DZ_53	1.9890	0.0	0.1891	0.0	0.53	1116.0	6.1	1111.1	4.0	1102.0	7.1	1102.0	7.1	101.3
EMB01DZ_10	1.7410	0.0	0.1645	0.0	0.71	981.8	4.1	1024.4	2.7	1104.9	3.0	1104.9	3.0	88.9
EMB01DZ_28	2.0070	0.0	0.1899	0.0	0.50	1121.0	7.1	1117.0	5.1	1111.0	9.7	1111.0	9.7	100.9
EMB01DZ_3	2.2030	0.0	0.1999	0.0	0.79	1174.0	17.3	1186.0	11.2	1192.0	12.2	1192.0	12.2	98.5

EMB01DZ_53	2.2770	0.0	0.2060	0.0	0.83	1207.0	8.2	1203.0	9.2	1202.0	12.8	1202.0	12.8	100.4
EMB01DZ_11	2.2940	0.0	0.2061	0.0	0.61	1208.0	7.7	1210.1	5.1	1218.0	7.1	1218.0	7.1	99.2
EMB01DZ_26	2.4260	0.0	0.2157	0.0	0.68	1262.0	7.1	1249.9	4.6	1230.0	6.1	1230.0	6.1	102.6
EMB01DZ_20	2.4200	0.0	0.2146	0.0	0.35	1253.0	7.1	1247.9	4.8	1235.0	9.2	1235.0	9.2	101.5
EMB01DZ_14	2.9440	0.0	0.2465	0.0	0.36	1420.0	5.6	1392.7	3.9	1357.0	6.1	1357.0	6.1	104.6
EMB01DZ_40	2.8730	0.0	0.2379	0.0	0.53	1375.6	4.7	1374.5	3.0	1382.7	3.6	1382.7	3.6	99.5
EMB01DZ_55	2.9490	0.0	0.2314	0.0	0.26	1341.7	4.6	1394.3	3.6	1487.0	5.6	1487.0	5.6	90.2
EMB01DZ_54	3.4120	0.0	0.2642	0.0	0.41	1511.5	4.5	1507.7	3.1	1515.2	4.9	1515.2	4.9	99.8
EMB01DZ_45	3.5930	0.0	0.2711	0.0	0.72	1546.0	7.7	1547.7	4.3	1541.4	4.2	1541.4	4.2	100.3
EMB01DZ_18	4.3000	0.1	0.2979	0.0	0.60	1680.0	19.9	1697.0	12.8	1739.0	12.8	1739.0	12.8	96.6
EMB01DZ_27	4.6020	0.0	0.3092	0.0	0.53	1737.0	11.7	1749.0	5.6	1779.0	6.6	1779.0	6.6	97.6
EMB01DZ_44	5.0430	0.0	0.3311	0.0	0.83	1843.0	9.2	1825.9	4.7	1797.7	4.0	1797.7	4.0	102.5
EMB01DZ_28	4.8660	0.0	0.3199	0.0	0.59	1789.0	6.6	1795.9	3.3	1815.2	3.6	1815.2	3.6	98.6
EMB01DZ_23	5.8640	0.0	0.3532	0.0	0.70	1950.0	7.7	1955.4	4.2	1964.3	4.0	1964.3	4.0	99.3
EMB01DZ_43	6.4700	0.1	0.3759	0.0	0.55	2057.0	11.7	2041.0	8.2	2026.0	9.7	2026.0	9.7	101.5
EMB01DZ_39	7.4420	0.0	0.4008	0.0	0.72	2172.0	13.3	2167.0	5.6	2144.4	4.7	2144.4	4.7	101.3
EMB01DZ_51	7.6110	0.0	0.4061	0.0	0.47	2197.0	6.1	2185.8	3.0	2187.5	3.8	2187.5	3.8	100.4
EMB01DZ_4	26.2600	0.2	0.6840	0.0	0.98	3359.0	21.9	3348.0	11.2	3331.0	5.6	3331.0	5.6	100.8

**EMB-03DZ, Miocene Guandacay Formation (N=126). 22.31°S, 64.51°W**

EMB03DZ_85	0.2999	0.0	0.0413	0.0	-0.28	260.8	3.9	266.3	3.7	319.0	23.0	260.8	3.9	81.8
EMB03DZ_28	0.3023	0.0	0.0423	0.0	0.31	266.8	1.1	268.2	1.4	279.0	6.6	266.8	1.1	95.6
EMB03DZ_38	0.3374	0.0	0.0460	0.0	0.78	290.7	1.9	295.7	1.9	333.0	5.6	290.7	1.9	87.3
EMB03DZ_9	0.3334	0.0	0.0467	0.0	0.35	294.1	1.9	292.0	3.5	310.0	16.8	294.1	1.9	94.9
EMB03DZ_77	0.3530	0.0	0.0477	0.0	0.28	300.1	1.9	307.0	5.6	380.0	33.2	300.1	1.9	79.0
EMB03DZ_1	0.4273	0.0	0.0574	0.0	0.20	359.5	1.6	362.3	2.9	387.0	12.8	359.5	1.6	92.9
EMB03DZ_78	0.4488	0.0	0.0592	0.0	0.59	370.7	1.6	376.3	2.0	404.0	7.1	370.7	1.6	91.8
EMB03DZ_30	0.4496	0.0	0.0603	0.0	0.11	377.6	1.7	376.8	2.3	381.0	8.7	377.6	1.7	99.1
EMB03DZ_96	0.5440	0.0	0.0703	0.0	0.50	437.9	1.9	441.7	2.1	458.0	7.1	437.9	1.9	95.6
EMB03DZ_117	0.5720	0.0	0.0733	0.0	0.59	456.2	2.7	459.1	3.4	467.0	12.2	456.2	2.7	97.7
EMB03DZ_50	0.5880	0.0	0.0757	0.0	0.13	470.7	1.8	470.0	2.4	462.0	9.7	470.7	1.8	101.9
EMB03DZ_26	0.6230	0.0	0.0763	0.0	0.55	474.5	2.8	491.0	4.4	565.0	13.8	474.5	2.8	84.0
EMB03DZ_62	0.6208	0.0	0.0776	0.0	0.56	481.5	2.8	491.0	3.2	522.0	8.2	481.5	2.8	92.2
EMB03DZ_51	0.6119	0.0	0.0778	0.0	0.47	482.9	2.7	484.6	2.4	502.0	8.7	482.9	2.7	96.2
EMB03DZ_46	0.6141	0.0	0.0782	0.0	0.41	485.4	2.6	485.9	2.7	508.0	12.2	485.4	2.6	95.6
EMB03DZ_36	0.6313	0.0	0.0788	0.0	0.10	488.6	1.9	496.8	1.9	532.0	8.2	488.6	1.9	91.8
EMB03DZ_66	0.6320	0.0	0.0788	0.0	0.78	488.6	3.6	497.3	2.1	554.0	5.6	488.6	3.6	88.2
EMB03DZ_68	0.6380	0.0	0.0806	0.0	0.90	500.0	6.1	500.9	4.2	524.0	7.1	500.0	6.1	95.4
EMB03DZ_16	0.6350	0.0	0.0812	0.0	0.26	503.4	2.6	499.1	2.0	484.0	7.1	503.4	2.6	104.0
EMB03DZ_31	0.6570	0.0	0.0814	0.0	0.15	504.2	2.9	512.3	3.4	553.0	14.3	504.2	2.9	91.2
EMB03DZ_48	0.6624	0.0	0.0828	0.0	0.28	513.0	2.0	515.9	2.4	520.0	7.7	513.0	2.0	98.7
EMB03DZ_110	0.6672	0.0	0.0830	0.0	0.54	514.2	3.0	518.9	2.2	535.0	6.6	514.2	3.0	96.1
EMB03DZ_32	0.6690	0.0	0.0832	0.0	0.03	515.3	2.3	519.9	3.5	540.0	12.8	515.3	2.3	95.4
EMB03DZ_18	0.6980	0.0	0.0835	0.0	0.05	517.0	7.7	537.0	10.2	606.0	33.2	517.0	7.7	85.3
EMB03DZ_79	0.6830	0.0	0.0841	0.0	0.83	520.4	4.6	528.2	3.1	555.0	5.6	520.4	4.6	93.8
EMB03DZ_37	0.6711	0.0	0.0844	0.0	0.49	522.0	1.7	521.3	1.9	514.0	6.1	522.0	1.7	101.6
EMB03DZ_56	0.6812	0.0	0.0851	0.0	0.28	526.6	1.5	527.4	1.5	535.0	4.4	526.6	1.5	98.4
EMB03DZ_93	0.6820	0.0	0.0855	0.0	0.58	528.8	2.7	528.3	2.7	521.0	7.1	528.8	2.7	101.5
EMB03DZ_29	0.6959	0.0	0.0859	0.0	0.36	531.3	2.8	536.7	2.6	565.0	7.7	531.3	2.8	94.0
EMB03DZ_112	0.7070	0.0	0.0861	0.0	0.34	532.3	3.5	543.0	3.1	602.0	10.7	532.3	3.5	88.4
EMB03DZ_63	0.6990	0.0	0.0865	0.0	0.84	535.0	7.1	538.2	4.7	573.0	6.1	535.0	7.1	93.4
EMB03DZ_55	0.6975	0.0	0.0869	0.0	0.20	537.0	2.8	537.2	2.5	527.0	7.7	537.0	2.8	101.9
EMB03DZ_111	0.6924	0.0	0.0875	0.0	0.38	540.7	2.3	534.1	2.2	504.0	8.2	540.7	2.3	107.3

EMB03DZ_27	0.7340	0.0	0.0877	0.0	0.67	542.0	5.1	558.6	4.4	598.0	12.8	542.0	5.1	90.6
EMB03DZ_107	0.7150	0.0	0.0887	0.0	0.10	547.5	3.3	548.5	3.3	543.0	12.2	547.5	3.3	100.8
EMB03DZ_88	0.7170	0.0	0.0887	0.0	0.53	547.9	5.1	548.0	5.6	575.0	11.2	547.9	5.1	95.3
EMB03DZ_86	0.7360	0.0	0.0895	0.0	0.19	552.5	4.0	560.0	5.1	619.0	15.3	552.5	4.0	89.3
EMB03DZ_40	0.7900	0.0	0.0898	0.0	0.61	554.0	6.6	591.0	7.7	741.0	13.3	554.0	6.6	74.8
EMB03DZ_34	0.7440	0.0	0.0900	0.0	0.17	555.7	4.0	566.3	4.7	590.0	14.8	555.7	4.0	94.2
EMB03DZ_24	0.7373	0.0	0.0903	0.0	0.36	557.0	2.4	560.7	1.8	573.4	4.2	557.0	2.4	97.1
EMB03DZ_122	0.7730	0.0	0.0908	0.0	0.83	560.0	6.6	581.0	6.1	665.0	10.7	560.0	6.6	84.2
EMB03DZ_49	0.7358	0.0	0.0908	0.0	0.46	560.3	2.4	559.8	2.0	549.0	6.6	560.3	2.4	102.1
EMB03DZ_115	0.7480	0.0	0.0911	0.0	0.36	562.1	1.8	567.0	1.9	587.2	5.1	562.1	1.8	95.7
EMB03DZ_42	0.7550	0.0	0.0917	0.0	0.23	565.8	2.9	571.7	3.7	572.0	7.7	565.8	2.9	98.9
EMB03DZ_71	0.7490	0.0	0.0929	0.0	0.36	572.0	7.7	568.0	7.7	553.0	14.3	572.0	7.7	103.4
EMB03DZ_70	0.7670	0.0	0.0933	0.0	0.32	574.8	2.4	577.6	3.0	581.0	9.2	574.8	2.4	98.9
EMB03DZ_127	0.7673	0.0	0.0938	0.0	0.03	577.9	3.7	578.2	1.1	564.0	16.3	577.9	3.7	102.5
EMB03DZ_59	0.7710	0.0	0.0939	0.0	0.27	578.7	1.6	580.2	2.0	593.0	5.6	578.7	1.6	97.6
EMB03DZ_5	0.7570	0.0	0.0942	0.0	0.47	580.3	4.2	572.0	6.1	542.0	11.7	580.3	4.2	107.1
EMB03DZ_106	0.7810	0.0	0.0950	0.0	0.38	584.9	2.1	585.9	2.0	586.0	6.1	584.9	2.1	99.8
EMB03DZ_61	0.7777	0.0	0.0952	0.0	0.58	586.4	2.2	584.6	2.5	575.0	5.1	586.4	2.2	102.0
EMB03DZ_57	0.7910	0.0	0.0955	0.0	0.62	588.2	2.2	591.6	1.9	610.1	3.5	588.2	2.2	96.4
EMB03DZ_113	0.8026	0.0	0.0972	0.0	0.41	597.8	1.9	598.3	1.6	606.4	4.2	597.8	1.9	98.6
EMB03DZ_102	0.8180	0.0	0.0973	0.0	0.30	598.5	2.6	606.6	3.1	638.0	9.7	598.5	2.6	93.8
EMB03DZ_120	0.8164	0.0	0.0985	0.0	0.35	605.8	2.3	605.8	2.7	610.0	7.1	605.8	2.3	99.3
EMB03DZ_121	0.8157	0.0	0.0988	0.0	0.38	607.3	1.7	605.6	1.4	595.3	4.0	607.3	1.7	102.0
EMB03DZ_103	0.8276	0.0	0.0990	0.0	0.22	608.5	2.9	612.8	2.4	621.0	7.1	608.5	2.9	98.0
EMB03DZ_69	0.8320	0.0	0.0993	0.0	0.38	610.3	2.7	614.4	3.8	648.0	14.8	610.3	2.7	94.2
EMB03DZ_89	0.8360	0.0	0.1003	0.0	0.20	616.0	3.5	616.3	3.8	631.0	12.8	616.0	3.5	97.6
EMB03DZ_25	0.8704	0.0	0.1024	0.0	0.53	628.6	2.4	635.6	2.3	658.0	5.1	628.6	2.4	95.5
EMB03DZ_82	0.8657	0.0	0.1034	0.0	0.43	634.2	2.4	633.1	2.3	633.0	7.1	634.2	2.4	100.2
EMB03DZ_91	0.8693	0.0	0.1035	0.0	0.34	634.9	2.1	635.0	2.1	626.4	4.7	634.9	2.1	101.4
EMB03DZ_124	0.8990	0.0	0.1054	0.0	0.14	645.8	2.9	650.7	4.2	653.0	10.2	645.8	2.9	98.9
EMB03DZ_20	0.9140	0.0	0.1071	0.0	0.44	656.0	3.5	659.7	3.5	639.0	7.7	656.0	3.5	102.7
EMB03DZ_98	0.9420	0.0	0.1079	0.0	0.29	661.3	3.5	675.4	4.0	696.0	10.2	661.3	3.5	95.0
EMB03DZ_80	0.9390	0.0	0.1098	0.0	0.63	671.4	4.5	672.7	3.6	673.0	7.7	671.4	4.5	99.8
EMB03DZ_45	0.9340	0.0	0.1100	0.0	0.52	672.4	3.5	669.7	2.7	660.0	4.5	672.4	3.5	101.9
EMB03DZ_14	0.9890	0.0	0.1133	0.0	0.52	692.0	2.6	698.2	2.8	719.0	6.1	692.0	2.6	96.2
EMB03DZ_94	1.0500	0.0	0.1168	0.0	0.63	712.0	9.2	729.0	9.2	781.0	15.8	712.0	9.2	91.2
EMB03DZ_125	1.1280	0.0	0.1253	0.0	0.20	761.0	2.3	766.2	4.0	776.0	9.7	761.0	2.3	98.1
EMB03DZ_105	1.1454	0.0	0.1277	0.0	0.55	774.9	3.0	774.9	2.3	776.4	4.7	774.9	3.0	99.8
EMB03DZ_100	1.2850	0.0	0.1357	0.0	0.44	820.4	4.2	838.7	4.1	875.0	8.7	820.4	4.2	93.8
EMB03DZ_75	1.4250	0.0	0.1467	0.0	0.56	882.4	3.7	900.6	3.8	937.0	6.6	882.4	3.7	94.2
EMB03DZ_22	1.4550	0.0	0.1489	0.0	0.80	894.5	3.5	911.7	3.8	949.2	4.5	894.5	3.5	94.2
EMB03DZ_72	1.5800	0.0	0.1559	0.0	0.64	934.0	5.1	962.1	3.6	1027.0	6.6	934.0	5.1	90.9
EMB03DZ_123	1.5750	0.0	0.1569	0.0	0.89	939.0	6.6	963.9	4.8	1014.9	3.3	939.0	6.6	92.5
EMB03DZ_41	1.5230	0.0	0.1573	0.0	0.37	941.5	2.9	939.2	3.6	935.0	7.1	941.5	2.9	100.7
EMB03DZ_53	1.6180	0.0	0.1577	0.0	0.62	943.9	4.3	976.9	3.6	1058.9	5.1	943.9	4.3	89.1
EMB03DZ_84	1.6080	0.0	0.1579	0.0	0.67	945.0	4.4	973.2	3.3	1047.0	5.1	945.0	4.4	90.3
EMB03DZ_92	1.6280	0.0	0.1622	0.0	0.68	974.0	8.7	980.9	4.7	966.0	9.2	966.0	9.2	100.8
EMB03DZ_60	1.7410	0.0	0.1726	0.0	0.70	1026.0	11.2	1023.0	9.2	977.0	15.3	977.0	15.3	105.0
EMB03DZ_7	1.6390	0.0	0.1649	0.0	0.58	983.8	4.9	984.8	3.6	984.0	6.1	984.0	6.1	100.0
EMB03DZ_15	1.7120	0.0	0.1708	0.0	0.43	1016.5	3.8	1012.4	4.0	1002.0	5.6	1002.0	5.6	101.4
EMB03DZ_3	1.7310	0.0	0.1716	0.0	0.67	1020.9	4.3	1019.7	3.2	1033.3	4.0	1033.3	4.0	98.8
EMB03DZ_12	1.7470	0.0	0.1733	0.0	0.05	1030.0	6.6	1025.0	6.1	1035.0	14.3	1035.0	14.3	99.5
EMB03DZ_81	1.7510	0.0	0.1718	0.0	0.53	1022.0	4.7	1027.0	3.6	1037.0	5.1	1037.0	5.1	98.6

EMB03DZ_2	1.7180	0.0	0.1684	0.0	0.76	1003.0	6.1	1015.1	3.8	1044.0	4.4	1044.0	4.4	96.1
EMB03DZ_74	1.8120	0.0	0.1772	0.0	0.48	1051.7	3.0	1050.1	2.5	1044.7	4.1	1044.7	4.1	100.7
EMB03DZ_83	1.7260	0.0	0.1690	0.0	0.52	1006.6	3.5	1018.1	2.7	1047.8	4.6	1047.8	4.6	96.1
EMB03DZ_108	1.7210	0.0	0.1650	0.0	0.71	984.0	8.7	1016.0	6.1	1052.0	8.2	1052.0	8.2	93.5
EMB03DZ_87	1.8040	0.0	0.1755	0.0	0.69	1042.4	3.6	1046.7	2.7	1055.4	3.2	1055.4	3.2	98.8
EMB03DZ_39	1.8130	0.0	0.1765	0.0	0.61	1048.0	5.1	1049.4	4.4	1056.0	6.1	1056.0	6.1	99.2
EMB03DZ_52	1.8030	0.0	0.1757	0.0	0.77	1043.0	5.6	1046.0	3.7	1056.5	4.8	1056.5	4.8	98.7
EMB03DZ_126	1.8190	0.0	0.1759	0.0	0.29	1044.3	4.0	1052.0	3.4	1059.0	6.1	1059.0	6.1	98.6
EMB03DZ_114	1.7130	0.0	0.1655	0.0	0.50	987.0	7.7	1013.0	8.7	1064.0	13.8	1064.0	13.8	92.8
EMB03DZ_8	1.8700	0.0	0.1810	0.0	0.48	1072.5	3.3	1070.3	2.3	1069.4	4.0	1069.4	4.0	100.3
EMB03DZ_67	1.8080	0.0	0.1757	0.0	0.85	1043.0	10.7	1048.0	7.7	1071.0	7.1	1071.0	7.1	97.4
EMB03DZ_21	1.7740	0.0	0.1702	0.0	0.74	1012.9	4.6	1036.4	3.0	1083.0	6.1	1083.0	6.1	93.5
EMB03DZ_11	1.8860	0.0	0.1826	0.0	0.38	1083.0	5.6	1075.7	4.2	1083.0	7.1	1083.0	7.1	100.0
EMB03DZ_95	1.9410	0.0	0.1846	0.0	0.71	1092.0	6.6	1095.1	3.5	1100.0	5.6	1100.0	5.6	99.3
EMB03DZ_19	1.7530	0.0	0.1668	0.0	0.72	994.0	5.6	1028.0	5.6	1102.0	7.7	1102.0	7.7	90.2
EMB03DZ_104	1.9360	0.0	0.1840	0.0	0.69	1088.6	4.0	1093.4	2.7	1102.4	4.2	1102.4	4.2	98.7
EMB03DZ_43	1.9360	0.0	0.1837	0.0	0.60	1087.0	5.6	1094.4	3.3	1113.0	6.1	1113.0	6.1	97.7
EMB03DZ_65	2.1250	0.0	0.1989	0.0	0.53	1169.0	5.6	1157.8	4.0	1131.0	5.6	1131.0	5.6	103.4
EMB03DZ_116	1.9120	0.0	0.1774	0.0	0.58	1052.0	7.1	1084.9	4.0	1137.0	7.7	1137.0	7.7	92.5
EMB03DZ_44	2.0010	0.0	0.1860	0.0	0.61	1099.0	5.6	1116.5	3.3	1144.0	5.6	1144.0	5.6	96.1
EMB03DZ_118	1.9850	0.0	0.1855	0.0	0.80	1097.0	7.7	1110.0	5.1	1147.0	5.1	1147.0	5.1	95.6
EMB03DZ_76	1.7460	0.0	0.1619	0.0	0.58	967.0	11.2	1025.0	9.7	1162.0	16.8	1162.0	16.8	83.2
EMB03DZ_13	2.2200	0.0	0.2023	0.0	0.66	1187.8	3.3	1188.2	2.2	1188.6	2.9	1188.6	2.9	99.9
EMB03DZ_119	2.1120	0.0	0.1920	0.0	0.39	1132.0	5.1	1152.6	4.0	1189.0	5.6	1189.0	5.6	95.2
EMB03DZ_64	3.0600	0.1	0.2470	0.0	0.95	1420.0	51.0	1415.0	32.1	1428.0	10.2	1428.0	10.2	99.4
EMB03DZ_4	3.4000	0.0	0.2575	0.0	0.59	1477.1	4.8	1504.3	2.3	1544.9	3.1	1544.9	3.1	95.6
EMB03DZ_58	4.2300	0.0	0.2959	0.0	0.21	1671.0	5.1	1680.5	3.2	1694.7	4.8	1694.7	4.8	98.6
EMB03DZ_33	4.6270	0.0	0.3130	0.0	0.70	1755.0	8.2	1754.7	3.8	1745.9	3.9	1745.9	3.9	100.5
EMB03DZ_73	4.6520	0.0	0.3130	0.0	0.60	1755.6	3.7	1759.0	2.0	1763.3	2.1	1763.3	2.1	99.6
EMB03DZ_47	6.1700	0.0	0.3654	0.0	0.38	2007.0	7.1	2000.0	3.6	1986.2	4.8	1986.2	4.8	101.0
EMB03DZ_54	5.8370	0.0	0.3397	0.0	0.95	1884.0	11.7	1951.0	5.6	2020.1	2.1	2020.1	2.1	93.3
EMB03DZ_101	6.4180	0.0	0.3644	0.0	0.81	2003.0	9.2	2034.6	4.2	2056.1	3.3	2056.1	3.3	97.4
EMB03DZ_6	6.3690	0.0	0.3634	0.0	0.56	1998.0	7.1	2027.7	3.2	2062.9	3.7	2062.9	3.7	96.9
EMB03DZ_109	6.6970	0.0	0.3708	0.0	0.72	2033.0	8.7	2072.1	3.2	2103.8	3.6	2103.8	3.6	96.6
EMB03DZ_90	7.4490	0.0	0.4002	0.0	0.64	2170.0	8.7	2166.5	4.1	2157.8	4.6	2157.8	4.6	100.6
EMB03DZ_99	7.2300	0.1	0.3888	0.0	0.29	2117.0	16.8	2142.0	8.7	2171.0	16.8	2171.0	16.8	97.5
EMB03DZ_23	7.5020	0.0	0.3975	0.0	0.69	2157.0	10.2	2173.0	5.1	2181.0	5.0	2181.0	5.0	98.9
EMB03DZ_35	11.2100	0.1	0.4685	0.0	0.93	2476.0	14.3	2540.0	6.6	2587.5	2.4	2587.5	2.4	95.7
EMB03DZ_97	11.6400	0.1	0.4787	0.0	0.83	2520.0	18.4	2576.0	8.2	2616.6	4.6	2616.6	4.6	96.3
EMB03DZ_17	13.3200	0.0	0.5231	0.0	0.77	2714.0	8.7	2702.2	3.2	2691.6	2.4	2691.6	2.4	100.8

#### EMB-05DZ, Pliocene Emborozú Formation (N=108). 22.31°S, 64.52°W

EMB05DZ_34	0.0107	0.0	0.0017	0.0	0.26	11.0	0.1	10.8	0.2	205.0	32.1	11.0	0.1	NA
EMB05DZ_66	0.0126	0.0	0.0020	0.0	-0.07	12.8	0.2	12.7	0.3	257.0	31.6	12.8	0.2	NA
EMB05DZ_29	0.0230	0.0	0.0030	0.0	0.26	19.0	0.2	23.1	0.4	503.0	31.6	19.0	0.2	NA
EMB05DZ_45	0.0202	0.0	0.0031	0.0	0.28	19.9	0.1	20.3	0.3	149.0	17.9	19.9	0.1	NA
EMB05DZ_84	0.0246	0.0	0.0034	0.0	-0.02	21.8	0.4	24.7	0.5	341.0	29.6	21.8	0.4	NA
EMB05DZ_113	0.3040	0.0	0.0419	0.0	0.64	264.5	2.4	269.4	2.6	330.0	10.7	264.5	2.4	80.2
EMB05DZ_19	0.3014	0.0	0.0420	0.0	0.67	265.3	1.5	267.4	1.5	298.0	7.1	265.3	1.5	89.0
EMB05DZ_1	0.3278	0.0	0.0453	0.0	0.32	285.5	1.8	287.8	1.6	354.0	10.2	285.5	1.8	80.6
EMB05DZ_109	0.4620	0.0	0.0609	0.0	0.77	381.0	4.1	385.2	3.8	438.0	10.2	381.0	4.1	87.0
EMB05DZ_77	0.4810	0.0	0.0617	0.0	0.38	387.1	3.1	398.4	3.5	485.0	12.8	387.1	3.1	79.8
EMB05DZ_57	0.5330	0.0	0.0670	0.0	0.57	418.1	3.8	433.4	3.5	518.0	9.7	418.1	3.8	80.7

EMB05DZ_111	0.5640	0.0	0.0724	0.0	0.43	450.6	2.0	454.6	1.8	482.0	6.1	450.6	2.0	93.5
EMB05DZ_46	0.5993	0.0	0.0751	0.0	0.18	466.6	2.4	477.4	2.7	505.0	9.2	466.6	2.4	92.4
EMB05DZ_87	0.5859	0.0	0.0758	0.0	0.16	470.7	2.2	468.0	2.6	465.0	8.2	470.7	2.2	101.2
EMB05DZ_25	0.5930	0.0	0.0758	0.0	0.62	471.2	3.7	472.7	3.7	501.0	12.2	471.2	3.7	94.1
EMB05DZ_103	0.5924	0.0	0.0761	0.0	0.77	472.6	2.8	472.2	2.2	478.1	5.0	472.6	2.8	98.8
EMB05DZ_70	0.5945	0.0	0.0761	0.0	0.60	473.3	2.9	473.5	2.8	470.0	6.1	473.3	2.9	100.7
EMB05DZ_72	0.6020	0.0	0.0779	0.0	0.48	483.4	3.0	478.4	2.8	452.0	8.2	483.4	3.0	106.9
EMB05DZ_37	0.6216	0.0	0.0788	0.0	0.38	488.8	3.3	490.7	2.5	517.0	8.7	488.8	3.3	94.5
EMB05DZ_95	0.6275	0.0	0.0809	0.0	0.40	501.5	2.2	494.4	2.3	468.0	7.7	501.5	2.2	107.2
EMB05DZ_33	0.6587	0.0	0.0810	0.0	0.25	502.2	2.3	513.6	2.9	555.0	9.2	502.2	2.3	90.5
EMB05DZ_92	0.6740	0.0	0.0811	0.0	0.40	502.7	2.8	523.7	3.2	619.0	9.7	502.7	2.8	81.2
EMB05DZ_56	0.6651	0.0	0.0824	0.0	0.58	510.7	3.8	517.7	2.9	533.0	10.2	510.7	3.8	95.8
EMB05DZ_93	0.6570	0.0	0.0825	0.0	0.84	511.0	5.1	512.4	4.9	539.0	8.2	511.0	5.1	94.8
EMB05DZ_78	0.6751	0.0	0.0831	0.0	0.37	514.8	2.2	524.3	2.0	568.0	6.6	514.8	2.2	90.6
EMB05DZ_104	0.7012	0.0	0.0841	0.0	0.79	520.6	2.3	539.4	1.7	621.4	3.4	520.6	2.3	83.8
EMB05DZ_62	0.7120	0.0	0.0845	0.0	0.20	522.9	3.4	545.2	4.7	660.0	13.8	522.9	3.4	79.2
EMB05DZ_96	0.6821	0.0	0.0853	0.0	0.41	527.4	2.6	527.8	2.7	538.0	6.6	527.4	2.6	98.0
EMB05DZ_68	0.6992	0.0	0.0871	0.0	0.63	538.3	2.7	538.1	2.2	542.0	5.6	538.3	2.7	99.3
EMB05DZ_65	0.7061	0.0	0.0871	0.0	0.32	538.4	3.0	542.3	2.2	559.0	9.2	538.4	3.0	96.3
EMB05DZ_89	0.6880	0.0	0.0874	0.0	0.53	539.9	2.8	531.4	3.3	520.0	7.1	539.9	2.8	103.8
EMB05DZ_60	0.7140	0.0	0.0884	0.0	0.41	545.8	1.8	547.0	2.0	550.0	6.1	545.8	1.8	99.2
EMB05DZ_42	0.7259	0.0	0.0886	0.0	0.28	547.3	2.9	553.9	2.7	581.0	7.1	547.3	2.9	94.2
EMB05DZ_59	0.7190	0.0	0.0890	0.0	0.42	549.5	3.4	549.8	3.2	567.0	7.1	549.5	3.4	96.9
EMB05DZ_32	0.7380	0.0	0.0898	0.0	-0.12	554.2	3.4	562.0	5.1	595.0	12.2	554.2	3.4	93.1
EMB05DZ_115	0.7440	0.0	0.0908	0.0	0.36	560.2	4.0	564.3	3.7	590.0	10.2	560.2	4.0	94.9
EMB05DZ_102	0.7520	0.0	0.0909	0.0	0.41	560.6	3.0	569.1	3.4	605.0	9.2	560.6	3.0	92.7
EMB05DZ_48	0.7600	0.0	0.0914	0.0	-0.06	563.7	2.3	573.0	7.1	573.0	18.4	563.7	2.3	98.4
EMB05DZ_22	0.7706	0.0	0.0917	0.0	0.72	565.4	2.4	580.6	1.9	641.9	3.8	565.4	2.4	88.1
EMB05DZ_30	0.7540	0.0	0.0933	0.0	0.49	574.8	3.7	568.8	3.8	538.0	7.7	574.8	3.7	106.8
EMB05DZ_81	0.7564	0.0	0.0934	0.0	0.66	575.4	2.8	572.4	2.8	569.0	6.1	575.4	2.8	101.1
EMB05DZ_99	0.7634	0.0	0.0938	0.0	0.39	577.9	2.5	576.4	2.6	558.0	7.1	577.9	2.5	103.6
EMB05DZ_116	0.7888	0.0	0.0938	0.0	0.46	578.1	2.3	590.3	2.2	640.8	4.9	578.1	2.3	90.2
EMB05DZ_52	0.7746	0.0	0.0939	0.0	0.56	578.6	2.8	582.2	2.4	597.0	6.6	578.6	2.8	96.9
EMB05DZ_110	0.7718	0.0	0.0943	0.0	0.67	581.2	3.2	581.2	2.3	570.8	4.3	581.2	3.2	101.8
EMB05DZ_11	0.7800	0.0	0.0950	0.0	0.01	584.8	2.3	585.1	3.0	588.0	7.1	584.8	2.3	99.5
EMB05DZ_94	0.7900	0.0	0.0950	0.0	-0.17	585.3	3.3	590.4	4.0	614.0	14.3	585.3	3.3	95.3
EMB05DZ_9	0.7887	0.0	0.0954	0.0	0.39	587.6	2.7	590.9	2.9	608.0	6.6	587.6	2.7	96.6
EMB05DZ_79	0.7853	0.0	0.0957	0.0	0.55	589.1	2.7	588.3	2.3	584.0	5.6	589.1	2.7	100.9
EMB05DZ_67	0.8211	0.0	0.0958	0.0	0.81	590.0	2.0	608.6	1.7	675.0	2.2	590.0	2.0	87.4
EMB05DZ_86	0.8110	0.0	0.0968	0.0	0.38	595.6	3.8	604.2	3.6	643.0	12.8	595.6	3.8	92.6
EMB05DZ_55	0.8144	0.0	0.0968	0.0	0.66	595.7	2.4	604.7	2.7	621.3	4.9	595.7	2.4	95.9
EMB05DZ_90	0.8650	0.0	0.0971	0.0	0.28	597.3	3.4	632.3	3.8	770.0	16.3	597.3	3.4	77.6
EMB05DZ_80	0.8511	0.0	0.1012	0.0	0.40	621.2	3.1	625.8	2.4	653.0	8.2	621.2	3.1	95.1
EMB05DZ_97	0.9020	0.0	0.1037	0.0	0.66	635.8	3.7	653.4	3.8	713.0	8.2	635.8	3.7	89.2
EMB05DZ_91	0.9030	0.0	0.1038	0.0	0.42	636.8	3.2	653.7	4.4	720.0	13.8	636.8	3.2	88.4
EMB05DZ_27	0.8980	0.0	0.1055	0.0	0.30	646.4	3.8	650.0	4.7	663.0	13.8	646.4	3.8	97.5
EMB05DZ_20	0.8936	0.0	0.1061	0.0	0.58	649.7	3.5	648.1	2.7	651.5	4.4	649.7	3.5	99.7
EMB05DZ_26	0.8940	0.0	0.1069	0.0	0.31	654.7	3.1	648.4	2.8	633.0	7.1	654.7	3.1	103.4
EMB05DZ_108	0.9150	0.0	0.1075	0.0	0.41	658.0	3.4	659.1	3.2	667.0	6.6	658.0	3.4	98.7
EMB05DZ_8	0.9300	0.0	0.1095	0.0	0.48	669.6	2.8	667.0	3.4	663.0	8.7	669.6	2.8	101.0
EMB05DZ_58	1.0240	0.0	0.1168	0.0	0.25	711.9	2.6	716.5	2.1	724.8	4.5	711.9	2.6	98.2
EMB05DZ_82	1.1010	0.0	0.1180	0.0	0.45	719.0	8.7	754.0	7.1	864.0	14.3	719.0	8.7	83.2
EMB05DZ_106	1.0764	0.0	0.1217	0.0	0.68	740.5	2.6	741.8	1.8	746.5	3.7	740.5	2.6	99.2

EMB05DZ_76	1.1580	0.0	0.1238	0.0	0.46	752.1	3.9	780.5	3.7	867.0	10.2	752.1	3.9	86.7
EMB05DZ_31	1.1290	0.0	0.1249	0.0	0.60	759.0	7.1	768.0	5.6	801.0	11.2	759.0	7.1	94.8
EMB05DZ_69	1.1210	0.0	0.1254	0.0	0.63	761.5	4.2	763.1	3.2	776.4	4.5	761.5	4.2	98.1
EMB05DZ_38	1.1570	0.0	0.1287	0.0	0.22	780.0	5.1	780.2	3.6	780.0	9.2	780.0	5.1	100.0
EMB05DZ_54	1.1840	0.0	0.1310	0.0	0.62	793.6	3.4	793.0	2.8	786.0	5.6	793.6	3.4	101.0
EMB05DZ_47	1.3070	0.0	0.1356	0.0	0.23	820.0	5.6	848.0	6.6	926.0	20.9	820.0	5.6	88.6
EMB05DZ_4	1.2290	0.0	0.1364	0.0	0.50	824.0	4.0	813.4	3.6	789.0	4.7	824.0	4.0	104.4
EMB05DZ_107	1.4060	0.0	0.1426	0.0	0.66	859.0	5.1	891.3	3.4	976.0	7.7	859.0	5.1	88.0
EMB05DZ_74	1.4110	0.0	0.1447	0.0	0.87	873.0	6.1	893.0	5.1	934.9	4.6	873.0	6.1	93.4
EMB05DZ_36	1.6830	0.0	0.1689	0.0	0.67	1006.0	4.1	1002.4	3.6	988.0	4.5	988.0	4.5	101.8
EMB05DZ_43	1.7550	0.0	0.1732	0.0	0.95	1029.0	7.1	1030.6	4.2	1021.8	2.7	1021.8	2.7	100.7
EMB05DZ_2	1.7310	0.0	0.1708	0.0	0.65	1017.0	5.1	1020.9	4.2	1032.0	5.6	1032.0	5.6	98.5
EMB05DZ_44	1.7190	0.0	0.1688	0.0	0.55	1005.0	7.7	1015.0	5.6	1035.0	9.2	1035.0	9.2	97.1
EMB05DZ_51	1.7750	0.0	0.1762	0.0	0.33	1046.0	8.7	1037.0	6.1	1035.0	11.7	1035.0	11.7	101.1
EMB05DZ_50	1.7790	0.0	0.1743	0.0	0.69	1035.0	6.1	1037.5	3.8	1038.0	5.6	1038.0	5.6	99.7
EMB05DZ_23	1.7720	0.0	0.1753	0.0	0.52	1041.0	7.1	1034.6	5.1	1041.0	7.1	1041.0	7.1	100.0
EMB05DZ_10	1.8490	0.0	0.1803	0.0	0.56	1068.3	4.3	1064.5	3.2	1052.5	5.0	1052.5	5.0	101.5
EMB05DZ_6	1.7530	0.0	0.1711	0.0	0.67	1018.0	5.1	1028.2	3.6	1057.0	5.1	1057.0	5.1	96.3
EMB05DZ_88	1.8270	0.0	0.1776	0.0	0.36	1053.8	4.6	1057.1	4.2	1065.0	7.1	1065.0	7.1	98.9
EMB05DZ_73	1.7160	0.0	0.1645	0.0	0.69	982.0	7.1	1015.0	6.1	1081.0	7.1	1081.0	7.1	90.8
EMB05DZ_114	1.9640	0.0	0.1893	0.0	0.68	1117.0	5.1	1102.8	3.4	1083.7	4.0	1083.7	4.0	103.1
EMB05DZ_3	1.8670	0.0	0.1798	0.0	0.78	1065.8	4.9	1069.2	2.8	1087.1	2.4	1087.1	2.4	98.0
EMB05DZ_21	1.9730	0.0	0.1879	0.0	0.57	1110.0	8.2	1106.0	4.8	1089.0	5.6	1089.0	5.6	101.9
EMB05DZ_112	1.9070	0.0	0.1824	0.0	0.59	1079.8	5.0	1082.9	3.9	1093.0	6.1	1093.0	6.1	98.8
EMB05DZ_41	2.0080	0.0	0.1888	0.0	0.54	1115.0	5.6	1117.8	4.4	1109.0	6.1	1109.0	6.1	100.5
EMB05DZ_98	1.8830	0.0	0.1790	0.0	0.75	1061.5	4.7	1075.0	3.3	1114.1	2.9	1114.1	2.9	95.3
EMB05DZ_105	2.0830	0.0	0.1928	0.0	0.41	1136.4	4.2	1142.8	3.7	1154.0	5.1	1154.0	5.1	98.5
EMB05DZ_49	2.2990	0.0	0.2040	0.0	0.49	1196.7	4.5	1212.5	2.8	1223.4	4.2	1223.4	4.2	97.8
EMB05DZ_83	2.4380	0.0	0.2086	0.0	0.68	1221.0	7.7	1255.0	6.1	1304.0	7.1	1304.0	7.1	93.6
EMB05DZ_71	2.8230	0.0	0.2358	0.0	0.83	1365.0	8.7	1362.3	4.9	1357.7	4.4	1357.7	4.4	100.5
EMB05DZ_16	3.2210	0.0	0.2491	0.0	0.55	1434.0	5.6	1462.0	3.7	1491.1	4.8	1491.1	4.8	96.2
EMB05DZ_13	2.6640	0.0	0.2041	0.0	0.88	1197.0	5.1	1318.1	5.1	1512.2	3.7	1512.2	3.7	79.2
EMB05DZ_28	4.8330	0.0	0.3253	0.0	0.68	1815.0	7.7	1791.4	3.6	1760.7	3.4	1760.7	3.4	103.1
EMB05DZ_40	3.9740	0.0	0.2611	0.0	0.94	1495.0	9.2	1628.2	4.9	1799.7	2.6	1799.7	2.6	83.1
EMB05DZ_100	4.7340	0.0	0.3126	0.0	0.66	1753.0	7.1	1773.0	5.1	1809.0	6.1	1809.0	6.1	96.9
EMB05DZ_61	4.7010	0.0	0.3034	0.0	0.82	1708.0	8.7	1769.0	5.6	1838.0	3.7	1838.0	3.7	92.9
EMB05DZ_35	5.9330	0.0	0.3501	0.0	0.85	1935.0	7.1	1965.5	4.0	2003.6	3.1	2003.6	3.1	96.6
EMB05DZ_64	6.3510	0.0	0.3663	0.0	0.93	2012.0	10.7	2024.0	5.6	2035.9	1.8	2035.9	1.8	98.8
EMB05DZ_53	7.0740	0.0	0.3965	0.0	0.42	2153.0	8.7	2121.9	4.4	2077.3	4.5	2077.3	4.5	103.6
EMB05DZ_14	7.8320	0.0	0.4091	0.0	0.94	2210.0	9.7	2211.3	4.4	2216.1	3.0	2216.1	3.0	99.7
EMB05DZ_18	8.2650	0.0	0.4200	0.0	0.55	2260.0	10.7	2259.8	4.4	2268.0	5.1	2268.0	5.1	99.6
EMB05DZ_101	9.5500	0.1	0.4360	0.0	0.85	2332.0	10.7	2391.7	4.9	2446.1	3.0	2446.1	3.0	95.3
EMB05DZ_17	12.1300	0.1	0.4943	0.0	0.77	2589.0	10.2	2613.8	3.9	2640.2	2.7	2640.2	2.7	98.1
EMB05DZ_75	23.1900	0.1	0.6223	0.0	0.91	3118.0	15.3	3234.0	6.1	3302.8	2.4	3302.8	2.4	94.4

#### VM-01, Oligocene-Miocene Petaca Formation (N=107). 21.26°S, 63.51°W

VM01_95	0.1438	0.0	0.0210	0.0	0.00	133.8	1.1	136.4	1.6	215.0	20.9	133.8	1.1	NA
VM01_58	0.1668	0.0	0.0243	0.0	0.09	155.0	0.9	156.9	1.0	186.0	10.7	155.0	0.9	83.3
VM01_73	0.3020	0.0	0.0419	0.0	0.24	264.4	0.9	267.9	1.6	291.0	7.1	264.4	0.9	90.9
VM01_35	0.3215	0.0	0.0449	0.0	0.20	283.0	1.7	283.6	2.6	287.0	13.3	283.0	1.7	98.6
VM01_83	0.6090	0.0	0.0747	0.0	0.35	464.2	2.1	482.8	2.0	574.0	8.2	464.2	2.1	80.9
VM01_64	0.6084	0.0	0.0781	0.0	0.25	484.6	1.8	482.4	2.2	457.0	8.2	484.6	1.8	106.0
VM01_97	0.6600	0.0	0.0781	0.0	0.51	484.9	5.1	517.0	9.2	684.0	23.0	484.9	5.1	70.9

VM01_29	0.6677	0.0	0.0835	0.0	0.40	516.8	2.1	519.2	1.9	530.0	6.1	516.8	2.1	97.5
VM01_74	0.6622	0.0	0.0837	0.0	0.48	518.3	2.7	515.8	2.4	514.0	8.7	518.3	2.7	100.8
VM01_65	0.6880	0.0	0.0839	0.0	0.23	519.5	2.3	531.0	3.4	568.0	10.2	519.5	2.3	91.5
VM01_66	0.6843	0.0	0.0865	0.0	0.32	534.8	2.3	529.1	2.7	503.0	8.7	534.8	2.3	106.3
VM01_72	0.7200	0.0	0.0867	0.0	0.03	537.0	5.6	547.0	9.7	590.0	30.6	537.0	5.6	91.0
VM01_47	0.6920	0.0	0.0869	0.0	0.34	537.3	2.0	533.8	2.7	519.0	7.7	537.3	2.0	103.5
VM01_24	0.7069	0.0	0.0879	0.0	0.59	543.2	1.9	542.8	1.8	551.4	4.4	543.2	1.9	98.5
VM01_88	0.7318	0.0	0.0900	0.0	0.35	555.2	2.5	558.3	2.9	578.0	7.7	555.2	2.5	96.1
VM01_38	0.7429	0.0	0.0916	0.0	0.54	565.1	2.4	563.9	2.9	561.0	7.1	565.1	2.4	100.7
VM01_112	0.7477	0.0	0.0916	0.0	0.45	565.1	2.3	568.0	2.2	588.6	4.9	565.1	2.3	96.0
VM01_56	0.7364	0.0	0.0922	0.0	0.32	568.4	2.4	560.8	2.9	523.0	8.2	568.4	2.4	108.7
VM01_79	0.7599	0.0	0.0926	0.0	0.39	570.6	2.6	573.7	2.7	585.0	8.2	570.6	2.6	97.5
VM01_93	0.7690	0.0	0.0926	0.0	0.11	570.9	3.7	578.0	6.1	639.0	14.3	570.9	3.7	89.3
VM01_13	0.7600	0.0	0.0926	0.0	0.27	571.1	3.1	574.0	7.1	622.0	19.9	571.1	3.1	91.8
VM01_54	0.7630	0.0	0.0929	0.0	0.34	572.8	2.8	575.5	2.7	577.0	8.7	572.8	2.8	99.3
VM01_100	0.7710	0.0	0.0940	0.0	0.33	579.5	2.4	580.2	3.5	577.0	10.7	579.5	2.4	100.4
VM01_12	0.7650	0.0	0.0943	0.0	0.21	580.7	2.1	577.6	3.0	564.0	9.2	580.7	2.1	103.0
VM01_32	0.7837	0.0	0.0951	0.0	0.33	585.4	2.1	587.4	2.6	595.0	6.6	585.4	2.1	98.4
VM01_25	0.7990	0.0	0.0952	0.0	0.31	586.3	3.1	596.2	3.6	636.0	9.7	586.3	3.1	92.2
VM01_87	0.8120	0.0	0.0953	0.0	0.58	586.9	3.3	604.6	2.8	655.0	5.6	586.9	3.3	89.6
VM01_96	0.7936	0.0	0.0962	0.0	0.10	592.3	3.0	593.8	3.0	606.0	10.2	592.3	3.0	97.7
VM01_3	0.8000	0.0	0.0966	0.0	-0.03	594.6	4.2	597.4	5.0	617.0	17.9	594.6	4.2	96.4
VM01_94	0.8030	0.0	0.0972	0.0	0.18	598.1	2.9	598.9	3.4	584.0	9.7	598.1	2.9	102.4
VM01_11	0.8026	0.0	0.0974	0.0	0.46	599.2	2.2	598.2	1.5	593.7	4.8	599.2	2.2	100.9
VM01_9	0.8280	0.0	0.0988	0.0	0.66	608.0	5.1	612.0	5.6	644.0	8.7	608.0	5.1	94.4
VM01_98	0.8430	0.0	0.0993	0.0	0.16	610.2	3.0	620.4	3.0	657.0	10.2	610.2	3.0	92.9
VM01_21	0.8230	0.0	0.0993	0.0	0.53	610.4	2.8	609.3	3.2	610.0	6.1	610.4	2.8	100.1
VM01_31	0.8476	0.0	0.0998	0.0	0.25	613.0	2.6	623.2	2.8	668.0	10.2	613.0	2.6	91.8
VM01_81	0.8410	0.0	0.1000	0.0	0.28	614.1	2.9	619.9	3.3	652.0	8.2	614.1	2.9	94.2
VM01_60	0.8322	0.0	0.1010	0.0	0.45	620.9	2.0	614.7	2.1	594.0	6.1	620.9	2.0	104.5
VM01_4	0.8240	0.0	0.1013	0.0	0.39	621.9	3.0	609.8	3.7	569.0	7.7	621.9	3.0	109.3
VM01_2	0.8462	0.0	0.1021	0.0	0.38	626.4	2.8	622.4	2.2	622.0	7.1	626.4	2.8	100.7
VM01_17	0.8590	0.0	0.1033	0.0	0.67	633.9	4.5	629.0	4.2	639.0	7.1	633.9	4.5	99.2
VM01_75	0.8696	0.0	0.1038	0.0	0.78	636.6	4.1	635.2	2.7	628.1	4.3	636.6	4.1	101.4
VM01_57	0.9001	0.0	0.1046	0.0	0.31	641.1	2.7	652.3	2.3	689.0	6.6	641.1	2.7	93.0
VM01_110	0.8970	0.0	0.1054	0.0	0.49	645.8	3.7	649.8	3.3	660.0	8.7	645.8	3.7	97.8
VM01_52	0.9980	0.0	0.1073	0.0	0.56	659.0	6.6	708.0	7.7	871.0	18.9	659.0	6.6	75.7
VM01_53	0.9098	0.0	0.1077	0.0	0.43	659.5	2.1	656.8	2.0	646.0	5.6	659.5	2.1	102.1
VM01_68	0.9190	0.0	0.1083	0.0	0.47	662.8	3.0	661.0	6.6	641.0	20.9	662.8	3.0	103.4
VM01_84	0.9253	0.0	0.1098	0.0	0.65	671.7	2.6	665.5	2.4	638.0	5.1	671.7	2.6	105.3
VM01_8	1.0590	0.0	0.1100	0.0	0.49	672.5	3.4	735.0	5.1	886.0	11.7	672.5	3.4	75.9
VM01_63	0.9550	0.0	0.1114	0.0	0.62	681.0	4.1	680.4	3.4	679.0	6.6	681.0	4.1	100.3
VM01_78	1.1470	0.0	0.1217	0.0	-0.05	740.0	9.2	775.0	9.7	888.0	19.4	740.0	9.2	83.3
VM01_92	1.1000	0.0	0.1245	0.0	0.48	756.3	3.3	752.8	3.9	741.0	9.2	756.3	3.3	102.1
VM01_6	1.2055	0.0	0.1337	0.0	0.45	809.2	3.1	803.0	2.0	797.0	5.1	809.2	3.1	101.5
VM01_20	1.3100	0.0	0.1385	0.0	0.41	835.9	4.6	850.0	3.2	888.0	7.7	835.9	4.6	94.1
VM01_10	1.4900	0.0	0.1474	0.0	0.79	886.0	6.6	926.0	5.1	1009.0	6.1	886.0	6.6	87.8
VM01_71	1.5310	0.0	0.1481	0.0	0.64	890.0	7.7	942.5	4.7	1065.0	6.6	890.0	7.7	83.6
VM01_77	1.4610	0.0	0.1517	0.0	0.16	910.2	4.3	914.0	5.1	925.0	9.2	910.2	4.3	98.4
VM01_106	1.5160	0.0	0.1579	0.0	0.40	944.8	2.8	936.8	2.4	922.0	5.1	944.8	2.8	102.5
VM01_15	1.5880	0.0	0.1617	0.0	0.33	966.1	3.3	964.9	3.6	961.0	7.7	961.0	7.7	100.5
VM01_59	1.5710	0.0	0.1587	0.0	0.46	950.0	5.6	959.0	5.1	982.0	7.1	982.0	7.1	96.7
VM01_107	1.8030	0.0	0.1785	0.0	0.32	1058.7	4.3	1046.1	3.5	1024.0	6.1	1024.0	6.1	103.4

VM01_34	1.7950	0.0	0.1773	0.0	0.48	1052.0	5.6	1045.0	5.1	1026.0	9.7	1026.0	9.7	102.5
VM01_27	1.8500	0.0	0.1829	0.0	0.56	1082.0	6.1	1063.0	5.1	1035.0	7.7	1035.0	7.7	104.5
VM01_113	1.7130	0.0	0.1683	0.0	0.45	1002.9	3.8	1013.1	3.4	1036.0	5.1	1036.0	5.1	96.8
VM01_89	1.7690	0.0	0.1731	0.0	0.25	1029.0	3.5	1034.9	3.8	1043.0	6.1	1043.0	6.1	98.7
VM01_70	1.8180	0.0	0.1775	0.0	0.32	1053.3	4.4	1051.5	3.3	1046.0	6.6	1046.0	6.6	100.7
VM01_40	1.8490	0.0	0.1795	0.0	0.59	1064.0	5.1	1062.5	4.2	1063.0	6.1	1063.0	6.1	100.1
VM01_111	1.8360	0.0	0.1783	0.0	0.52	1058.0	6.1	1057.7	4.1	1064.0	6.1	1064.0	6.1	99.4
VM01_80	1.7410	0.0	0.1703	0.0	0.59	1013.0	9.2	1023.0	6.6	1065.0	13.8	1065.0	13.8	95.1
VM01_90	1.8610	0.0	0.1809	0.0	0.60	1071.8	3.5	1067.2	2.5	1066.9	4.5	1066.9	4.5	100.5
VM01_39	1.6860	0.0	0.1601	0.0	0.58	957.0	6.6	1003.0	6.1	1078.0	9.7	1078.0	9.7	88.8
VM01_41	1.9240	0.0	0.1844	0.0	0.56	1090.9	4.3	1088.7	5.1	1079.0	9.2	1079.0	9.2	101.1
VM01_109	1.8530	0.0	0.1777	0.0	0.70	1054.0	5.1	1063.0	5.1	1088.0	8.7	1088.0	8.7	96.9
VM01_104	1.7940	0.0	0.1721	0.0	0.43	1023.6	4.3	1042.9	3.8	1089.5	4.9	1089.5	4.9	94.0
VM01_36	2.0130	0.0	0.1893	0.0	0.44	1117.0	5.6	1120.4	3.9	1125.0	7.7	1125.0	7.7	99.3
VM01_19	2.1080	0.0	0.1973	0.0	0.63	1160.8	4.0	1151.3	2.1	1137.8	3.4	1137.8	3.4	102.0
VM01_103	2.0940	0.0	0.1948	0.0	0.28	1147.0	6.6	1146.8	3.6	1143.0	5.6	1143.0	5.6	100.3
VM01_86	2.0530	0.0	0.1805	0.0	0.90	1069.0	10.7	1134.0	6.6	1258.0	5.6	1258.0	5.6	85.0
VM01_91	2.7120	0.0	0.2259	0.0	0.09	1313.0	8.7	1331.0	5.1	1340.0	11.2	1340.0	11.2	98.0
VM01_99	2.7080	0.0	0.2290	0.0	0.55	1328.9	4.2	1330.5	2.7	1342.9	3.5	1342.9	3.5	99.0
VM01_5	2.8660	0.0	0.2395	0.0	0.53	1384.0	6.1	1373.5	4.0	1358.0	5.6	1358.0	5.6	101.9
VM01_101	2.8430	0.0	0.2360	0.0	0.61	1366.0	7.1	1368.2	3.2	1365.7	4.9	1365.7	4.9	100.0
VM01_108	2.9590	0.0	0.2416	0.0	0.33	1394.8	4.7	1396.9	3.4	1403.0	5.6	1403.0	5.6	99.4
VM01_28	2.9850	0.0	0.2425	0.0	0.37	1399.0	6.6	1404.0	7.7	1407.0	15.8	1407.0	15.8	99.4
VM01_18	3.0800	0.0	0.2494	0.0	0.47	1435.0	6.6	1430.4	3.7	1413.0	5.1	1413.0	5.1	101.6
VM01_50	2.5930	0.0	0.2038	0.0	0.18	1196.0	5.6	1298.1	4.5	1454.0	8.7	1454.0	8.7	82.3
VM01_46	3.0070	0.0	0.2392	0.0	0.31	1382.0	9.7	1410.0	6.1	1471.0	10.7	1471.0	10.7	93.9
VM01_49	3.9880	0.0	0.2907	0.0	0.71	1645.0	6.1	1632.3	3.6	1608.7	3.3	1608.7	3.3	102.3
VM01_42	4.1570	0.0	0.2959	0.0	0.68	1671.0	7.7	1665.2	3.9	1650.1	3.7	1650.1	3.7	101.3
VM01_102	4.5760	0.0	0.3098	0.0	0.59	1740.0	5.1	1745.4	2.6	1749.9	2.8	1749.9	2.8	99.4
VM01_51	4.8530	0.0	0.3230	0.0	0.78	1804.0	11.2	1795.0	7.7	1792.0	5.6	1792.0	5.6	100.7
VM01_76	4.7520	0.0	0.3145	0.0	0.49	1764.0	6.6	1776.2	3.2	1795.0	4.0	1795.0	4.0	98.3
VM01_85	5.4310	0.0	0.3426	0.0	0.71	1899.0	6.6	1889.2	3.8	1875.8	3.8	1875.8	3.8	101.2
VM01_33	5.2200	0.0	0.3239	0.0	0.90	1808.0	12.2	1855.0	4.9	1911.6	4.8	1911.6	4.8	94.6
VM01_45	5.9390	0.0	0.3653	0.0	0.55	2007.0	7.7	1966.6	4.5	1928.0	5.6	1928.0	5.6	104.1
VM01_22	5.6040	0.0	0.3312	0.0	0.88	1843.0	11.2	1917.0	6.1	1988.7	3.1	1988.7	3.1	92.7
VM01_30	6.3240	0.0	0.3729	0.0	-0.03	2042.0	12.2	2022.0	6.1	2000.0	7.7	2000.0	7.7	102.1
VM01_16	6.7700	0.1	0.3818	0.0	0.95	2083.0	14.8	2082.0	7.1	2084.6	2.7	2084.6	2.7	99.9
VM01_43	7.2470	0.0	0.4043	0.0	0.57	2189.0	8.7	2141.9	4.2	2110.9	4.7	2110.9	4.7	103.7
VM01_48	7.1710	0.0	0.3948	0.0	0.24	2145.0	9.7	2132.0	5.6	2121.0	6.6	2121.0	6.6	101.1
VM01_62	9.8000	0.0	0.4507	0.0	0.85	2401.0	9.7	2418.5	4.0	2427.5	3.2	2427.5	3.2	98.9
VM01_37	13.2600	0.1	0.5183	0.0	0.72	2692.0	11.7	2697.8	4.1	2705.2	3.5	2705.2	3.5	99.5
VM01_61	12.3100	0.1	0.4791	0.0	0.87	2522.0	13.3	2627.0	5.1	2706.9	3.4	2706.9	3.4	93.2
VM01_23	15.7820	0.0	0.5517	0.0	0.80	2834.0	8.2	2864.1	3.0	2882.6	2.0	2882.6	2.0	98.3
VM01_55	22.7600	0.2	0.6479	0.0	0.98	3219.0	17.9	3216.0	7.1	3213.1	1.9	3213.1	1.9	100.2

#### VM-05, Miocene Guandacay Formation (N=106). 21.27°S, 63.50°W

VM05_68	0.0203	0.0	0.0032	0.0	0.09	20.4	0.1	20.5	0.2	134.0	11.7	20.4	0.1	NA
VM05_114	0.2955	0.0	0.0404	0.0	0.49	255.2	1.3	262.7	1.6	340.0	10.7	255.2	1.3	75.1
VM05_66	0.3000	0.0	0.0418	0.0	0.08	264.1	1.2	266.3	1.7	288.0	10.7	264.1	1.2	91.7
VM05_54	0.3110	0.0	0.0435	0.0	0.04	274.5	1.2	274.9	1.7	281.0	10.7	274.5	1.2	97.7
VM05_48	0.3098	0.0	0.0436	0.0	0.09	275.3	1.2	273.9	1.9	286.0	11.7	275.3	1.2	96.3
VM05_2	0.4705	0.0	0.0607	0.0	0.32	379.7	2.0	391.4	2.5	449.0	11.7	379.7	2.0	84.6
VM05_5	0.5810	0.0	0.0739	0.0	0.52	459.5	3.0	466.4	3.9	519.0	13.8	459.5	3.0	88.5

VM05_64	0.6020	0.0	0.0769	0.0	0.40	477.3	2.2	478.3	2.7	473.0	9.2	477.3	2.2	100.9
VM05_27	0.6120	0.0	0.0785	0.0	0.56	486.9	2.4	484.7	2.0	487.0	6.1	486.9	2.4	100.0
VM05_32	0.6580	0.0	0.0803	0.0	0.72	498.0	6.1	513.0	6.6	595.0	14.3	498.0	6.1	83.7
VM05_71	0.6640	0.0	0.0838	0.0	0.41	519.0	2.4	516.8	3.2	511.0	10.2	519.0	2.4	101.6
VM05_26	0.6880	0.0	0.0848	0.0	0.18	524.6	3.3	531.6	3.7	595.0	12.8	524.6	3.3	88.2
VM05_99	0.7050	0.0	0.0873	0.0	0.62	539.2	2.7	541.6	2.2	548.0	6.1	539.2	2.7	98.4
VM05_41	0.7046	0.0	0.0880	0.0	0.42	543.5	2.8	541.9	2.6	541.0	7.1	543.5	2.8	100.5
VM05_73	0.7125	0.0	0.0882	0.0	0.56	544.9	1.9	546.1	2.0	543.3	4.3	544.9	1.9	100.3
VM05_81	0.7313	0.0	0.0889	0.0	0.64	548.7	2.0	557.2	2.0	578.1	4.7	548.7	2.0	94.9
VM05_63	0.7220	0.0	0.0900	0.0	0.38	555.6	3.0	551.3	3.0	539.0	8.7	555.6	3.0	103.1
VM05_40	0.7230	0.0	0.0902	0.0	0.28	556.7	3.2	551.5	4.5	521.0	13.3	556.7	3.2	106.9
VM05_80	0.7279	0.0	0.0903	0.0	0.58	557.4	2.3	555.8	2.3	542.2	4.1	557.4	2.3	102.8
VM05_107	0.7351	0.0	0.0912	0.0	0.73	562.6	3.1	560.1	2.7	569.0	5.6	562.6	3.1	98.9
VM05_88	0.7550	0.0	0.0935	0.0	0.11	575.9	4.0	570.7	4.6	558.0	14.3	575.9	4.0	103.2
VM05_77	0.7907	0.0	0.0939	0.0	0.63	578.4	2.6	591.3	2.8	626.0	6.6	578.4	2.6	92.4
VM05_18	0.7880	0.0	0.0941	0.0	0.21	580.0	3.4	590.0	5.6	623.0	14.3	580.0	3.4	93.1
VM05_1	0.7820	0.0	0.0949	0.0	0.40	584.6	2.8	587.0	2.7	618.0	7.7	584.6	2.8	94.6
VM05_46	0.7715	0.0	0.0952	0.0	0.43	586.0	2.2	581.1	2.4	573.0	7.1	586.0	2.2	102.3
VM05_10	0.8009	0.0	0.0958	0.0	0.27	589.9	2.2	597.2	1.9	637.0	7.1	589.9	2.2	92.6
VM05_49	0.7836	0.0	0.0962	0.0	0.44	592.1	2.7	587.3	2.8	568.0	7.1	592.1	2.7	104.2
VM05_112	0.8290	0.0	0.0963	0.0	0.57	593.0	5.6	613.2	4.1	680.0	10.2	593.0	5.6	87.2
VM05_29	0.7955	0.0	0.0967	0.0	0.48	595.4	2.6	595.4	2.4	603.0	7.1	595.4	2.6	98.7
VM05_108	0.8042	0.0	0.0976	0.0	0.22	600.3	2.1	598.9	2.6	599.0	7.1	600.3	2.1	100.2
VM05_84	0.8222	0.0	0.0995	0.0	0.64	611.5	2.7	609.2	1.8	603.9	4.2	611.5	2.7	101.3
VM05_37	0.8610	0.0	0.1000	0.0	0.59	614.0	5.6	630.7	3.4	699.0	12.8	614.0	5.6	87.8
VM05_9	0.8554	0.0	0.1020	0.0	0.50	626.3	2.3	627.4	2.4	630.0	6.1	626.3	2.3	99.4
VM05_109	0.8810	0.0	0.1023	0.0	0.20	627.6	4.0	641.0	5.1	678.0	16.8	627.6	4.0	92.6
VM05_92	0.8740	0.0	0.1024	0.0	0.25	628.2	4.0	637.4	3.6	670.0	12.2	628.2	4.0	93.8
VM05_55	0.8569	0.0	0.1026	0.0	0.45	629.8	2.0	628.2	2.4	618.0	5.6	629.8	2.0	101.9
VM05_43	0.8589	0.0	0.1029	0.0	0.73	631.6	3.1	629.4	1.9	633.7	4.7	631.6	3.1	99.7
VM05_61	0.8750	0.0	0.1045	0.0	0.56	640.8	2.9	637.9	3.4	610.0	7.7	640.8	2.9	105.0
VM05_104	0.9480	0.0	0.1061	0.0	0.47	649.9	4.7	676.0	5.1	763.0	13.3	649.9	4.7	85.2
VM05_38	0.9250	0.0	0.1063	0.0	0.79	651.1	4.9	664.0	6.6	722.0	10.2	651.1	4.9	90.2
VM05_53	0.9090	0.0	0.1072	0.0	0.18	656.2	3.0	656.4	2.9	678.0	8.2	656.2	3.0	96.8
VM05_42	0.9070	0.0	0.1074	0.0	0.79	657.3	4.5	655.1	3.4	656.0	5.1	657.3	4.5	100.2
VM05_57	0.9120	0.0	0.1074	0.0	0.29	657.8	3.8	657.3	4.2	658.0	11.7	657.8	3.8	100.0
VM05_102	0.9370	0.0	0.1079	0.0	0.43	660.3	3.3	671.1	3.5	714.0	8.2	660.3	3.3	92.5
VM05_33	0.9220	0.0	0.1085	0.0	0.68	664.0	5.1	663.7	4.2	677.0	9.2	664.0	5.1	98.1
VM05_70	0.9140	0.0	0.1090	0.0	0.36	666.7	4.0	658.6	4.6	635.0	12.2	666.7	4.0	105.0
VM05_47	0.9790	0.0	0.1123	0.0	0.57	686.0	3.2	692.7	3.6	727.0	6.6	686.0	3.2	94.4
VM05_60	1.0021	0.0	0.1152	0.0	0.44	703.1	2.2	704.7	1.9	709.5	4.4	703.1	2.2	99.1
VM05_50	1.2250	0.0	0.1329	0.0	0.42	804.0	5.6	813.0	5.6	835.0	13.3	804.0	5.6	96.3
VM05_85	1.2430	0.0	0.1346	0.0	0.32	815.0	3.3	820.1	3.1	827.0	9.7	815.0	3.3	98.5
VM05_21	1.2270	0.0	0.1351	0.0	0.53	818.0	3.5	812.7	2.6	809.0	5.6	818.0	3.5	101.1
VM05_105	1.4410	0.0	0.1395	0.0	0.91	842.0	6.1	905.0	6.6	1032.0	6.6	842.0	6.1	81.6
VM05_35	1.3650	0.0	0.1470	0.0	0.24	884.0	6.1	873.2	4.8	844.0	11.2	884.0	6.1	104.7
VM05_14	1.4760	0.0	0.1544	0.0	0.48	925.0	5.6	919.9	4.9	910.0	8.2	925.0	5.6	101.6
VM05_79	1.5740	0.0	0.1576	0.0	0.52	943.4	4.1	961.1	3.3	996.0	5.1	943.4	4.1	94.7
VM05_34	1.6770	0.0	0.1693	0.0	0.44	1008.1	4.3	999.7	2.8	978.0	6.1	978.0	6.1	103.1
VM05_25	1.6660	0.0	0.1682	0.0	0.61	1002.0	5.1	995.4	3.5	985.8	4.7	985.8	4.7	101.6
VM05_16	1.8120	0.0	0.1792	0.0	0.53	1062.3	3.9	1050.3	3.2	1030.7	4.2	1030.7	4.2	103.1
VM05_17	1.7430	0.0	0.1723	0.0	0.35	1025.0	5.6	1023.7	4.5	1034.0	8.7	1034.0	8.7	99.1
VM05_82	1.8160	0.0	0.1789	0.0	0.60	1061.0	4.4	1050.7	3.5	1034.0	5.1	1034.0	5.1	102.6

VM05_62	1.7030	0.0	0.1676	0.0	0.30	998.0	6.1	1012.0	5.6	1037.0	12.2	1037.0	12.2	96.2
VM05_22	1.8090	0.0	0.1779	0.0	0.49	1056.8	4.2	1048.3	3.3	1041.6	4.3	1041.6	4.3	101.5
VM05_8	1.7420	0.0	0.1708	0.0	0.51	1016.5	4.5	1023.6	3.6	1043.0	6.1	1043.0	6.1	97.5
VM05_111	1.8340	0.0	0.1799	0.0	0.88	1066.0	6.1	1057.3	3.8	1043.2	4.1	1043.2	4.1	102.2
VM05_106	1.8020	0.0	0.1766	0.0	0.23	1049.0	3.8	1046.7	2.6	1051.7	4.9	1051.7	4.9	99.7
VM05_100	1.7710	0.0	0.1731	0.0	0.71	1029.0	9.2	1034.0	5.6	1056.0	8.7	1056.0	8.7	97.4
VM05_78	1.7610	0.0	0.1713	0.0	0.28	1019.0	7.1	1030.0	5.6	1073.0	11.2	1073.0	11.2	95.0
VM05_115	1.7520	0.0	0.1708	0.0	0.42	1016.6	4.7	1028.7	2.7	1077.0	6.1	1077.0	6.1	94.4
VM05_12	1.8230	0.0	0.1768	0.0	0.27	1049.0	5.6	1052.8	4.9	1077.0	9.7	1077.0	9.7	97.4
VM05_93	1.9620	0.0	0.1871	0.0	0.18	1105.3	4.8	1102.1	3.9	1082.0	8.7	1082.0	8.7	102.2
VM05_83	1.8650	0.0	0.1775	0.0	0.70	1053.3	4.2	1068.1	3.7	1095.0	5.6	1095.0	5.6	96.2
VM05_86	1.9020	0.0	0.1794	0.0	0.31	1063.5	3.4	1081.4	3.7	1112.0	6.6	1112.0	6.6	95.6
VM05_19	2.0130	0.0	0.1902	0.0	0.61	1122.0	7.1	1119.1	4.7	1116.0	7.1	1116.0	7.1	100.5
VM05_15	1.9670	0.0	0.1844	0.0	0.66	1090.7	4.0	1103.7	3.7	1138.9	4.0	1138.9	4.0	95.8
VM05_89	2.0950	0.0	0.1959	0.0	0.41	1153.0	5.1	1146.6	3.7	1139.0	6.6	1139.0	6.6	101.2
VM05_45	2.1410	0.0	0.1997	0.0	0.74	1174.0	6.6	1161.9	4.5	1147.0	5.6	1147.0	5.6	102.4
VM05_94	2.1530	0.0	0.1989	0.0	0.47	1169.0	6.1	1167.9	4.7	1160.0	7.7	1160.0	7.7	100.8
VM05_69	2.1340	0.0	0.1971	0.0	0.46	1159.6	4.1	1159.7	3.4	1162.0	5.6	1162.0	5.6	99.8
VM05_11	1.8700	0.0	0.1764	0.0	-0.12	1047.0	10.7	1067.0	12.8	1167.0	24.5	1167.0	24.5	89.7
VM05_59	2.2100	0.0	0.2028	0.0	0.66	1190.0	7.1	1183.6	4.3	1183.0	7.1	1183.0	7.1	100.6
VM05_65	2.1040	0.0	0.1920	0.0	0.75	1132.2	3.5	1150.0	2.4	1191.4	2.9	1191.4	2.9	95.0
VM05_96	2.4870	0.0	0.2214	0.0	0.38	1289.0	5.1	1269.2	4.9	1227.0	8.7	1227.0	8.7	105.1
VM05_95	2.2630	0.0	0.2014	0.0	0.60	1182.6	4.6	1200.6	3.1	1234.6	3.5	1234.6	3.5	95.8
VM05_87	2.5280	0.0	0.2213	0.0	0.26	1288.0	5.6	1279.5	3.7	1255.1	4.3	1255.1	4.3	102.6
VM05_91	2.8390	0.0	0.2363	0.0	0.50	1367.3	4.7	1365.5	3.1	1356.6	4.2	1356.6	4.2	100.8
VM05_52	2.5570	0.0	0.2108	0.0	0.67	1233.0	8.2	1287.0	7.1	1386.0	8.2	1386.0	8.2	89.0
VM05_58	2.9310	0.0	0.2409	0.0	0.70	1391.0	9.2	1392.0	6.6	1392.0	7.1	1392.0	7.1	99.9
VM05_113	2.9170	0.0	0.2355	0.0	0.45	1363.0	9.2	1385.0	6.1	1415.0	8.7	1415.0	8.7	96.3
VM05_75	2.9530	0.0	0.2375	0.0	0.40	1373.0	11.7	1395.0	5.6	1420.0	9.7	1420.0	9.7	96.7
VM05_28	2.9880	0.0	0.2431	0.0	0.55	1406.0	8.2	1404.0	5.1	1423.0	7.1	1423.0	7.1	98.8
VM05_13	4.1330	0.0	0.2918	0.0	0.67	1650.0	9.7	1660.0	5.6	1658.0	7.1	1658.0	7.1	99.5
VM05_56	4.1330	0.0	0.2923	0.0	0.21	1653.0	8.2	1662.3	3.1	1680.0	6.1	1680.0	6.1	98.4
VM05_36	4.3980	0.0	0.3077	0.0	0.94	1729.0	7.7	1711.3	4.2	1704.5	4.8	1704.5	4.8	101.4
VM05_6	3.9130	0.0	0.2718	0.0	0.72	1550.0	7.1	1617.0	4.1	1716.4	4.0	1716.4	4.0	90.3
VM05_23	4.6680	0.0	0.3162	0.0	0.75	1771.0	8.7	1762.0	4.2	1751.0	5.1	1751.0	5.1	101.1
VM05_90	4.8370	0.0	0.3228	0.0	0.48	1803.0	6.6	1790.0	5.6	1782.0	6.1	1782.0	6.1	101.2
VM05_7	5.2990	0.0	0.3382	0.0	0.69	1878.0	8.7	1869.6	4.3	1863.4	3.8	1863.4	3.8	100.8
VM05_24	5.4000	0.0	0.3440	0.0	0.70	1909.0	10.2	1886.7	3.9	1879.5	4.9	1879.5	4.9	101.6
VM05_3	5.9490	0.0	0.3502	0.0	0.43	1935.0	6.6	1967.6	4.9	2010.0	8.2	2010.0	8.2	96.3
VM05_98	6.5680	0.0	0.3748	0.0	0.75	2051.0	11.7	2054.1	5.0	2053.0	5.1	2053.0	5.1	99.9
VM05_101	6.7600	0.0	0.3848	0.0	0.57	2098.0	7.1	2080.3	2.9	2081.0	3.4	2081.0	3.4	100.8
VM05_44	6.8150	0.0	0.3647	0.0	0.62	2007.0	9.2	2087.2	4.8	2173.0	5.6	2173.0	5.6	92.4
VM05_110	7.8420	0.0	0.4121	0.0	0.37	2227.0	9.2	2212.6	3.6	2201.0	6.1	2201.0	6.1	101.2
VM05_39	8.9400	0.1	0.4080	0.0	0.89	2205.0	13.3	2331.0	7.7	2449.8	3.7	2449.8	3.7	90.0
VM05_103	10.8700	0.1	0.4646	0.0	0.95	2459.0	19.4	2510.0	10.2	2551.0	5.6	2551.0	5.6	96.4
VM05_72	13.9730	0.1	0.5442	0.0	0.51	2800.0	8.7	2747.5	3.4	2711.9	3.5	2711.9	3.5	103.2

**RPAR-1, Quaternary Rio Parapeti sand (N=109). 20.02°S, 63.19°W**

RPAR_15	0.0034	0.0	0.0634	0.0	0.00	21.6	0.5	20.7	0.7	335.0	34.7	21.6	0.5	NA
RPAR_47	0.0038	0.0	0.0875	0.0	0.00	24.3	0.7	26.3	1.1	464.0	37.8	24.3	0.7	NA
RPAR_105	0.0411	0.0	0.2185	0.0	0.00	260.3	1.7	269.5	2.6	365.0	12.8	260.3	1.7	71.3
RPAR_4	0.0479	0.0	0.3461	0.0	0.00	301.4	2.3	305.6	3.6	378.0	14.8	301.4	2.3	79.7
RPAR_28	0.0517	0.0	0.3640	0.0	0.00	325.1	3.3	340.2	3.9	438.0	13.3	325.1	3.3	74.2

RPAR_55	0.0542	0.0	0.0597	0.0	0.00	340.0	1.6	336.7	3.4	334.0	13.8	340.0	1.6	101.8
RPAR_69	0.0553	0.0	0.1825	0.0	0.00	346.6	2.4	344.4	2.7	379.0	13.3	346.6	2.4	91.5
RPAR_60	0.0788	0.0	0.3484	0.0	0.00	488.8	3.1	497.8	4.5	564.0	14.3	488.8	3.1	86.7
RPAR_17	0.0800	0.0	0.2162	0.0	0.00	496.3	3.7	523.9	3.6	643.0	12.2	496.3	3.7	77.2
RPAR_82	0.0803	0.0	0.2688	0.0	0.00	497.7	4.1	508.0	5.1	551.0	17.9	497.7	4.1	90.3
RPAR_64	0.0826	0.0	0.2319	0.0	0.00	511.6	4.2	515.0	6.6	572.0	18.4	511.6	4.2	89.4
RPAR_87	0.0834	0.0	0.1587	0.0	0.00	516.0	5.6	553.0	5.6	734.0	18.9	516.0	5.6	70.3
RPAR_67	0.0838	0.0	0.0646	0.0	0.00	519.0	7.1	514.0	11.7	533.0	34.2	519.0	7.1	97.4
RPAR_104	0.0840	0.0	0.1324	0.0	0.00	519.6	3.6	518.0	6.6	532.0	20.9	519.6	3.6	97.7
RPAR_9	0.0844	0.0	0.3271	0.0	0.00	522.0	2.5	546.3	4.0	650.0	10.2	522.0	2.5	80.3
RPAR_14	0.0852	0.0	0.3201	0.0	0.00	526.8	3.0	544.1	3.3	613.0	9.2	526.8	3.0	85.9
RPAR_27	0.0853	0.0	0.4152	0.0	0.00	527.3	4.6	529.7	4.4	534.0	13.8	527.3	4.6	98.7
RPAR_110	0.0863	0.0	0.1902	0.0	0.00	533.5	4.3	554.2	4.2	656.0	17.3	533.5	4.3	81.3
RPAR_109	0.0865	0.0	0.2887	0.0	0.00	534.9	2.3	542.2	4.1	586.0	15.3	534.9	2.3	91.3
RPAR_70	0.0871	0.0	0.5255	0.0	0.00	538.5	2.6	541.1	2.3	578.0	6.1	538.5	2.6	93.2
RPAR_19	0.0871	0.0	0.1771	0.0	0.00	539.3	4.3	556.0	6.1	620.0	21.4	539.3	4.3	87.0
RPAR_86	0.0886	0.0	0.4027	0.0	0.00	547.4	2.6	557.1	3.2	600.0	8.7	547.4	2.6	91.2
RPAR_112	0.0887	0.0	0.8572	0.0	0.00	548.0	7.7	560.0	9.7	626.0	21.4	548.0	7.7	87.5
RPAR_48	0.0895	0.0	0.7087	0.0	0.00	552.0	7.1	545.0	8.7	516.0	20.9	552.0	7.1	107.0
RPAR_3	0.0903	0.0	0.8807	0.0	0.00	557.0	6.6	585.0	6.6	694.0	11.2	557.0	6.6	80.3
RPAR_22	0.0903	0.0	0.2821	0.0	0.00	557.1	2.4	553.0	2.8	544.0	9.7	557.1	2.4	102.4
RPAR_20	0.0906	0.0	0.2833	0.0	0.00	559.3	2.6	562.8	3.7	593.0	11.2	559.3	2.6	94.3
RPAR_78	0.0911	0.0	0.6973	0.0	0.00	561.8	4.3	564.3	4.0	598.0	12.8	561.8	4.3	93.9
RPAR_46	0.0925	0.0	0.2076	0.0	0.00	570.3	4.2	575.0	5.6	629.0	17.3	570.3	4.2	90.7
RPAR_35	0.0937	0.0	0.2167	0.0	0.00	577.2	4.0	588.6	4.6	649.0	16.8	577.2	4.0	88.9
RPAR_76	0.0956	0.0	0.3139	0.0	0.00	589.0	5.6	636.0	7.7	822.0	18.9	589.0	5.6	71.7
RPAR_38	0.0972	0.0	0.0897	0.0	0.00	598.0	7.7	608.0	10.7	689.0	33.7	598.0	7.7	86.8
RPAR_102	0.0991	0.0	0.2741	0.0	0.00	609.2	3.3	605.7	4.5	603.0	10.7	609.2	3.3	101.0
RPAR_24	0.0993	0.0	0.2813	0.0	0.00	610.0	4.5	613.3	4.9	643.0	13.3	610.0	4.5	94.9
RPAR_58	0.1006	0.0	0.1912	0.0	0.00	618.0	6.1	653.0	8.2	786.0	19.4	618.0	6.1	78.6
RPAR_66	0.1013	0.0	0.1179	0.0	0.00	621.8	2.5	636.1	3.6	713.0	11.7	621.8	2.5	87.2
RPAR_108	0.1015	0.0	0.5429	0.0	0.00	623.0	2.6	667.0	8.2	834.0	25.5	623.0	2.6	74.7
RPAR_25	0.1024	0.0	0.0333	0.0	0.00	628.3	4.3	617.3	4.9	586.0	15.3	628.3	4.3	107.2
RPAR_96	0.1023	0.0	0.0994	0.0	0.00	630.0	7.1	627.0	8.7	637.0	23.0	630.0	7.1	98.9
RPAR_31	0.1028	0.0	0.2395	0.0	0.00	630.7	3.3	646.4	4.3	688.0	11.2	630.7	3.3	91.7
RPAR_81	0.1031	0.0	0.2993	0.0	0.00	634.0	6.6	679.0	7.1	847.0	17.3	634.0	6.6	74.9
RPAR_10	0.1042	0.0	0.5169	0.0	0.00	639.0	5.1	704.6	4.7	886.0	13.3	639.0	5.1	72.1
RPAR_116	0.1050	0.0	0.1794	0.0	0.00	643.6	3.7	640.2	3.5	643.0	12.8	643.6	3.7	100.1
RPAR_71	0.1054	0.0	0.4169	0.0	0.00	647.1	4.3	642.7	3.9	640.0	10.7	647.1	4.3	101.1
RPAR_43	0.1058	0.0	0.3484	0.0	0.00	648.1	3.1	657.6	2.9	670.0	7.7	648.1	3.1	96.7
RPAR_79	0.1068	0.0	0.1028	0.0	0.00	654.4	3.0	655.2	3.3	655.0	11.2	654.4	3.0	99.9
RPAR_80	0.1074	0.0	0.6769	0.0	0.00	657.0	5.6	662.0	5.6	677.0	9.7	657.0	5.6	97.0
RPAR_95	0.1119	0.0	0.7343	0.0	0.00	683.0	6.6	718.8	4.8	864.0	11.2	683.0	6.6	79.1
RPAR_117	0.1235	0.0	0.2453	0.0	0.00	750.3	3.2	774.5	4.7	861.0	13.3	750.3	3.2	87.1
RPAR_26	0.1307	0.0	0.2816	0.0	0.00	792.0	8.7	804.0	9.7	813.0	20.4	792.0	8.7	97.4
RPAR_98	0.1341	0.0	0.2983	0.0	0.00	811.0	8.2	803.0	9.7	826.0	21.4	811.0	8.2	98.2
RPAR_56	0.1368	0.0	0.5004	0.0	0.00	826.0	9.2	828.0	7.7	875.0	15.3	826.0	9.2	94.4
RPAR_77	0.1367	0.0	0.5037	0.0	0.00	829.0	13.3	845.0	16.3	943.0	27.0	829.0	13.3	87.9
RPAR_84	0.1422	0.0	0.6937	0.0	0.00	857.0	5.1	878.3	4.5	941.0	6.1	857.0	5.1	91.1
RPAR_30	0.1441	0.0	0.5967	0.0	0.00	867.0	14.8	903.0	13.8	984.0	25.0	867.0	14.8	88.1
RPAR_90	0.1447	0.0	0.6098	0.0	0.00	871.0	5.1	888.6	4.7	930.0	7.1	871.0	5.1	93.7
RPAR_2	0.1519	0.0	0.6600	0.0	0.00	912.0	5.6	919.0	5.1	937.0	7.1	912.0	5.6	97.3

RPAR_52	0.1536	0.0	0.5084	0.0	0.00	921.0	7.1	968.1	4.4	1056.0	11.2	921.0	7.1	87.2
RPAR_39	0.1569	0.0	0.7409	0.0	0.00	939.0	7.1	965.0	6.1	1027.0	8.2	939.0	7.1	91.4
RPAR_83	0.1609	0.0	0.1071	0.0	0.00	961.8	4.2	953.1	4.5	949.0	10.2	949.0	10.2	101.3
RPAR_65	0.1596	0.0	0.1649	0.0	0.00	954.0	11.2	957.0	10.2	950.0	26.0	950.0	26.0	100.4
RPAR_1	0.1764	0.0	0.3223	0.0	0.00	1047.1	4.6	1035.7	4.0	1025.0	6.6	1025.0	6.6	102.2
RPAR_89	0.1724	0.0	0.2423	0.0	0.00	1025.0	5.0	1026.8	5.1	1041.0	11.7	1041.0	11.7	98.5
RPAR_62	0.1684	0.0	0.3605	0.0	0.00	1003.0	6.1	1012.0	4.9	1044.0	10.2	1044.0	10.2	96.1
RPAR_75	0.1747	0.0	0.4539	0.0	0.00	1037.9	4.5	1035.7	3.8	1051.0	7.1	1051.0	7.1	98.8
RPAR_114	0.1595	0.0	0.7252	0.0	0.00	954.0	6.6	980.0	5.0	1051.0	8.2	1051.0	8.2	90.8
RPAR_54	0.1774	0.0	0.5051	0.0	0.00	1052.0	6.6	1052.0	5.6	1069.0	9.7	1069.0	9.7	98.4
RPAR_101	0.1710	0.0	0.5189	0.0	0.00	1017.7	4.8	1027.6	3.9	1069.0	6.6	1069.0	6.6	95.2
RPAR_63	0.1768	0.0	0.4531	0.0	0.00	1049.0	5.6	1053.0	5.6	1076.0	10.2	1076.0	10.2	97.5
RPAR_36	0.1737	0.0	0.4646	0.0	0.00	1032.0	5.6	1055.0	5.6	1077.0	8.7	1077.0	8.7	95.8
RPAR_119	0.1728	0.0	0.4438	0.0	0.00	1027.2	5.0	1043.8	3.7	1093.0	6.1	1093.0	6.1	94.0
RPAR_68	0.1823	0.0	0.2011	0.0	0.00	1079.0	8.2	1087.0	6.1	1100.0	12.8	1100.0	12.8	98.1
RPAR_53	0.1824	0.0	0.2015	0.0	0.00	1082.0	7.7	1100.0	7.1	1142.0	14.8	1142.0	14.8	94.7
RPAR_18	0.1840	0.0	0.2208	0.0	0.00	1088.0	8.2	1094.0	7.7	1146.0	15.8	1146.0	15.8	94.9
RPAR_93	0.1880	0.0	0.4544	0.0	0.00	1110.0	5.6	1121.0	5.1	1158.0	8.2	1158.0	8.2	95.9
RPAR_94	0.1738	0.0	0.5517	0.0	0.00	1033.0	6.6	1085.1	4.6	1187.0	5.6	1187.0	5.6	87.0
RPAR_13	0.2100	0.0	0.1766	0.0	0.00	1229.0	5.1	1215.8	4.2	1202.0	7.1	1202.0	7.1	102.2
RPAR_61	0.2062	0.0	0.4346	0.0	0.00	1208.5	5.0	1201.1	4.0	1213.0	6.6	1213.0	6.6	99.6
RPAR_99	0.1978	0.0	0.3348	0.0	0.00	1163.0	8.7	1173.0	8.2	1222.0	12.2	1222.0	12.2	95.2
RPAR_11	0.1967	0.0	0.4444	0.0	0.00	1157.0	6.1	1180.9	4.7	1224.0	7.7	1224.0	7.7	94.5
RPAR_34	0.1599	0.0	0.0630	0.0	0.00	956.0	8.2	1049.0	11.2	1240.0	32.1	1240.0	32.1	77.1
RPAR_42	0.1770	0.0	0.0582	0.0	0.00	1051.0	5.1	1119.0	8.7	1249.0	24.5	1249.0	24.5	84.1
RPAR_73	0.1705	0.0	0.3911	0.0	0.00	1014.0	10.2	1096.0	8.7	1275.0	16.8	1275.0	16.8	79.5
RPAR_92	0.2294	0.0	0.4351	0.0	0.00	1331.0	4.6	1335.6	3.0	1349.7	4.2	1349.7	4.2	98.6
RPAR_57	0.2323	0.0	0.3447	0.0	0.00	1347.0	6.1	1348.8	3.7	1351.0	6.6	1351.0	6.6	99.7
RPAR_5	0.2419	0.0	0.5426	0.0	0.00	1396.0	6.6	1392.9	4.2	1368.0	6.6	1368.0	6.6	102.0
RPAR_115	0.2250	0.0	0.3091	0.0	0.00	1308.0	7.1	1329.0	5.6	1368.0	9.7	1368.0	9.7	95.6
RPAR_40	0.2279	0.0	0.3539	0.0	0.00	1323.0	5.6	1352.3	3.7	1390.0	6.6	1390.0	6.6	95.2
RPAR_44	0.2272	0.0	0.4787	0.0	0.00	1319.0	13.3	1359.0	10.7	1425.0	12.8	1425.0	12.8	92.6
RPAR_23	0.2318	0.0	0.5955	0.0	0.00	1344.0	8.7	1384.0	7.7	1457.0	11.2	1457.0	11.2	92.2
RPAR_12	0.2478	0.0	0.7694	0.0	0.00	1427.0	8.7	1457.0	5.1	1497.0	4.4	1497.0	4.4	95.3
RPAR_6	0.2664	0.0	0.2154	0.0	0.00	1522.0	8.2	1540.2	4.2	1571.0	7.1	1571.0	7.1	96.9
RPAR_50	0.2971	0.0	0.3354	0.1	0.00	1676.0	11.2	1714.0	5.6	1755.0	8.7	1755.0	8.7	95.5
RPAR_29	0.3017	0.0	0.4363	0.1	0.00	1700.0	6.6	1737.5	3.4	1768.0	5.1	1768.0	5.1	96.2
RPAR_41	0.3037	0.0	0.2825	0.1	0.00	1712.0	9.2	1745.0	7.1	1780.0	8.7	1780.0	8.7	96.2
RPAR_97	0.3215	0.0	0.6599	0.1	0.00	1797.0	6.6	1790.2	3.4	1794.8	3.4	1794.8	3.4	100.1
RPAR_16	0.3243	0.0	0.2496	0.1	0.00	1810.0	8.2	1818.0	9.7	1808.0	17.3	1808.0	17.3	100.1
RPAR_118	0.2981	0.0	0.5370	0.1	0.00	1682.0	9.2	1774.0	11.7	1894.0	20.9	1894.0	20.9	88.8
RPAR_103	0.3160	0.0	0.1417	0.1	0.00	1770.0	8.2	1827.0	5.6	1908.0	7.7	1908.0	7.7	92.8
RPAR_7	0.3423	0.0	0.3314	0.1	0.00	1897.0	9.7	1917.7	4.3	1942.0	7.7	1942.0	7.7	97.7
RPAR_45	0.3350	0.0	0.5472	0.1	0.00	1862.0	10.2	1894.0	5.6	1942.0	6.6	1942.0	6.6	95.9
RPAR_100	0.3363	0.0	0.6419	0.1	0.00	1869.0	9.7	1940.0	5.1	2034.0	5.6	2034.0	5.6	91.9
RPAR_107	0.3261	0.0	0.7354	0.1	0.00	1819.0	10.2	1921.0	7.7	2048.0	7.1	2048.0	7.1	88.8
RPAR_59	0.3648	0.0	0.3686	0.1	0.00	2004.0	9.7	2033.3	4.8	2079.0	6.6	2079.0	6.6	96.4
RPAR_51	0.4047	0.0	0.7742	0.1	0.00	2190.0	12.8	2246.4	4.8	2291.9	4.3	2291.9	4.3	95.6
RPAR_106	0.5020	0.0	0.7669	0.1	0.00	2622.0	7.1	2614.3	3.0	2620.5	2.1	2620.5	2.1	100.1
RPAR_91	0.5002	0.0	0.6008	0.1	0.00	2614.0	10.2	2642.0	3.7	2668.0	4.0	2668.0	4.0	98.0
RPAR_37	0.4674	0.0	0.7020	0.1	0.00	2472.0	7.1	2610.1	2.6	2699.4	2.6	2699.4	2.6	91.6
RPAR_88	0.4821	0.0	0.6141	0.1	0.00	2536.0	8.7	2627.2	3.7	2700.7	4.2	2700.7	4.2	93.9

**RGRA-1, Quaternary Rio Grande sand (N=115). 18.91°S, 63.40°W**

RGRA1_108	0.0136	0.0	0.0020	0.0	0.06	12.9	0.3	13.7	0.6	424.0	45.9	12.9	0.3	NA
RGRA1_4	0.0926	0.0	0.0138	0.0	-0.06	88.6	1.3	89.6	3.3	309.0	33.2	88.6	1.3	NA
RGRA1_25	0.3120	0.0	0.0404	0.0	-0.10	255.8	2.5	274.9	4.0	457.0	19.9	255.8	2.5	NA
RGRA1_75	0.4134	0.0	0.0560	0.0	0.04	351.0	1.8	351.2	2.3	351.0	12.2	351.0	1.8	100.0
RGRA1_6	0.4401	0.0	0.0587	0.0	0.28	367.5	2.2	370.0	3.2	377.0	10.2	367.5	2.2	97.5
RGRA1_97	0.5650	0.0	0.0677	0.0	-0.01	422.1	3.3	454.5	4.8	592.0	18.4	422.1	3.3	71.3
RGRA1_83	0.5690	0.0	0.0682	0.0	0.72	425.3	2.9	458.2	3.0	607.0	8.7	425.3	2.9	70.1
RGRA1_50	0.5580	0.0	0.0688	0.0	0.65	428.0	6.1	449.2	4.6	588.0	17.3	428.0	6.1	72.8
RGRA1_1	0.5700	0.0	0.0707	0.0	0.36	440.4	3.5	457.0	6.6	525.0	21.9	440.4	3.5	83.9
RGRA1_98	0.5940	0.0	0.0734	0.0	0.68	456.3	4.9	473.2	3.4	563.0	11.2	456.3	4.9	81.0
RGRA1_74	0.5770	0.0	0.0734	0.0	0.14	456.6	2.3	462.3	3.4	499.0	11.7	456.6	2.3	91.5
RGRA1_21	0.5610	0.0	0.0735	0.0	0.29	457.4	3.6	451.4	3.8	455.0	14.8	457.4	3.6	100.5
RGRA1_95	0.5983	0.0	0.0737	0.0	0.41	458.4	2.8	475.9	3.0	558.0	11.7	458.4	2.8	82.2
RGRA1_106	0.6056	0.0	0.0757	0.0	0.46	470.4	3.0	480.5	3.0	532.0	11.2	470.4	3.0	88.4
RGRA1_31	0.6050	0.0	0.0766	0.0	0.43	475.8	3.0	479.8	3.8	488.0	13.3	475.8	3.0	97.5
RGRA1_35	0.6220	0.0	0.0781	0.0	0.39	484.6	2.7	490.4	3.8	515.0	11.7	484.6	2.7	94.1
RGRA1_41	0.6050	0.0	0.0787	0.0	0.03	488.3	3.1	482.1	4.3	494.0	14.8	488.3	3.1	98.8
RGRA1_63	0.6280	0.0	0.0791	0.0	0.20	490.7	3.5	494.0	5.1	532.0	17.3	490.7	3.5	92.2
RGRA1_85	0.6230	0.0	0.0795	0.0	0.22	493.0	3.9	494.3	3.6	504.0	11.7	493.0	3.9	97.8
RGRA1_67	0.6495	0.0	0.0809	0.0	0.36	501.6	2.8	508.0	2.8	538.0	12.2	501.6	2.8	93.2
RGRA1_16	0.6860	0.0	0.0816	0.0	0.36	505.5	2.6	530.0	4.1	639.0	11.7	505.5	2.6	79.1
RGRA1_3	0.6700	0.0	0.0823	0.0	0.72	510.0	3.2	520.4	3.9	566.0	8.2	510.0	3.2	90.1
RGRA1_110	0.6910	0.0	0.0828	0.0	0.51	513.3	3.0	534.2	3.0	618.0	8.7	513.3	3.0	83.1
RGRA1_48	0.7080	0.0	0.0862	0.0	0.23	532.7	4.1	545.8	4.9	602.0	13.3	532.7	4.1	88.5
RGRA1_79	0.6970	0.0	0.0865	0.0	0.12	534.5	4.2	536.3	4.2	547.0	11.7	534.5	4.2	97.7
RGRA1_34	0.7590	0.0	0.0881	0.0	0.45	544.0	3.4	573.0	3.0	670.0	9.2	544.0	3.4	81.2
RGRA1_103	0.7012	0.0	0.0881	0.0	0.18	544.5	2.6	539.2	2.8	538.0	8.7	544.5	2.6	101.2
RGRA1_38	0.7050	0.0	0.0885	0.0	-0.02	546.7	3.2	541.2	4.0	553.0	13.3	546.7	3.2	98.9
RGRA1_28	0.7960	0.0	0.0886	0.0	0.48	547.0	5.0	594.2	3.9	755.0	12.2	547.0	5.0	72.5
RGRA1_117	0.7240	0.0	0.0886	0.0	0.02	547.3	3.6	552.2	4.0	558.0	13.8	547.3	3.6	98.1
RGRA1_8	0.7006	0.0	0.0887	0.0	0.18	547.6	3.1	538.9	3.0	519.0	10.2	547.6	3.1	105.5
RGRA1_55	0.7091	0.0	0.0889	0.0	0.20	548.9	2.8	544.0	2.7	540.0	9.2	548.9	2.8	101.6
RGRA1_71	0.7160	0.0	0.0895	0.0	0.12	552.7	2.7	547.6	4.2	535.0	12.8	552.7	2.7	103.3
RGRA1_18	0.7670	0.0	0.0898	0.0	0.00	554.2	4.6	578.0	7.1	686.0	26.5	554.2	4.6	80.8
RGRA1_114	0.7350	0.0	0.0904	0.0	0.27	557.6	3.8	560.4	4.6	590.0	14.8	557.6	3.8	94.5
RGRA1_90	0.7620	0.0	0.0927	0.0	0.66	571.4	3.4	574.7	4.1	565.0	10.2	571.4	3.4	101.1
RGRA1_109	0.7870	0.0	0.0928	0.0	0.28	572.1	4.0	588.0	6.1	689.0	18.4	572.1	4.0	83.0
RGRA1_33	0.7700	0.0	0.0929	0.0	0.59	573.0	5.6	579.2	5.1	611.0	11.7	573.0	5.6	93.8
RGRA1_46	0.7740	0.0	0.0933	0.0	0.34	575.0	6.6	583.0	7.7	646.0	22.4	575.0	6.6	89.0
RGRA1_53	0.8180	0.0	0.0934	0.0	0.23	575.7	4.8	606.0	5.0	690.0	17.3	575.7	4.8	83.4
RGRA1_52	0.8070	0.0	0.0940	0.0	0.21	579.0	5.6	602.0	6.6	696.0	17.9	579.0	5.6	83.2
RGRA1_9	0.8310	0.0	0.0948	0.0	0.74	583.9	4.4	613.5	3.7	725.0	6.1	583.9	4.4	80.5
RGRA1_58	0.7980	0.0	0.0955	0.0	0.01	588.0	5.1	595.1	5.0	598.0	18.4	588.0	5.1	98.3
RGRA1_99	0.8580	0.0	0.0969	0.0	0.40	596.3	4.4	628.7	3.6	746.0	12.8	596.3	4.4	79.9
RGRA1_118	0.7970	0.0	0.0973	0.0	0.20	598.3	3.0	595.6	3.2	599.0	9.2	598.3	3.0	99.9
RGRA1_91	0.8310	0.0	0.0985	0.0	0.52	605.0	5.6	616.0	6.1	637.0	17.3	605.0	5.6	95.0
RGRA1_5	0.8203	0.0	0.0984	0.0	0.51	605.2	2.3	608.0	2.2	628.0	6.1	605.2	2.3	96.4
RGRA1_32	0.8230	0.0	0.0987	0.0	0.01	606.7	4.4	604.0	5.1	594.0	19.9	606.7	4.4	102.1
RGRA1_116	0.8270	0.0	0.0989	0.0	0.69	607.8	4.4	611.7	3.6	596.0	8.2	607.8	4.4	102.0
RGRA1_56	0.8230	0.0	0.0994	0.0	0.75	610.7	4.7	609.5	3.4	632.0	6.1	610.7	4.7	96.6
RGRA1_59	0.8408	0.0	0.0995	0.0	0.49	611.2	3.4	619.3	2.7	633.0	7.1	611.2	3.4	96.6
RGRA1_7	0.8480	0.0	0.1000	0.0	0.78	614.0	6.1	624.7	4.7	677.0	8.2	614.0	6.1	90.7

RGRA1_19	0.8410	0.0	0.1003	0.0	-0.02	616.0	3.2	618.6	5.1	622.0	17.9	616.0	3.2	99.0
RGRA1_96	0.8580	0.0	0.1005	0.0	0.25	617.3	3.5	629.8	4.6	653.0	15.8	617.3	3.5	94.5
RGRA1_81	0.8720	0.0	0.1014	0.0	0.02	622.5	3.6	637.0	5.0	701.0	18.4	622.5	3.6	88.8
RGRA1_115	0.8450	0.0	0.1021	0.0	0.20	626.5	3.5	621.7	3.8	616.0	12.8	626.5	3.5	101.7
RGRA1_88	0.8550	0.0	0.1028	0.0	0.39	630.7	3.4	626.9	3.5	616.0	8.7	630.7	3.4	102.4
RGRA1_43	0.8820	0.0	0.1045	0.0	0.20	641.0	5.1	641.0	5.6	657.0	15.3	641.0	5.1	97.6
RGRA1_80	0.8820	0.0	0.1050	0.0	0.40	643.8	3.5	641.4	4.2	656.0	10.2	643.8	3.5	98.1
RGRA1_107	0.9670	0.0	0.1097	0.0	0.10	670.9	4.7	686.0	5.6	723.0	16.3	670.9	4.7	92.8
RGRA1_45	0.9030	0.0	0.1103	0.0	0.09	674.6	4.3	652.8	3.9	614.0	11.7	674.6	4.3	109.9
RGRA1_100	0.9680	0.0	0.1122	0.0	0.62	685.7	4.3	687.0	3.3	725.0	6.6	685.7	4.3	94.6
RGRA1_23	1.0330	0.0	0.1141	0.0	0.46	696.4	3.8	720.2	3.1	810.0	9.7	696.4	3.8	86.0
RGRA1_104	1.0340	0.0	0.1154	0.0	0.28	703.8	4.2	720.0	5.1	769.0	10.7	703.8	4.2	91.5
RGRA1_70	1.1610	0.0	0.1300	0.0	0.31	787.6	4.6	781.5	5.1	792.0	10.7	787.6	4.6	99.4
RGRA1_51	1.5000	0.0	0.1487	0.0	0.61	893.8	5.1	929.0	6.1	1033.0	12.8	893.8	5.1	86.5
RGRA1_2	1.4690	0.0	0.1521	0.0	0.28	912.7	4.1	916.7	4.9	923.0	9.2	912.7	4.1	98.9
RGRA1_68	1.4840	0.0	0.1549	0.0	0.38	928.0	6.6	924.0	6.1	920.0	11.7	928.0	6.6	100.9
RGRA1_20	1.5480	0.0	0.1553	0.0	0.49	930.8	4.8	949.0	6.6	982.0	12.8	930.8	4.8	94.8
RGRA1_77	1.6380	0.0	0.1699	0.0	0.80	1012.0	9.2	986.0	8.7	937.0	10.7	937.0	10.7	108.0
RGRA1_54	1.5310	0.0	0.1569	0.0	0.17	939.0	6.6	941.0	7.1	948.0	17.3	939.0	6.6	99.1
RGRA1_120	1.7270	0.0	0.1714	0.0	0.53	1019.9	3.7	1018.3	3.2	1016.9	4.3	1016.9	4.3	100.3
RGRA1_11	1.7330	0.0	0.1711	0.0	0.37	1017.9	4.8	1020.6	3.4	1036.0	8.2	1036.0	8.2	98.3
RGRA1_42	1.7570	0.0	0.1743	0.0	-0.06	1035.0	6.6	1028.0	6.6	1064.0	12.8	1064.0	12.8	97.3
RGRA1_36	1.7100	0.0	0.1659	0.0	0.36	989.0	7.1	1010.0	8.7	1069.0	14.3	1069.0	14.3	92.5
RGRA1_22	1.8690	0.0	0.1768	0.0	0.93	1049.0	18.4	1066.0	15.8	1100.0	14.3	1100.0	14.3	95.4
RGRA1_30	1.9500	0.0	0.1863	0.0	0.46	1101.0	5.1	1097.8	3.9	1105.0	6.6	1105.0	6.6	99.6
RGRA1_17	2.2420	0.0	0.1975	0.0	0.55	1162.0	6.6	1195.0	5.1	1258.0	7.7	1258.0	7.7	92.4
RGRA1_61	2.7740	0.0	0.2329	0.0	0.81	1349.0	7.7	1348.0	5.1	1341.0	6.1	1341.0	6.1	100.6
RGRA1_89	2.7690	0.0	0.2281	0.0	0.56	1324.2	5.0	1346.9	3.2	1379.0	5.1	1379.0	5.1	96.0
RGRA1_102	2.9900	0.0	0.2468	0.0	0.43	1422.0	8.7	1404.0	6.1	1385.0	10.2	1385.0	10.2	102.7
RGRA1_15	3.4480	0.0	0.2659	0.0	0.20	1520.0	7.7	1514.7	4.7	1518.0	7.7	1518.0	7.7	100.1
RGRA1_78	2.9600	0.0	0.2264	0.0	0.57	1315.0	7.7	1397.0	3.9	1543.0	5.6	1543.0	5.6	85.2
RGRA1_94	3.7140	0.0	0.2811	0.0	0.35	1596.0	9.7	1573.7	4.8	1549.0	8.7	1549.0	8.7	103.0
RGRA1_57	3.7760	0.0	0.2840	0.0	0.53	1611.0	8.2	1587.0	5.6	1553.0	6.6	1553.0	6.6	103.7
RGRA1_69	3.5490	0.0	0.2678	0.0	0.52	1530.0	8.7	1539.3	5.0	1555.0	7.7	1555.0	7.7	98.4
RGRA1_44	3.9460	0.0	0.2862	0.0	0.57	1622.0	9.7	1622.0	7.7	1634.0	5.6	1634.0	5.6	99.3
RGRA1_62	4.1970	0.0	0.2952	0.0	0.34	1667.0	9.2	1672.0	5.6	1678.0	9.2	1678.0	9.2	99.3
RGRA1_37	4.8530	0.0	0.3296	0.0	0.43	1836.0	8.7	1796.2	4.6	1761.0	5.6	1761.0	5.6	104.3
RGRA1_84	5.5420	0.0	0.3503	0.0	0.35	1936.0	9.2	1909.1	5.1	1875.0	7.1	1875.0	7.1	103.3
RGRA1_72	6.1100	0.1	0.3630	0.0	0.55	1999.0	12.2	1987.0	10.2	1962.0	13.3	1962.0	13.3	101.9
RGRA1_76	6.0140	0.0	0.3612	0.0	0.55	1988.0	6.1	1978.4	3.0	1967.2	4.0	1967.2	4.0	101.1
RGRA1_27	4.8600	0.1	0.2900	0.0	0.74	1641.0	13.3	1793.0	9.7	1991.0	8.7	1991.0	8.7	82.4
RGRA1_82	6.8300	0.1	0.3901	0.0	0.70	2123.0	16.3	2089.0	10.2	2044.0	13.8	2044.0	13.8	103.9
RGRA1_24	6.3530	0.0	0.3642	0.0	0.51	2004.0	7.7	2025.4	3.3	2055.0	4.0	2055.0	4.0	97.5
RGRA1_92	6.7450	0.0	0.3760	0.0	0.54	2057.0	8.7	2078.0	5.6	2077.0	5.6	2077.0	5.6	99.0
RGRA1_12	6.7320	0.0	0.3729	0.0	0.59	2043.0	8.2	2078.6	4.3	2107.0	5.1	2107.0	5.1	97.0
RGRA1_105	6.6100	0.1	0.3654	0.0	0.64	2007.0	12.8	2059.0	7.7	2126.0	7.7	2126.0	7.7	94.4
RGRA1_101	7.7000	0.1	0.4132	0.0	0.57	2228.0	22.4	2198.0	10.7	2142.0	12.8	2142.0	12.8	104.0
RGRA1_60	7.3400	0.1	0.3926	0.0	0.46	2134.0	11.2	2155.0	13.3	2170.0	20.4	2170.0	20.4	98.3
RGRA1_87	7.1800	0.1	0.3697	0.0	0.29	2027.0	12.8	2135.0	7.7	2233.0	9.2	2233.0	9.2	90.8
RGRA1_64	10.4400	0.1	0.4710	0.0	0.96	2487.0	11.7	2474.0	6.6	2457.4	4.4	2457.4	4.4	101.2
RGRA1_111	13.4900	0.1	0.5077	0.0	0.78	2646.0	15.8	2714.0	8.2	2780.0	6.6	2780.0	6.6	95.2
RGRA1_73	13.4600	0.1	0.4546	0.0	0.86	2414.0	18.4	2710.0	10.2	2945.0	6.1	2945.0	6.1	82.0

**Appendix 3. SHRIMP U-Pb data from detrital zircon sample VLE07-109 from Escayola et al. (2011)**

Spot name	ppm U	ppm Th	ppm Rad 206	232Th/ 238U	% err	Total 206Pb/ 238U	% err	Total 208Pb/ 232Th	% err	204corr 206Pb/ 238U age	1 err	207 corr 206Pb/ 238U age
9579-1.2	546	44	162.4	0.08	0.67	0.346	1.1	0.1072	3.3	1917	18	1906
9579-4.1	89	88	11.4	1.01	0.47	0.148	1.5	0.0490	3.6	892	12	890
9579-4.2	204	109	17.3	0.55	0.44	0.099	1.3	0.0315	4.0	608	8	609
9579-5.1	305	70	25.7	0.24	0.55	0.098	1.2	0.0338	4.7	603	7	604
9579-6.1	279	352	79.6	1.30	0.27	0.332	1.1	0.0959	1.7	1847	18	1846
9579-6.2	175	246	47.2	1.46	0.31	0.314	1.2	0.0937	2.9	1761	19	1741
9579-7.1	1310	578	125.6	0.46	0.20	0.112	1.1	0.0341	1.9	682	7	683
9579-8.1	253	67	58.2	0.27	0.56	0.268	1.1	0.0821	3.2	1531	16	1531
9579-8.2	414	101	98.0	0.25	0.47	0.276	1.1	0.0784	2.7	1570	15	1573
9579-10.1	194	91	26.9	0.49	0.49	0.162	1.3	0.0562	3.4	967	11	967
9579-10.2	203	41	27.9	0.21	0.74	0.160	1.3	0.0490	5.2	957	11	957
9579-11.1	430	128	57.5	0.31	0.41	0.156	1.1	0.0477	3.0	933	10	931
9579-11.2	81	1	7.0	0.01	5.98	0.100	1.7	0.1278	27.6	618	11	609
9579-12.1	165	108	23.3	0.68	0.45	0.164	1.3	0.0506	3.3	979	12	977
9579-14.1	278	183	24.6	0.68	0.35	0.103	1.2	0.0344	3.0	633	7	633
9579-15.1	156	74	28.5	0.49	0.55	0.213	1.3	0.0699	3.4	1241	14	1242
9579-15.2	183	64	32.9	0.36	0.57	0.210	1.2	0.0675	4.9	1226	14	1225
9579-19.1	170	79	25.2	0.48	0.52	0.174	1.3	0.0552	3.6	1030	12	1028
9579-20.1	156	53	13.9	0.35	0.87	0.105	1.4	0.0449	4.8	633	9	632
9579-20.2	199	133	15.1	0.69	0.40	0.089	1.4	0.0274	3.9	546	7	548
9579-21.1	114	67	51.2	0.60	0.58	0.522	1.2	0.1512	2.6	2707	27	2735
9579-21.2	82	50	31.2	0.63	0.65	0.446	1.3	0.1420	3.8	2372	26	2355
9579-22.1	128	42	18.3	0.34	0.71	0.167	1.4	0.0493	5.0	995	13	996
9579-23.1	128	44	10.9	0.35	0.73	0.100	1.5	0.0342	6.3	607	9	611
9579-23.2	84	26	7.1	0.32	0.91	0.100	1.7	0.0384	7.2	605	11	609
9579-23.3	229	77	19.7	0.35	0.54	0.101	1.3	0.0331	4.6	617	8	615
9579-25.1	44	30	5.7	0.70	0.85	0.150	1.9	0.0549	5.9	894	16	899
9579-30.1	225	55	34.0	0.25	0.62	0.176	1.2	0.0531	5.7	1045	12	1041
9579-33.1	194	100	21.4	0.54	0.46	0.129	1.3	0.0442	3.5	780	10	779
9579-36.1	227	104	28.4	0.48	0.45	0.146	1.2	0.0479	3.3	877	10	876
9579-39.1	55	20	9.3	0.38	1.04	0.200	1.7	0.0680	6.4	1164	21	1157
9579-39.2	145	74	24.0	0.53	0.55	0.194	1.3	0.0598	3.7	1137	14	1138
9579-42.1	316	421	27.0	1.38	0.24	0.100	1.2	0.0326	2.3	611	7	612
9579-42.2	210	244	17.8	1.20	0.33	0.099	1.4	0.0313	3.2	607	8	608

9579-47.1	129	52	21.9	0.42	0.64	0.198	1.3	0.0654	4.0	1166	14	1163
9579-51.1	424	318	36.2	0.77	0.26	0.099	1.2	0.0316	2.4	610	7	609
9579-52.1	258	122	38.8	0.49	0.43	0.175	1.2	0.0550	3.0	1039	11	1037
9579-53.1	133	148	11.1	1.15	0.36	0.098	1.4	0.0310	3.4	600	8	599
9579-53.2	401	163	34.4	0.42	0.75	0.100	1.3	0.0347	4.2	613	8	614
9579-58.1	90	58	24.3	0.67	0.60	0.313	1.3	0.0937	3.3	1754	21	1752
9579-60.1	129	39	27.6	0.31	0.70	0.249	1.3	0.0769	4.0	1434	16	1428
9579-62.1	61	77	27.3	1.30	0.51	0.520	1.4	0.1454	2.5	2696	30	2695
9579-63.1	536	234	148.7	0.45	0.43	0.324	1.1	0.0989	2.5	1803	18	1797
9579-64.1	19	21	1.4	1.14	0.96	0.083	3	0.0361	8.2	510	15	499
9579-67.1	131	145	57.6	1.14	0.37	0.510	1.2	0.1469	1.9	2658	26	2635
9579-67.2	514	296	207.7	0.60	0.49	0.472	1.2	0.1497	2.2	2487	24	2425
9579-71.1	178	154	28.1	0.89	0.35	0.184	1.2	0.0564	2.5	1087	12	1084
9579-73.1	247	114	51.2	0.48	0.41	0.241	1.1	0.0765	2.5	1392	14	1383
9579-76.1	406	104	35.3	0.26	0.43	0.101	1.2	0.0306	3.8	622	7	622
9579-79.1	257	152	20.6	0.61	0.36	0.094	1.2	0.0318	3.2	575	7	576
9579-85.1	110	69	12.8	0.65	0.52	0.136	1.4	0.0430	4.0	816	11	822
9579-86.1	293	141	43.3	0.50	0.38	0.172	1.2	0.0571	2.6	1024	11	1025
9579-88.1	34	27	3.1	0.82	0.86	0.109	2.2	0.0344	7.4	660	14	664

## References

- Adams, C.J., Miller, H., Aceñolaza, F.G., Toselli, a. J., and Griffin, W.L., 2011, The Pacific Gondwana margin in the late Neoproterozoic–early Paleozoic: Detrital zircon U–Pb ages from metasediments in northwest Argentina reveal their maximum age, provenance and tectonic setting: *Gondwana Research*, v. 19, p. 71–83.
- Ayaviri, A., 1971, El Terciario Subandino: Yacimientos Petrolíferos Fiscales Bolivianos internal report, 6 p.
- Baby, P., Héral, G., Salinas, R. and Sempere T., 1992, Geometry and kinematic evolution of passive roof duplexes deduced from cross section balancing: example from the foreland thrust system of the southern Bolivian Subandean zone: *Tectonics*, v. 11, p. 523–536.
- Bahlburg, H., Moya, C. and Zeil, W., 1994, Geodynamic evolution of the early Paleozoic continental margin of Gondwana in the Southern Central Andes of Northwestern Argentina and Northern Chile; in: Reutter, K.-J., Scheuber, E. & Wigger, P. (editors): *Tectonics of the Southern Central Andes*, Springer Verlag, Berlin, Heidelberg, New York, p. 293–302.
- Bahlburg, H., and Hervé, F., 1997, Geodynamic evolution and tectonostratigraphic terranes of northwestern Argentina and northern Chile: *Geological Society of America Bulletin*, v. 109, p. 869–884.
- Bahlburg, H., Vervoort, J.D., Andrew DuFrane, S., Carlotto, V., Reimann, C., and Cárdenes, J., 2011, The U–Pb and Hf isotope evidence of detrital zircons of the Ordovician Ollantaytambo Formation, southern Peru, and the Ordovician provenance and paleogeography of southern Peru and northern Bolivia: *Journal of South American Earth Sciences*, v. 32, p. 196–209.
- Barnes, J.B., Ehlers, T. a., McQuarrie, N., O’Sullivan, P.B., and Pelletier, J.D., 2006, Eocene to recent variations in erosion across the central Andean fold-thrust belt, northern Bolivia: Implications for plateau evolution: *Earth and Planetary Science Letters*, v. 248, p. 118–133,
- Barnes, J.B., Ehlers, T. A., McQuarrie, N., O’Sullivan, P.B., and Tawackoli, S., 2008, Thermochronometer record of central Andean Plateau growth, Bolivia (19.5°S): *Tectonics*, v. 27, p. 1–25.
- Barnes, J.B., Ehlers, T.A., Insel, N., McQuarrie, N., and Poulsen, C.J., 2012, Linking orography, climate, and exhumation across the central Andes: *Geology*, v. 40, p. 1135–1138.

- Barnes, J.B., and Heins, W. A., 2009, Plio-Quaternary sediment budget between thrust belt erosion and foreland deposition in the central Andes, southern Bolivia: Basin Research, v. 21, p. 91–109.
- Beck, S.L., and Zandt, G., 2002. The nature of orogenic crust in the central Andes: Journal of Geophysical Research, v. 107, p. 2230.
- Bettencourt, J.S., Leite, W.B., Ruiz, A.S., Matos, R., Payolla, B.L., and Tosdal, R.M., 2010, The Rondonian-San Ignacio Province in the SW Amazonian Craton: An overview: Journal of South American Earth Sciences, v. 29, p. 28–46.
- Blanco, J. a., Armenteros, I., and Huerta, P., 2008, Silcrete and alunite genesis in alluvial palaeosols (late Cretaceous to early Palaeocene, Duero basin, Spain): Sedimentary Geology, v. 211, p. 1–11.
- Brierley,G., Ferguson, R.J. and Wolfe, K.J., 1997, What is a fluvial levee ?: Sedimentary Geology, v. 114, p. 1–9.
- Brusset, S., Rochat, P., Baby, P., and Flinch, J., 2002, Thrust kinematics and foreland basin dynamics of the southern Subandean zone in Bolivia: new insight from apatite fission track analysis: ISAG.International Symposium on Andean Geodynamics, p. 101–104.
- Butler, R., 1992. Paleomagnetism: magnetic domains to geologic terranes, Oxford, Blackwell Scientific, 1992, 237 p.
- Chew, D., Magna, T., Kirkland, C., Miskovic, a, Cardona, a, Spikings, R., and Schaltegger, U., 2008, Detrital zircon fingerprint of the Proto-Andes: Evidence for a Neoproterozoic active margin?: Precambrian Research, v. 167, p. 186–200, doi: 10.1016/j.precamres.2008.08.002.
- Colombo, F., 1994, Normal and reverse unroofing sequences in syntectonic conglomerates as evidence of progressive basinward deformation: Geology, v.22, p. 235–238.
- DeCelles,, P.G., Gray, M.B., Ridgway, R. B., Cole, P., Srivastava, P., Pquera, P. and Pivnik, D.A., 1991. Kinematic history of a foreland uplift from Paleocene synorogenic conglomerate, Beartooth Range, Wyoming and Montana: Geological Society of America Bulletin, v. 103, p. 1458-1475.
- DeCelles, P.G., and Giles, K.N., 1996, Foreland basin systems: Basin Research, v. 8, p.105–123.
- DeCelles, P.G., Gehrels, G.E., Quade, J., Ojha, T.P., Kapp, P. a., and Upreti, B.N., 1998, Neogene foreland basin deposits, erosional unroofing, and the kinematic history of the Himalayan fold-thrust belt, western Nepal: Geological Society of America Bulletin, v. 110, p. 2–21.

- DeCelles, P.G., Cavazza, W., 1999. A comparison of fluvial mega-fans in the Cordilleran (Upper Cretaceous) and modern Himalayan foreland systems. Geological Society of America Bulletin 111, 1315–1334.
- DeCelles, P.G., and Horton, B.K., 2003, Early to middle Tertiary foreland basin development and the history of Andean crustal shortening in Bolivia: Geological Society of America Bulletin, v. 115, p. 58–77.
- Dickinson, W.R., 1985, Interpreting provenance relation from detrital modes of sandstones: in Zuffa, G.G. (ed.), Provenance of Arenites: NATO ASI Series, C 148, D. Reidel Publishing Company, Dordrecht, p. 333–363.
- Dickinson, W.R., and Suczek, C. A., 1979, Plate tectonics and sandstone compositions, in: American Association of Petroleum Geologists Bulletin, v. 63, p. 2164–2182.
- Dunn, J. F., Hartshorn, K. G., and Hartshorn, P.W., 1995, Structural styles and hydrocarbon potential of the Subandean belt of southern Bolivia, in Tankard, A. J., Suárez, S. R., and Welsink, H. J., eds., Petroleum basins of South America:American Association of Petroleum Geologists Memoir 62, p. 523–543.
- Eberth, D. a., and Miall, A.D., 1991, Stratigraphy, sedimentology and evolution of a vertebrate-bearing, braided to anastomosed fluvial system, Cutler Formation (Permian-Pennsylvanian), north-central New Mexico: Sedimentary Geology, v. 72, p. 225–252.
- Echavarria, L., Hernández, R., Allmendinger, R., and Reynolds, J., 2003, Subandean thrust and fold belt of northwestern Argentina: Geometry and timing of the Andean evolution: AAPG Bulletin, v. 87, p. 965–985.
- Ege, H., Sobel, E.R., Scheuber, E., and Jacobshagen, V., 2007, Exhumation history of the southern Altiplano plateau (southern Bolivia) constrained by apatite fission track thermochronology: Tectonics, v. 26, p. 1–24.
- Egenhoff, S.O., 2007. Life and death of a Cambrian-Ordovician basin: An Andean three-act play featuring Gondwana and the Arequipa-Antofalla terrane, in Limmermann, U., Nance, R.D., Kraft, P., and Zulauf, G. eds., The evolution of the Rheic Ocean: from Avalonian-Cadomian active margin to Alleghenian-Variscan collision: Geological Society of America Special Paper 423, p. 511-524.
- Egenhoff, S.O. and Lucassen, F., 2003, Chemical and Isotopic Composition of Lower to Upper Ordovician Sedimentary Rocks (Central Andes / South Bolivia ): Implications for Their Source: The Journal of Geology, v. 111, p. 487–497.
- Erikson, J. P., and Kelley, S. A., 1995, Late Oligocene initiation of foreland-basin formation in Bolivia based on newly dated volcanic ash, in IX Congreso Latinoamericano de Geología: Caracas, Venezuela, Ministerio de Energía y Minas, 14 p.

- Escayola, M. P., van Staal, C. R. and Davis, W. J., 2011, The age and tectonic setting of the Puncoviscana Formation in northwestern Argentina: An accretionary complex related to Early Cambrian closure of the Puncoviscana Ocean and accretion of the Arequipa-Antofalla block: *Journal of South American Earth Sciences*, v. 32, p. 438–459.
- Folk, R.L., 1980, Petrology of Sedimentary Rocks: Austin, Texas, Hemphill, 190 p.
- Galloway, W.E. and Hobday, D.K., 1996, Terrigenous clastic depositional systems, application to fossil fuel and groundwater resources, 2nd. ed., Springer, p. 60-90.
- Gibling, M.R., 2006, Width and Thickness of Fluvial Channel Bodies and Valley Fills in the Geological Record: A Literature Compilation and Classification: *Journal of Sedimentary Research*, v. 76, p. 731–770.
- Giraudo, R. and Limachi, R., 2001, Pre-Silurian control in the genesis of the central and southern Bolivian fold belt: *Journal of South American Earth Sciences*, v. 14, p. 665–680.
- Gradstein, F., Ogg, J., Schmitz, M. and Ogg G., 2012, The geologic time scale 2012, Elsevier, 1176 p.
- Gubbels, T. L., Isacks, B. L., and Farrar, E., 1993, High-level surfaces, plateau uplift, and foreland development, Bolivian central Andes: *Geology*, v. 21, p. 695–698.
- Hauser, N., Matteini, M., Omarini, R.H., and Pimentel, M.M., 2011, Combined U–Pb and Lu–Hf isotope data on turbidites of the Paleozoic basement of NW Argentina and petrology of associated igneous rocks: Implications for the tectonic evolution of western Gondwana between 560 and 460Ma: *Gondwana Research*, v. 19, p. 100–127.
- Hernandez, R.M., Jordan, T.E., Farjat, A.D., Echavarria, L., Idleman, B.D., Reynolds, J.H., 2005, Age, distribution, tectonics, and eustatic controls of the Paranense and Caribbean marine transgressions in southern Bolivia and Argentina: *Journal of South American Earth Sciences*, v. 19, p. 495–512.
- Horton, B. K., and DeCelles, P. G., 1997, The modern foreland basin system adjacent to the Central Andes: *Geology*, v. 25, p. 895–898.
- Horton, B.K., 1998, Sediment accumulation on top of the Andean orogenic wedge: Oligocene to late Miocene basins of the Eastern Cordillera, southern Bolivia: *Geological Society of America Bulletin*, v. 110, p. 1174–1192.
- Horton, B.K., and DeCelles, P.G., 2001, Modern and ancient fluvial megafans in the foreland basin system of the central Andes, southern Bolivia: implications for drainage network evolution in fold-thrust belts: *Basin Research*, v. 13, p. 43–63.
- Horton, B.K., Hampton, B. a., and Waanders, G.L., 2001, Paleogene synorogenic sedimentation in the Altiplano plateau and implications for initial mountain

- building in the central Andes: Geological Society of America Bulletin, v. 113, p. 1387–1400.
- Horton, B.K., 2005, Revised deformation history of the central Andes: Inferences from Cenozoic foredeep and intermontane basins of the Eastern Cordillera, Bolivia: Tectonics, v. 24.
- Hulka C., 2005. . Sedimentary and tectonic evolution of the Cenozoic Chaco foreland basin, Southern Bolivia: PhD Dissertation, Freie Universität Berlin.
- Hulka, C., Grafe, K., Sames, B., Uba, C., and Heubeck, C., 2006, Depositional setting of the Middle to Late Miocene Yecua Formation of the Chaco Foreland Basin, southern Bolivia: Journal of South American Earth Sciences, v. 21, p. 135–150.
- Hulka, C. and Heubeck, C., 2010, Composition and provenance history of Late Cenozoic sediments in southeastern Bolivia: Implications for Chaco foreland basin evolution and Andean uplift, Journal of Sedimentary Research, v. 80, p. 288–299.
- Ingersoll, R.V., Bullard, T.F., Ford, R.L., Grimm, J.P., Pickle, J.D., and Sares, S.W., 1984, The effect of grain size on detrital modes: A test of the Gazzi-Dickinson point-counting method: Journal of Sedimentary Petrology, v. 54, p. 103–116.
- Isacks, B.L., 1988, Uplift of the central Andean plateau and bending of the Bolivian orocline: Journal of Geophysical Research, v. 93, p. 3211–3231.
- Jacobshagen, V., Müller, J., Wemmer, K., Ahrendt, H., and Manutsoglu, E., 2002, Hercynian deformation and metamorphism in the Cordillera Oriental of Southern Bolivia, Central Andes: Tectonophysics, v. 345, p. 119–130.
- Jaillard, E., Hérail, G., Montfret, T., Diáz-Martinez, E., Baby, P., Laveno, A., Dumon, J.F., 2000, Tectonic evolution of the Andes of Ecuador, Peru, Bolivia and northern-most Chile, in: Cordani, U.G., Milani, E.J., Thomaz Filho, A.M., Campos, D.A. eds., Tectonic evolution of South America, 31st International Geological Congress, Rio de Janeiro, p. 481–559.
- Jordan, T. E., Reynolds, J. H., and Erikson, J. P., 1997, Variability in age of initial shortening and uplift in the central Andes, 16–33°30' S, in Ruddiman, W. F., ed., Tectonic uplift and climate change: New York, Plenum Press, p. 41–61.
- Kennan, L., Lamb, S., and Rundle, C., 1995, K-Ar dates from the Altiplano and Cordillera Oriental of Bolivia: Implications for Cenozoic stratigraphy and tectonics: Journal of South American Earth Sciences, v. 8, p. 163–186.
- Kley, J. 1993, Der Übergang vom Subandin zur Ostkordillere in Südbolivien: Geologische Struktur und Kinematik.- Berliner Geowissenschaftliche Abhandlungen, Reihe A, Band 156 : 1-88.
- Kley, J., 1996, Transition from basement-involved to thin-skinned thrusting in the Cordillera Oriental of southern Bolivia:Tectonics, v. 15, p. 763–775

- Kley, J., Müller, J., Tawackoli, S., Jacobshagen, V. and Manutsoglu, E., 1997,. Preandean and Andean-Age deformation in the Eastern Cordillera of Southern Bolivia. *Journal of South American Earth Sciences*, v. 10, p. 1-19.
- Kley, J., 1999a, Geologic and geometric constraints on a kinematic model of the Bolivian orocline: *Journal of South American Earth Sciences*, v. 12, p. 221–235.
- Lamb, S., Hoke, L., Kennan, L. and Dewey, J., 1997, Cenozoic evolution of the Central Andes in Bolivia and northern Chile, in: J.-P. Burg, M. Ford., eds., *Orogenes Through Time*, Special Publication Geological Society of London, v. 121, p. 237–264.
- Leier, a. L., McQuarrie, N., Horton, B.K., and Gehrels, G.E., 2010, Upper Oligocene Conglomerates of the Altiplano, Central Andes: The Record of Deposition and Deformation Along the Margin of a Hinterland Basin: *Journal of Sedimentary Research*, v. 80, p. 750–762.
- Litherland, M., Bloomfield, K., 1981. The proterozoic history of eastern Bolivia: *Precambrian Research*, v. 15, p. 157–179.
- Litherland, M., Annells, R.N., Derbyshire, D.P.F., Fletcher, C.J.N., Hawkins, M.P., Klinck, B. a., Mitchell, W.I., O'Connor, E. a., Pitfield, P.E.J., Power, G., and Webb, B.C., 1989, The Proterozoic of Eastern Bolivia and its relationship to the Andean mobile belt: *Precambrian Research*, v. 43, p. 157–174.
- Lopez-Pugliesi, M., 1995, Grupo Tacuru de las Sierras Subandinas de Bolivia, nominación de las unidades formacionales que lo integran, *Revista Técnica de Yacimientos Petrolíferos Fiscales Bolivianos*, v. 16 (1-2), p. 55-68.
- Loewy, S.L., Connelly, J.N., and Dalziel, I.W.D., 2004, An orphaned basement block: The Arequipa-Antofalla Basement of the central Andean margin of South America: *Geological Society of America Bulletin*, v. 116, p. 171-187.
- Marshall, L.G., Sempere, T., 1991, The Eocene to Pleistocene vertebrates of Bolivia and their stratigraphic context: a review. In: Suarez-Soruco, R. (Ed.), *Fósiles y Facies de Bolivia: Ver-tebrados*, *Revista Técnica de Yacimientos Petrolíferos Fiscales Bolivianos*, v. 12, p. 631–652.
- Marshall, L.G., Sempere, T., Gayet, M., 1993, The Petaca (Upper Oligocene–Middle Miocene) and Yecua (Upper Miocene) formations of the Subandean–Chaco basin, Bolivia, and their tectonic significance: *Documents des Laboratoires de Géologie de Lyon* 125, p. 291–301.
- Mascle, G., and Zubieta-Rossetti, D., 2005, Erosion in the Andes and sedimentation in the foreland basin of eastern Bolivia: 6th International Symposium on Andean Geodynamics, extended abstracts, p. 497–498.

- Matos Salinas, G.R., 2010, Geocronologia e evolucao tectónica Paleo-Mesoproterozoica do Oriente Boliviano – Regiao sudoeste do cratón Amazonico, PhD Dissertation, Universidade de Sao Paulo.
- McCarthy, P.J., and Martini, I.P., 1997, Anatomy and evolution of a Lower Cretaceous alluvial plain: sedimentology and palaeosols in the upper Blairmore Group , south-western Alberta, Canada: *Sedimentology*, v. 44, p. 197–220.
- McLeod, C.L., Davidson, J.P., Nowell, G.M., de Silva, S.L. and Schmitt, A.K., 2013, Characterizing the continental basement of the Central Andes: Constraints from Bolivian crustal xenoliths: *Geological Society of America Bulletin*, v. 125, 985-997.
- McQuarrie, N., 2002, The kinematic history of the central Andean fold-thrust belt, Bolivia: Implications for building a high plateau: *Geological Society of America Bulletin*, v. 114, p. 950–963.
- McQuarrie, N., Horton, B., Zandt, G., Beck, S., and Decelles, P., 2005, Lithospheric evolution of the Andean fold?thrust belt, Bolivia, and the origin of the central Andean plateau: *Tectonophysics*, v. 399, p. 15–37.
- Miall, A.D., 1977, A review of the braided-river depositional environment: *Earth-Science Reviews*, v. 13, p. 1–62.
- Miall, A.D., 1996, *The Geology of Fluvial Deposits*: Springer- Verlag, Berlin. 581 p.
- Moretti, I., Baby, P., Mendez, E. and Zubieta D., 1996, Hydrocarbon generation in relation to thrusting in the Sub Andean Zone from 18° to 22°S, Bolivia: *Petroleum Geoscience*, v. 2, p. 17-28.
- Mulch, A., Uba, C.E., Strecker, M.R., Schoenberg, R., and Chamberlain, C.P., 2010, Late Miocene climate variability and surface elevation in the central Andes: *Earth and Planetary Science Letters*, v. 290, p. 173–182.
- Müller, J.P., Kley, J., and Jacobshagen, V., 2002, Structure and Cenozoic kinematics of the Eastern Cordillera, southern Bolivia (21°S): *Tectonics*, v. 21, p. 1–23.
- Nash, D.J., McLaren, S.J., and Webb, J. a., 2004, Petrology, geochemistry and environmental significance of silcrete-calcrete intergrade duricrusts at Kang Pan and Tswaane, central Kalahari, Botswana: *Earth Surface Processes and Landforms*, v. 29, p. 1559–1586.
- Norabuena, E., 1998, Space Geodetic Observations of Nazca-South America Convergence Across the Central Andes: *Science*, v. 279, p. 358–362.
- Oiler, J. and Sempere, T., 1990, A fluvio-eolian sequence of probable Middle Triassic-Jurassic age in both Andean and Subandean Bolivia, in International Symposium.. "Geodynamique Andine", Résumés communication. ORSTOM Collection, Paris, p. 237-240.

- Oncken, O., Hindle, D., Kley, J., Elger, K., Victor, P., and Schemann, K., 2006, Deformation of the Central Andean upper plate system - facts, fiction, and constraints for plateau models, in Oncken, o., Chong, G., Franz, G., Glese, P., Götze H.J., Ramos, V., Strecker, M. and Wigger., P., eds.: The Andes: Active Subduction Orogeny, Berlin, Springer, p. 3-27.
- Oviedo, C., 1974, Correlaciones estratigráficas y evolución paleotectónica entre Monteagudo e Iñiguzo – Faja Subandina del sur, Internal report Yacimientos Petrolíferos Fiscales Bolivianos, 13 p.
- Perez, N. D., 2009, Late Miocene sedimentation in the central Andean foreland basin, southern Bolivia: constraint from magnetostratigraphy, Undergraduate Senior Honors thesis, The University of Texas at Austin.
- Ramos, V. a., 2008, The Basement of the Central Andes: The Arequipa and Related Terranes: Annual Review of Earth and Planetary Sciences, v. 36, p. 289–324.
- Ramos, V. a., 2010, The Grenville-age basement of the Andes: Journal of South American Earth Sciences, v. 29, p. 77–91.
- Reimann, C.R., Bahlburg, H., Kooijman, E., Berndt, J., Gerdes, a., Carlotto, V., and López, S., 2010, Geodynamic evolution of the early Paleozoic Western Gondwana margin 14°–17°S reflected by the detritus of the Devonian and Ordovician basins of southern Peru and northern Bolivia: Gondwana Research, v. 18, p. 370–384.
- Salinas, R., 1981, Informe final Sección Geológica Regional No. 2, Latitud Río Azero – Lagunillas: Internal YPFB report, Santa Cruz, Bolivia, 41 p.
- Schonian, F. and Egenhoff, S.O., 2007. A late Ordovician ice sheet in South America: evidence from the Cancañiri tillites, southern Bolivia, in Limmermann, U., Nance, R.D., Kraft, P., and Zulauf, G. eds., The evolution of the Rheic Ocean: from Avalonian-Cadomian active margin to Alleghenian-Variscan collision: Geological Society of America Special Paper 423, p. 525-548.
- Sempere, T., Héral, G., Oller, J., and Bonhomme M.G., 1990, Late Oligocene-early Miocene major tectonic crisis and related basins in Bolivia: Geology, v.. 18, p. 946–949.
- Sempere, T., 1995, Phanerozoic evolution of Bolivia and adjacent regions, in Tankard, A.J., Suarez, R., Wel- sink, H.J., eds., Petroleum basins of South America: American Association of Petroleum Geologists Memoir 62, p. 207–230.
- SERGEOTECMIN – YPFB, 2000, Mapa geológico de Bolivia, 1:1000000
- Siks, B.C., 2011, Sedimentary , structural , and provenance record of the Cianzo basin , Puna plateau-Eastern Cordillera boundary , NW Argentina, MSc. thesis The University of Texas at Austin.

- Simpson, G. D., 2006, Modelling interactions between fold-thrust belt deformation, foreland flexure and surface mass transport: *Basin Research*, v. 18(2), p. 125-143.
- Starck, D., and Del Papa, C., 2006, The northwestern Argentina Tarija Basin: Stratigraphy, depositional systems, and controlling factors in a glaciated basin: *Journal of South American Earth Sciences*, v. 22, p. 169–184.
- Stow, D.A.V., 2012. Sedimentary rocks in the field- a color guide, London, Elsevier Inc, 319 p.
- Suarez-Soruco, R., 2000, Compendio de Geología de Bolivia. Revista Técnica de Yacimientos Petrolíferos Fiscales Bolivianos, v. 18, p. 1–166.
- Teixeira, W., Geraldes, M.C., Matos, R., Ruiz, A.S., Saes, G., and Vargas-Mattos, G., 2010, A review of the tectonic evolution of the Sunsás belt, SW Amazonian Craton: *Journal of South American Earth Sciences*, v. 29, p. 47–60.
- Thiry, M. and Márechal, B., 2001, Development of tightly cemented sandstone lenses in uncemented sand: example of the fontainebleau sand (Oligocene) in the Paris basin: *Journal of Sedimentary Research*, v. 71, p. 473-483.
- Toselli, A.J., Aceñolaza, G.F., Miller, H., Adams, C., Aceñolaza, F.G., and Rossi, J.N., 2012, Basin evolution of the margin of Gondwana at the Neoproterozoic/Cambrian transition: the Puncoviscana Formation of Northwest Argentina: *Neues Jahrbuch für Geologie und Paläontologie - Abhandlungen*, v. 265, p. 79–95.
- Tucker, M.E., 2003, Sedimentary rocks in the field, 3rd. ed., West Sussex, Wiley, 234 p.
- Uba, C.E., Heubeck, C., and Hulka, C., 2005, Facies analysis and basin architecture of the Neogene Subandean synorogenic wedge, southern Bolivia: *Sedimentary Geology*, v. 180, p. 91-123.
- Uba, C.E., Strecker, M.R., Schmitt, A.K., 2007. Increased sediment accumulation rates and climatic forcing in the central Andes during the late Miocene: *Geology* 35, 979–982.
- Uba, C. E., Kley, J., Strecker, M. R., and Schmitt, A. K., 2009, Unsteady evolution of the Bolivian Subandean thrust belt: The role of enhanced erosion and clastic wedge progradation: *Earth and Planetary Science Letters*, v. 281, p.134-146.
- Wotzlaw, J.F., Decou, A., von Eynatten, H., Worner, G. and Frei, D., 2011, Jurassic to Palaeogene tectono-magmatic evolution of northern Chile and adjacent Bolivia from detrital zircon U-Pb geochronology and heavy mineral provenance: *Terra Nova*, v. 23, p. 399-406.
- Zandt, G., Beck, S. L., Ruppert, S. R., Ammon, C. J., Rock, D., Minaya, E., Wallace, T.C. N., and Silver, P. G., 1996, Anomalous crust of the Bolivian Altiplano, Central Andes: Constraints from broad- band regional seismic waveforms: *Geophysical Research Letters*, v. 23, p. 1159–1162.

## Vita

Amanda Zulema Calle was born in La Paz, Bolivia. Amanda obtained a Bachelor's degree of Engineering geology in 2008 from the Universidad Mayor de San Andres (UMSA). For four consecutive years, she was recognized as an academically distinguished student by the Provost of the University and Mr. Guido Capra, an ex-Bolivian senator, for obtaining the school's highest grades. After preparing her thesis and working as a geological susceptibility researcher at the Servicio Nacional de Geologia y Tecnico de Minas of Bolivia (SERGEOTECMIN), she joined Repsol YPF Bolivia oil company in 2006. In August 2011, she enrolled in The University of Texas at Austin to pursue a Master of Science degree in Geological Sciences at the Jackson School of Geosciences, with research focused on tectonics and sedimentology. After her graduation, she will pursue doctoral studies in the Jackson School of Geosciences at The University of Texas at Austin.

Permanent email address: amyzcp@gmail.com

This thesis was typed by the author.